GEOCHEMISTRY AND PETROGENESIS OF THE BELKNAP MOUNTAINS COMPLEX AND PLINY RANGE, WHITE MOUNTAIN SERIES, NEW HAMPSHIRE

by

MARC CHARLES LOISELLE

B.S., University of California, Riverside
(1973)

SUBMITTED IN PARTIAL FULFILLMENT
OF THE REQUIREMENTS FOR THE
DEGREE OF

DOCTOR OF PHILOSOPHY

at the

MASSACHUSETTS INSTITUTE OF TECHNOLOGY

OCTOBER, 1978

Signature of Author.....
Department of Earth and Planetary Sciences
October, 1978

Certified by.....
Thesis Supervisor

Accepted by.....
Chairman, Department Committee

GEOCHEMISTRY AND PETROGENESIS OF THE BELKNAP MOUNTAINS COMPLEX AND PLINY RANGE, WHITE MOUNTAIN SERIES, NEW HAMPSHIRE

by

MARC CHARLES LOISELLE

Submitted to the Department of Earth and Planetary Sciences October, 1978, in partial fulfillment of the requirements for the Degree of Doctor of Philosophy.

ABSTRACT

The anorogenic White Mountain series intrusives of northern New England consist of sub-alkaline to alkaline complexes composed of dominantly syenitic to granitic plutonic rocks. A detailed geochemical study was made of the Belknap Mountains complex in south central New Hampshire to determine the genesis and evolution of the intrusive rocks. The Belknap Mountains complex consists of (in order of decreasing age) a gabbro, a diorite, the Gilmanton monzodiorite (GMD), Ames monzodiorite (AMD), Belknap Mountain syenite (BMS), Cobble Hill syenite (CHS), Lake quartz syenite (LQS), Albany quartz syenite (AQS), Sawyer quartz syenite (SQS), and Conway granite (CG).

Results of Sr isotope analyses indicate the gabbro, diorite, BMS, CHS, SQS, and CG have similar initial ratios of $\sim$0.7035, and define an isochron with age $\sim$168 m.y. The AQS defines a whole rock isochron with a significantly higher initial Sr isotope ratio of $\sim$0.7040. The remaining units (GMD, AMD, LQS) do not fall on or define isochrons, and yield greater model initial ratios in the range 0.7040 to 0.7045. Some of this scatter is due to weathering of samples, particularly in the GMD where mineral separates yielded discordant ages.

Major and trace element modeling supports an origin for the gabbro as a partial cumulate from the diorite. Modeling of the more silicic units with low initial Sr isotope ratio as residual liquids derived by fractional crystallization of the diorite yielded ambiguous and inconsistent results due to the large gap in SiO_2 and lack of intermediate samples in the suite studied. A comagmatic relation for the series BMS$\rightarrow$SQS$\rightarrow$CG is strongly supported by the major and trace element data. The samples of Conway granite represent partial cumulates of quartz and feldspar, and were not formed by closed system crystallization of a liquid. The CHS appears to have evolved under more anhydrous conditions than the BMS.

It is suggested that the AQS (and possibly the GMD, AMD, and LQS) formed by assimilation of metamorphosed tholeiitic

basalt at the base of the crust.

The low initial Sr isotope ratios of the SQS and CG, the lack of a significant iron enrichment trend, and the large role of fractional crystallization in the evolution of the silicic rocks contrasts strongly with the model proposed by Barker et al. (1975) for the genesis of similar complexes. The AQS (and possibly the monzodiorites and LQS) do show the effects of assimilation or reaction with older crust.

Because no isotope data was obtained on samples from the Pliny Range, northern New Hampshire, no detailed geochemical modeling was undertaken. Preliminary examination of the results support Czamanske et al.'s (1977) conclusions that a model involving derivation of the magmas in the complex from a single source is precluded. One unit (the hastingsite quartz syenite) shows extreme iron enrichment, and in this respect is similar to rocks from the Pikes Peak batholith and the Nigerian Younger granite complexes. The older syenites are geochemically distinct from other White Mountain series syenitic and quartz syenitic rocks studied, and may have been produced by melting of eclogitic material at the base of the crust.

Thesis Supervisor: Dr. Frederick A. Frey
Associate Professor of Geochemistry

TABLE OF CONTENTS

Page

LIST OF FIGURES

Page

Page

LIST OF TABLES

Page

ACKNOWLEDGEMENTS

But when the dust had finally settled,
And the air had quickly cleared
Things were not as bad as I had feared.....

J. Buffett

The person who must be acknowledged first on these pages is my wife, Ellen, not only for her typing and drafting during the last months in Cambridge, but for her understanding, patience, and encouragement during all those other months.

I also want to thank:

Fred Frey, my advisor, for providing what turned out to be the right mix of critical comment and knowledgeable non-interference during the course of this research, and for essential financial support while the bulk of the text was being written;

Stan Hart, for financial support during several summers, for patient instruction in mass spectrometry, and for a new slant on how to hunt deer;

John S. Dickey, Jr., for my introduction to the White Mountain Series, and for an interesting viewpoint on lots of things;

R.S. Naylor, Northeastern University, for many helpful discussions on New England regional geology and tectonics;

D.R. Wones, Virginia Polytechnic Institute and State University, for providing samples of Pliny Range material analyzed by the USGS, for critically reading the first draft

of this thesis 1½ times, and for providing a place to go after finishing at MIT;

H.E. Gaudette, University of New Hampshire, for providing sample material from the Belknap Mountains;

J.C. Eichelberger, Los Alamos, for several days spent showing me around the Pliny Range;

My graduate student contemporaries in the department at MIT, not so much for any comment or suggestions they may have made regarding this thesis, but for the type of interaction that is essential to a graduate education. These include: Bruce Watson, Bruce Loeffler, John Suen, Mike Batzle, Carla Montgomery, Bill Olsewski, Karleen Davis, Mark Sneeringer, Maggie Riggs-Sneeringer, Alan Zindler, Hubert (The Hun) Staudigel, Bob Houghton, Kay Parkin, Rosemary Hickey, and a host of others. Most of these people have gone on to bigger(?) and better(!) things, and those that haven't most certainly will. Just remember: enjoy it while you can!!

The departmental administrative assistants Lynn Dickey and Debbie Gilette, as well as a cast of thousands on the 9^{th} floor, for making my stay at (and exit from) MIT a smooth one;

B.W. Chappell, Australian National University, for XRF analyses on splits of the Belknap Mountains samples;

G. Thompson, Woods Hole Oceanographic Institute, for providing access to their XRF facility;

Staff at the MIT Reactor Facility for the efficient

irradiation of samples analyzed by INAA. (Additional samples were irradiated at the Georgia Institute of Technology.)

J. Melanson, Wolfboro, N.H., for access to his property on Rattlesnake Island.

CHAPTER 1. INTRODUCTION

The White Mountain rock series consists of small to medium-sized intrusions of dominantly syenitic and granitic material, aligned in a roughly linear trend from northern New Hampshire to southeastern Maine (Figure 1). The largest body, the White Mountain Batholith, is a composite body of syenite, quartz syenite, and granite (several varieties) (Billings, 1956; Creasy, 1974; Henderson et al., 1977). The syenites and quartz syenites frequently occur as partial ring dikes, indicating cauldron subsidence during emplacement of the magmas.

While plutonic rocks dominate at the present level of erosion, there are occurrences of volcanic material in scattered localities (Ossipee, Moat Mountain), usually preserved in down-faulted wedges. In most cases, the volcanics predate the plutonics, as is common in similar complexes preserved at higher structural levels (Jacobson et al., 1958). Silica-saturated and oversaturated rocks are predominant in the White Mountain intrusives, with only minor occurrances of undersaturated rock types, notably at Red Hill (Quinn, 1937; Wellman, 1971; Size, 1972).

K/Ar dating of most of the White Mountain complexes (Foland and Faul, 1977) yield ages ranging from ∿220 m.y. to ∿100 m.y. The ages of the complexes fall into three groups - between 240-220 m.y.; 200-156 m.y.; and 125-100 m.y. (Foland

and Faul, 1977, Figure 4). Individual complexes, however, were emplaced over a relatively short period of time (<5 m.y.). An exception is the White Mountain Batholith which spans a range of 10-12 m.y. (Foland and Faul, 1977). K/Ar dating by Foland et al. (1971) and Foland and Faul (1977) indicates an age of ∿158 m.y. for the Belknap Mountains complex. (Rb/Sr work in this study indicates an age ∿6% higher, or ∿168 m.y.) K/Ar dating of granitic material from the Pliny Range yielded an age of 188 ±4 m.y. (Foland et al., 1971, corrected in Foland and Faul, 1977).

The broad linear trend of White Mountain intrusives (Figure 1) suggests some major tectonic control on their generation and emplacement. Morgan (1971) suggested the movement of the North American plate over a fixed mantle plume. In contrast, Ballard and Uchupi (1972) proposed emplacement along a fracture zone produced by translation of crustal blocks prior to the initiation of seafloor spreading, whereas Chapman (1968) suggested that the location of White Mountain intrusives was controlled by the intersection of two fracture systems.

Foland and Faul (1977) present age data on nearly all the White Mountain intrusives and discuss the implications for the various theories. They concluded that the distribution of ages is not consistent with a "simple" hot spot model, but is consistent with generation and emplacement along a fracture system which was reactivated several times during the Mesozoic.

Recently, Barker et al. (1975) presented a model for the genesis of the Pikes Peak Batholith and similar rock associations (including the White Mountain complexes). The model is complex and includes reaction of a mantle-derived alkali basalt with lower and intermediate crustal material (Figure 2). It is clear that the nature of the crustal section will have considerable control on the composition of the later magmas. This model contrasts strongly with the much simpler model of a fractional crystallization (comagmatic model, Figure 2) origin for the more silicic members of such complexes.

Both models (in some form) have been suggested as mechanisms for the origin of the White Mountains complex. Chapman and Williams (1935), in an early review paper believed that a mixture of reaction, assimilation, and crystallization was responsible for the compositional variations of the White Mountain magmas. Chapman (1976) presented a model for the evolution of White Mountain complexes based on structural criteria, and suggested that granitic material was generated by selective fusion of crustal material while syenitic material developed from basaltic magma through fraction crystallization and assimilation. Other studies of individual complexes have suggested fractional crystallization (Roy and Freedman, 1944; Size, 1972, Gaudette and Bothner, 1969), or more complex models (Modell, 1936; Czamanske et al., 1977) for the origin of the intrusives. The lack of abundant mafic material necessary in any comagmatic/fractional

crystallization model using basalt as a parent magma was a major point against adoption of this model, but Sharp and Simmons (1978) show that the necessary cumulate material may lie at depth beneath many of the complexes.

The two models (Figure 2) are not mutually exclusive in that in the more complex reaction melting models, fractional crystallization will almost certainly act to modify the magma composition.

With these two simplified, end-member models for the genesis of the White Mountain and similar complexes in mind this geochemical study was undertaken. One special objective was to determine the role of reaction and assimilation of older crustal material in the genesis of the Belknap Mountains complex, and its effect on the composition of the magmas. The Belknaps have a wide range of rock types exposed (Chapter 2), a good geologic map is available (Modell, 1936; Bothner and Gaudette, 1971), and the relative age relations of the rocks are well known. Therefore, it was considered a good choice for a detailed geochemical study. Since the Barker et al. (1975) model involves older crust, the initial Sr isotopic composition of the rock units appears to be a straightforward way of determining the involvement of older material. For this reason, Sr isotope data was obtained on all the plutonic rocks in the complex. In addition, major and trace element data were obtained in order to quantitatively evaluate possible comagmatic relations and determine the relative importance of mineral phases in controlling the

magma composition.

The petrology and mineralogy of the Pliny Range has recently been studied (Czamanske et al., 1977), and trace element and additional major element data were obtained in order to compare the geochemistry of the two complexes. Because the two intrusives were emplaced in different structural and stratigraphic belts (Chapter 2), these studies might allow an estimate of the effect of the crustal section on the magma chemistry.

The overall objective of this thesis was a detailed geochemical study of two sub-alkaline intrusive complexes of the White Mountain rock series, New Hampshire. Specific objectives were to determine the role of older crustal material in the genesis of the complexes, to quantitatively evaluate possible comagmatic relations, and to assess the effect of contrasting crustal sections on magma composition. An additional objective was to examine the geochemistry of continental igneous activity associated with continental breakup, specifically the opening of the Atlantic Ocean.

Figure Captions

Figure 1. Distribution of White Mountain series intrusive complexes in Maine, New Hampshire, and Vermont.

Figure 2. Schematic diagram illustrating two contrasting end member theories for the genesis of alkaline igneous complexes. Comagmatic model derives more silicic magmas through fractional crystallization of a basaltic magma; reaction melting model (Barker et al., 1975) derives more silicic magmas by reaction of a mantle-derived basaltic magma with lower and intermediate crustal rocks.

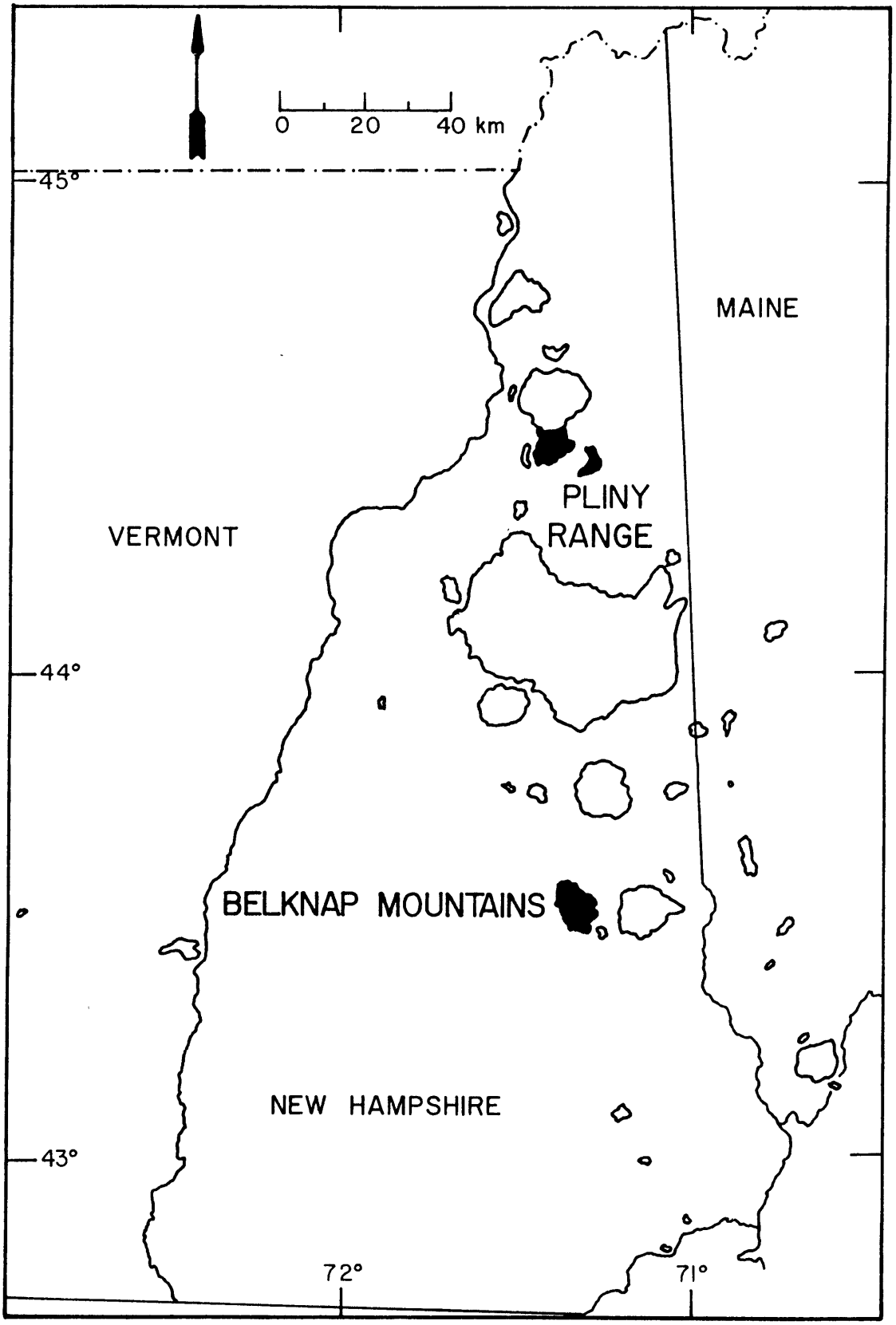
0 20 40 km
45°
MAINE
PLINY
RANGE
VERMONT
44°
BELKNAP MOUNTAINS
NEW HAMPSHIRE
43°
72°
71°

THEORIES FOR THE GENESIS OF IGNEOUS ALKALINE COMPLEXES

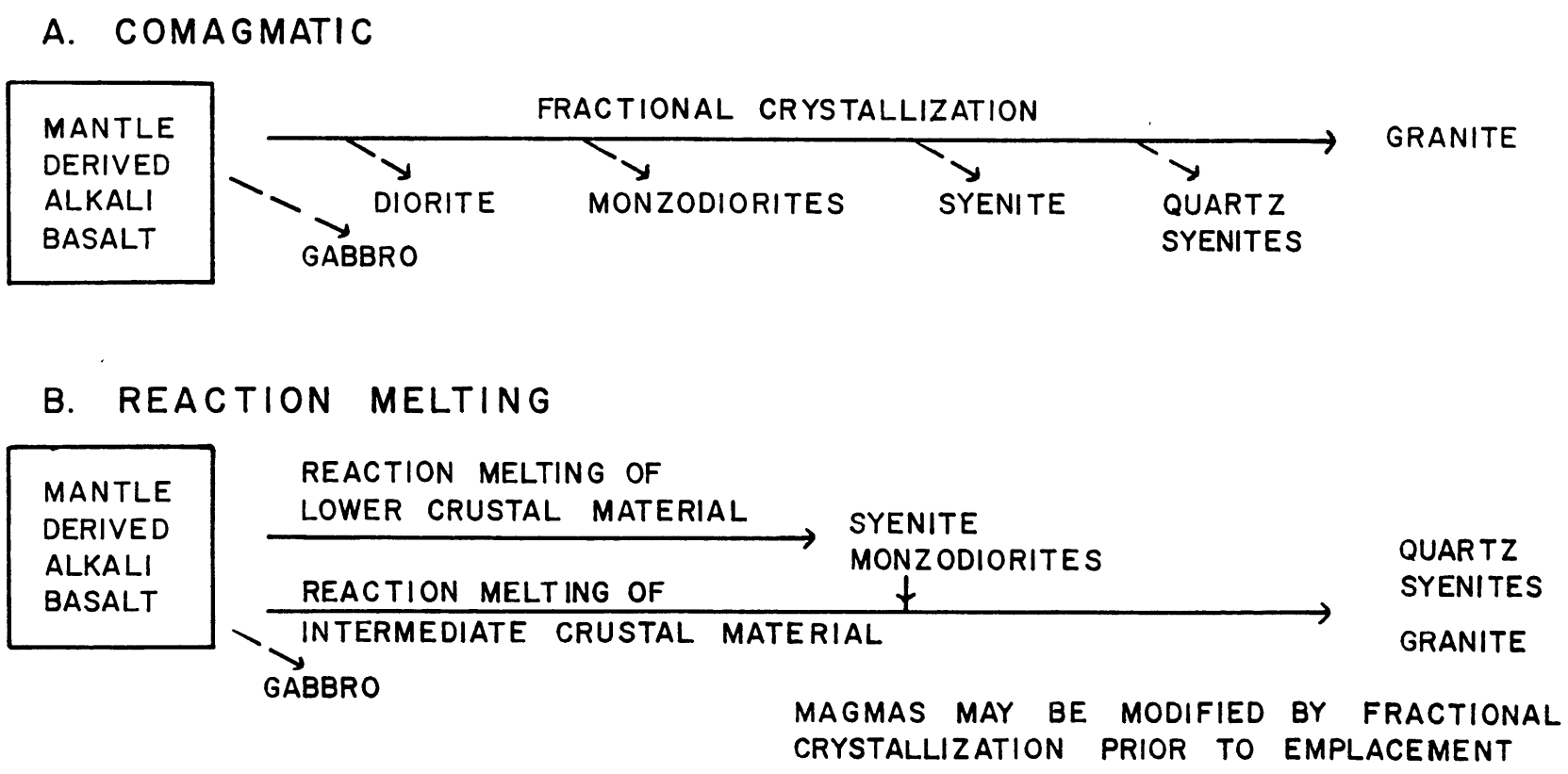

Figure 2

CHAPTER 2. REGIONAL GEOLOGY AND TECTONICS

From the discussion on possible formation mechanisms for the White Mountain and similar mildly alkaline complexes, it is clear that the reaction melting model is sensitive to the age and nature of the precursor crustal section. Therefore, it is necessary to attempt to characterize the crustal section into which the Pliny Range and Belknap Mountain complexes were emplaced.

As shown in Figure 3, the trend of White Mountain igneous activity cuts the older northern Appalachian structural trends at an angle of ∿50°-60°. At the latitude of the main White Mountain intrusives (∿44°N) the structural elements that make up the northern Appalachians consist of (from west to east) (Rodgers, 1970): the Green Mountain anticlinorium; Connecticut-Gaspé synclinorium; Bronson Hill-Boundary Mountain anticlinorium; and the Merrimack synclinorium. With the exception of several complexes in Vermont, all the White Mountain intrusions were emplaced in the latter two structural belts. The Pliny Range was intruded into the Bronson Hill anticlinorium, the Belknap Mountains into the Merrimack synclinorium.

The Bronson Hill anticlinorium has not been extensively studied recently at the latitude of the Pliny Range. Chapman et al. (1944) and Chapman (1948) did earlier structural and petrologic studies in this portion of the

anticlinorium. More recently the stratigraphy and structure of the anticlinorium has been examined both to the north (Green, 1964; Green and Guidotti, 1968; Boudette and Boone, 1976) and south (Thompson et al., 1968) of the Pliny Range. Recent work in northern New Hampshire and northwestern Maine appears to be most relevant to the area around the Pliny Range. Green and Guidotti (1968) examined the stratigraphy of the anticlinorium in this area and indicated a history of eugeosynclinal deposition and volcanic activity during much of the Ordovician, terminated by the Taconic orogeny and the intrusion of the Ordovician Oliverian/ Highlandcroft magmas (Naylor, 1968, 1969).

Following the Taconic orogeny, the Bronson Hill-Boundary Mountain anticlinorium was locally emergent through much of the Silurian, although scattered remnants of Silurian rocks (unconformably overlying the Ordovician rocks) are present. The anticlinorium was then subjected to folding and metamorphism during the Devonian Acadian orogeny. Coincident with the highest degrees of deformation and metamorphism during the Acadian was the generation and emplacement of Billing's (1956) New Hampshire Plutonic Series, dominantly calc-alkaline intermediate and silicic rocks. Gravity studies of New Hampshire Plutonic Series intrusives (Nielson et al., 1976) indicate these bodies are shallow, sheet-like bodies and recent Sr isotopic work by Lyons and Livingston (1977) yield high initial ratios

indicative of a crustal source.

Boudette and Boone (1976) describe a block of older metamorphic basement dated at ∿1500 m.y. (Naylor et al., 1973) in the Boundary Mountain anticlinorium. This raises the possibility that other portions of the Bronson Hill-Boundary Mountain anticlinorium may be either floored by or contain blocks of much older crustal material.

Therefore, in the Bronson Hill anticlinorium there was a complex geologic history prior to White Mountain igneous activity. This is summarized in Table 1. Notable is the occurrence of several igneous episodes which may have produced a heterogeneous middle and upper crustal section while depleting portions of the lower crust in volatiles and large ion lithophile elements.

At this point the position of the older Pliny Range syenites in the sequence of igneous events should be mentioned. Chapman (1944) placed them in the Oliverian Magma Series because of their porphyritic texture similar to the Oliverian gneisses and their weak to moderate foliation that is wholly absent in White Mountain rocks. Eichelberger (1971) and Czamanske et al. (1977) noted that the syenites clearly truncate structures in the older rocks and do not show the multiple deformations characteristic of the Oliverian/Highlandcroft. They suggest the syenites represent an earlier phase of White Mountain activity unique to the Pliny Range. Page (1968) has emphasized the occurrence of a late Devonian post-tectonic episode of mildly alkaline

TABLE 1. COMPARISON OF CRUSTAL DEVELOPMENT IN THE BRONSON HILL ANTICLINORIUM VS. THE MERRIMACK SYNCLINORIUM.

Bronson Hill Anticlinorium	Merrimack Synclinorium
	∿168 m.y. - Belknap Mtns. Complex.
∿188 m.y. - Pliny Complex.	White Mountain activity ca. 200 m.y. (Red Hill).
Devonian Plutonism (New Hampshire Plutonic Series).	Devonian Plutonism (New Hampshire Plutonic Series).
Restricted Siluro-Devonian sedimentation. Acadian Orogeny.	Siluro-Devonian eugeosynclinal sedimentation. Acadian Orogeny.
Minor post-Highlandcroft/Oliverian plutonism and volcanism.	
Ordovician plutonism (Highlandcroft/ Oliverian).	Ordovician sedimentation and volcanism (?)
Cambro-Ordovician eugeosynclinal sedimentation and volcanism. Taconic Orogeny.	
Possible Precambrian blocks and/or basement; migmitization (Chain Lakes Block).	(?)

plutonism in New England. As mentioned by Czamanske et al. (1977), these older syenites may belong to this Late Devonian magmatic episode. However, the assignment of the older syenites of the Pliny Range to the White Mountain rocks is tenuous until isotopic work underway at the University of Pennsylvania (K. Foland, pers. comm.) is completed.

In contrast to the complex pre-White Mountain history in the Bronson Hill anticlinorium, the Merrimack synclinorium apparently has had a much less complex history. Detailed studies in the vicinity of the Belknap Mountains are lacking, but there are detailed stratigraphic and structural studies of the central and southeastern portions of the synclinorium in central Maine (Osberg et al., 1968; Boudette and Boone, 1976; Ludman, 1976; and Pankiwskyj et al., 1976) where the lower degree of metamorphism and presence of fossil control provide better structural control. These studies indicate the synclinorium consists of a tightly folded sequence of Ordovician to Devonian clastic metasediments and minor metavolcanics, and that sedimentation in the synclinorium was continuous throughout this period (Osberg et al., 1968). In the vicinity of the Belknap Mountains the country rock is the Devonian Littleton Formation (Billings, 1956), an amphibolite facies pelitic schist composed of quartz, feldspar, and mica, with less abundant garnet and sillimanite (Modell, 1936). The Littleton was intruded in the Devonian by magmas of the New Hampshire Plutonic Series. These quartz

diorite and porphyritic granite bodies are most likely shallow, probably not more than a few kilometers thick (Nielson et al., 1976). Migmatization of the Littleton Formation in some localities and abundant pegmatites throughout this part of New Hampshire indicate that regional metamorphic conditions were sufficient for anatexis of crustal material. Naylor (1975) summarized isotopic ages on basement in the northern Appalachians, and felt that the sediments of the Merrimack synclinorium are not underlain by an older (Precambrian) sialic basement, but acknowledged that the presently available data cannot resolve the question of whether a continuous sialic basement underlies the northern Appalachians.

K/Ar age dating of other White Mountain complexes in the vicinity of the Belknaps (Armstrong and Stump, 1971; Foland and Faul, 1977) yield ages of 194 m.y. and 198 m.y. for the Red Hill complex approximately 20 km to the north. Rb/Sr work by Foland and Friedman (1977) support these ages for Red Hill. From this it is apparent that White Mountain plutonism (and volcanism) started in southcentral New Hampshire some 30 m.y. before the emplacement of the Belknap Mountains complex (ca. 168 m.y.).

A schematic pre-White Mountain series history for the Merrimack synclinorium is given in Table 1. Note that unlike the Bronson Hill anticlinorium there is no evidence for an older crystalline basement, and no Taconic/Ordovician plutonic event. However, White Mountain magmatic activity

in this portion of New Hampshire commenced ∿30 m.y. prior to the generation of the Belknap Mountain complex.

Geologic Relations in the Pliny Range

White Mountain plutonic rocks in the Pliny and Crescent Ranges were first mapped in detail by Chapman (1942). The complex was remapped by Eichelberger (1971), and a study of the petrology and mineralogy of the rocks in the Pliny Range was made by Czamanske et al. (1977).

Figure 4 is a geologic map of the Pliny and Crescent Ranges (from Eichelberger, 1971) and summarizes the geologic relations leading to the relative age assignments of the White Mtn. rocks. A large mass of older syenite was intruded by a central mass of diorite and partial ring dikes of quartz monzodiorite, quartz monzonite, and quartz syenite. These units were intruded by small stocks of hastingsite-biotite granite and Conway granite. Sample locations for Czamanske et al. (1977) and for samples collected for the study are also given.

Following are brief descriptions of the rock units from Czamanske et al. (1977). More detailed descriptions of the units are given in Czmanske et al. (1977). Detailed petrographic descriptions and modes of new samples collected for this study are given in Appendix I, and modal data for all samples are summarized in Figure 5.

Older Syenites - Coarse syenite is composed of pink perthite phenocrysts up to 2 cm long and smaller, less abundant plagioclase phenocrysts in a matrix of quartz, plagioclase, perthite, amphibole, biotite, sphene, and magnetite. The medium syenite is similar except for the smaller grain size ($\sim$3 mm perthites) and lower mafic content. Primary hematite is observed in one sample. Both rock types have textures suggestive of recrystallization.

Diorite - This unit is composed dominantly of plagioclase, with amphibole, biotite, and pyroxene (the mafic phases in order of decreasing abundance). Quartz and alkali feldspar are minor interstitial phases. Also opaques, minor sphene, and apatite are present.

Quartz Monzodiorite - Mineralogy is dominantly plagioclase, with amphibole and biotite as mafic phases. Quartz and alkali feldspar are considerably more abundant than in the diorite, but generally less than 30%. Minor phases are opaques, sphene, and apatite.

Hastingsite Quartz Syenite - The mineralogy is dominantly perthite with interstitial quartz. Amphibole is the dominant mafic phase. Plagioclase is present, but variable in amount. Minor opaques and allanite are also present.

Porphyritic Quartz Monzonite - This unit is composed of intergrown quartz, alkali feldspar, and plagioclase, with minor amphibole and biotite, and accessory opaques

and sphene. The quartz-feldspar intergrowths show some evidence of recrystallization.

Pink Biotite Granite - A medium grained, equigranular rock composed of perthite, plagioclase, and quartz, with biotite and minor amphibole. Opaques, sphene, and allanite are also present, as are numerous xenoliths of country rock. This unit was mapped by Chapman (1942) as a "shatter zone."

Granite Porphyry - This rock consists of phenocrysts of perthite, plagioclase, and quartz (showing resorbed grain boundaries) in a fine matrix of quartz and feldspar. Biotite and amphibole occur as irregular grains. Minor opaques and allanite are also present.

Hastingsite Biotite Granite - Mineralogy is perthite, plagioclase, and interstitial quartz with minor amphibole, biotite, opaques, allanite, and sphene. This rock can be distinguished from the Conway granite by its higher mafic content, smaller grain size, and interstitial nature of the quartz.

Conway Granite - This unit is similar to the Hastingsite biotite granite except it is coarser grained and less mafic, and the quartz is subhedral as opposed to interstitial.

Geologic Relations in the Belknap Mountains

The geology and petrography of the Belknap Mountains were first examined by Pirsson and Washington (1905, 1906), but the first detailed work was by Modell (1936). He mapped the complex, examined the structure of the ring dikes and the relation to the country rocks and the other White Mountain units, and examined (in a limited way) the petrography and petrology of the complex. Gaudette and Bothner (1969) studied the geochemistry of selected major and trace elements, and Bothner and Gaudette (1971) published a slightly modified map of the complex.

Figure 6 is a geologic map of the Belknap Mountains complex after Bothner and Gaudette (1971). The complex is elliptical in plan form, approximately 13 km x 9 km. There are several well developed partial ring dikes, most notably the Albany quartz syenite, the Lake quartz syenite, and the Conway granite. These and other intermediate and silicic units surround an early stock of diorite and were intruded by the late central mass of Conway granite. Modell (1936) recognized two masses of syenite (both termed the Belknap syenite). These two masses of syenitic material will be treated separately as they show important compositional and modal differences. The syenitic rocks on the western edge of the complex will be called the Belknap Mountain syenite, while the syenite stock in the northcentral portion of the complex will be called the Cobble Hill syenite, an informal

term used by Modell (1936).

There are restricted occurrences of volanics and volcanic breccias in the Belknap Mountains, but these units were not studied. The Moat volcanics consist of both trachytic and rhyolitic material in a fault slice along the inner side of the Albany quartz syenite ring dike (Figure 6), and are badly fractured and altered. More suitable localities for the study of White Mountain volcanics are the Ossipee ring dike complex and Moat Mountain (Billings, 1956).

Figure 6 also illustrates schematically the relative age relations of the White Mountain rocks in the Belknap Mountains. Data for this figure come from Modell (1936) and my own observations. It is strongly recommended that Modell's paper be read as this represents a major and primary source of information on the geologic relations summarized in Figure 6. The relative ages of the units are fairly well known, with several exceptions:

- The relative age of the gabbro with respect to the diorite is not known because the contact on Locke's Hill is not exposed.
- The Ames monzodiorite is certainly older than the Conway granite which truncates it, but its age relative to the other units is not known. Because of the small outcrop area and extremely limited data collected for this study, this is not a particularly critical age assignment. It is given a relative age

similar to the Gilmanton monzodiorite.

- The contact between the Gilmanton monzodiorite and Belknap Mountain syenite is "not sharp" (Modell, 1936, p. 1902), and thus their relative age is uncertain. The contact relation between the monzodiorite and the syenite may be critical to an interpretation of the genesis of the complex, and the suggestion of the lack of a sharp contact may be significant.
- The relative age of the Lake quartz syenite is not constrained on the young side. It's position is in accordance with the relative ages of quartz syenite intrusions in other complexes.

As with the Pliny Range, detailed petrographic descriptions and modes of samples are given in Appendix I. Brief descriptions of the units are given below, with the modal data summarized in Figure 7. Sample locations are shown in Figure 6.

Gilford Gabbro - A dark, medium to coarse grained rock composed primarily of plagioclase, clinopyroxene (partially altered to hornblende), and ilmenite with large, poiklitic brown hornblende crystals up to 3 cm across evenly distributed through the rock. Accessories include minor biotite and chlorite, epidote, and late sphene.

Endicott Diorite - A light to dark grey, fine to medium grained equigranular rock, with dominant plagioclase,

hornblende, and biotite with minor clinopyroxene and ilmenite. Accessories include abundant apatite, minor chlorite, sphene, and epidote. Interstitial alkali feldspar is present in samples 17 and 18. Evidence of recrystallization in the irregular grain boundaries is most likely due to intrusion of the Conway granite. Much of the Endicott diorite has been intruded and brecciated by the Conway granite, and in places the diorite only remains as inclusions (50%) in a matrix of granitic material. Samples 5 and 18 of the diorite come from large inclusions of diorite in such brecciated outcrops. Sample 17 is from a large mass of diorite cut by thin veins of granitic material.

Gilmanton Monzodiorite - A medium grained rock with plagioclase, alkali feldspar (microperthite), hornblende, and biotite, minor clinopyroxene and opaques, and very minor interstitial quartz. Accessories include apatite, sphene, zircon, chlorite, and epidote. Plagioclase is in subhedral to anhedral crystals with interstitial alkali feldspar. Hornblende and biotite contents are variable. Irregular grain boundaries, wavy plagioclase twin lamellae, undulose extinction, and small stringers of crushed and recrystallized minerals between larger grains suggest minor cataclasis.

Ames Monzodiorite - A light grey, medium grained rock with plagioclase, alkali feldspar (microperthite), biotite, hornblende (with a few cores of clinopyroxene), and

quartz. Accessories include apatite, sphene, and chlorite. Opaques are rounded and show evidence of resorption or reaction. A few large subhedral grains of feldspar occur, but most alkali feldspar is anhedral to interstitial. Quartz is interstitial. Small (up to 1-2 cm) inclusions of mafic-rich material are common in outcrop. Care was taken to avoid these in selecting fragments for geochemical study.

Belknap Mountain Syenite - A medium to coarse grained, light grey to buff colored, rock consisting of perthitic alkali feldspar, plagioclase, hornblende, biotite, and minor clinopyroxene (core of hornblende), opaques, and interstitial quartz. Minor apatite, zircon, sphene, and chlorite occur as accessories. Discrete grains of alkali feldspar are much more abundant than primary (not exsolution) plagioclase which sometimes cores the perthite. It has higher mafic content and plagioclase content than the Cobble Hill syenite.

Cobble Hill Syenite - A light grey to white, medium grained rock, with dominantly perthitic alkali feldspar, plus hornblende and minor biotite. Primary plagioclase is extremely minor. Accessories include clinopyroxene (especially in G7), apatite (also much more abundant in G7), opaques, sphene, zircon, and chlorite. Sample G8 consists of primarily euhedral to subhedral alkali feldspar with conspicuous interstitial quartz. G7 is

much more allotriomorphic in texture.

Lake Quartz Syenite - A medium grained, porphyritic rock. Two contrasting samples were studied; a relatively basic sample from the inside margin of the ring dike and an interior sample. Phenocrysts of feldspar occur in a matrix of feldspar, quartz, and mafics (hornblende and minor biotite), with accessory opaques, apatite, sphene, zircon, and chlorite.

Sawyer Quartz Syenite - A pink, medium grained equigranular rock with coarsely perthitic alkali feldspar and quartz as major constituents. The amount of primary plagioclase varies considerably in the samples. Mafic minerals include hornblende and biotite, and accessories are apatite, zircon, sphene, allanite, opaques, and chlorite. The quartz is anhedral and at times interstitial. Some of the plagioclase appears to be a late crystallizing phase.

Albany Quartz Syenite - A medium to coarse grained subporphyritic quartz syenite with perthitic alkali feldspar in a matrix of feldspar, quartz, and mafics (primarily hornblende with some biotite). Accessories include opaques, apatite, zircon, sphene, and chlorite. Sample 1 shows good porphyritic texture and this sample also contains several slightly rounded but obviously euhedral grains of quartz.

Conway Granite - A medium grained, equigranular rock,

composed dominantly of perthitic alkali feldspar, quartz, plagioclase, biotite, and minor hornblende, plus accessory opaques, apatite, zircon, sphene, and traces of allanite. Fluorite occurs in samples 6, G28, and G29. Sample G28 is much more akin to Sawyer quartz syenite. In general, the granite has very "clean" grain boundaries. Samples 6 and 7 of the Conway granite are material intruding and brecciating the diorite.

Figure Captions

Figure 3. Major structural belts in northern New England and distribution of White Mountain series intrusives.

Figure 4. Geologic map of the Pliny Region, New Hampshire, with relative stratigraphy and locations of samples analyzed for this study.

Figure 5. Modal proportions of quartz, alkali feldspar, and plagioclase for samples from the Pliny Region, New Hampshire. Includes samples described in Czamanske et al. (1977), as well as samples collected for this study. IUGS Classification (1973).

Figure 6. Geologic map of the Belknap Mountains Complex, New Hampshire, with relative stratigraphy and location of samples analyzed for this study.

Figure 7. Modal proportions of quartz, alkali feldspar, and plagioclase for samples from the Belknap Mountains Complex, New Hampshire. IUGS Classification (1973).

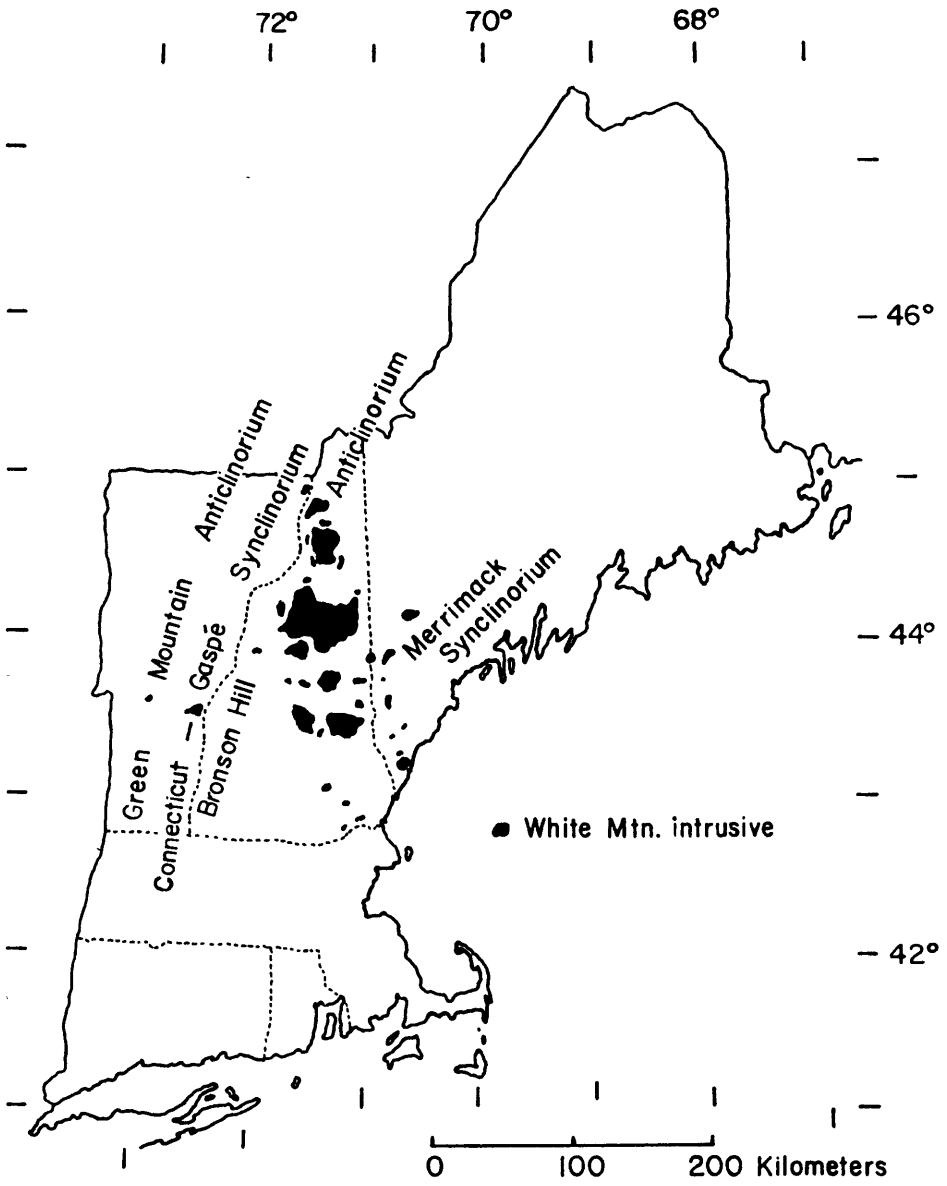
72°
70°
68°
46°
44°
42°
Anticlinorium
Synclinorium
Anticlinorium
Merrimack Synclinorium
Mountain
Gaspé
Bronson Hill
Green
Connecticut
White Mtn. intrusive
0
100
200 Kilometers

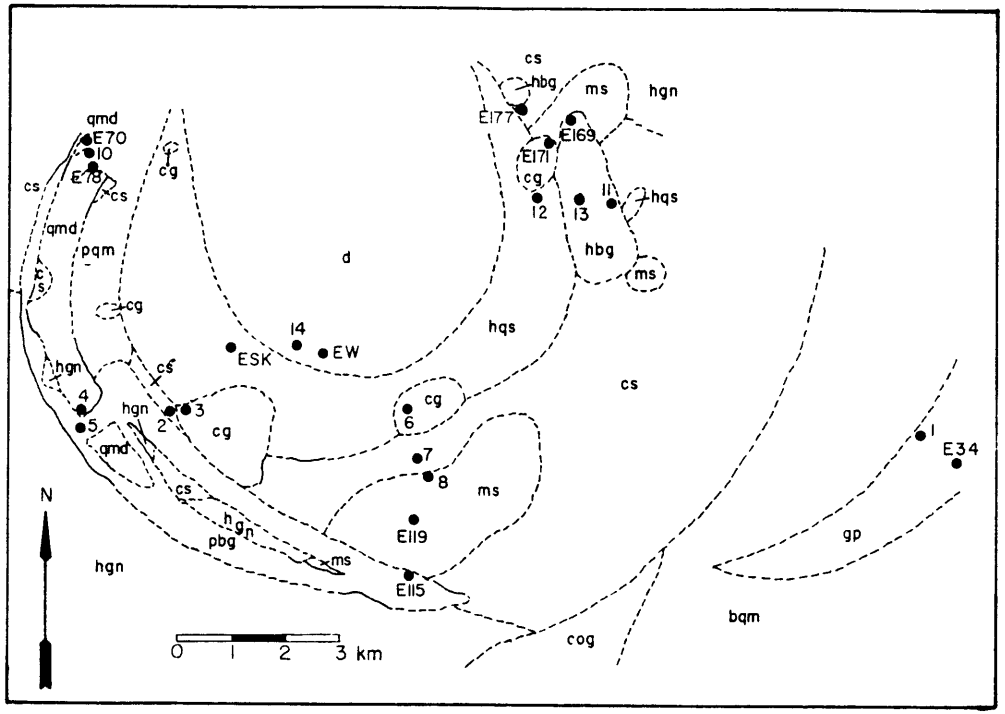

GEOLOGIC MAP OF THE PLINY REGION, N.H.

Geology from Eichelberger (1971), Czamanske et al. (1977), Chapman (1942).

LEGEND AND RELATIVE STRATIGRAPHY

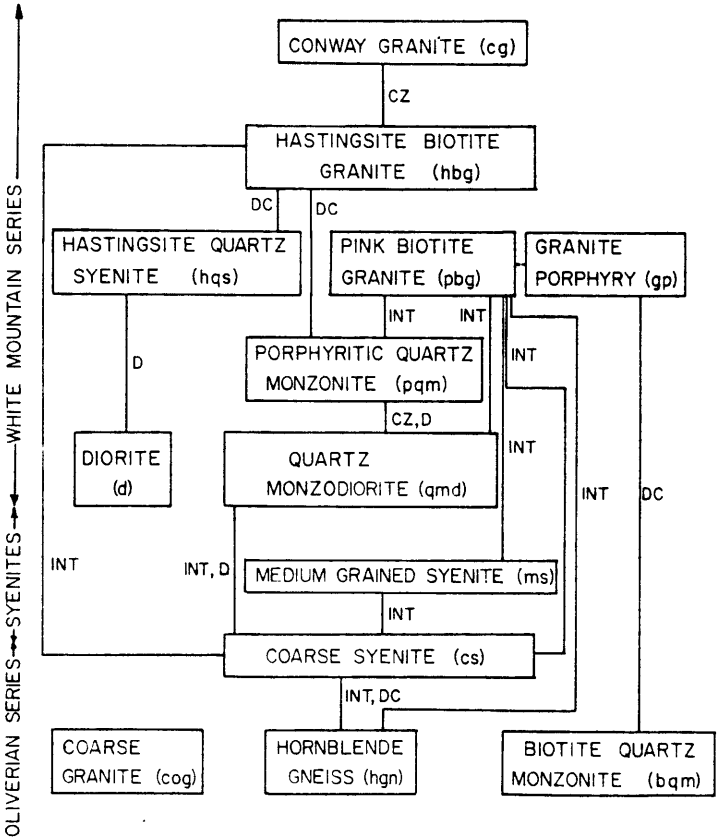

● E119 Sample Location

Figure 4

PLINY RANGE - MODAL DATA

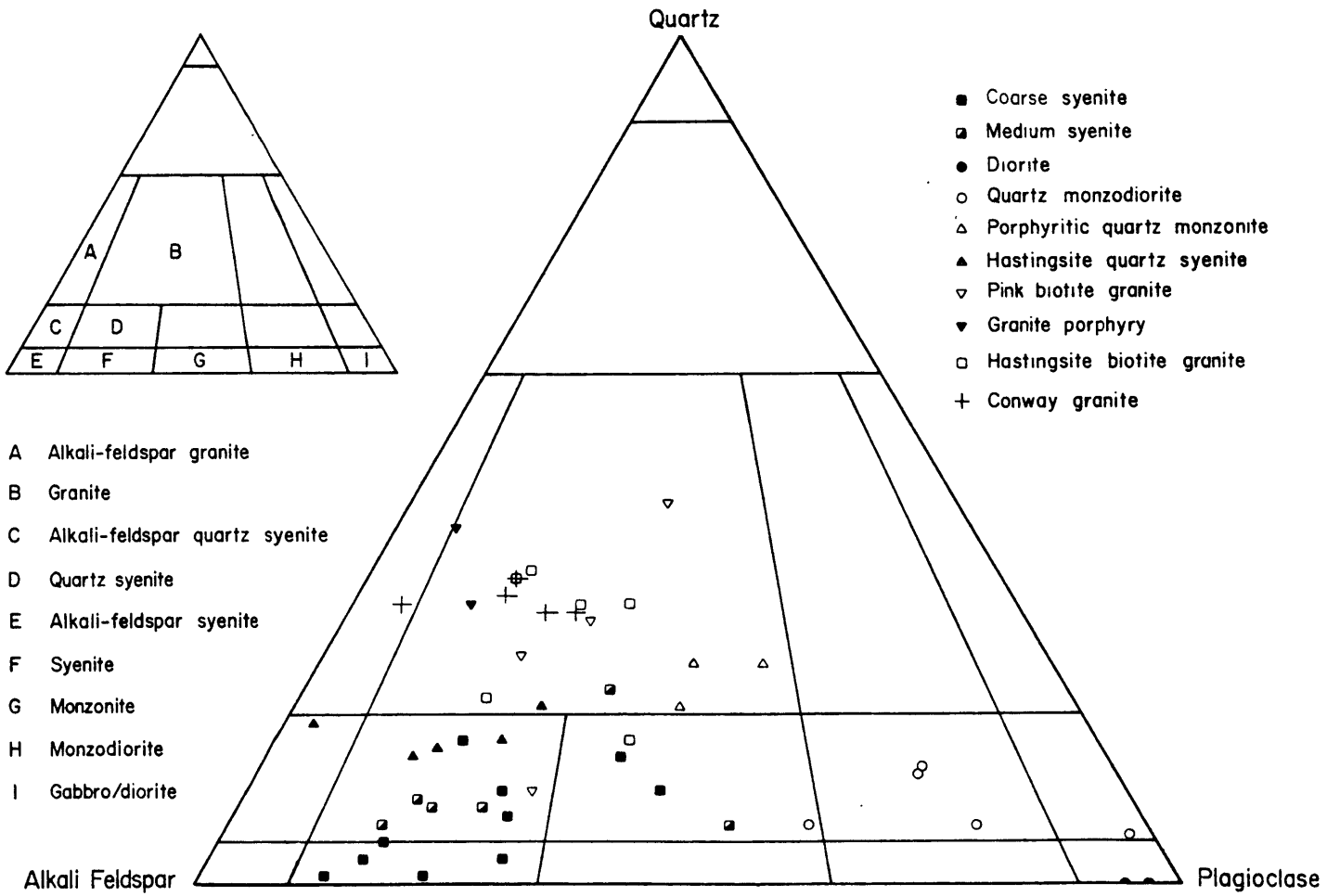

Figure 5

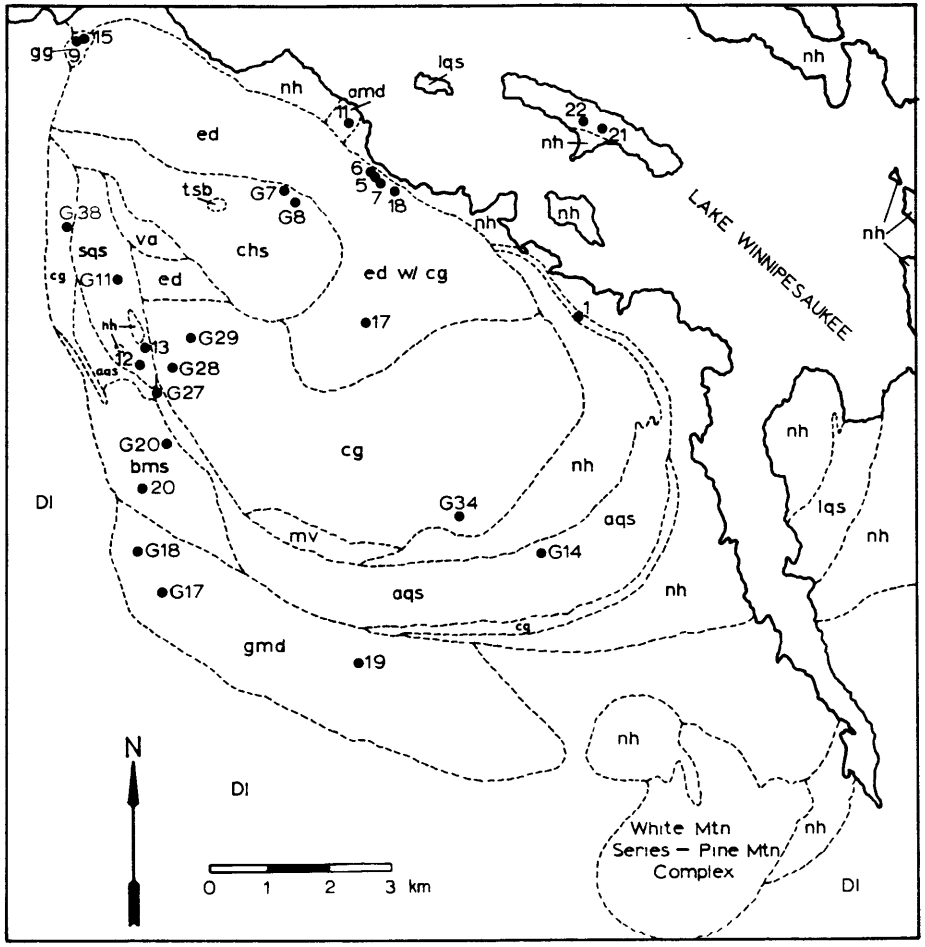

GEOLOGIC MAP OF THE BELKNAP MOUNTAINS, N.H.

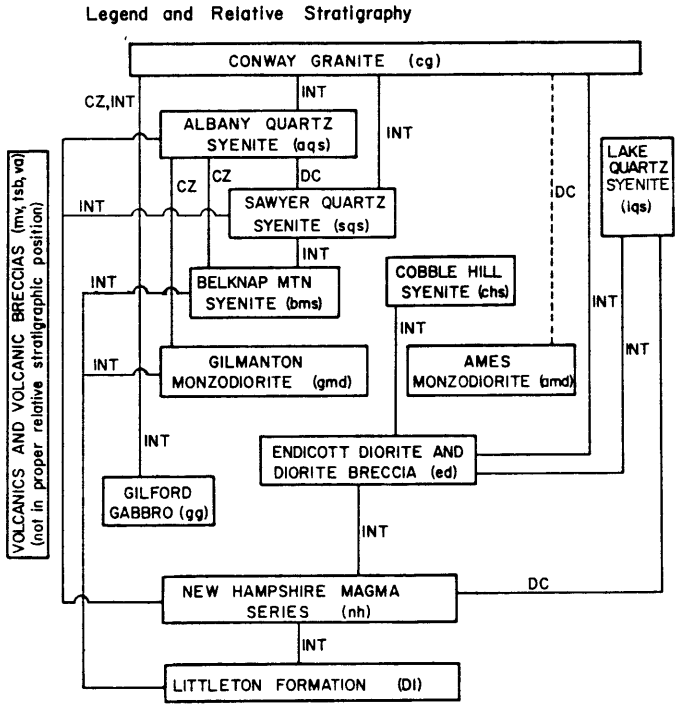

● 12 Sample Location

Geology from Modell (1936) and Bothner and Gaudette (1971)

Figure 6

BELKNAP MOUNTAINS - MODAL DATA

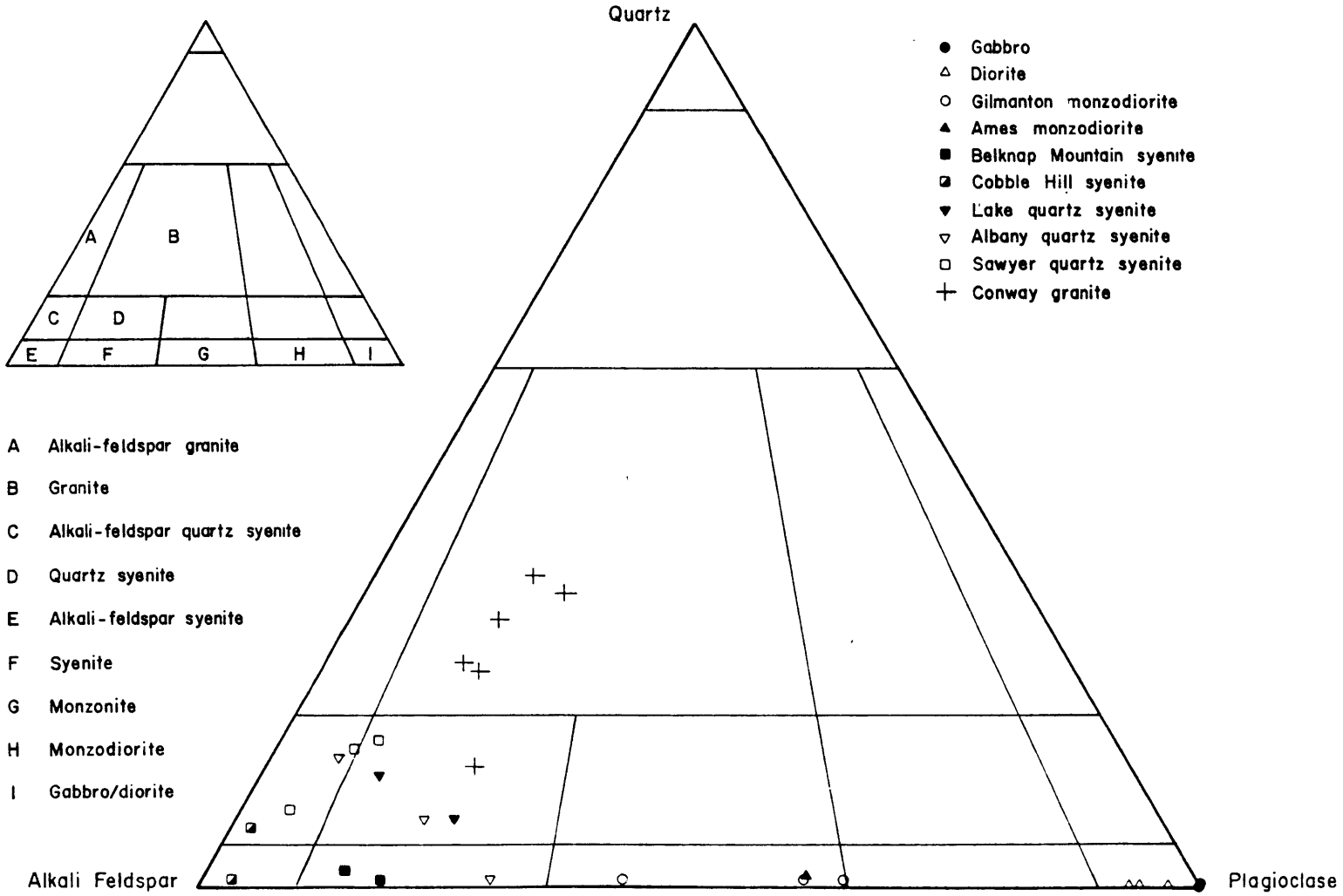

Figure 7

CHAPTER 3. Rb/Sr ISOTOPE SYSTEMATICS OF THE BELKNAP MOUNTAINS COMPLEX

The major distinction between the reaction melting model and the comagmatic model (Figure 2) for the genesis of the White Mountain and similar alkaline complexes is that of a multi-source vs. single source origin for the magmas. Detailed isotopic studies of individual rock units within a complex may allow determination if more than one source was involved in the genesis of the rocks. For example, if reaction melting or a similar process was involved in the evolution of a complex, a series of magmas with different $^{87}Sr/^{86}Sr$ ratios is expected. K/Ar results (Foland and Faul, 1977) on several Belknap rock units indicate that all the magmas in the complex were emplaced within $\sim$5 million years. Therefore, for a reaction melting process, the Sr isotopic data will form a series of parallel whole rock isochrons for each rock with significantly different initial $^{87}Sr/^{86}Sr$. The greater the variation in initial $^{87}Sr/^{86}Sr$ ratio of the various rocks, the easier it will be to distinguish between the two models. In particular, a large variation in initial $^{87}Sr/^{86}Sr$ is expected from an old, differentiated crust which has had time to develop significant variations in $^{87}Sr/^{86}Sr$. Because of the longer, more complex crustal history of the Bronson Hill anticlinorium compared to the Merrimack synclinorium,

the rocks from the Pliny Range may have a larger variation in initial $^{87}Sr/^{86}Sr$ ratio than the Belknap Mountains rocks provided that reaction melting was involved. The Belknap Mountains, however, have a larger compositional range of rock types and were selected for isotopic study.

Several detailed isotopic studies on igneous complexes displaying characteristics similar to the Belknaps have been published. Foland and Henderson (1976) found that both the saturated and undersaturated rocks of the Marangudzi ring dike complex in Rhodesia fell on a single isochron and possessed the same initial $^{87}Sr/^{86}Sr$ ratio (0.7077). They indicated the distinctive chemistry of the rocks could be produced by fractional crystallization of a single magma. In contrast, Hedge and Barker (1975) report that the Pikes Peak batholith (Barker et al., 1975) represents a nearly ideal example of reaction melting with considerable variation in initial Sr isotope ratio. Gabbro and anorthosite have low initial ratios of 0.7044; syenites and quartz syenites range from 0.7052 to 0.7063; and granite from 0.7063 to 0.7117.

Van Breeman et al. (1975) studied a group of syenites and granites from ring dike complexes in central Nigeria and also found considerable variation in initial $^{87}Sr/^{86}Sr$. They considered that the variation in initial Sr ratio was due to crustal enrichment processes, but did not elaborate other than to point out the similarity in initial ratio of the late peraluminous biotite granites to the ca. 600 m.y.

Pan-African granites in the area. In addition, they found extremely high values of $^{87}Sr/^{86}Sr)_o$ in granites which had undergone metasomatic alteration (albitisation).

In a study of the Kangerdlugssuag alkaline complex in East Greenland, Pankhurst et al. (1976) found differences in initial ratio between the over- and under-saturated rocks. They concluded, on the basis of combined oxygen and strontium isotope data, that the $^{87}Sr/^{86}Sr$ ratio of the parental magma for the complex was modified through interaction with meteoric water that had equilibrated with the surrounding Precambrian country rocks. This produced an initial decrease in δO^{18} plus a minor increment in $^{87}Sr/^{86}Sr$ (both at magmatic temperatures) in the inner undersaturated syenites, but the interaction of water with outer quartz normative syenites at post-magmatic temperatures produced increases in both δO^{18} and $^{87}Sr/^{86}Sr$ in these rocks.

Taylor (1974, 1978) has found numerous examples of large scale depletion of O^{18} in igneous complexes due to post-magmatic interaction of meteoric water with the rocks. The effects on other isotope systematics (such as Sr and Pb) are not known, but the interpretation by Moorbath and Bell (1965) and Moorbath and Welke (1969) that late granitic rocks at the Isle of Skye were not related to earlier basalts by simple fractional crystallization because of a significant crustal component in their Pb and Sr has been complicated by oxygen isotope studies by Forester and Taylor (1977). They showed that the plutonic rocks of Skye

have undergone massive exchange of oxygen isotopes with meteoric water.

Finally, Foland and Friedman (1977) examined Sr and O isotope relations in the White Mountain complex at Red Hill. They found uniform and low initial $^{87}Sr/^{86}Sr$ ratios in the syenites, but higher and variable values for $^{87}Sr/^{86}Sr)_o$ in later nepheline-sodalite syenite and interior granite. An increase in δO^{18} correlates with the increase in $^{87}Sr/^{86}Sr)_o$ and apparently occurred at magmatic temperatures. They concluded that the isotope variations, and probably the distinctive oversaturated-undersaturated nature of the complex, were due to crustal contamination.

If one thing is clear from all these studies, it is the extreme variability of the isotope relations in the complexes that have been studied in detail. Variations range from rather simple systematics in comagmatic suites (Marangudzi, Foland and Henderson, 1976) to classic cases of development through progressive reaction melting (Pikes Peak, Hedge and Barker, 1975). The isotopic relations may be further complicated by Sr and O exchange with groundwater at both the magmatic and post-magmatic stage. Thus, if a multi-source model is indicated by the isotope systematics (excluding the possibility of post-magmatic effects on Sr isotope ratios) it may not be possible to uniquely identify the characteristics or degree of involvement of crustal material(s) because of the number of variables that enter into such a mixing relation. However, one of the most

important constraints that Sr isotope studies can provide is identification of units in a complex that may be related by simple fractional crystallization. Even in the reaction melting model, fractional crystallization will almost certainly have important effects on magma composition; therefore, isochron relations between rock units will identify rocks that may be related by fractional crystallization.

Details of the analytical procedure used for isotope dilution analysis of Rb and Sr and Sr isotopic analysis are given in Appendix II. Precision of the $^{87}Rb/^{86}Sr$ ratio and $^{87}Sr/^{86}Sr$ ratio (based on duplicate analyses) is 1.0% and 0.02%, respectively. $^{87}Sr/^{86}Sr$ ratios have been normalized to a value of 0.7080 for the Eimer and Armand Standard $SrCO_3$. Determinations of this ratio made throughout the isotope analyses gave an average value of 0.70765 ±.00011 (2σ standard deviation of six determinations). Table 2 lists the results of analyses on whole rocks and minerals.

In Figure 8 all the whole rock Rb/Sr isotope data are plotted. The data are very linear at high $^{87}Rb/^{86}Sr$, but there is considerable scatter at low values of Rb/Sr. A regression of all the Belknap Mountains' whole rock data does not yield an isochron relation because of the scatter greatly in excess of experimental error at low Rb/Sr. However, a regression of the data obtained from the gabbro, diorite, Belknap Mountain and Cobble Hill syenites, Sawyer

TABLE 2. BELKNAP MTNS RB/SR WHOLE ROCK ISOTOPE DATA

Rock Type/Sample No.	ppm Rb	ppm Sr	μmoles Rb^{87} [a]	μmoles Sr^{86} [a]	Rb^{87}/Sr^{86}	Sr^{87}/Sr^{86} [b]
Gabbro/ 15	12.4	788.	0.04033	0.88802	0.045416	0.70368±7
9	14.5	831.	0.04728	0.93540	0.050545	0.70355±6
Diorite/17	83.6	966.	0.27200	1.08720	0.25018	0.70415±6
18	109.	789.	0.35412	0.88781	0.39887	0.70420±7
5	132.	818.	0.43101	0.98856	0.43600	0.70461±6
Belknap Mtn. Syenite/20	147.	276.	0.47695	0.31040	1.53657	0.70738±9
Cobble Hill Syenite/G7	153.	35.	0.49644	0.03953	12.5586	0.73239±9
G8	193.	23.5	0.62883	0.02628	23.9281	0.76031±23
Sawyer Quartz Syenite/13	187.	35.	0.60861	0.03977	15.3032	0.74016±5
12	224.	33.	0.72959	0.03682	19.8150	0.75152±9
Conway Granite/ 7	189.	116.	0.61563	0.12996	4.73707	0.71489±15
G34	181.	102.	0.59080	0.11462	5.15442	0.71528±10
G29	255.	65.	0.83142	0.07372	11.2781	0.72943±10
G28	194.	43.	0.63247	0.04871	12.9844	0.73450±11

TABLE 2. (continued)

Rock Type/Sample No.	ppm Rb	ppm Sr	μmoles Rb^{87}[a]	μmoles Sr^{86}[a]	Rb^{87}/Sr^{86}	Sr^{87}/Sr^{86}[b]
Gilmanton Monzodiorite/G18	126.	727.	0.40983	0.81819	0.50090	0.70554±7
G17	112.	549.	0.36533	0.61850	0.59067	0.70518±10
19	124.	455.	0.40370	0.51209	0.78834	0.70619±6
Ames Monzodiorite/11	136.	419.	0.44206	0.47160	0.93736	0.70619±6
Albany Quartz Syenite/G14	147.	273.	0.47812	0.30771	1.55380	0.70780±6
G27	151.	203.	0.49079	0.22838	2.14901	0.70898±11
1	137.	79.	0.44564	0.08872	5.02299	0.71604±5
Lake Quartz Syenite/22	139.	366.	0.45169	0.41198	1.09639	0.70754±9
21	193.	204.	0.62692	0.23000	2.72572	0.71037±10

[a] Constants used: Rb85/Rb87 = 2.5907; Sr84/Sr88 = 0.006695; Sr86/Sr88 = 0.11940.

[b] Normalized to Sr86/Sr88 = 0.11940 during run. Uncertainties in last digit(s) represent 2 sigma deviation from the mean obtained during run.

quartz syenite, and Conway granite yields a line which is consistent with a single age and initial ratio. This is the solid regression line plotted in Figure 8. Table 3 gives the results of this and other regressions. In order to verify the similar age and initial ratio of the basic and felsic units, the gabbro plus diorite, and the syenites, Sawyer quartz syenite, and granite were regressed as independent data sets. As the results in Table 3 show, the age and initial ratios are identical within the uncertainties given.

The remaining data points shown in Figure 8 plot significantly above the regression line shown. Figure 9 is an enlargement of the area of Figure 8 with $^{87}Rb/^{86}Sr < 6.0$. Three lines are shown on the figure. The lower solid line is the regression line from Figure 8. The initial ratio is 0.70349 ±12 (2σ). The other solid line is a regression line obtained from the three Albany quartz syenite samples. The age is identical to the age of the lower line. However, the initial ratio of 0.70397 ±38 (2σ) overlaps the possible values of $^{87}Sr/^{86}Sr)_o$ for the lower line at the 95% confidence level, but it is significantly different at the 90% confidence level.

The third, dashed, line is not an isochron, but a line of slope ∿168 m.y. drawn through two of the three Gilmanton monzodiorite data points. The three whole rock samples of Gilmanton do not yield an isochron, but the significantly higher present day values of $^{87}Sr/^{86}Sr$ strongly suggest a

TABLE 3. REGRESSION PARAMETERS FOR

BELKNAP MOUNTAINS COMPLEX WHOLE ROCK Rb/Sr DATA.

Regression based on method of York (1969) as discussed by Brooks et al. (1972). Uncertainties given at the 2σ (95%) confidence level. $\lambda = 1.42 \times 10^{-11}$/yr.

Unit(s)	No. Samples	Age (m.y.)	Initial $^{87}Sr/^{86}Sr$	Σx^2 [a]
All whole rock data	23	164.9 ±4.2	0.70388 ±24	2.85
Gabbro, diorite, Belknap Mtn. syenite, Cobble Hill syenite, Sawyer quartz syenite, Conway granite	14	166.3 ±1.6	0.70349 ±12	1.65
Gabbro, diorite	5	154. ±54	0.70352 ±22	1.10
Belknap Mtn. syenite, Cobble Hill syenite, Sawyer quartz syenite, Conway granite	9	166.1 ±2.0	0.70356 ±26	2.02
Albany quartz syenite	3	168.5 ±9.2	0.70397 ±38	1.19
Ames monzodiorite (whole rock plus minerals)	4	146.6 ±3.0	0.70426 ±18	0.26

[a] The Σx^2 may be used as an index to discriminate between an isochron and an errorchron (Brooks et al., 1972). A value of ∿2.0 has been adopted as a cut-off. Values of Σx^2 greater than ∿2.0 indicate scatter about the regression line in excess of that expected from a consideration of experimental error, while values less than ∿2.0 indicate there is no scatter in excess of that associated with the analyses.

higher initial Sr isotope ratio at the time of emplacement. Since geologic relations indicate the Gilmanton is younger than the diorite but older than the Albany quartz syenite and Conway granite, it must have been emplaced ca. 168 m.y. The lack of an isochron relation for the Gilmanton whole rock samples does not allow precise definition of the initial ratio, but the data indicate an initial ratio higher than that obtained from the lower regression line in Figure 9. The cause of the scatter among the Gilmanton samples will be discussed later when the effect of whole rock weathering on Rb/Sr isotope systematics is considered.

The remaining whole rock data for the Ames monzodiorite and Lake quartz syenite are insufficient to draw any definite conclusions about their initial ratios. However, their $^{87}Sr/^{86}Sr$ values fall significantly above the lower isochron in Figure 9, indicating the possibility of higher $^{87}Sr/^{86}Sr)_o$.

Even though the regression line shown in Figure 8 may be considered an isochron (footnote, Table 3), several points lie off the line by greater than the 2σ experimental error in Rb/Sr or $^{87}Sr/^{86}Sr$ ratio. Samples 5 (diorite), G7 (Cobble Hill syenite), G29 and G34 (Conway granite) fall below the line, and samples 20 (Belknap Mountain syenite), 12 and 13 (Sawyer quartz syenite) fall above the line. Studies of the effect of weathering on whole rock Rb/Sr ages (Bottino and Fullagar, 1968; Blaxton, 1974; Fullagar and Ragland, 1975) have shown that incipient chemical weathering tends to lower the age of the whole rock slightly, either by

preferential loss of radiogenic ^{87}Sr from the Rb site or by an increase in Rb/Sr ratio through clay mineralization. In this case a regression line for an array of slightly weathered whole rocks may provide a reasonably good fit, but with some scatter of data points to either side of the line. The points on the low side of the line are samples which have undergone a change in either Rb/Sr or $^{87}Sr/^{86}Sr$, while points to the high side of the line represent essentially unaltered samples. Since no weathering process has been suggested for granitic rocks that would move a point up and/or to the left of an isochron, a regression of whole rock samples from the gabbro, diorite, syenites, Sawyer quartz syenite, and granite was made excluding those points which fell significantly below the best fit line of Figure 8. This line has been termed the "high" regression line or the "high" line. Table 4 compares the two regressions. The age of the "high" line is increased slightly to 168.3 m.y., but it is not significantly different from the earlier value of 166.3 m.y. at the 2σ confidence level. Similarly, the initial ratio is identical within uncertainties - 0.70356 ±12 vs. 0.70349 ±12. However, the Σx^2 for the "high" line is significantly lower than the value for a regression including the points falling below the regression line in Figure 8. Also, all of the points fall within experimental error of the regression line. Therefore, exclusion of samples which are assumed to have undergone incipient chemical weathering has produced a much better fit to a regression line. No obvious petrographic

TABLE 4. COMPARISON OF REGRESSION PARAMETERS FOR "HIGH" REGRESSION LINE VS. ALL SAMPLES FROM GRABBRO, DIORITE, SYENITES, SAWYER QUARTZ SYENITE, AND GRANITE.

Regression method and uncertainties as in Table 3. $\lambda = 1.42 \times 10^{-11}$/yr.

Samples Included in Regression Analysis	Age (m.y.)	Initial $^{87}Sr/^{86}Sr$	Σx^2
Gabbro - 9, 15 Diorite - 5, 17, 18 Belknap Mtn. syenite - 20 Cobble Hill syenite - G7, G8 Conway granite - 7, G28, G29 G34 Sawyer quartz syenite - 12, 13	166.3 ±1.6	0.70349 ±12	1.65
High line - excluding samples 18, G7, G29, G34	168.3 ±1.8	0.70356 ±12	0.70

features differentiate the four samples which fall below the regression line from the remaining samples.

As a check on the suggestion that points which fall below the isochron of Figure 8 have been displaced due to minor chemical weathering, a hornblende separate from one of the low samples (G7, Cobble Hill syenite) was analyzed. The analysis is given in Table 5 with other analyses of mineral separates. It is concordant with the "high" regression line, and this result lends support to the idea that the points below the isochron contain weathered alkali feldspar and biotite.

Mineral separates from sample G28 (Conway granite) were also analyzed. The alkali feldspar falls on the "high" line, and the hornblende lies slightly above (but within experimental error for the $^{87}Rb/^{86}Sr$ ratio). This is to be expected because sample G28 was considered an unweathered sample in the determination of the "high" line. The spread in Rb/Sr ratio is not sufficient to yield a whole rock-mineral isochron with low enough uncertainty in initial ratio to be meaningful.

As mentioned earlier, whole rock samples of the Gilmanton monzodiorite do not define an isochron. A reasonable explanation is weathering of sample G17 which causes it to fall significantly below the other two rocks (Figure 9). Hornblende, biotite, and feldspar separates were picked from sample G18 in order to generate a whole rock-mineral isochron. Results of the analyses are listed

TABLE 5. BELKNAP MTNS. RB/SR MINERAL ISOTOPE DATA

Sample No./Mineral Type[a]	ppm Rb	ppm Sr	μmoles Rb^{87}[b]	μmoles Sr^{86}[b]	Rb^{87}/Sr^{86}	Sr^{87}/Sr^{86}[c]
15 (H)	3.6	412.	0.01171	0.46345	0.25267	0.70398 ±14
G7 (H)	28.2	11.1	0.09192	0.01242	7.40097	0.72113 ±18
G28 (H)	157.	26.6	0.51014	0.02982	17.1073	0.74487 ±8
G28 (F)	266.	47.6	0.86545	0.05339	16.2100	0.74240 ±12
11 (H)	20.2	23.9	0.06565	0.02693	2.43780	0.70932 ±15
11 (F)	144.	461.	0.47000	0.51875	0.90602	0.70614 ±31
11 (B)	651.	8.2	2.12007	0.00877	241.74	1.20792 ±84
G18 (H1)	12.1	46.8	0.03944	0.05269	0.74853	0.70579 ±17
G18 (H2)	44.6	50.4	0.14502	0.05671	2.55722	0.70969 ±9
G18 (F1)	269.	798.	0.87499	0.89791	0.97447	0.70640 ±11
G18 (F2)	212.	571.	0.69033	0.64279	1.07366	0.70606 ±6
G18 (B)	811.	24.0	2.63848	0.02670	98.82	0.82897 ±10

[a] H = hornblende; F = feldspar; B = biotite.

[b] Constants used, as in Table 1.

[c] Ratio and uncertainty as in Table 1.

in Table 5 and all the Gilmanton whole rock and mineral data are plotted in Figure 10. From Figure 10 it is obvious no isochron relation was obtained for the G18 whole rock and minerals. That weathering is involved is clear from the model age of the biotite separate. With any reasonable initial ratio an age of ∿90 m.y. is obtained. This low age is due to massive loss of radiogenic ^{87}Sr during weathering. Similar low ages for biotites from weathered rocks are reported by Goldich and Gast (1966). Other mineral separates also yield low model ages (assuming 0.7043 as $^{87}Sr/^{86}Sr)_o$, ranging from ∿125 m.y. (G18 (F2)) to ∿150 m.y. (G18 (F1)). If all the minerals analyzed from sample G18 fall below the whole rock data point, mass balance demands some phase with low Rb/Sr which has a higher $^{87}Sr/^{86}Sr$ ratio (most likely pure plagiocalse). Thus, the whole rock model $^{87}Sr/^{86}Sr)_o$ at 168 m.y. must be considered a minimum initial ratio for the rock. Several facts may explain why the Gilmanton monzodiorite whole rocks and minerals give such scattered results. Despite a large map area (Figure 6) the Gilmanton is not well exposed. No roads (and no roadcuts of fresh material) penetrate the map area. The relatively coarse grain size and mildly cataclastic nature (see Appendix I, Petrography) may have contributed to the weathering.

Mineral separates (feldspar, hornblende, biotite) from the Ames monzodiorite (sample 11) were also analyzed. The results are given in Table 5 and plotted in Figure 11.

The four points fall on a regression line with no scatter outside of experimental error. The age obtained from the line is ∿147 m.y. and the initial ratio is 0.70436 ±18 (2σ).

The age of ∿147 m.y. is geologically unreasonable since the Ames is truncated by the Conway granite. This is another case of weathering producing a low age. In this example the minerals and whole rock appear to define a valid isochron, but considering the variability in mineral separates from the Gilmanton, no significance can be attached to the age. Since mass balance for the Ames demands a low Rb/Sr phase (plagioclase) to make up for the large contribution of the biotite (∿7 modal %) to the whole rock Rb/Sr, the initial ratio of 0.7042-0.7043 may be a more reasonable value for $^{87}Sr/^{86}Sr)_o$ than the model initial ratio calculated from the whole rock assuming an age of 168 m.y. (0.70395).

The whole rock Rb/Sr age of 168.3 ±1.8 m.y. obtained from the "high" regression line, and the age obtained from the Albany quartz syenite samples are approximately 6% higher than published K/Ar ages for units in the Belknaps (Foland and Faul, 1977). The K/Ar ages most likely represent cooling ages; the Rb/Sr age the actual age of emplacement. While some White Mountain complexes have concordant K/Ar and Rb/Sr ages (i.e., Red Hill; Foland and Friedman, 1977), others have significant time periods between intrusion and cooling below the K/Ar blocking temperature (Mad River; Foland and Faul, 1977).

Figure 12 shows model initial $^{87}Sr/^{86}Sr$ calculated for all the whole rock samples and selected mineral separates (separates from samples 15, G7, G28). The age used in the calculation was 168.3 m.y., the age from the "high" regression line. Geologic relations constrain all the units to have ages close to this value. The only exception is the Lake quartz syenite, which is not constrained on the young side. However, there is no reason to believe that the Lake quartz syenite (if it is related to the Belknap complex) was not emplaced prior to the late Conway granite. The larger uncertainty in calculated initial ratios for the felsic units is due to the 1% uncertainty in $^{87}Rb/^{86}Sr$ ratio. This uncertainty has little effect at $^{87}Rb/^{86}Sr$ less than $\sim$1.5, where the uncertainty in $^{87}Sr/^{86}Sr$ dominates. The initial ratios of the gabbro and diorite are very well constrained at $\sim$0.7035. The lower dashed line represents the initial ratio of 0.70356 obtained from the "high" regression line. The scatter of syenitic and granitic points below this line is due to weathering. Note that the hornblende from sample G7 (Cobble Hill syenite) falls right next to the regression initial ratio. Initial $^{87}Sr/^{86}Sr$ values of the felsic units near the low regression line show more scatter, but from a consideration of the regression results they are considered to be the same as the gabbro and diorite values within the uncertainty of the data.

The Albany quartz syenite, however, has a significantly higher $^{87}Sr/^{86}Sr)_o$ of $\sim$0.7040. This is indicated by the

regression of the three Albany samples (Table 3) and the model initial ratios. Also, the initial ratio of the Gilmanton monzodiorite shown by the upper dashed line at 0.7043 must be considered a minimum initial ratio that has been lowered by weathering effects. In addition, the Ames monzodiorite and Lake quartz syenite units have model initial ratios higher than that of the gabbro and diorite. As discussed for the Ames, the regression ratio (shown by a box in Figure 12) may more closely approach the actual initial ratio. The two Lake quartz syenite samples have considerably different initial ratios. Without additional analyses for the Ames monzodiorite and Lake quartz syenite, it is not possible to say much more than that there is evidence for suspecting a higher initial ratio in these units.

Conclusions based on the isotopic data regarding the sources involved in the genesis of the Belknap magmas must take into account factors such as the small spread in observed initial ratios (0.7035 to 0.7045), the lack of data at low Rb/Sr to tie down the initial ratios of the felsic units, and the problem of weathering in the Gilmanton monzodiorite. In addition, implicit in a discussion of the data up to this point has been the assumption that the only process affecting the Rb/Sr isotope systematics subsequent to the emplacement of the magmas has been weathering. The possibility of post-magmatic Sr isotope exchange with meteoric water has not been considered because of the

inability to determine whether any interaction with ground-water took place (i.e., no oxygen isotope data). The position of the Gilmanton on the outer margin of the complex with a large area in contact with the surrounding Littleton Formation makes it (along with the Lake quartz syenite) one of the better candidates for such an exchange process. (Forester and Taylor, 1976, show an increase in oxygen exchange at the margins of the Skye complex.) Thus, the lack of an isochron relation between the Gilmanton whole rock samples and whole rock G18 and its minerals could be due to variable degrees of Sr exchange in the whole rocks and minerals, coupled with weathering (as in G18-biotite). In this case sample G17 may represent the closest approach to the true Gilmanton initial $^{87}Sr/^{86}Sr)_o$. However, the isochron relation among the basic and felsic units on the regression line in Figure 8 and the isochron defined by the Albany quartz syenite make Sr isotope exchange in these samples unlikely.

With the last few paragraphs' discussion as a background, the following conclusions are made based on the isotope results:

(A) The gabbro and diorite have low initial ratios in the range 0.70356 ±12. This is similar to the initial ratio of 0.70330 ±16 for the syenites at Red Hill (Foland and Friedman, 1977), but lower than ratios of presumably related lamprophyres in New England (0.7039-0.7053) (McHone et al., 1976). These low ratios indicate a mantle

derivation for the basic rocks in the Belknaps. The initial ratios are higher than present day mid-ocean ridge values, but lower than many oceanic island basalts (Hofmann and Hart, 1978). Thus the mantle source has probably been depleted in Rb and other large ion lithophile elements relative to the source of some oceanic island basalts, but not to the degree of present day sources of mid-ocean ridge basalts.

(B) The Albany quartz syenite, and possibly the Gilmanton monzodiorite, Ames monzodiorite, and Lake quartz syenite (discounting post-magmatic Sr isotope exchange) possess higher initial ratios in the range 0.7040-0.7045. These ratios are consistent with:

(1) Partial melting of a crustal source with relatively low $^{87}Sr/^{86}Sr$ at 168 m.y. ($\sim$0.7040); this would imply either a short residence time in the crust for this crustal source, a low Rb/Sr ratio, or both;

(2) An admixture of mantle Sr with $^{87}Sr/^{86}Sr$ $\sim$0.7035, with crustal strontium of undefined but higher $^{87}Sr/^{86}Sr$.

(C) The low initial ratio for the sequence syenites, Sawyer quartz syenite, granite is consistent with an origin for these units by fractional crystallization of the basic (dioritic) material. This possibility is treated in the sections dealing with major and trace element geochemistry. In terms of a multi-source model, the low initial ratio of the felsic suite, essentially identical to that of the basic

rocks, places severe constraints on any material involved in its genesis. One possibility is to remelt the products of earlier White Mountain igneous activity. This would satisfy the constraint of $^{87}Sr/^{86}Sr)_o$ identical to the basic Belknap rocks. This alternative is also discussed in the sections on major and trace element geochemistry.

(D) If the Gilmanton has undergone Sr isotope exchange with meteoric water subsequent to its emplacement, the monzodiorite may also have a low initial ratio and be part of a comagmatic suite. Because of this possibility the major and trace element geochemistry of the Gilmanton is also evaluated in terms of the comagmatic model in the chapters dealing with the geochemistry.

Figure Captions

Figure 8. Rb-Sr whole rock data for the Belknap Mountains complex. Solid regression line (166.3 ±1.6 m.y. $^{87}Sr/^{86}Sr)_o$ = 0.70349 ±12) based on data from underlined units. Dashed line is a line of similar age drawn through two of the three Gilmanton monzodiorite data points.

Figure 9. Rb-Sr whole rock data for Belknap Mountains complex samples with $^{87}Rb/^{86}Sr < 6.0$. Lower solid regression line is from Figure 8; upper solid regression line based on three Albany quartz syenite samples; dashed line is line of slope ∿168 m.y. drawn through two of the three Gilmanton monzodiorite samples (see text).

Figure 10. Rb-Sr whole rock and mineral data for the Gilmanton monzodiorite. Solid regression line is from Figure 8. 168 m.y. line with $^{87}Sr/^{86}Sr)_o \simeq 0.7043$ drawn through two of the Gilmanton monzodiorite whole rock points for comparison with solid regression line. ∿90 m.y. dashed line drawn through G18 (biotite) calculated assuming $^{87}Sr/^{86}Sr)_o \simeq 0.7043$ (see text).

Figure 11. Rb-Sr whole rock and mineral data for the Ames monzodiorite. Solid regression line from Figure 8. Dashed line is a regression line based on four Ames monzodiorite whole rock and mineral data points (see text).

Figure 12. Model $^{87}Sr/^{86}Sr)_o$ for whole rocks and selected minerals from the Belknap Mountains complex. Initial ratio calculated assuming an age of 168 m.y. Vertical bars represent 2σ uncertainty in the calculated initial ratio.

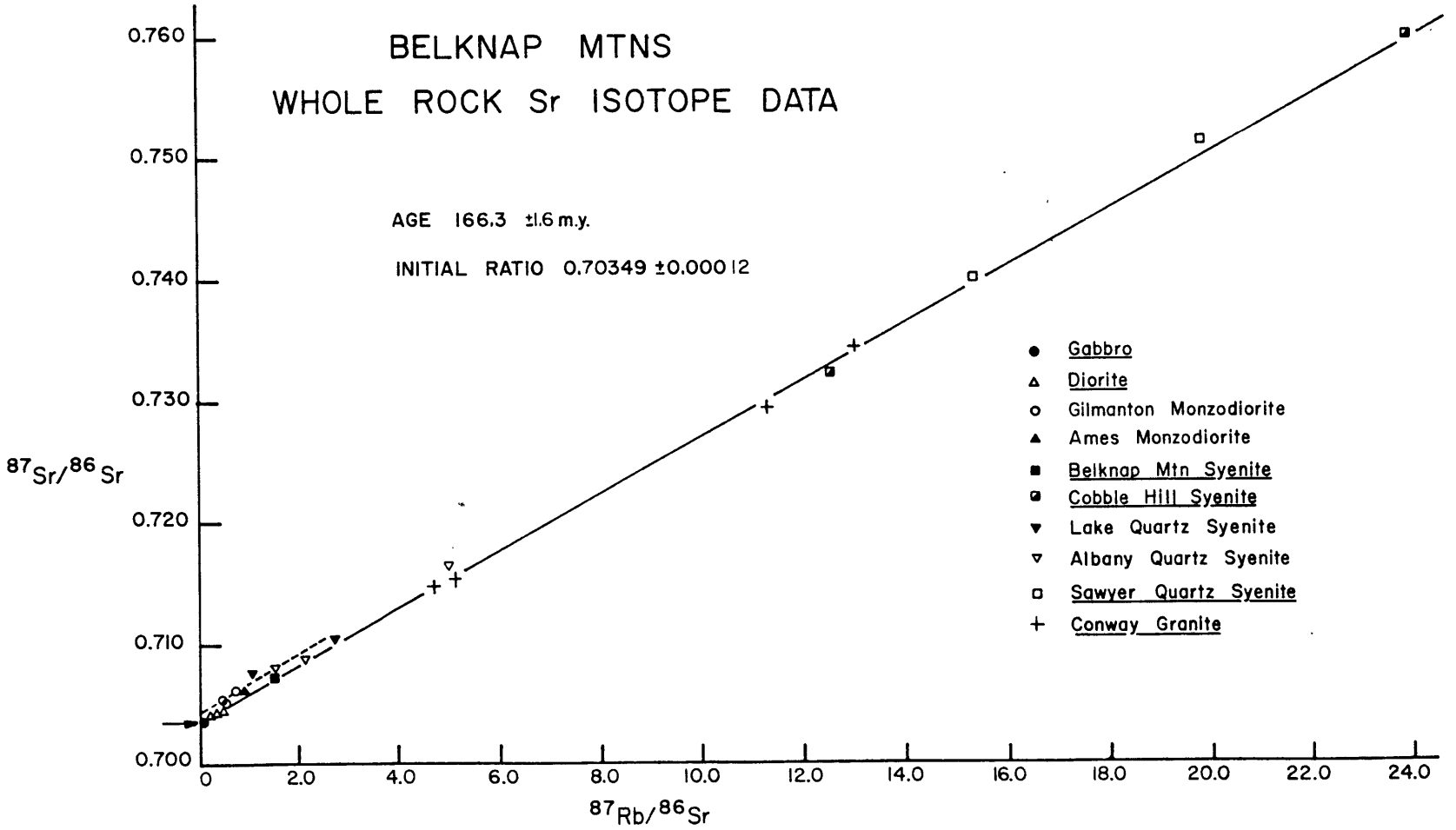
BELKNAP MTNS
WHOLE ROCK Sr ISOTOPE DATA
AGE 166.3 ±1.6 m.y.
INITIAL RATIO 0.70349 ±0.00012
Gabbro
Diorite
Gilmanton Monzodiorite
Ames Monzodiorite
Belknap Mtn Syenite
Cobble Hill Syenite
Lake Quartz Syenite
Albany Quartz Syenite
Sawyer Quartz Syenite
Conway Granite
0.760
0.750
0.740
0.730
0.720
0.710
0.700
87Sr/86Sr
0
2.0
4.0
6.0
8.0
10.0
12.0
14.0
16.0
18.0
20.0
22.0
24.0
87Rb/86Sr

Figure 8

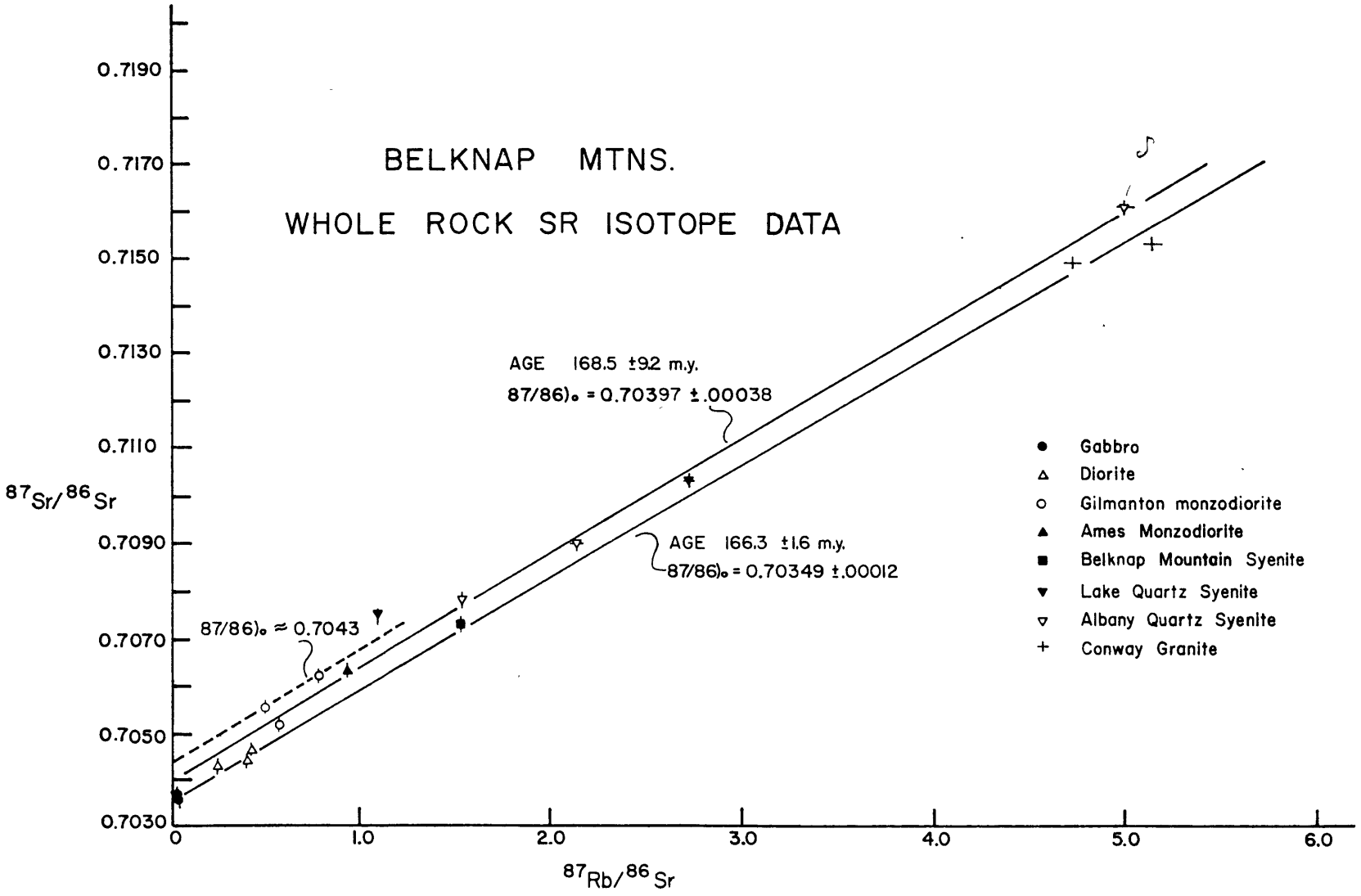
BELKNAP MTNS.
WHOLE ROCK SR ISOTOPE DATA
AGE 168.5 ±92 m.y.
87/86)₀ = 0.70397 ±.00038
AGE 166.3 ±1.6 m.y.
87/86)₀ = 0.70349 ±.00012
87/86)₀ ≈ 0.7043
Gabbro
Diorite
Gilmanton monzodiorite
Ames Monzodiorite
Belknap Mountain Syenite
Lake Quartz Syenite
Albany Quartz Syenite
Conway Granite
0.7190
0.7170
0.7150
0.7130
0.7110
0.7090
0.7070
0.7050
0.7030
87Sr/86Sr
0
1.0
2.0
3.0
4.0
5.0
6.0
87Rb/86Sr

Figure 9

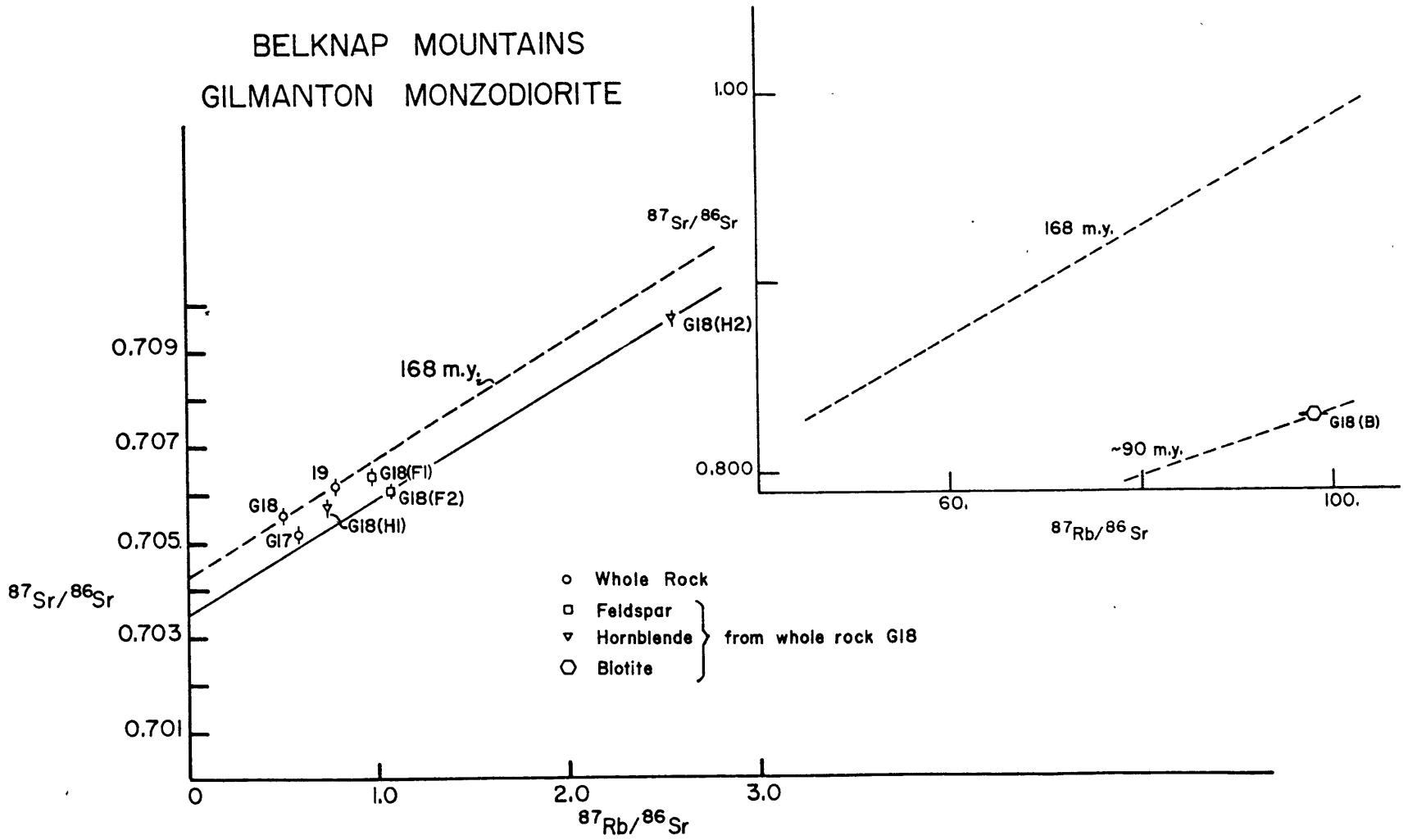
BELKNAP MOUNTAINS
GILMANTON MONZODIORITE
87Sr/86Sr
0.709
0.707
0.705
0.703
0.701
168 m.y.
G18
G17
19
G18(F1)
G18(F2)
G18(H1)
G18(H2)
0
1.0
2.0
3.0
87Rb/86Sr
Whole Rock
Feldspar
Hornblende
Biotite
from whole rock G18
1.00
0.800
168 m.y.
~90 m.y.
G18(B)
60.
100.
87Rb/86Sr

Figure 10

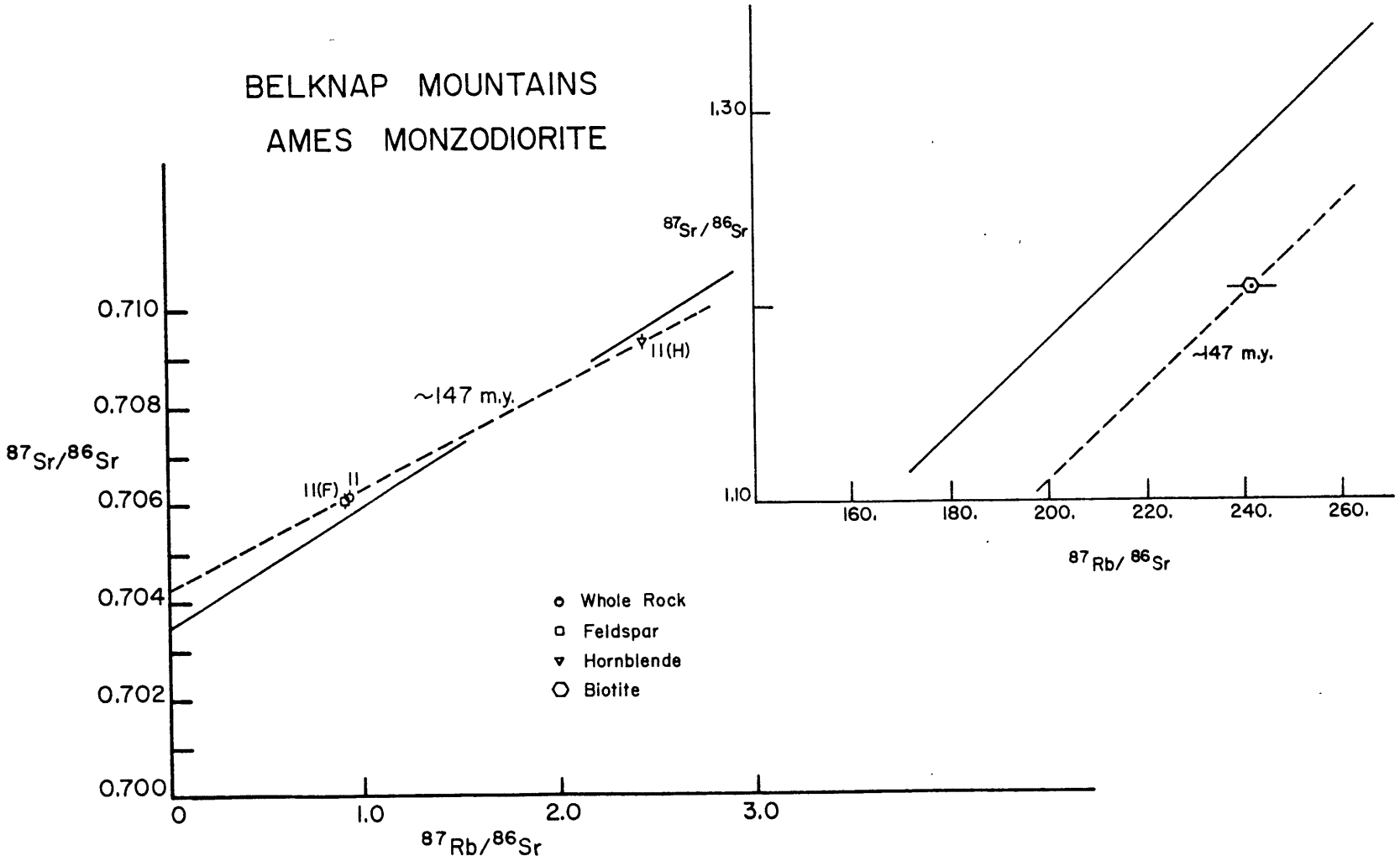
BELKNAP MOUNTAINS
AMES MONZODIORITE
0.710
0.708
0.706
0.704
0.702
0.700
87Sr/86Sr
0
1.0
2.0
3.0
87Rb/86Sr
~147 m.y.
11(F)
11(H)
Whole Rock
Feldspar
Hornblende
Biotite
1.30
1.10
160.
180.
200.
220.
240.
260.
87Rb/86Sr
~147 m.y.

Figure 11

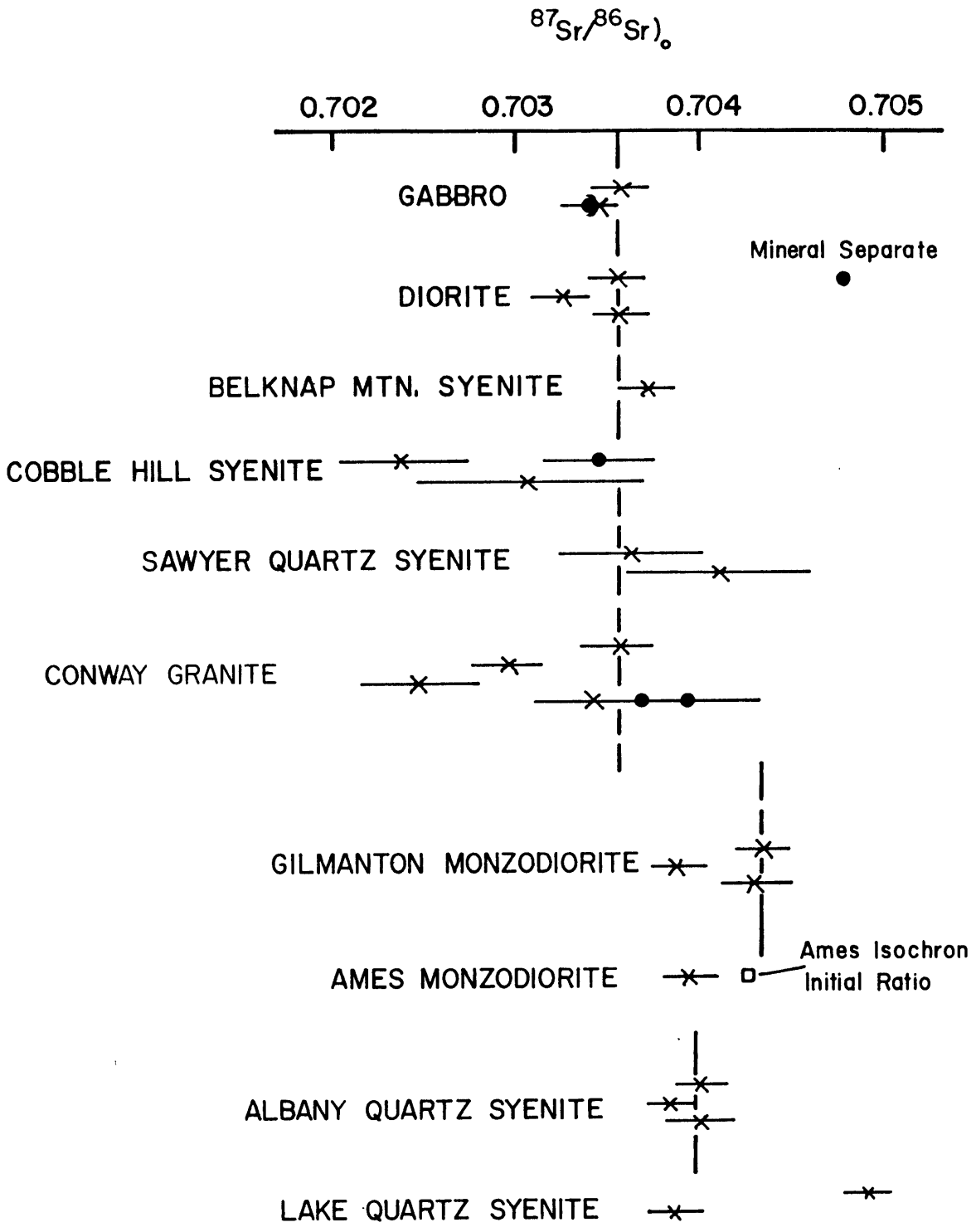
$^{87}Sr/^{86}Sr)_o$
0.702
0.703
0.704
0.705
GABBRO
Mineral Separate
DIORITE
BELKNAP MTN. SYENITE
COBBLE HILL SYENITE
SAWYER QUARTZ SYENITE
CONWAY GRANITE
GILMANTON MONZODIORITE
Ames Isochron Initial Ratio
AMES MONZODIORITE
ALBANY QUARTZ SYENITE
LAKE QUARTZ SYENITE

CHAPTER 4. MAJOR ELEMENT GEOCHEMISTRY

In Chapter 3 isotopic data were used to evaluate whether more than one source was involved in the genesis of the Belknap Mountains magmas. In this and the following chapters major and trace element abundances are used to further evaluate multiple source models. Where multiple sources are indicated by the isotopic data, the geochemical abundance data are used to identify differences in source composition. Barker et al. (1975) note that the composition of crustal rocks involved in the formation of the Pikes Peak batholith played a large role in the end products of reaction melting. The crustal section in the Merrimack synclinorium is not as evolved as that in the Front Range of Colorado, so the compositional trends produced by reaction melting at the base of the New Hampshire crust will be different from those observed at Pikes Peak. The following discussion shows that there is only minor variation in whole rock compositions despite the variation in initial $^{87}Sr/^{86}Sr$ ratios.

Several felsic units were shown to have initial $^{87}Sr/^{86}Sr$ ratios consistent with an origin by fractional crystallization of basic material. Evaluation of the major (and trace) element composition should allow verification of this origin by geochemical modeling. While such modeling has inevitable uncertainties, the existence of viable mechanisms

for derivation of one rock type from another by crystallization processes, combined with the isotope data, provide very strong evidence for a fractional crystallization model. However, absence of geologically and geochemically reasonable mechanisms for such a relationship does not wholly disprove such a link, but indicates that other models consistent with the geologic relations and geochemistry (particularly isotope systematics) should be examined.

The next two chapters present major and trace element data for the Belknap Mountains samples. This is followed by chapters discussing major and trace element geochemical modeling, and finally, a discussion of models for the genesis of the complex consistent with the accumulated data.

Details of the analytical procedure for major elements are given in Appendix II but, in brief, analyses were by X-ray fluorescence on a Phillips ASX automated spectrometer. Fused glass discs were prepared following the procedure of Norrish and Hutton (1969) as modified by Harvey et al. (1973). FeO/Fe_2O_3 (weight ratio), H_2O, and CO_2 data were obtained on separate splits of most samples by analyses performed at the Australian National University by B.W. Chappell. For the remaining samples iron is reported as FeO*, and H_2O and CO_2 are not reported. Major element data and CIPW norms are given in Table 6.

Consideration of the isotope data indicated that the Gilmanton monzodiorite, Ames monzodiorite, Albany quartz syenite, and Lake quartz syenite showed evidence of

TABLE 6. MAJOR ELEMENT ANALYSES AND CIPW NORMS

FOR BELKNAP MOUNTAINS SAMPLES

	Gabbro		Diorite			Gilmanton Monzodiorite			Ames Monzodiorite
	9	15	5	17	18	G17	G18	19	11
SiO_2	37.4	38.6	47.5	51.0	51.9	61.6	60.2	60.3	60.2
TiO_2	7.01	6.46	3.07	2.30	2.24	0.81	0.81	0.97	1.30
Al_2O_3	14.6	14.4	16.7	17.7	17.1	18.0	19.1	17.7	16.2
Fe_2O_3[a]	4.87	--	2.19	--	--	1.50	1.33	--	1.29
FeO	11.3	16.0	8.63	8.62	8.19	2.28	2.34	5.08	4.56
MgO	6.28	6.11	3.80	3.06	2.89	0.93	0.93	1.27	1.75
CaO[b]	13.2	13.5	7.81	5.82	5.95	2.76	3.65	3.06	3.67
Na_2O[b]	1.87	2.01	4.38	4.82	4.62	5.74	5.13	4.82	4.26
K_2O	0.59	0.47	2.34	3.40	3.79	5.22	4.76	5.64	4.88
P_2O_5	0.52	0.32	1.09	1.06	1.26	0.36	0.30	0.30	0.36
H_2O+[c]	1.52	--	0.75	--	--	0.67	0.46	--	0.54
CO_2[c]	0.55	--	0.33	--	--	0.16	0.18	--	0.59
TOTAL	99.71	97.86	98.59	97.78	97.94	100.03	99.19	99.14	99.60

TABLE 6. continued (CIPW Norms)

	Gabbro		Diorite			Gilmanton Monzodiorite			Ames Monzodiorite
	9	15	5	17	18	G17	G18	19	11
Q	--	--	--	--	--	2.02	3.18	2.49	6.21
C	--	--	--	--	--	--	--	--	--
Or	3.52	2.82	14.07	20.51	22.83	30.89	28.41	33.56	29.14
Ab	5.26	6.23	28.65	34.98	35.96	48.63	43.85	41.07	36.42
An	29.84	29.41	19.28	17.02	14.99	7.84	15.21	10.08	10.73
Lc	--	--	--	--	--	--	--	--	--
Ne	5.80	5.97	4.92	3.60	2.11	--	--	--	--
Wo	13.66	15.15	5.39	2.25	2.80	1.47	0.46	1.35	2.21
En	9.44	9.90	2.71	1.10	1.38	2.32	2.34	3.19	4.40
Fs	3.11	4.20	2.57	1.10	1.37	1.61	1.88	2.79	5.12
Fo	4.44	3.90	4.85	4.68	4.17	--	--	--	--
Fa	1.61	1.82	5.07	5.16	4.57	--	--	--	--
Mt	7.13	7.34	3.23	2.64	2.50	2.18	1.95	2.92	1.89
Hm	--	--	--	--	--	--	--	--	--
Il	13.44	12.47	5.94	4.46	4.34	1.54	1.55	1.86	2.49
Ap	1.24	0.77	2.63	2.56	3.04	0.85	0.72	0.72	0.86
Fe/Fe+Mg	0.58	0.60	0.61	0.51	0.61	0.69	0.68	0.69	0.64
Na+K/Al	0.26	0.26	0.59	0.66	0.70	0.83	0.69	0.77	0.76

TABLE 6. continued

	Belknap Mountain Syenite		Cobble Hill Syenite		Lake Quartz Syenite		Sawyer Quartz Syenite		
	G20	20	G7	G8	21	22	G11	12	13
SiO_2	63.3	61.3	64.3	67.4	66.2	61.5	69.3	69.5	66.9
TiO_2	0.47	0.82	0.36	0.26	0.55	1.16	0.28	0.22	0.40
Al_2O_3	18.1	17.4	17.3	16.6	16.1	16.2	15.36	15.6	16.0
Fe_2O_3[a]	1.29	--	1.38	1.26	--	--	1.30	1.05	1.52
FeO	2.17	4.83	2.37	1.46	3.49	5.23	1.19	1.43	2.50
MgO	0.42	0.85	0.39	0.21	0.58	1.55	0.21	0.21	0.25
CaO[b]	1.52	2.11	0.91	0.48	1.56	2.93	0.62	0.59	0.81
Na_2O[b]	5.95	5.31	6.76	6.26	4.74	4.36	5.07	5.37	5.27
K_2O	6.20	5.99	5.72	5.63	5.74	5.03	5.47	5.85	5.86
P_2O_5	0.09	0.32	0.05	0.01	0.14	0.28	n.d.	n.d.	0.02
H_2O+[c]	0.39	--	0.25	0.36	--	--	0.26	0.16	0.43
CO_2[c]	0.21	--	0.35	0.28	--	--	0.25	0.03	0.16
TOTAL	100.11	98.93	100.14	100.21	99.10	98.24	99.31	100.01	100.12

TABLE 6. continued (CIPW Norms)

	Belknap Mountain Syenite		Cobble Hill Syenite		Lake Quartz Syenite		Sawyer Quartz Syenite		
	G20	20	G7	G8	21	22	G11	12	13
Q	0.92	2.02	0.42	7.99	12.53	9.05	17.11	14.12	10.77
C	--	--	--	--	--	--	--	--	--
Or	36.68	35.69	33.87	33.28	34.18	30.20	32.63	34.58	34.65
Ab	50.40	45.30	57.26	52.98	40.42	37.49	43.31	45.45	44.62
An	4.37	6.03	--	0.60	5.61	9.83	3.03	1.05	2.75
Lc	--	--	--	--	--	--	--	--	--
Ne	--	--	--	--	--	--	--	--	--
Wo	1.08	1.01	1.75	0.72	0.53	1.29	0.03	0.79	0.48
En	1.05	2.14	0.97	0.52	1.46	3.92	0.53	0.52	0.62
Fs	2.15	2.58	2.64	1.21	1.57	1.82	0.66	1.40	2.68
Fo	--	--	--	--	--	--	--	--	--
Fa	--	--	--	--	--	--	--	--	--
Mt	1.87	2.92	1.98	1.83	2.32	3.51	1.90	1.52	2.21
Hm	--	--	--	--	--	--	--	--	--
Il	0.89	1.57	0.69	0.49	1.05	2.24	0.54	0.42	0.76
Ap	0.21	0.77	0.12	0.02	0.33	0.67	--	--	0.05
Fe/Fe+Mg	0.84	0.87	0.81	0.76	0.77	0.65	0.86	0.86	0.90
Na+K/Al	0.90	0.88	1.02	0.98	0.86	0.84	0.92	0.88	0.94

TABLE 6. continued

	Albany Quartz Syenite			Conway Granite					
	G14	G27	1	G28	G29	G34	G38	7	6
SiO_2	64.5	66.8	69.5	67.6	73.1	75.1	74.8	75.9	75.3
TiO_2	0.66	0.57	0.27	0.32	0.21	0.21	0.17	0.14	0.19
Al_2O_3	16.8	16.2	14.8	16.4	14.0	13.2	13.2	12.3	13.39
Fe_2O_3[a]	1.06	1.03	0.90	1.11	1.08	0.89	0.63	0.71	1.39
FeO	2.85	2.19	1.69	1.62	0.71	0.62	0.84	0.65	0.49
MgO	0.73	0.55	0.24	0.17	0.17	0.17	0.17	0.10	0.07
CaO[b]	1.96	1.56	1.02	0.82	0.37	0.53	0.48	0.47	0.36
Na_2O[b]	5.23	5.13	4.77	5.74	4.38	3.99	4.48	3.99	3.88
K_2O	5.68	5.57	5.36	6.01	5.49	5.08	5.02	4.66	5.57
P_2O_5	0.18	0.13	0.01	0.02	n.d.	n.d.	n.d.	n.d.	n.d.
H_2O+[c]	0.42	0.40	0.39	0.30	0.31	0.27	0.27	0.22	0.39
CO_2[c]	0.22	0.22	0.38	0.30	0.10	0.27	0.15	0.26	0.02
TOTAL	100.29	100.35	99.33	100.41	99.92	100.33	100.21	99.40	101.05

TABLE 6. continued (CIPW Norms)

	Albany Quartz Syenite			Conway Granite					
	G14	G27	1	G28	G29	G34	G38	7	6
Q	6.71	11.24	18.83	9.13	25.58	30.99	28.13	30.22	33.93
C	--	--	--	--	0.22	0.20	--	0.32	--
Or	33.57	32.88	32.24	35.49	32.49	30.01	29.64	32.58	27.79
Ab	44.26	43.36	41.01	48.53	37.11	33.75	37.87	32.50	34.07
An	5.48	4.78	1.69	1.21	1.84	2.63	1.19	1.77	1.85
Lc	--	--	--	--	--	--	--	--	--
Ne	--	--	--	--	--	--	--	--	--
Wo	1.28	0.88	1.41	1.14	--	--	0.50	--	0.21
En	1.82	1.37	0.61	0.42	0.42	0.42	0.42	0.17	0.25
Fs	3.27	2.23	1.95	1.53	0.07	0.06	0.74	--	0.38
Fo	--	--	--	--	--	--	--	--	--
Fa	--	--	--	--	--	--	--	--	--
Mt	1.54	1.49	1.33	1.61	1.57	1.29	0.91	1.02	1.04
Hm	--	--	--	--	--	--	--	0.67	--
Il	1.25	1.08	0.52	0.61	0.40	0.40	0.32	0.35	0.27
Ap	0.43	0.31	0.02	0.05	--	--	--	--	--
Fe/Fe+Mg	0.75	0.76	0.85	0.90	0.85	0.82	0.82	0.93	0.88
Na+K/Al	0.88	0.88	0.92	0.98	0.94	0.92	0.98	0.92	0.94

TABLE 6. continued

[a] Where Fe_2O_3 not given, total iron reported as FeO.

[b] See Appendix II for details of CaO and Na_2O analysis.

[c] H_2O^+ and CO_2 determined on separate splits by B.W. Chappell at the Australian National University.

n.d. Not detected.

-- Not determined.

significantly higher $^{87}Sr/^{86}Sr)_o$ than units on the lower regression line in Figure 8 (Chapter 3). If the higher model initial ratios are primary (as in the case of the Albany quartz syenite), the source may have produced a characteristic major element composition as well as Sr isotopic composition.

Figures 13 to 19 are variation diagrams for the major oxides plotted against SiO_2. For clarity, fields have been drawn around the plotted points. The most significant feature of the variation diagrams is that for most oxides (except K_2O (not shown) and FeO*), and for whole rock Fe/Fe+Mg (Figure 20) there is a significant difference between felsic units with low initial ratio (Belknap Mtn. syenite; Cobble Hill syenite; Sawyer quartz syenite; Conway granite) and felsic units with higher initial ratios (Lake quartz syenite; Albany quartz syenite). MgO, CaO, and TiO_2, and to a lesser degree P_2O_5 and FeO*, are all higher at a given SiO_2 in the Lake and Albany, while total alkalis, whole rock Fe/Fe+Mg, and, to some extent Al_2O_3, are lower in these units. Thus, the major element composition correlates with the model $^{87}Sr/^{86}Sr)_o$ differences in Figure 12. These major element differences are interpreted as representing a distinct source composition for the Lake quartz syenite and Albany quartz syenite.

While the Gilmanton monzodiorite shows distinct differences from the Belknap Mountain syenite in some cases (CaO, total alkalis, Fe/Fe+Mg), in other cases it is

indistinguishable from the syenite-granite trend (TiO_2, Al_2O_3, FeO*, P_2O_5). The lack of any clear separation between the Gilmanton and felsic units of the lower regression line (Figure 8) suggests the possibility that the monzodiorite is in some way related to these low initial ratio units, as discussed in Chapter 3.

The whole rock Fe/Fe+Mg of the gabbro is considerably higher than would be expected from a trend line connecting the diorite to the felsic rocks (Figure 20). This is due to the unusually high modal ilmenite in the gabbro (Table 19), which has Fe/Fe+Mg of near unity. The high modal ilmenite is also reflected by the unusually high TiO_2 content of the gabbro and the low SiO_2 (Table 6, Figure 13). The mineralogy and composition of the gabbro are consistent with a cumulate of clinopyroxene, calcic plagioclase, and ilmenite (high CaO, high TiO_2, high CaO/Al_2O_3, low SiO_2, Na_2O, and K_2O).

When plotted on a molecular A-F-M diagram (Figure 21) the Belknap Mountains samples follow a broadly calc-alkaline or alkaline trend (see, for instance, Carmichael et al., 1974). They do not display any great iron enrichment. There is also no separation of the units on the lower regression line from the Albany and Lake quartz syenites. Since the gabbro bulk composition does not represent a liquid, its position on the A-F-M diagram does not constitute the extension of a liquid trend. On the basis of clinopyroxene

and hornblende major element compositional data discussed below, the liquid which precipitated the mafic minerals in the gabbro most likely had an Fe/Fe+Mg of ∿0.45, indicating a curve in the trend toward the M apex of the triangle, as is common in igneous suites.

Figures 22 and 23 are plots of normative An-Ab-Or and Q-Or-Ab for Belknap samples with >60 wt.% SiO_2 (more silicic than monzodiorite). For samples that did not have ferrous iron determined independently, the average FeO/Fe_2O_3 weight ratio for the rock unit was used to partition total iron between Fe^{+2} and Fe^{+3} for the norm calculation. In the case of the Lake quartz syenite a ratio of 1.3 was used.

During late stage crystallization the composition of a liquid in equilibrium with quartz and feldspar(s) is approximately controlled by the location of the ternary minimum or eutectic (or two feldspar cotectic) in the simplified granite system Q-Or-Ab-An. Conclusions based on the position of samples on either of the two projections (An-Ab-Or and Q-Or-Ab) are only significant if there is reason to believe the bulk rock composition represents a liquid in equilibrium with quartz and feldspar(s). Position in the Q-Or-Ab diagram may also be controlled by the marked thermal trough connecting the Or-Ab sideline with the ternary minimum (or two feldspar cotectic in the case of the existence of a ternary eutectic (Tuttle and Bowen, 1958)). However, the restriction that the bulk rock represent a liquid composition in equilibrium with the phase(s) in

question still holds if any meaningful conclusions about the conditions of crystallization are to be made. An additional complication is the effect of P_{Total}, P_{H_2O}, and other intensive parameters on the position of the minimum or eutectic. There is considerable variation with both P_{Total} and P_{H_2O} (Tuttle and Bowen, 1958; Luth et al., 1964; Luth, 1969; Winkler, 1974).

Figure 22 is a plot of normative Ab-Or-An normalized to 100%. Also shown are projections of the 1 kb and 2 kb $P_{H_2O} = P_{Total}$ quartz-saturated cotectics in the system Q-Or-Ab-An from James and Hamilton (1969) and data in Winkler (1974). With the restrictions discussed above kept in mind, the only rocks which are likely to represent liquids in equilibrium with quartz plus feldspar are the Conway granite samples. The position of the monzodiorites well toward the Ab-An sideline show the effect of considerable plagioclase crystallization prior to the crystallization of quartz, as is indicated by the petrography. This is also true for sample 22 of the Lake quartz syenite. Petrographic evidence for the remaining samples (except the Conway granite) indicate quartz was a late crystallizing phase, and that the bulk composition of the rock does not represent a liquid in equilibrium with quartz plus two feldspars.

The position of the Conway granite displaced towards the Or apex from the 1 kb $P_{H_2O} = P_{Total}$ cotectic may indicate crystallization at $P_{H_2O} = P_{Total} < 1$ kb. Since the effect

of $P_{H_2O} < P_{Total}$ is to shift the cotectics toward the Or-An sideline (Steiner et al., 1975), the position of the Conway is also consistent with crystallization at 1-2 kb $P_{H_2O} < P_{Total}$. The lack of pegmatites and scarcity of miarolitic features in the Conway granite suggest the latter conditions are more likely.

The two samples of Cobble Hill syenite plot well away from the rest of the Belknap felsic units with a normative anorthite content of essentially zero and a much higher normative Ab. In this respect they are similar to syenites from the Nigerian younger granite province (MacLeod et al., 1971) and some syenitic rocks from the Sabaloka igneous complex in the Sudan (Almond, 1977).

These features are consistent with an origin for the Cobble Hill syenite by accumulation of alkali feldspar. In particular, sample G8 exhibits a texture indicative of alkali feldspar accumulation (Appendix I). Conjugation lines in the system Q-Or-Ab-H_2O (Bowen and Tuttle, 1958) and Q-Or-Ab-An-H_2O (James and Hamilton, 1969) show that alkali feldspar crystallizing from liquids similar to the Sawyer quartz syenite will be higher in normative Ab content than the liquid. The low An content is consistent with James and Hamilton's (1969) observation that alkali feldspar crystallizing from low An liquids contain less An than the liquid. MacLeod et al. (1971) and Toulmin (1960) suggest a similar origin for syenitic rocks in Nigeria and in the Cape Ann, Massachusetts, area. However, as will be

discussed in the next chapter, some trace element data (notably low Sr and Ba) in the Cobble Hill make an origin by accumulation of alkali feldspar difficult to accept.

Figure 23 is a plot of normative Q-Or-Ab for Belknap samples with less than 5% normative An. Liquid compositions with An > 5% are not likely to have their position controlled by minima (eutectics) or thermal valleys in or close to the Q-Or-Ab plane. Also shown are the position of the ternary minima and eutectics for $P_{H_2O} = P_{Total}$ (Tuttle and Bowen, 1968; Luth et al., 1964), the anhydrous ternary minima (Luth, 1969), and projections of piercing points for the quartz-saturated cotectic at 1 kb $P_{H_2O}=P_{Total}$ for various An contents (James and Hamilton, 1969). Along the bottom of the figure the position of the extensions of the thermal valleys connecting the Ab-Or sideline with the minimum or piercing points at 1 kb $P_{H_2O}=P_{Total}$ are shown.

The felsic units fall in the thermal valley corresponding to a normative An content of ∿3% and a crystallization pressure of 1-2 kb at $P_{H_2O} < P_{Total}$. There is no distinction between the units with low initial ratio and the Albany quartz syenite. However, no difference is expected since the bulk composition of a liquid at late stages of crystallization is controlled by the position of minima and thermal valleys in Q-Or-Ab-An, not by the original characteristics of the liquid inherited from the source. Note that the two Cobble Hill syenite samples have significantly higher Ab contents than the felsic units which lie

in the thermal trough.

Analyses of minerals from samples of the gabbro, diorite, Gilmanton monzodiorite, Belknap Mountain syenite, Cobble Hill syenite, Sawyer quartz syenite, and Conway granite were made via electron microprobe. The analyses were performed chiefly to allow quantitative modeling of the major element chemistry by a least squares mixing program, but some features of the mineral compositions are worth mentioning.

Chemical analyses of pyroxenes, amphiboles, and biotites are given in Table 7. Because it was not possible to obtain MnO data due to standard problems, and the Fe^{+3}/Fe^{+2} ratio of the amphiboles and biotites are not known, no attempt has been made to calculate structural formulae. The following discussion is based on the similarity of chemical compositions to Pliny Range mafic phases (Czamanske et al., 1977), and on ratios such as Fe/Fe+Mg which do not depend on structural formula.

A comparison of the Belknap Mountains amphiboles to those from the Pliny Range given in Czamanske et al. (1977) shows the remarkable similarity of the amphiboles in the two complexes. These amphiboles are also similar to the low-Al hastingsites found by Creasy in the North Conway quadrangle (Creasy, 1974). The sole exception to the similarity of Pliny and Belknap amphiboles is the Cobble Hill syenite (G8) amphibole, which has much less Al_2O_3 and CaO and considerably more Na_2O than the other amphiboles.

TABLE 7. COMPOSITIONS OF MAFIC SILICATES FROM BELKNAP MOUNTAIN ROCKS[a]

	Gabbro (9)			Diorite (5)		
	clinopyroxene (4)	green hornblende (4)	brown hornblende (4)	clinopyroxene (2)	hornblende (4)	biotite (2)
SiO_2	52.9	42.2	40.1	51.3	42.0	34.9
TiO_2	0.10	1.93	4.76	0.18	1.66	3.63
Al_2O_3	0.84	10.8	11.8	0.71	9.75	13.4
FeO*	7.93	16.0	13.4	12.4	20.3	22.4
MgO	13.7	11.5	11.9	11.3	9.05	9.89
CaO	23.6	11.9	11.8	22.6	11.4	0.03
Na_2O	0.25	2.19	2.35	0.45	2.25	0.16
K_2O	n.d.	0.98	1.21	0.09	1.24	9.35
	99.32	97.50	97.32	99.03	97.65	93.76

TABLE 7. continued

	Gilmanton Monzodiorite (G18)			Belknap Mountain Syenite (G20)	
	clinopyroxene (1)	hornblende (3)	biotite (2)	hornblende (3)	biotite (2)
SiO_2	51.3	45.7	37.3	45.5	35.7
TiO_2	n.d.	1.57	3.54	1.14	3.89
Al_2O_3	0.22	6.73	12.1	6.13	12.8
FeO*	12.5	18.3	21.8	20.7	23.7
MgO	11.8	11.7	11.5	9.79	9.51
CaO	22.4	10.6	n.d.	10.9	n.d.
Na_2O	0.15	1.93	0.08	1.70	0.16
K_2O	n.d.	0.95	9.11	0.80	9.16
	98.37[b]	97.48	95.43	96.66	94.92

TABLE 7. CONTINUED

	Cobble Hill Syenite (G8)	Sawyer Quartz Syenite (G11)		Conway Granite (7)
	hornblende (4)	hornblende (3)	biotite (2)	biotite (2)
SiO_2	45.6	41.9	36.6	36.6
TiO_2	1.19	1.24	2.84	3.14
Al_2O_3	2.97	6.79	11.3	11.9
FeO*	30.8	27.7	28.9	22.3
MgO	3.09	4.68	6.46	11.3
CaO	7.15	10.1	n.d.	n.d.
Na_2O	3.37	2.34	0.09	0.11
K_2O	0.97	1.13	9.38	8.94
	95.14[c]	95.88	95.57	94.29

[a] Analyses by electron microprobe. Total iron reported as FeO*. Analyses represent the average of several grains in a thin section (number in parenthesis by mineral type), with 6 or more point analyses per grain. Sample number next to rock type.

[b] Low analysis may be due to late stage alteration as clinopyroxenes in G18 occur as cores in hornblende.

[c] Low total probably due to considerable Fe^{3+} in this hornblende.

n.d. Not detected.

In this respect, it is intermediate between calcic amphiboles characteristic of subaluminous and peraluminous granites in similar complexes and the alkali amphiboles of peralkaline granites (cf. MacLeod et al., 1971, for analyses of calcic and alkali amphiboles from the Nigerian ring dike complexes). The Cobble Hill syenite is also the only unit with molar Na+K/Al > 1.0 (sample G7) (Table 6).

The mafic minerals of the Belknaps do differ from those in the Pliny range in that there is a broad correlation between whole rock Fe/Fe+Mg and mineral Fe/Fe+Mg (Figure 24). While the correlation is not perfect, it indicates that the variation of intensive parameters during crystallization of the Belknap magmas was not as extreme as in the Pliny Range (Czamanske et al., 1977, p. 1087). That intensive parameters (i.e., fo_2) had some control over Fe/Fe+Mg of the mafic silicates is seen in the tendency for whole rocks with higher Fe^{+3}/Fe^{+2} ratios to have lower Fe/Fe+Mg minerals, e.g., an extreme example is sample 7 (Conway granite) where Fe/Fe+Mg biotite is only 0.53 while Fe/Fe+Mg whole rock is 0.93. This suggests considerably higher fo_2 during crystallization of sample 7 (cf. Czamanske and Wones, 1973), possibly due to buildup and loss of volatiles during the last stages of crystallization.

Using the values of $Fe/Fe+Mg)_{min}/Fe/Fe+Mg)_{w.r.}$ obtained from the diorite and monzodiorite an estimate of the Fe/Fe+Mg of the liquid which precipitated the clinopyroxene and hornblende in the gabbro was calculated. An

average value of 0.46 was obtained. While this is only an approximation since the exact Fe/Mg partitioning between mineral and liquid will be a function of T and fo_2 (at the least), it is probably much closer to the actual Fe/Fe+Mg of the gabbro's parent than the analyzed gabbro whole rock value of 0.58-0.60, which is abnormally high because of cumulate ilmenite.

The range of plagioclase composition in the samples (obtained via microprobe analysis) is shown in Figure 25. The extremely calcic plagioclase in the gabbro (occurring in cores and as inclusions in clinopyroxene and hornblende) also indicates that the diorite is too fractionated to serve as a parent liquid for the gabbro.

Figure Captions

Figure 13. Plot of TiO_2 (wt.%) vs. SiO_2 (wt.%) for Belknap Mountains complex samples.

- ● Gabbro
- △ Diorite
- ○ Gilmanton monzodiorite
- ▲ Ames monzodiorite
- ■ Belknap Mountain syenite
- ◪ Cobble Hill syenite
- ▼ Lake quartz syenite
- ▽ Albany quartz syenite
- □ Sawyer quartz syenite
- + Conway granite

Figure 14. Plot of Al_2O_3 (wt.%) vs. SiO_2 (wt.%) for Belknap Mountains complex. Legend same as for Figure 13.

Figure 15. Plot of total iron as FeO (wt.%) vs. SiO_2 (wt.%) for Belknap Mountains complex. Legend same as for Figure 13.

Figure 16. Plot of MgO (wt.%) vs. SiO_2 (wt.%) for Belknap Mountains complex. Legend same as for Figure 13.

Figure 17. Plot of CaO (wt.%) vs. SiO_2 (wt.%) for Belknap Mountains complex. Legend same as for Figure 13.

Figure 18. Plot of $Na_2O + K_2O$ (wt.%) vs. SiO_2 (wt.%) for Belknap Mountains complex. Legend same as for Figure 13.

Figure 19. Plot of P_2O_5(wt.%) vs. SiO_2 (wt.%) for Belknap Mountains complex. Legend same as for Figure 13.

Figure 20. Plot of whole rock Fe/Fe+Mg vs. SiO_2 (wt.%) for Belknap Mountains complex samples. Fe/Fe+Mg calculated from total iron content of samples.

Figure 21. Molecular A(Na_2O+K_2O) - F(total iron as FeO) - M(MgO) diagram for Belknap Mountains complex samples. Because of overlap of points, fields for various rock units are shown instead of individual data points.

Figure 22. Normative Ab-An-Or (recalculated to 100%) for Belknap Mountains complex samples. 1 and 2 kilobar ($P_{H_2O}=P_{Total}$) cotectics (quartz plus two feldspars) from James and Hamilton (1969) and data in Winkler (1974), respectively.

Figure 23. Normative Q-Or-Ab (recalculated to 100%) for

Belknap Mountains complex samples.

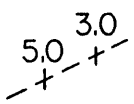

Ternary minima and eutectic at $P_{H_2O}=P_{Total}$ (kilobars) from Tuttle and Bowen (1958) and Luth et al. (1964).

Ternary minima at P_{H_2O}= 0 (P_{Total} in kilobars) from Luth (1969).

Projections of piercing points for the quartz-saturated cotectic (quartz plus two feldspars) at $P_{H_2O}=P_{Total}$= 1 kilobar for various An contents from James and Hamilton (1969).

Position of the extension of the thermal valleys connecting the Ab-Or sideline with the ternary minimum or piercing points at P_{H_2O}= P_{Total} = 1 kilobar.

Figure 24. Mineral Fe/Fe+Mg vs. whole rock Fe/Fe+Mg for mafic silicates from the Belknap Mountains complex.

Figure 25. Range of primary plagioclase variation in selected Belknap Mountains complex samples.

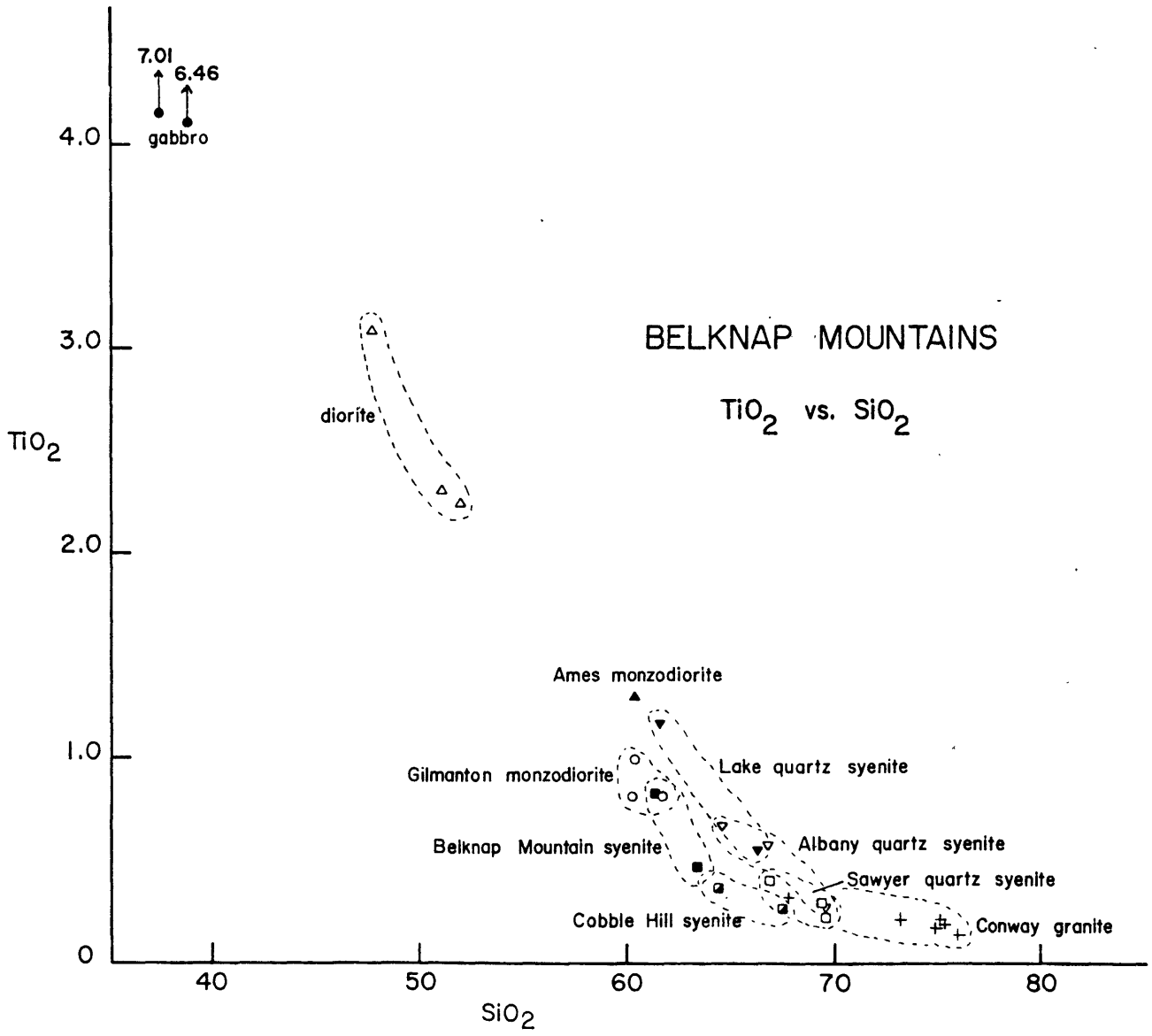
7.01
6.46
gabbro
4.0
3.0
2.0
1.0
0
TiO_2
diorite
BELKNAP MOUNTAINS
TiO_2 vs. SiO_2
Ames monzodiorite
Gilmanton monzodiorite
Lake quartz syenite
Belknap Mountain syenite
Albany quartz syenite
Sawyer quartz syenite
Cobble Hill syenite
Conway granite
40
50
60
70
80
SiO_2

Figure 13

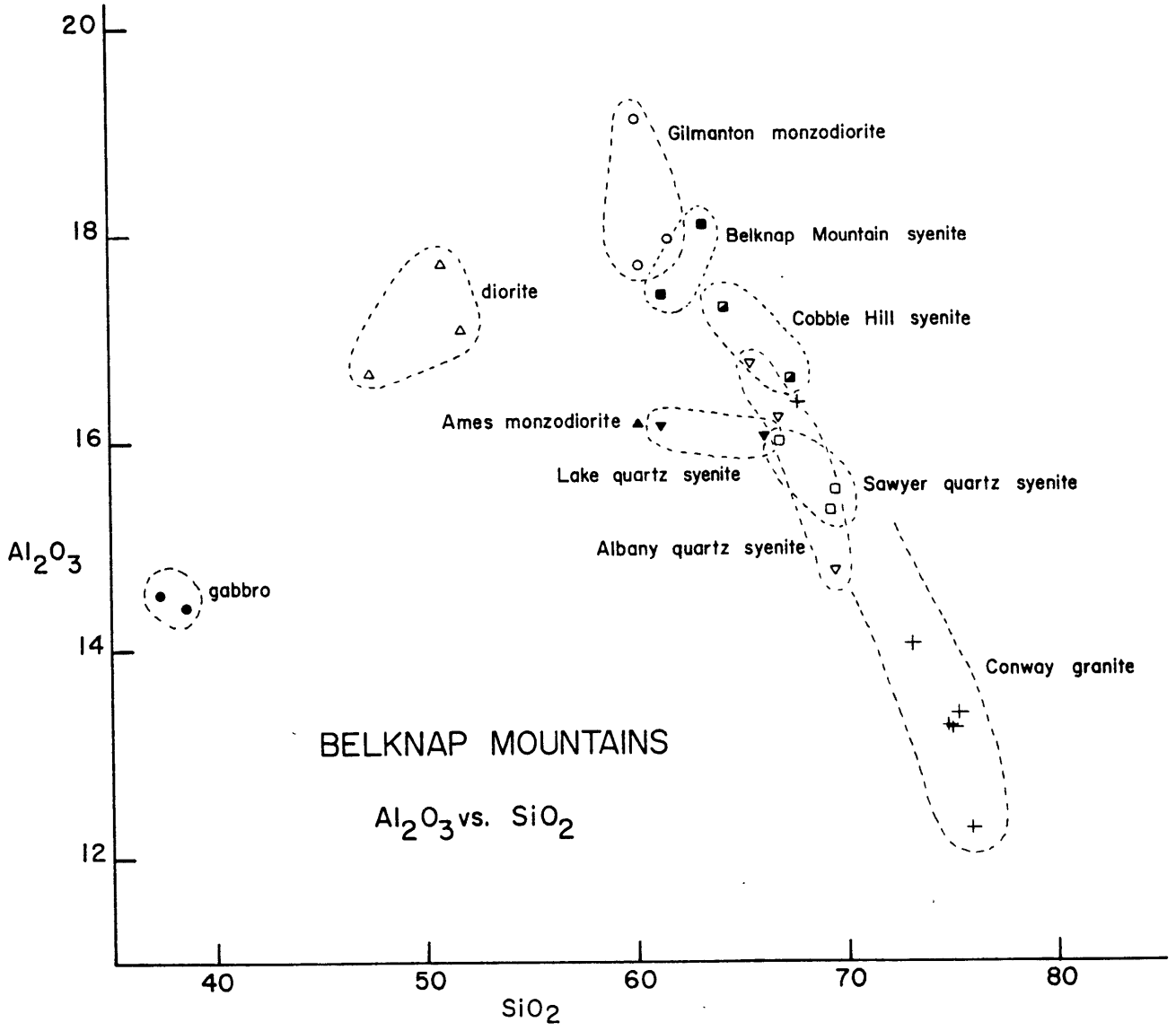
20
18
16
14
12
Al_2O_3
40
50
60
70
80
SiO_2
Gilmanton monzodiorite
Belknap Mountain syenite
diorite
Cobble Hill syenite
Ames monzodiorite
Lake quartz syenite
Sawyer quartz syenite
Albany quartz syenite
gabbro
Conway granite
BELKNAP MOUNTAINS
Al_2O_3 vs. SiO_2

Figure 14

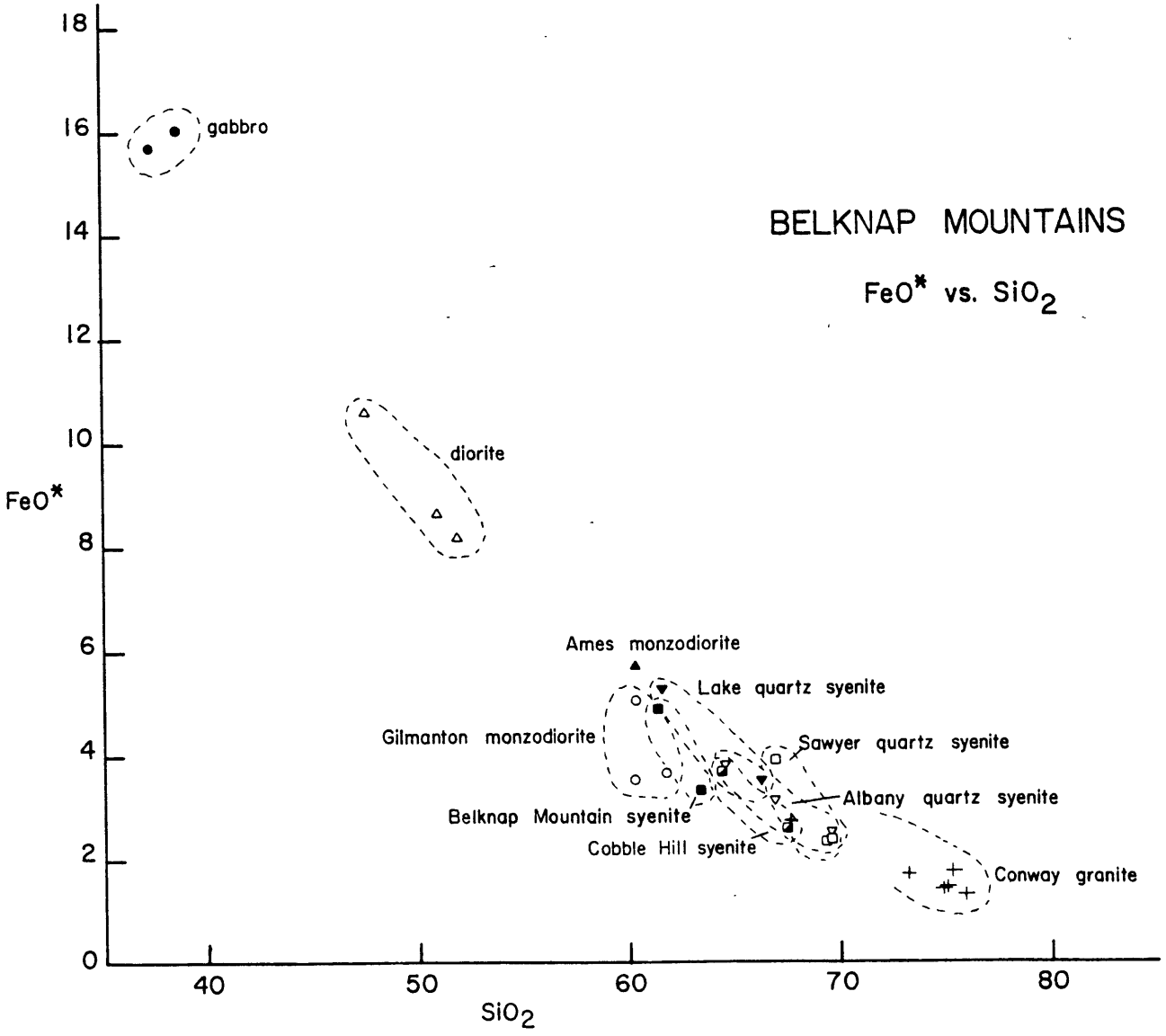
BELKNAP MOUNTAINS
FeO* vs. SiO2
FeO*
SiO2
18
16
14
12
10
8
6
4
2
0
40
50
60
70
80
gabbro
diorite
Ames monzodiorite
Lake quartz syenite
Gilmanton monzodiorite
Sawyer quartz syenite
Albany quartz syenite
Belknap Mountain syenite
Cobble Hill syenite
Conway granite

Figure 15

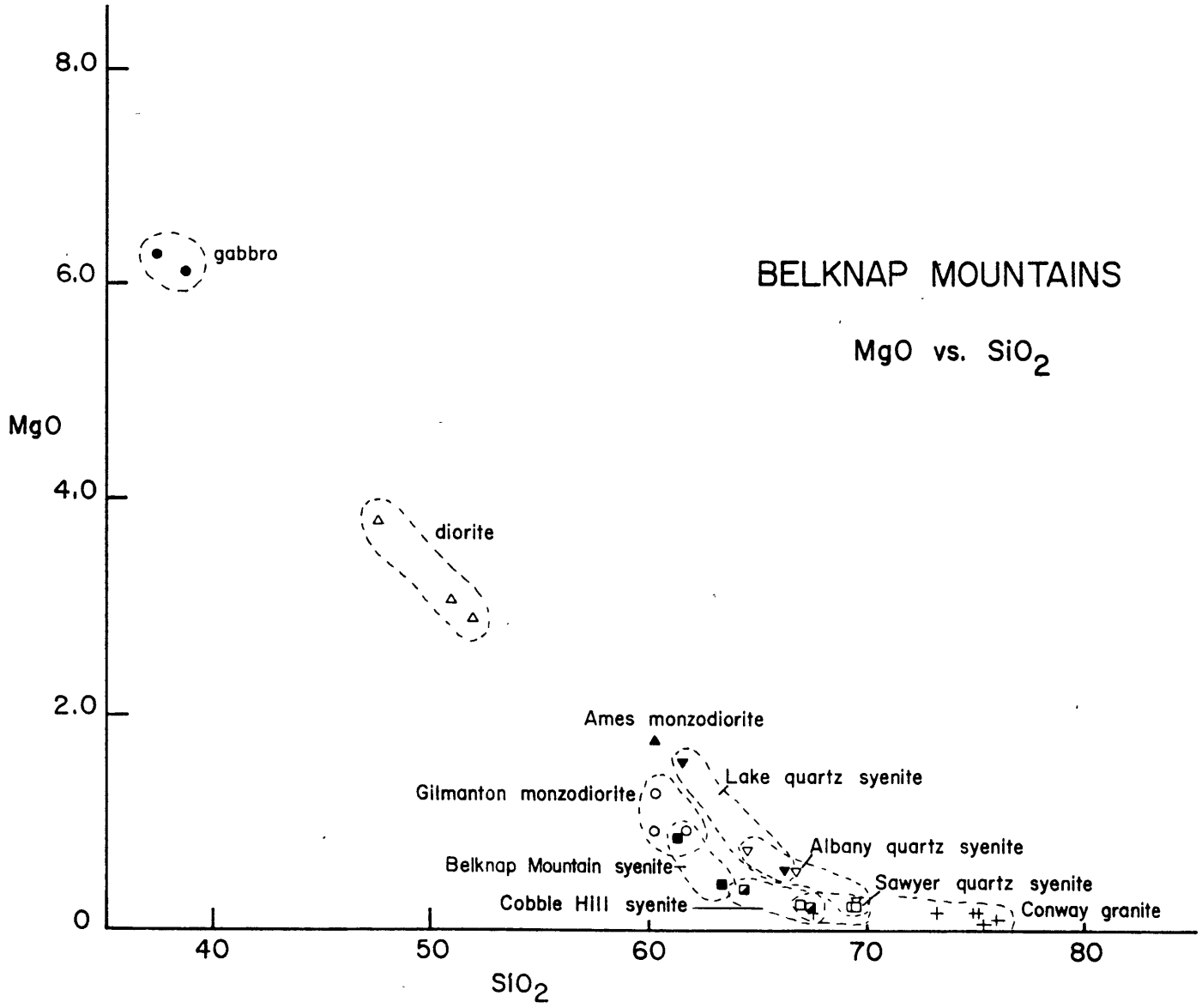
BELKNAP MOUNTAINS
MgO vs. SiO2
MgO
SiO2
8.0
6.0
4.0
2.0
0
40
50
60
70
80
gabbro
diorite
Ames monzodiorite
Gilmanton monzodiorite
Lake quartz syenite
Albany quartz syenite
Belknap Mountain syenite
Sawyer quartz syenite
Cobble Hill syenite
Conway granite

Figure 16

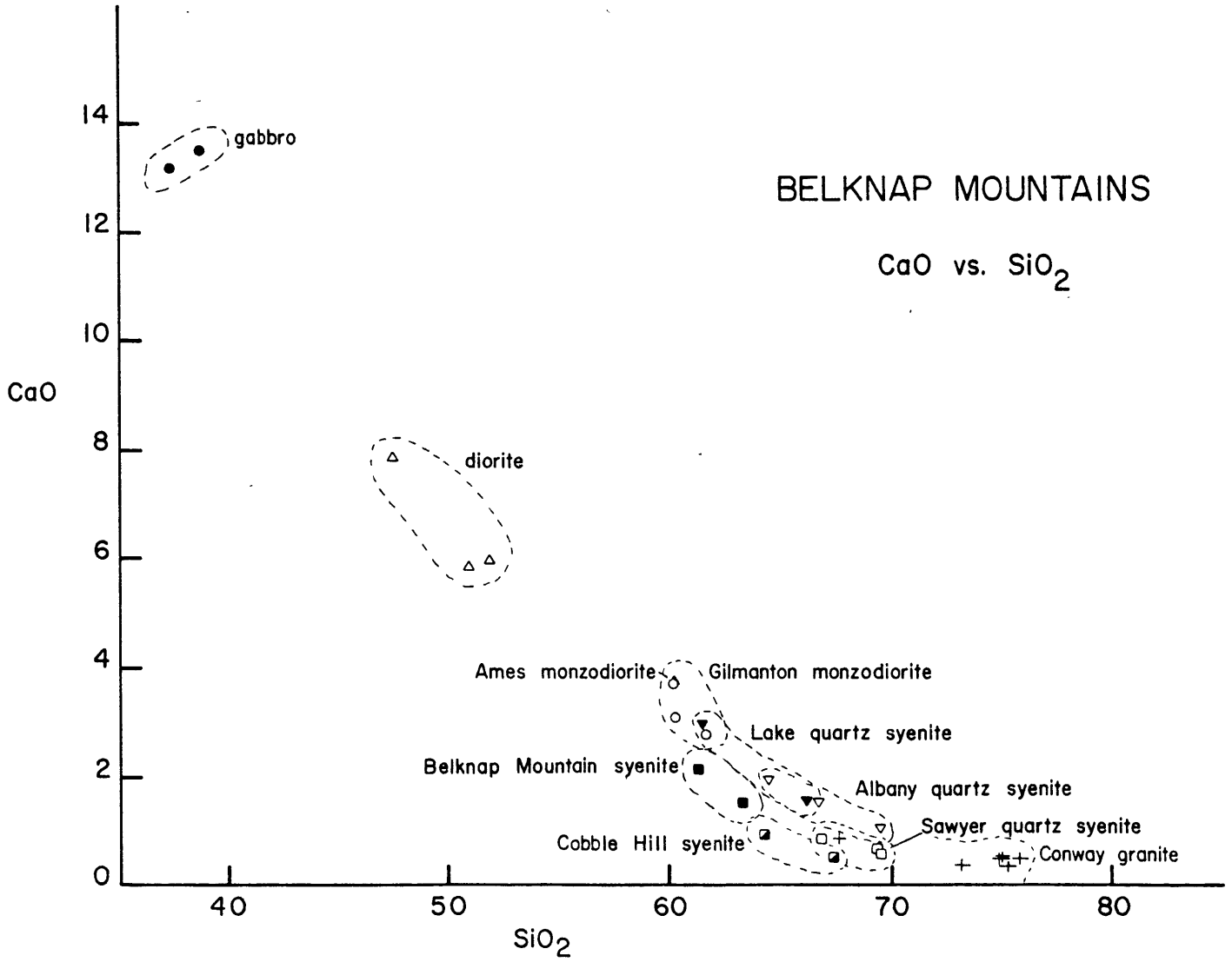
BELKNAP MOUNTAINS
CaO vs. SiO2
CaO
SiO2
0
2
4
6
8
10
12
14
40
50
60
70
80
gabbro
diorite
Ames monzodiorite
Gilmanton monzodiorite
Lake quartz syenite
Belknap Mountain syenite
Albany quartz syenite
Sawyer quartz syenite
Cobble Hill syenite
Conway granite

Figure 17

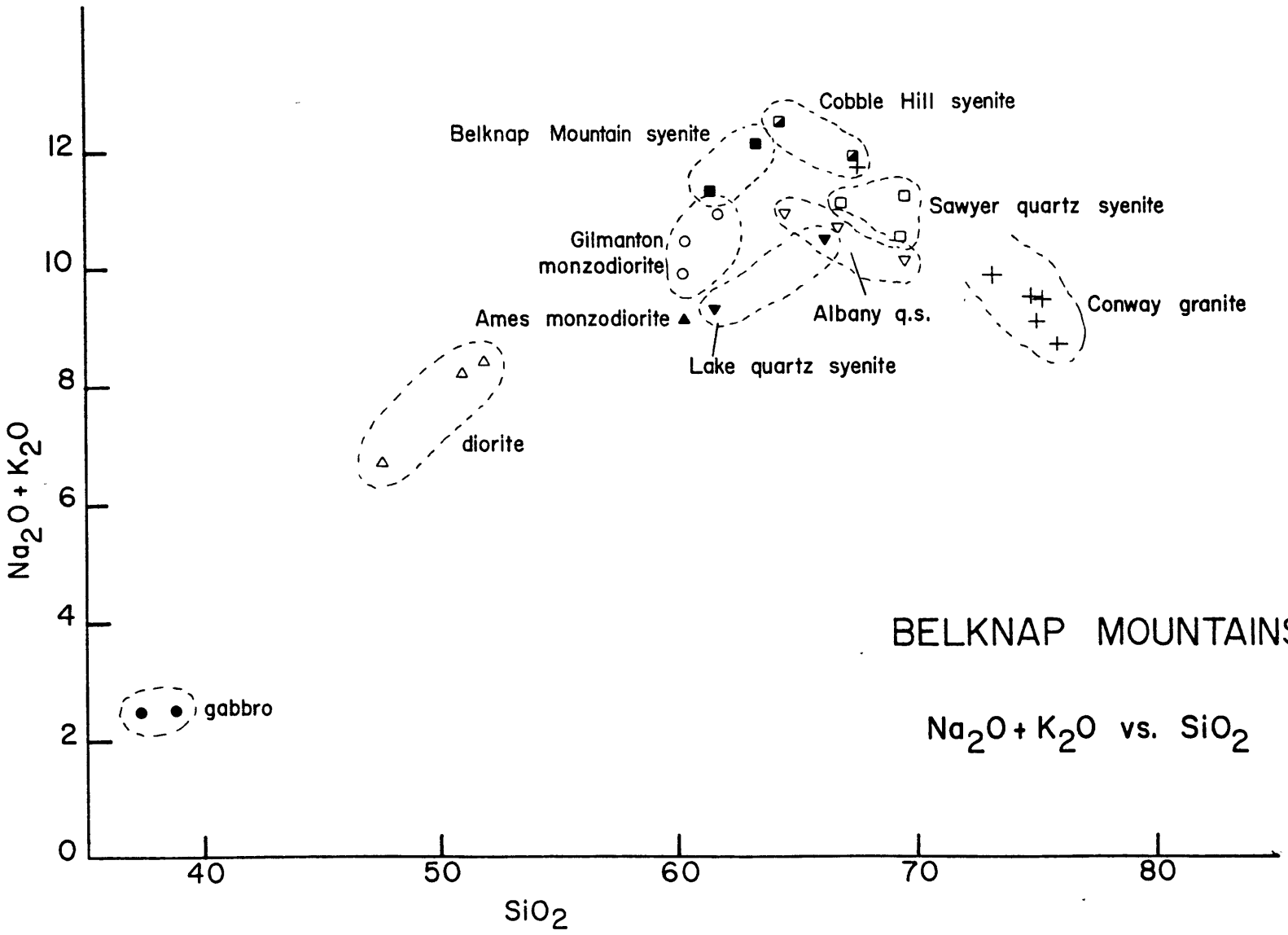
Cobble Hill syenite
Belknap Mountain syenite
Sawyer quartz syenite
Gilmanton monzodiorite
Ames monzodiorite
Albany q.s.
Conway granite
Lake quartz syenite
diorite
gabbro
BELKNAP MOUNTAINS
Na2O + K2O vs. SiO2
Na2O + K2O
SiO2
0
2
4
6
8
10
12
40
50
60
70
80

Figure 18

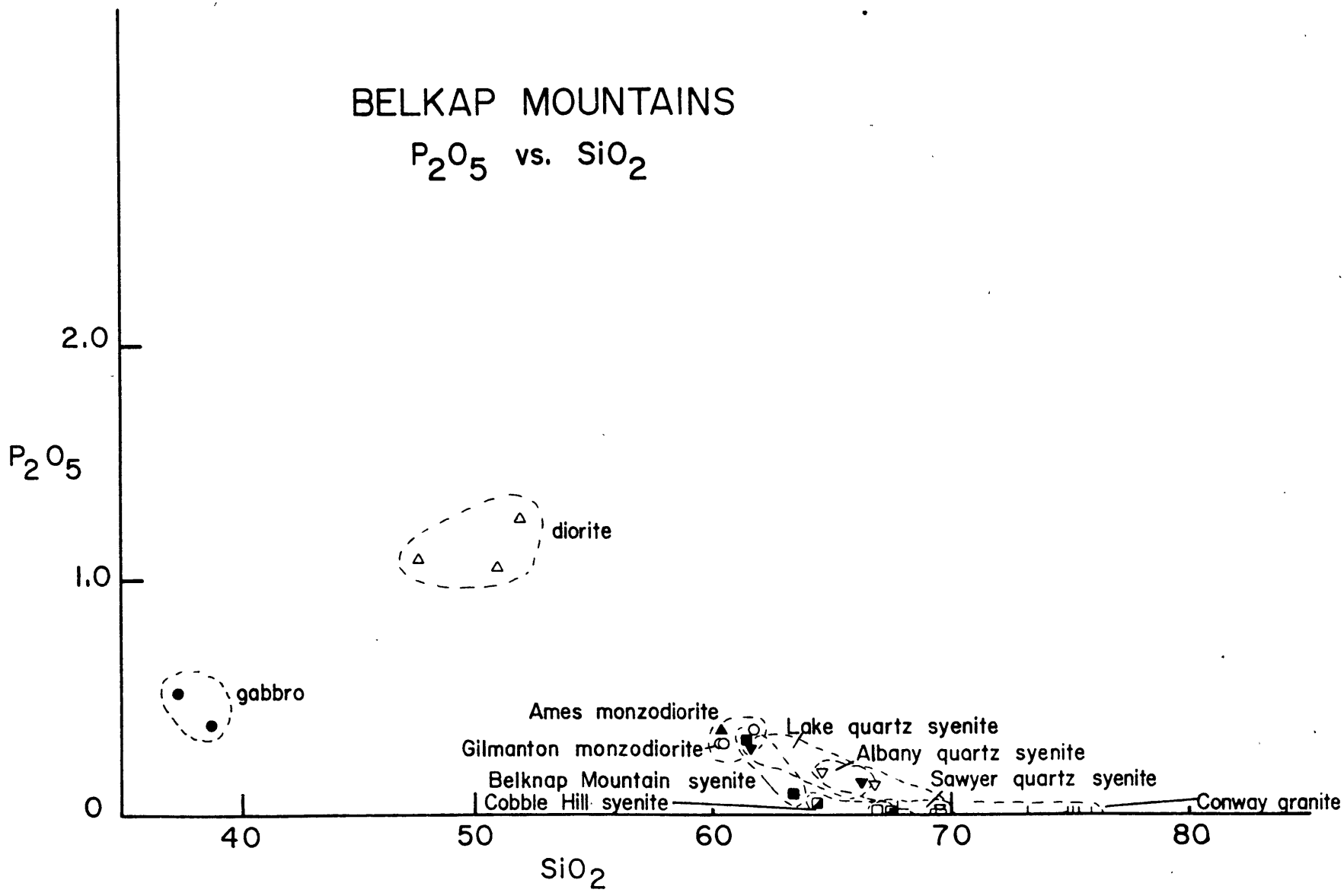
BELKAP MOUNTAINS
P_2O_5 vs. SiO_2
2.0
1.0
0
P_2O_5
40
50
60
70
80
SiO_2
diorite
gabbro
Ames monzodiorite
Gilmanton monzodiorite
Belknap Mountain syenite
Cobble Hill syenite
Lake quartz syenite
Albany quartz syenite
Sawyer quartz syenite
Conway granite

Figure 19

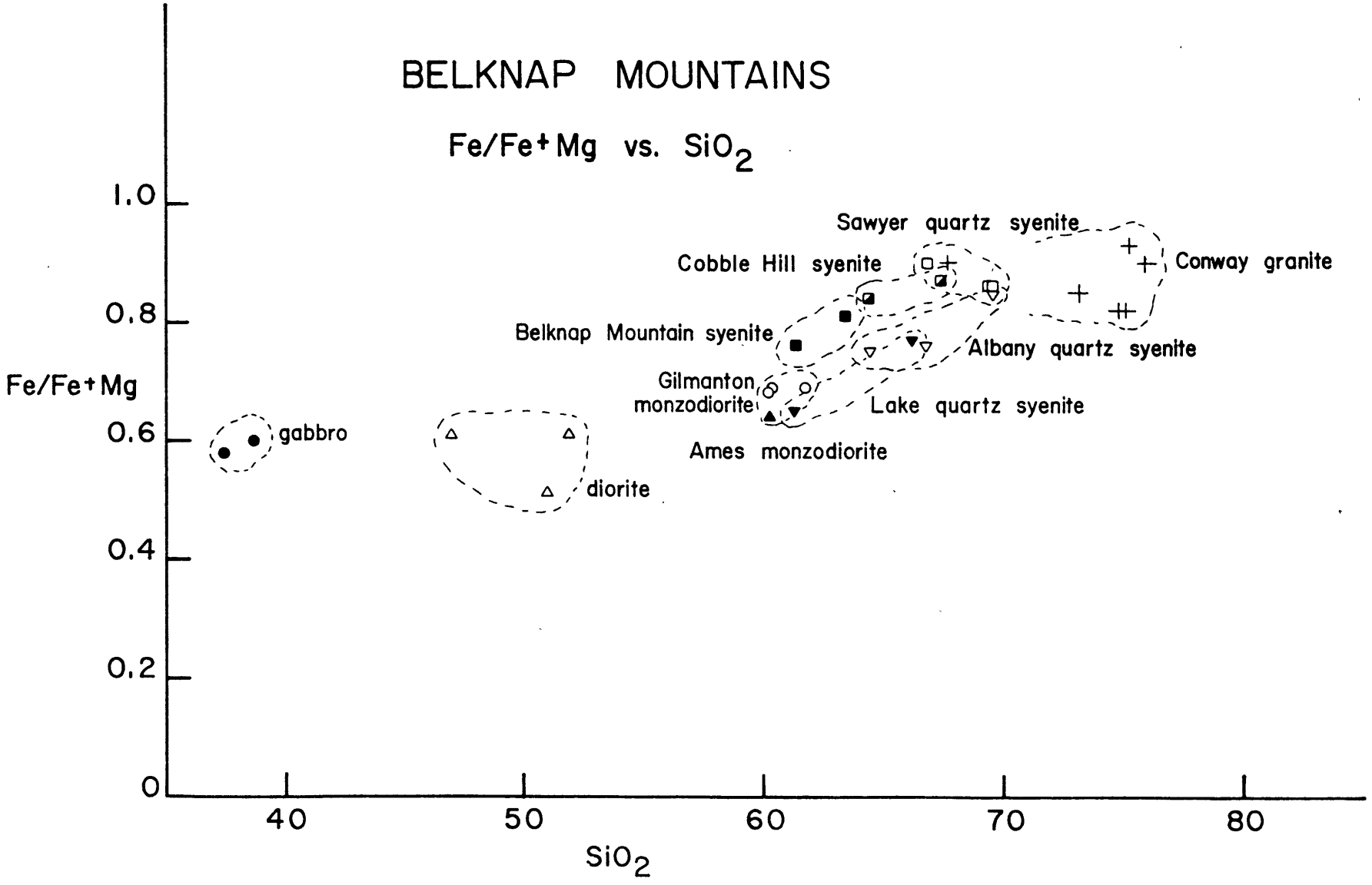
BELKNAP MOUNTAINS
Fe/Fe+Mg vs. SiO2
Fe/Fe+Mg
1.0
0.8
0.6
0.4
0.2
0
40
50
60
70
80
SiO2
Sawyer quartz syenite
Cobble Hill syenite
Conway granite
Belknap Mountain syenite
Albany quartz syenite
Gilmanton monzodiorite
Lake quartz syenite
Ames monzodiorite
gabbro
diorite

Figure 20

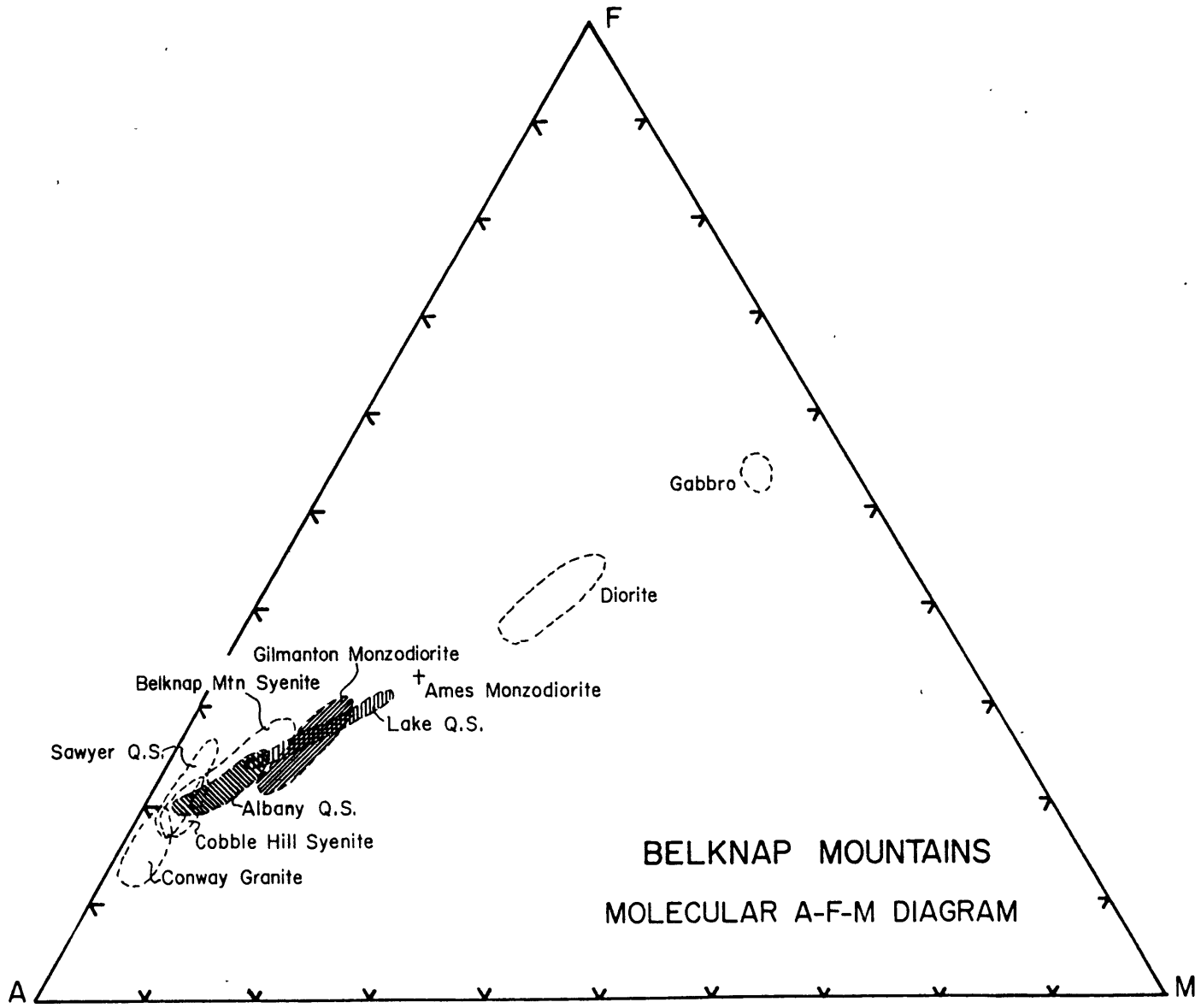
F
A
M
Gabbro
Diorite
Gilmanton Monzodiorite
+Ames Monzodiorite
Belknap Mtn Syenite
Lake Q.S.
Sawyer Q.S.
Albany Q.S.
Cobble Hill Syenite
Conway Granite
BELKNAP MOUNTAINS
MOLECULAR A-F-M DIAGRAM

Figure 21

BELKNAP MOUNTAINS: NORMATIVE Ab-An-Or

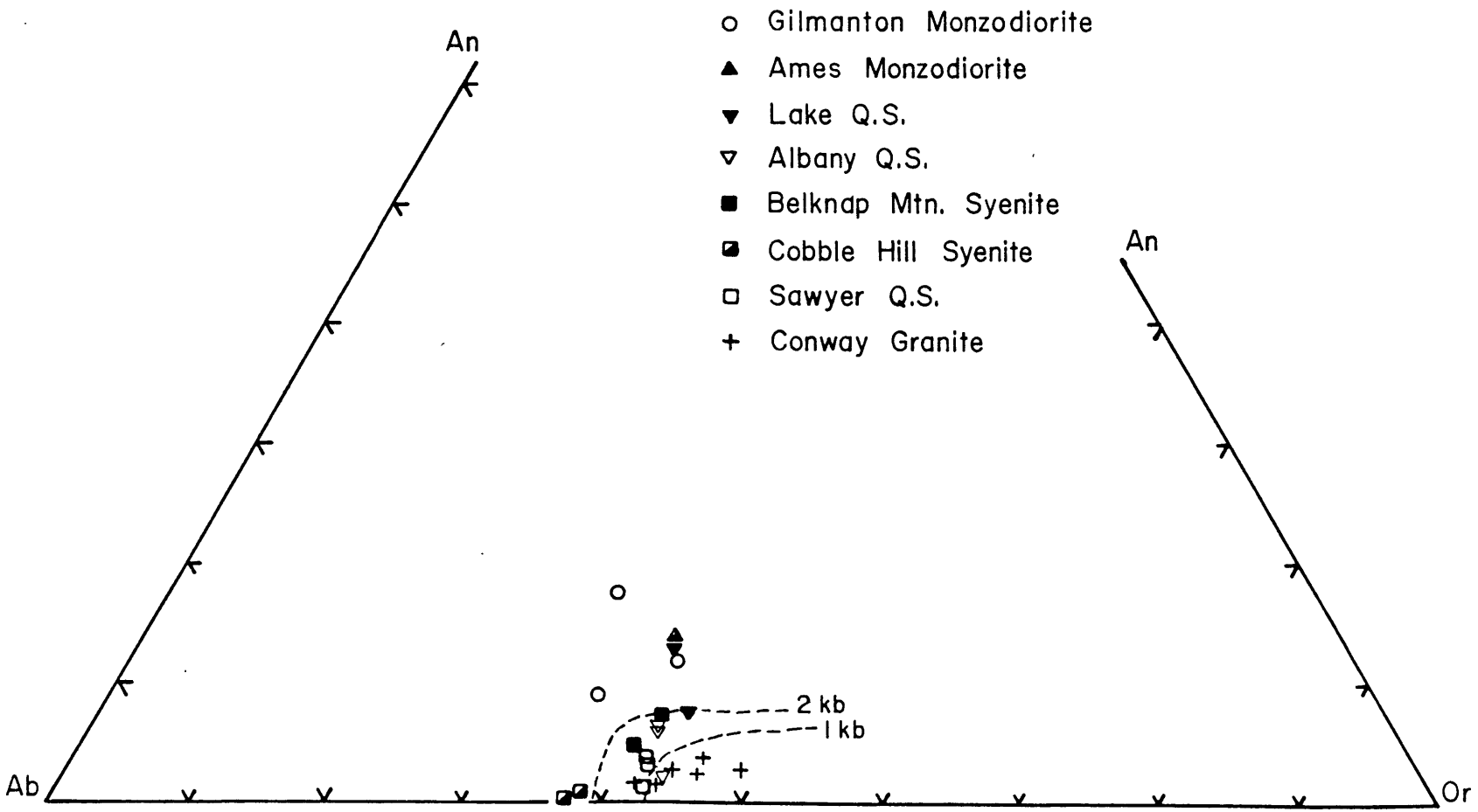

Figure 22

BELKNAP MOUNTAINS: NORMATIVE Q-Or-Ab

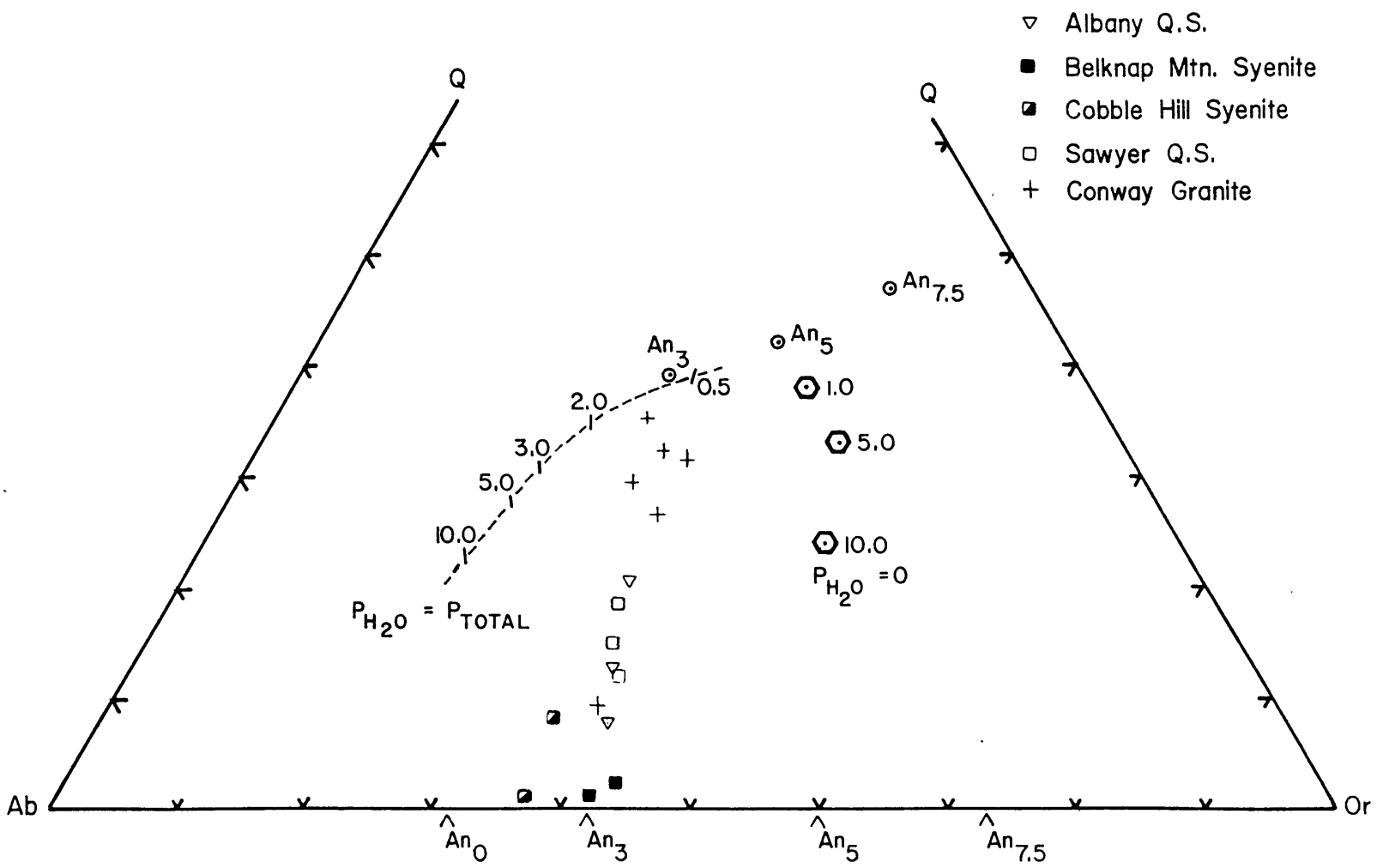

Figure 23

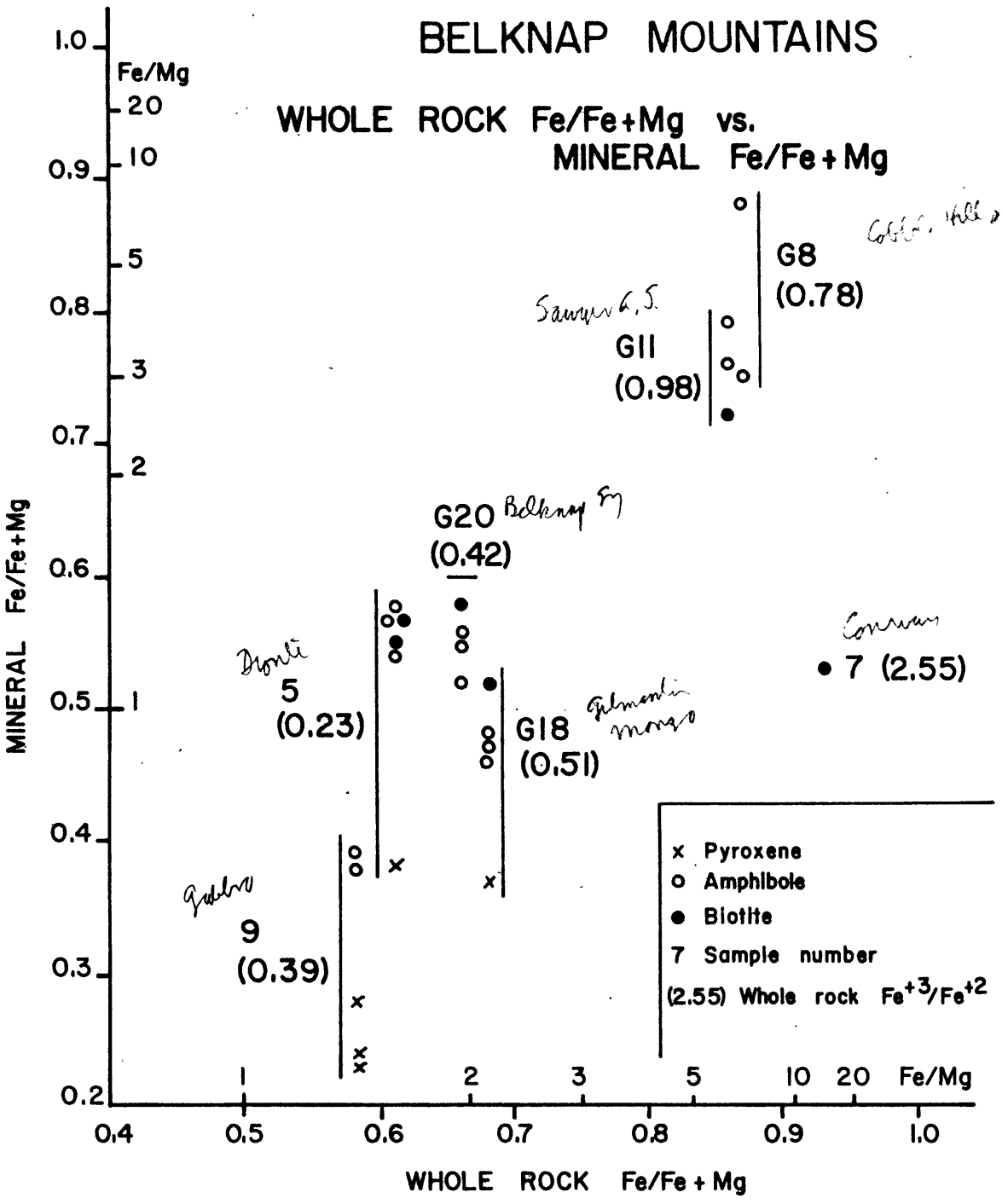
BELKNAP MOUNTAINS
WHOLE ROCK Fe/Fe+Mg vs.
MINERAL Fe/Fe+Mg
MINERAL Fe/Fe+Mg
WHOLE ROCK Fe/Fe+Mg
Fe/Mg
1.0
0.9
0.8
0.7
0.6
0.5
0.4
0.3
0.2
20
10
5
3
2
1
0.4
0.5
0.6
0.7
0.8
0.9
1.0
1
2
3
5
10
20
G8
(0.78)
G11
(0.98)
G20
(0.42)
G18
(0.51)
5
(0.23)
9
(0.39)
7 (2.55)
x Pyroxene
o Amphibole
● Biotite
7 Sample number
(2.55) Whole rock Fe+3/Fe+2

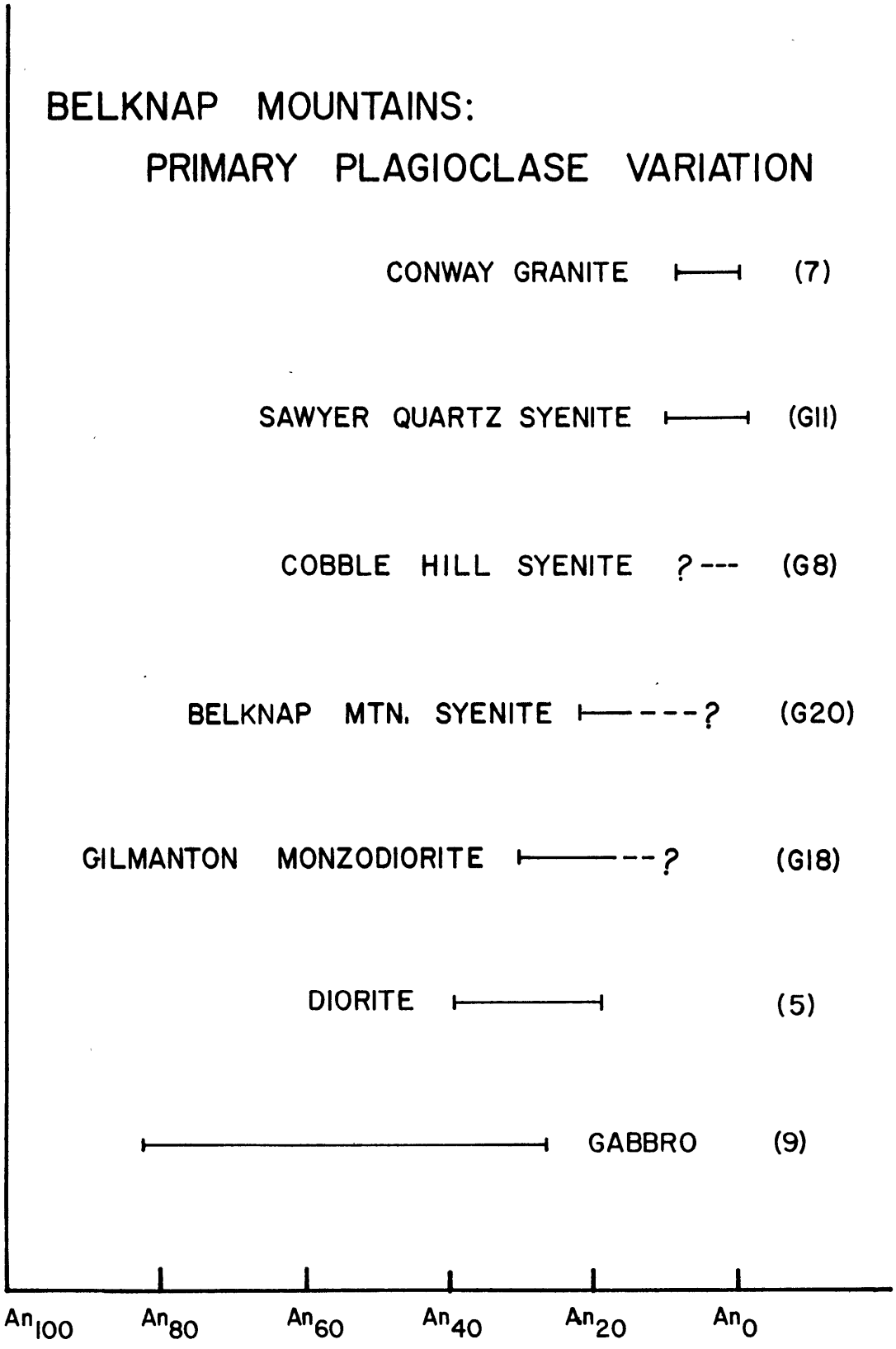
BELKNAP MOUNTAINS:
PRIMARY PLAGIOCLASE VARIATION
CONWAY GRANITE (7)
SAWYER QUARTZ SYENITE (GII)
COBBLE HILL SYENITE ?--- (G8)
BELKNAP MTN. SYENITE ---? (G20)
GILMANTON MONZODIORITE ---? (GI8)
DIORITE (5)
GABBRO (9)
An100
An80
An60
An40
An20
An0

CHAPTER 5. TRACE ELEMENT GEOCHEMISTRY

As in the case of major elements, trace element abundances might be expected to show unique characteristics in rock units with different initial $^{87}Sr/^{86}Sr$ inherited from the source region. Because trace element contents vary by several orders of magnitude in igneous rocks where major element abundances may vary by no more than a factor of 10 (in extreme cases), trace elements may be more sensitive to source characteristics than major elements. However, the variability of trace elements may also lead to a problem in interpretation. Several accessory phases in granites (e.g., apatite, allanite, zircon, sphene) may contain 50 percent or more of the rare earths and other trace elements in a rock, so trace element differences may be due to inhomogeneous distribution of minor phases in rocks or in splits of samples. The question of trace element variation between independently prepared splits of the same rock is discussed in Appendix II.

The behavior of trace elements during igneous processes can be described by relatively simple equations (see Allegre and Minster, 1978 and Hanson, 1978). While there are uncertainties in trace element modeling (see Chapter 6 for a discussion), the development of geologically and petrologically reasonable fractionation models for Belknap Mountain rocks with similar $^{87}Sr/^{86}Sr)_o$ would be strong evidence for a comagmatic relation between units. Conversely, trace element

relations may preclude a comagmatic relation under any reasonable circumstances.

Details of analytical procedure are given in Appendix II. The rare earths, Cs, Sc, Hf, Ta, Th, U, Ba, and in some samples, Co, were determined via instrumental neutron activation analysis (Gordon et al., 1968). Rb and Sr were determined by isotope dilution analysis, except for four samples, which have Rb and Sr values from XRF. Zr was determined in 12 samples by XRF. The data for the Belknap Mountains samples are given in Table 8.

To determine the suitability of using trace elements as indicators of primary petrogenetic processes, Hon (1976) compared analyses of fresh Mount Katahdin granite samples with material which had suffered post-magmatic alteration (weathering, mylonitization, hydrothermal alteration). He concluded that Cs, U, and Ta were not suitable. U values also possess large uncertainty due to the difficulty of analyzing for the element by INAA (Appendix II, Table 21). Hon (1976) suggested the problem with Ta in the rocks he analyzed may have been the solubility of Ta as a fluoride, and pointed out that the Katahdin granites were fluorite-bearing. Fluorite occurs in the Conway granite, but is otherwise not present in the Belknap samples examined. Furthermore, there is also very little evidence of water saturation and the presence of a vapor phase in the Belknaps, whereas pegmatites and aplites are abundant at Mount Katahdin. Therefore, it is not surprising that Ta shows coherent

TABLE 8. TRACE ELEMENT DATA FOR BELKNAP MOUNTAIN SAMPLES[a]

	Gabbro		Diorite			Gilmanton Monzodiorite			Ames Monzodiorite
	9	15	5	17	18	G17	G18	19	11
Rb[e]	14.5	12.4	132.	83.6	109.	112.	126.	124.	136.
Cs	b	b	2.9	1.5	2.5	2.8	3.1	2.7	3.8
Sr[e]	831.	788.	818.	966.	789.	549.	727.	455.	419.
Ba	319.	287.	602.	1010.	753.	795.	1380.	1330.	848.
Sc	38.1	34.4	15.1	9.4	11.2	3.6	4.5	9.2	8.8
Co		56.9			16.4		5.9		17.6
La	19.2	16.8	39.5	45.5	70.4	47.6	50.6	69.3	88.6
Ce	47.0	37.5	97.2	113.	148.	89.5	97.2	144.	186.
Nd	27.4	20.0	53.0	56.0	63.1	33.5	32.7	51.8	68.5
Sm	6.6	4.8	10.5	10.6	10.8	5.7	5.8	9.4	10.9
Eu	2.2	1.7	3.7	3.5	3.3	2.4	3.1	3.0	2.1
Ho	0.8	0.6	1.2	1.1	1.2	0.9	0.8	0.9	1.3
Yb	1.4	1.0	2.1	2.2	2.4	1.6	1.6	2.7	3.3
Lu	0.20	0.17	0.36	0.35	0.43	0.28	0.27	0.40	0.54
Zr	118.				355.		384.	638.[f]	449.
Hf	3.2	2.9	6.7	8.8	8.5	9.7	12.1	15.7	12.6
Ta	3.6	3.1	5.0	6.7	6.3	6.4	5.5	6.2	7.9
Th	1.0	1.5	4.3	5.5	9.6	14.4	13.0	12.5	22.3
U	0.4	c	1.0	2.4	2.2	3.0	3.9	3.9	4.0

TABLE 8. continued

	Belknap Mountain Syenite		Cobble Hill Syenite		Lake Quartz Syenite		Sawyer Quartz Syenite		
	G20[g]	20	G7	G8	21	22	G11[g]	12	13
Rb[e]	175.	147.	153.	193.	193.	139.	212.	224.	187.
Cs	2.4	2.2	2.8	6.1	5.8	2.9	2.7	1.7	4.5
Sr[e]	256.0	276.0	35.0	24.0	204.0	366.0	62.0	33.0	35.0
Ba	651.	688.	323.	98.5	509.	709.	<100.0[d]	<60.0[d]	<60.0[d]
Sc	3.5	7.0	2.2	1.7	4.6	8.1	3.9	5.9	3.0
Co			0.8					1.2	
La	49.9	63.3	72.1	47.4	114.	103.	132.	207.	196.
Ce	113.	134.	162.	101.	222.	202.	263.	461.	378.
Nd	39.1	56.7	60.4	38.2	72.8	68.2	85.0	133.	123.
Sm	7.2	10.2	10.0	7.4	12.8	12.1	12.5	20.1	17.2
Eu	1.9	2.4	1.2	0.52	1.4	1.9	0.48	0.48	0.36
Ho	1.0	1.6	1.2	1.3	2.1	1.6	1.4	2.2	1.5
Yb	2.4	2.6	2.8	3.0	4.4	4.0	3.3	5.0	4.0
Lu	0.40	0.34	0.46	0.44	0.67	0.59	0.56	0.83	0.67
Zr		905.[f]		230.	538.				426.
Hf	12.4	21.0	8.2	7.4	15.3	13.8	14.4	26.3	14.9
Ta	9.4	7.3	7.3	9.7	11.1	7.6	9.9	9.9	13.7
Th	15.7	10.4	15.6	20.3	29.4	22.5	31.0	56.2	60.4
U	4.0	4.7	4.7	4.7	3.9	2.6	6.1	7.4	9.4

TABLE 8. continued

	Albany Quartz Syenite			Conway Granite					
	G14	G27	1	G28	G29	G34	G38[g]	7	6[g]
Rb[e]	147.	151.	137.	194.	255.	181.	174.	189.	217.
Cs	2.2	2.1	1.6	2.0	6.3	2.6	2.3	1.7	3.7
Sr[e]	273.	203.	79.0	43.0	65.0	102.	84.0	116.	84.
Ba	778.	482.	319.	187.	201.	255.	348.	298.	387.
Sc	5.7	3.5	2.5	3.9	0.8	1.1	1.5	0.7	0.3
Co			1.4	1.2					
La	68.3	55.4	64.8	110.	109.	39.8	76.8	84.5	29.5
Ce	147.	110.	131.	248.	188.	80.7	166.	169.	65.8
Nd	49.4	39.8	47.3	75.1	53.9	21.1	45.6	39.6	21.0
Sm	9.3	7.0	8.5	11.6	8.4	4.1	9.3	6.5	5.2
Eu	1.9	1.3	0.81	0.49	0.60	0.68	0.67	0.47	0.43
Ho	1.4	1.3	1.1	1.6	1.3	0.7	1.5	1.0	2.4
Yb	2.8	2.6	2.9	3.4	3.6	2.3	4.1	2.8	5.4
Lu	0.43	0.42	0.46	0.62	0.52	0.33	0.54	0.43	0.69
Zr	460.			590.[f]				202.	
Hf	11.9	11.8	10.1	17.6	8.8	6.2	8.0	8.7	9.5
Ta	6.3	8.9	8.4	11.6	15.7	9.9	10.9	14.6	18.9
Th	17.6	23.6	28.3	33.3	52.3	30.9	44.9	45.1	60.8
U	3.9	5.2	5.0	7.4	8.7	4.5	5.6	5.4	23.7

TABLE 8. continued

	K/Rb	Rb/Sr	Ba/Sr	$(La/Yb)_{cn}$
Gabbro				
9	33.7	0.017	0.38	8.3
15	314.	0.016	0.36	10.2
Diorite				
5	146.	0.16	0.73	11.4
17	337.	0.086	1.05	12.5
18	288.	0.14	0.95	17.8
Gilmanton Monzodiorite				
G17	386.	0.20	1.45	18.0
G18	312.	0.17	1.90	19.2
19	376.	0.27	2.93	15.6
Ames Monzodiorite				
11	297.	0.32	2.02	16.3
Belknap Mountain Syenite				
G20	293.	0.68	2.54	12.6
20	337.	0.53	2.49	14.8
Cobble Hill Syenite				
G7	309.	4.37	9.22	15.6
G8	241.	8.04	4.10	9.5
Lake Quartz Syenite				
21	246.	0.95	2.50	15.7
22	299.	0.40	1.94	15.6

TABLE 8. continued

	K/Rb	Rb/Sr	Ba/Sr	$La/Yb)_{cn}$
Sawyer Quartz Syenite				
G11	214.	3.42	<1.61	24.2
12	216.	6.78	<1.82	25.1
13	259.	5.34	<1.71	29.7
Albany Quartz Syenite				
G14	320.	0.54	2.85	14.8
G27	304.	0.74	2.37	12.9
1	324.	1.73	4.04	13.5
Conway Granite				
G28	256.	4.51	4.34	19.6
G29	178.	3.92	3.09	18.4
G34	231.	1.77	2.50	10.5
G38	239.	2.07	4.14	11.4
7	243.	1.63	2.57	18.3
6	178.	2.58	4.61	3.3

TABLE 8. continued

a See Appendix II for details of analytical procedure.

b Below detection limit.

c Below detection limit.

d Calculated detection limit.

e Isotope dilution analysis unless indicated.

f These values of Zr beyond standard range. See Appendix II.

g Rb and Sr by XRF.

behavior in the Belknap samples and, as a result, primary significance is attached to the Ta data.

Hart (1969) and Blaxland (1974) indicate that Rb may also be affected considerably during alteration and weathering in basic and silicic rocks. The discussion of Sr isotope systematics shows that some samples have probably undergone changes in Rb/Sr ratio (and probably K/Rb as well). For this reason, Rb data must be used with caution in evaluating igneous relationships.

Figures 26-28 are the chondrite normalized rare earth patterns for the Belknap Mountains samples. Figure 29 is a plot of Sr vs. SiO_2; Figures 30, 31, 32, and 33 are plots of K_2O vs. Ba, Sr vs. Ba, Ta vs. Sc, and La_{cn} vs. Yb_{cn}.

The gabbros possess the lowest overall rare earth abundances in the complex. They also have a slight (+)Eu anomaly and low abundances of Rb, Th, Zr, Hf, and Ta, lower Ba than the diorites, and very high Sc and Co. Taken together these are consistent with an origin (in part) as a cumulate. As discussed in Chapter 3, the range of plagioclase composition in the diorite and the Fe/Fe+Mg of the mafic silicates preclude the diorite as a suitable parent for the gabbro. This problem will be discussed in more detail in the chapter on geochemical modeling.

Samples 5 and 17 of the diorite are similar to many basic continental alkaline rocks in their REE pattern (for example, Kay and Gast, 1973; Price and Taylor, 1973). They are very similar in their abundances to volcanics from the

Belknap Mountains (R. Houghton, pers. commn). Note that sample 18 is considerably more enriched in the light rare earths and Th than samples 5 and 17, however. This may be due to contamination during intrusion of the Conway granite, as the sample shows evidence of injection of K-rich material in the form of stringers of alkali feldspar in stained section. For this reason sample 18 must be considered contaminated. Some features of the major element composition of sample 18 may also be due to contamination with granitic material (low TiO_2, FeO, MgO), but the major oxide variation diagrams (Figures 13-19) do not indicate a simple mixing relation between diorite sample 5 and granitic material to yield sample 18.

Sample 5 also has very high Rb, and an extremely low K/Rb with may be due to the presence of biotite without an accompanying high K/Rb potassic phase such as alkali feldspar. However, the possibility of Rb exchange with Conway granite material with relatively high Rb (samples 6 and 7) cannot be ruled out. Sample 17 has K/Rb very similar to the gabbros, and this is probably a good estimate of the "primary" K/Rb for the dioritic rocks.

Samples 5 and 17 also have slight (+)Eu anomalies (comparable to the gabbro) and moderately high Sr concentrations, indicating possible assimilation of feldspar, although this is not indicated in the petrography. Sample 17 has considerably higher Ba than sample 5, reflecting the presence of interstitial alkali feldspar. A comparison of

the major and trace element contents of samples 5 and 17 indicates that in all cases (except Rb) 17 is more fractionated (assuming removal of calcic plagioclase, mafics, and oxides) than 5.

Samples G17 and G18 of the Gilmanton monzodiorite have low REE contents and display a pronounced (+)Eu anomaly and higher Sr contents compared to sample 19, which has significantly higher REE overall and essentially no Eu anomaly. The (+)Eu anomaly in samples G17 and G18 is interpreted as due to plagioclase accumulation reducing the concentration of "incompatible" elements in these samples while increasing the Sr. This is also reflected in the high CaO and Al_2O_3 of sample G18. The cumulate nature of G17 and G18 is discussed in detail in the chapter on geochemical modeling. As a consequence of the cumulate plagioclase in G17 and G18, sample 19, the most mafic sample (Table 6) with the highest Sc content, has the largest amounts of the rare earths, Ba (relative to G17), Zr, and Hf.

In contrast to the Gilmanton, the Ames monzodiorite (sample 11) shows a significant (-)Eu anomaly with considerably higher REE overall. Sample 11 also has relatively high Sc and Co content, and high Th and U content.

The Belknap Mountain syenite is very similar in LREE abundances to the Gilmanton monzodiorite, but with a moderate (-)Eu anomaly and higher HREE. As in the case of sample 19 in the Gilmanton, Belknap Mountain syenite (sample 20) is more basic than G20 (lower SiO_2, Th, Ta; higher TiO_2, FeO*,

MgO, and Sc) but is significantly enriched in the LREE, Zr, and Hf relative to G20. Sample 20 also has considerably more P_2O_5 (and modal apatite) than G20. Since both zircon and apatite have large values of REE mineral/liquid distribution coefficients, the higher rare earth content of 20 may reflect the higher modal zircon and apatite. Also, the high total alkalis and high Al_2O_3 in G20 may indicate some contribution of cumulate alkali feldspar, thereby lowering the REE abundances (note that sample G20 has a smaller negative Eu anomaly, Eu/Eu* = 0.89 for G20 versus Eu/Eu* = 0.73 for 20).

The Cobble Hill syenite samples (G7 and G8) have light and heavy rare earth abundances similar to the range in the Belknap Mountain syenite samples, but have significantly larger negative Eu anomalies (Eu/Eu* = 0.22 and 0.39). The Cobble Hill syenite samples are also extremely depleted in Sr, have very low Sc and Co contents (sample G7), and lower Zr, Hf, and Ba abundances than the Belknap Mountain syenite samples. The REE content, low Sc, Co, Zr, and Hf abundances, combined with the high total alkalis of the Cobble Hill samples and the position of the samples on the normative Or-Ab-An and Q-Or-Ab diagrams (Figures 22 and 23) are all consistent with an origin by accumulation of alkali feldspar.

With respect to a cumulate model a plot of Ta versus Sc is of interest (Figure 32). In general, Sc decreases during fractional crystallization due to its incorporation in mafic silicates (Ewart and Taylor, 1969; Higuchi and Nagasawa, 1969; Paster et al., 1974), whereas Ta is often

utilized as a very incompatible element (Allegre et al., 1977). A liquid evolution path on a plot of Ta versus Sc would be similar to the general distribution of Belknap samples in Figure 32. The gabbro, with high Sc and low Ta contents, represents a mafic partial cumulate and it should lie to the right of a liquid trend. However, a rock composed of accumulated feldspar, which excludes both Ta and Sc, would lie to the left of the liquid trend. The two samples of Cobble Hill syenite lie well to the left of any line drawn through the samples of diorite, Belknap Mountain syenite, and Sawyer quartz syenite (other units with low $^{87}Sr/^{86}Sr)_o$). Samples G17 and G18 of the Gilmanton (which have significant (+)Eu anomalies and much lower Sc than sample 19) also lie well to the left of this possible liquid line.

The chief obstacle to acceptance of this model is the extremely low Sr values in the Cobble Hill syenites. Sr values are 35 ppm (G7) and 25 ppm (G8), lower even than the highly evolved Sawyer quartz syenite (30-60 ppm). Since feldspars (plagioclase and alkali feldspars) have mineral/liquid distribution coefficients for Sr greater than 1 (Arth, 1976) a rock composed of cumulate feldspar would have Sr values 2-3 times the parent liquid (depending on percentage of trapped liquid). This implies a liquid even more fractionated than the Sawyer quartz syenite as a parent for the Cobble Hill syenite. Details of this difficulty in modeling the Cobble Hill as a cumulate from a Sawyer-type liquid are outlined in Chapter 6. An additional complication is the

unique composition of the hornblende in the Cobble Hill. It has an intermediate composition between the high-Al hastingsite present in the other Belknap samples and sodic amphiboles (Table 7).

Relative to the Belknap Mountain syenite, the Lake quartz syenite samples are moderately enriched in the REE and Th, but have similar Ba and Sr abundances. On a plot of La_{cn} versus Yb_{cn} (Figure 33), the Lake samples plot well away from any of the other Belknap units.

The Albany quartz syenite has rare earth abundance patterns similar to the range of the Belknap Mountain and Cobble Hill syenites (Figure 27). There is considerable internal variation in trace elements Sc, Th, Sr, Ba, and Eu/Eu*, and in major elements such as TiO_2, FeO, MgO, and CaO. Decreasing Sr and Ba contents correlate with a increase in the europium anomaly, indicating the role of feldspar fractionation. There is a very large range for the Albany samples on plots of Ba versus Sr and Ba versus K_2O (Figures 30 and 31). Mafic mineral fractionation has also been important since Sc decreases with FeO, MgO, and CaO. Consideration of major elements, trace elements, and modal data indicate a fractionation sequence for the Albany quartz syenite in the sequence G14 → G27 → 1. The only difficulty is that the overall REE patterns (excluding Eu) do not show this trend.

Among the Belknap Mountains samples the Sawyer quartz syenite shows the greatest enrichment in the light rare earths

and the largest negative Eu anomaly (Eu/Eu* = 0.16-0.13) (Figure 28). The quartz syenite is extremely depleted in Ba and Sr, and relative to the Belknap Mountain syenite it is enriched in Th, U, and to some degree Ta and Hf. The enrichment of Th, U, Ta, and Hf (elements incompatible in feldspars) and depletion of Eu, Ba, and Sr (feldspar compatible elements) indicate that the Sawyer quartz syenite formed after large degrees of feldspar fractionation. Because the La_{cn}/Yb_{cn} ratio of the Sawyer is the largest of the Belknap units (Figure 33), a phase with large HREE/LREE partitioning ratio must have been involved in the fractionation process (a likely phase is amphibole). Feldspar fractionation alone would decrease the La_{cn}/Yb_{cn} ratio because of the slight preference of feldspars for the LREE; hornblende, however, has large HREE distribution coefficients (Arth, 1976) and its removal would tend to create lower HREE abundances, thereby increasing La_{cn}/Yb_{cn}.

The Conway granite, in spite of being the most fractionated unit in terms of major elements (Figures 13-18), has significantly lower abundances of most "incompatible" elements than the Sawyer quartz syenite, e.g., the rare earths (except Eu), Th, Zr, and Hf. An extreme example is sample G34 with La at only ∿120 times chondrites and Lu at ∿10 times chondrites. In contrast, Ba, Sr, and Eu contents and (Eu/Eu*) are all higher in the Conway than the Sawyer quartz syenite. These elements are concentrated in feldspars.

For this reason, the trace element features of the

Conway granite are interpreted as resulting from accumulation of early crystallizing feldspar (and later quartz) and the removal of varying amounts of residual, incompatible element-enriched liquid prior to final crystallization. In this sense, the granite may be considered partly a cumulate of early crystallized feldspar and quartz, with a relationship to the Sawyer quartz syenite (or some more evolved liquid) equivalent to that of a cumulate to a parent liquid. The mechanism of separation of early crystals from the residual liquid is discussed in the chapter on geochemical modeling, as are the large variations in REE abundances among the Conway granite samples (Figure 28).

Sample G28 is much more like the Sawyer quartz syenite in terms of major and trace elements and petrography than the other Conway samples. There are two possible explanations. The first is that the sample collected as Conway granite is actually from a large inclusion of Sawyer quartz syenite in the granite. Modell (1936) commented on the occurrence of xenoliths of Sawyer quartz syenite in Conway granite, but did not comment on their size or distribution. The actual assignment of sample G28 to the Conway granite is not critical, and has no effect on conclusions discussed earlier. The second possibility is that sample G28 is a transitional member of a series ranging from Sawyer liquid (sample 12) to dominantly early formed feldspar and quartz (sample G34). In this model, sample G28 contains a high percentage of liquid component.

Sample 6 of the Conway granite is anomalous in its very low La_{cn}/Yb_{cn}, very high Th and Ta, and extremely high U. These features are discussed in Chapter 6.

In general, the felsic rocks in the Belknap Mountains are characterized by considerable light rare earth enrichment, small to extreme negative Eu anomalies, and relatively flat heavy rare earth distributions on a chondrite normalized diagram. The Belknap samples are similar in these characteristics to rocks from the Pikes Peak batholith (Barker et al., 1976).

A plot of Sr versus SiO_2 (Figure 29) is very similar in general relations to the plot of CaO versus SiO_2, as might be expected. A significant difference is that the Conway granite shows variable and higher Sr abundances than the Sawyer quartz syenite. The plots of Ba versus K_2O and Ba versus Sr (Figures 30 and 31) are useful for looking at the effects of alkali feldspar and plagioclase fractionation. There is an initial increase in Ba from the diorite to the Gilmanton monzodiorite, followed by a consistent decrease in the more felsic units (up to the Sawyer quartz syenite). Sr decreases continuously from the diorite to the Sawyer. The extreme range of the three Albany quartz syenite samples illustrates the major effect of feldspar fractionation. On both plots the Conway shows higher values of Sr and Ba than the Sawyer. On Figure 30 (Ba vs. K_2O) Ba drops very sharply while K_2O remains approximately constant. This is because the amount of K_2O removed from the liquid is fixed by the

stoichiometry of potassium feldspar and the percentage of K-feldspar component in the alkali feldspar. For the more felsic units, this amounts to between 6 and 7 percent based on modal abundance of alkali feldspar and the normative Ab/Or ratio. This yields an effective "partition coefficient" for K_2O in alkali feldspar slightly greater than 1, while the Ba partition coefficient in alkali feldspar is on the order of 6 or higher (Arth, 1976). For this reason, Ba decreases much more rapidly in the residual liquids of the Belknap Mountain syenite-Sawyer quartz syenite and Albany quartz syenite.

Trace element abundances are not particularly useful in characterizing the possible source rocks for the various Belknap magmas. Some features such as the relatively low total rare earths in Albany quartz syenite, the high REE and Th in the Lake quartz syenite and the contrasting rare earth patterns in the monzodiorites are probably reflections of the source chemistry or conditions of origin. But, in general, Ba, Rb, K/Rb, and a number of other trace element characteristics show little variation between units with different $^{87}Sr/^{86}Sr$ initial ratio.

A probable explanation for this is that the low values and small range of $^{87}Sr/^{86}Sr)_o$ require low Rb/Sr (and low abundances for other incompatible trace elements) in any possible source region. As a result, the lack of distinctive trace element features in the various Belknap magmas is not

so surprising.

Equally important, fractional crystallization has modified the trace element abundances, so that distinctive features in the original magma inherited from the source have been obscured.

Figure Captions

Figure 26. Chondrite normalized rare earth diagram for the gabbro, diorite, Gilmanton monzodiorite, and Ames monzodiorite. Data normalized to chondrite values of Haskin et al. (1968).

Figure 27. Chondrite normalized rare earth diagram for the Belknap Mountain syenite, Cobble Hill syenite, Albany quartz syenite, and Lake quartz syenite. Data normalized to chondrite values of Haskin et al. (1968).

Figure 28. Chondrite normalized rare earth diagram for the Sawyer quartz syenite and Conway granite. Data normalized to chondrite values of Haskin et al. (1968).

Figure 29. Plot of Sr (ppm) vs. SiO_2 (%) for the Belknap Mountains complex. Legend as in Figure 13.

Figure 30. Plot of K_2O (%) vs. Ba (ppm) for the Belknap Mountains complex. Legend as in Figure 13.

Figure 31. Plot of Sr vs. Ba for the Belknap Mountains complex. Legend as in Figure 13.

Figure 32. Plot of Ta vs. Sc for the Belknap Mountains complex. Legend as in Figure 13.

Figure 33. Plot of chondrite normalized La vs. chondrite normalized Yb for the Belknap Mountains complex. Legend as in Figure 13. Data normalized to chondrite values of Haskin et al. (1968).

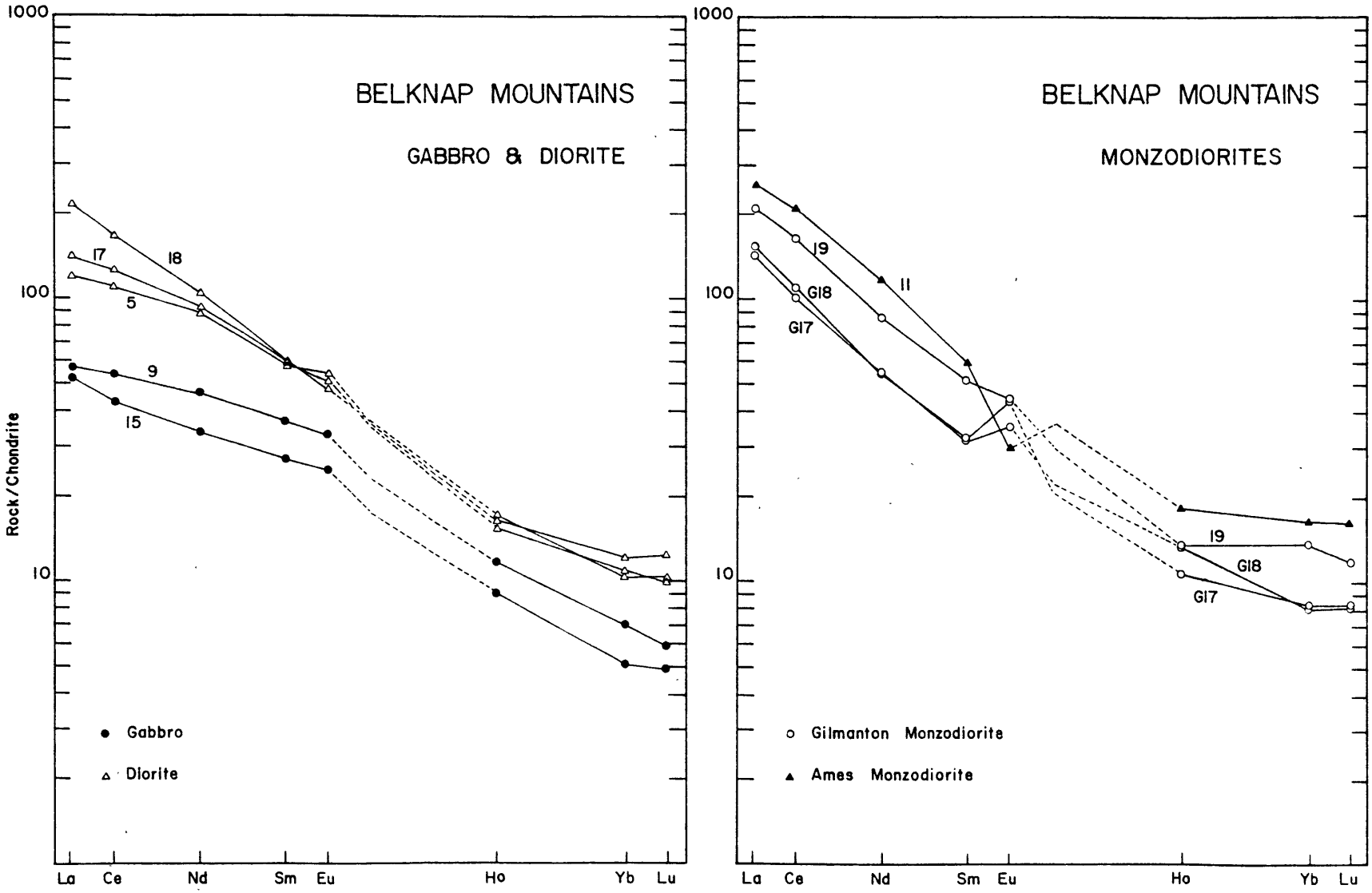
BELKNAP MOUNTAINS
GABBRO & DIORITE
Rock/Chondrite
1000
100
10
17
18
5
9
15
Gabbro
Diorite
La
Ce
Nd
Sm
Eu
Ho
Yb
Lu
BELKNAP MOUNTAINS
MONZODIORITES
19
11
GI8
GI7
Gilmanton Monzodiorite
Ames Monzodiorite

Figure 26

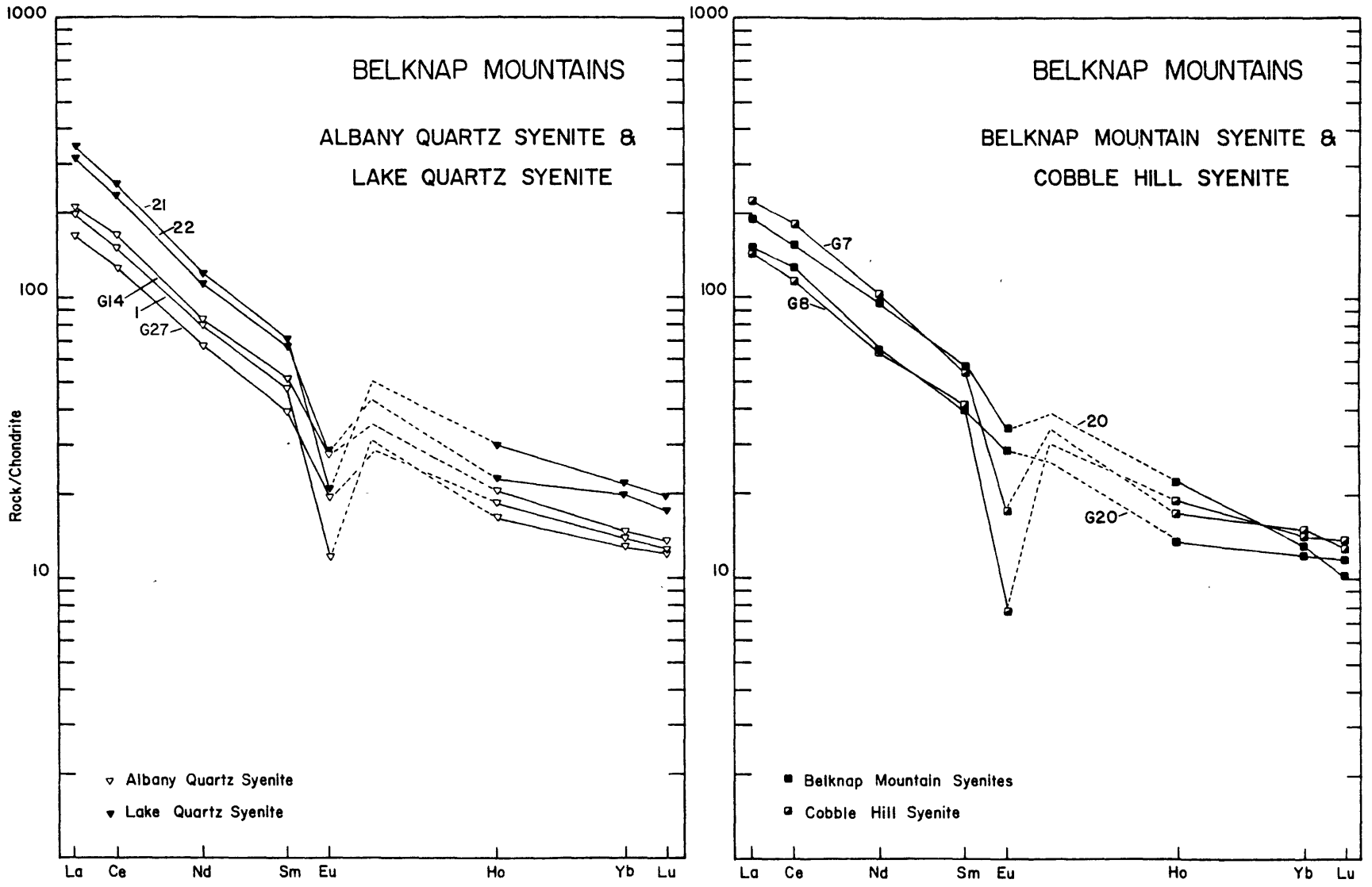
BELKNAP MOUNTAINS
ALBANY QUARTZ SYENITE &
LAKE QUARTZ SYENITE
1000
100
10
Rock/Chondrite
21
22
G14
1
G27
La
Ce
Nd
Sm
Eu
Ho
Yb
Lu
Albany Quartz Syenite
Lake Quartz Syenite
BELKNAP MOUNTAINS
BELKNAP MOUNTAIN SYENITE &
COBBLE HILL SYENITE
G7
G8
20
G20
Belknap Mountain Syenites
Cobble Hill Syenite

Figure 27

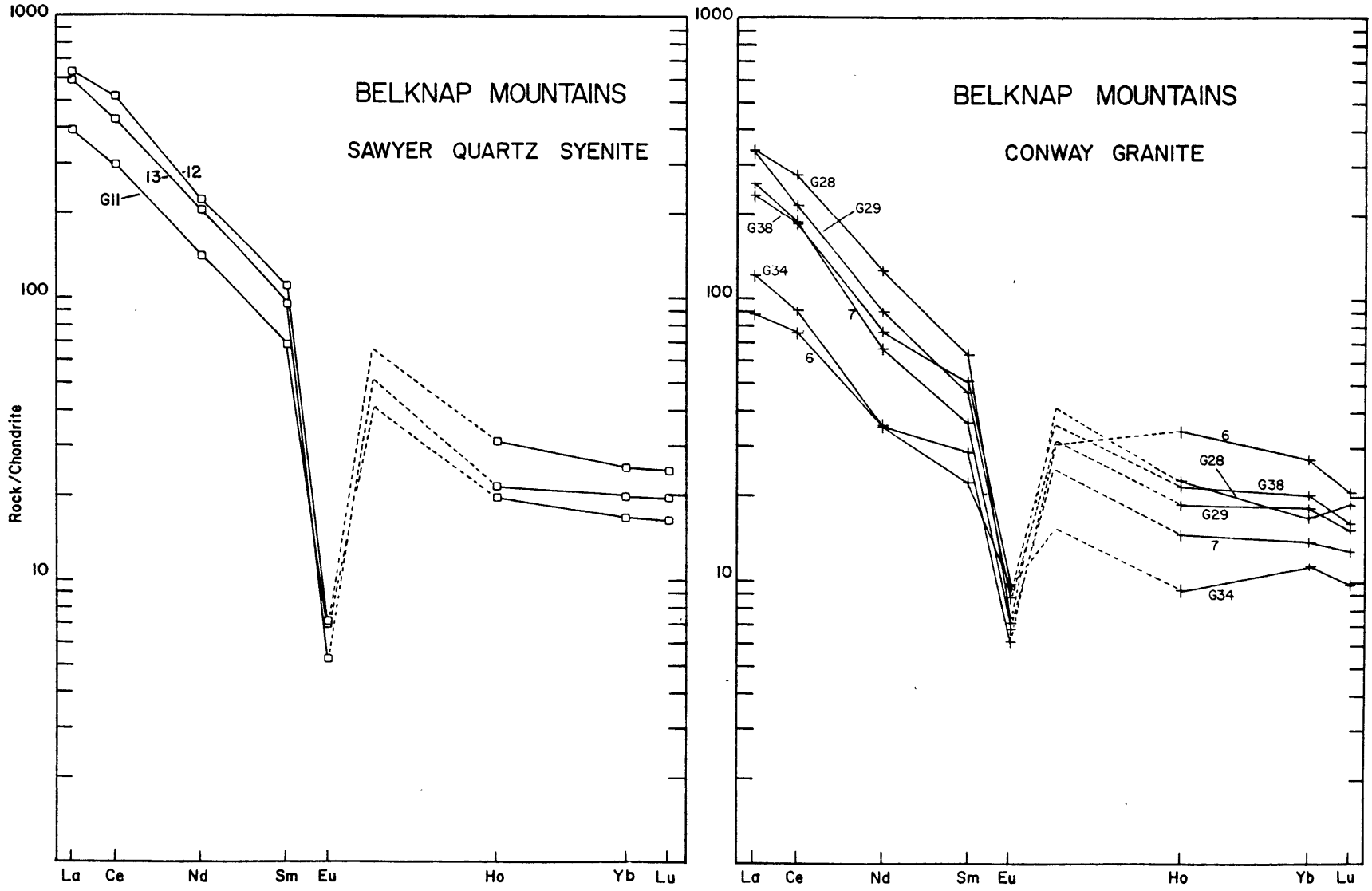
BELKNAP MOUNTAINS
SAWYER QUARTZ SYENITE
1000
100
10
Rock/Chondrite
13
12
G11
La
Ce
Nd
Sm
Eu
Ho
Yb
Lu
BELKNAP MOUNTAINS
CONWAY GRANITE
G28
G29
G38
G34
7
6

Figure 28

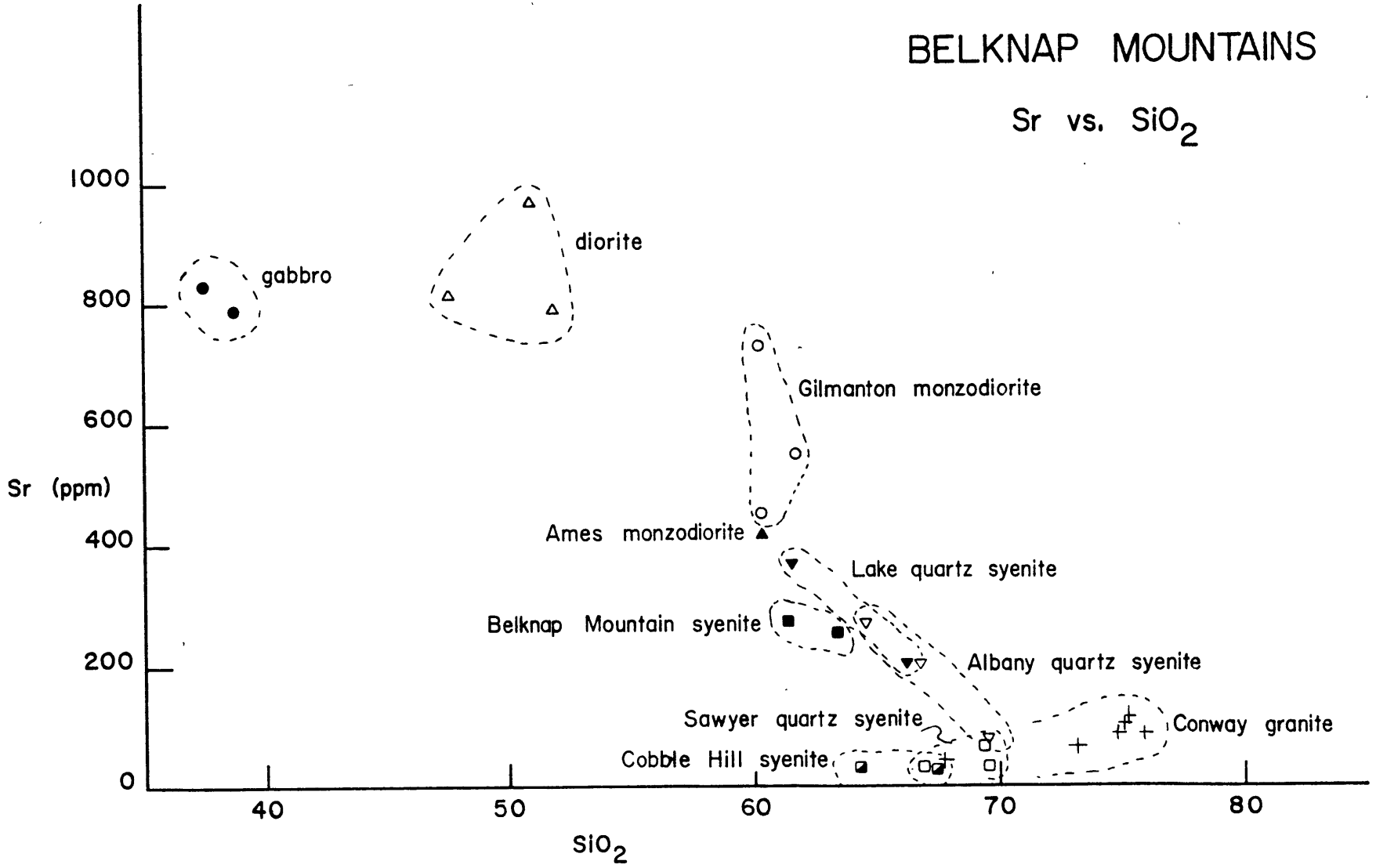
BELKNAP MOUNTAINS
Sr vs. SiO2
1000
800
600
400
200
0
Sr (ppm)
40
50
60
70
80
SiO2
gabbro
diorite
Gilmanton monzodiorite
Ames monzodiorite
Lake quartz syenite
Belknap Mountain syenite
Albany quartz syenite
Sawyer quartz syenite
Conway granite
Cobble Hill syenite

Figure 29

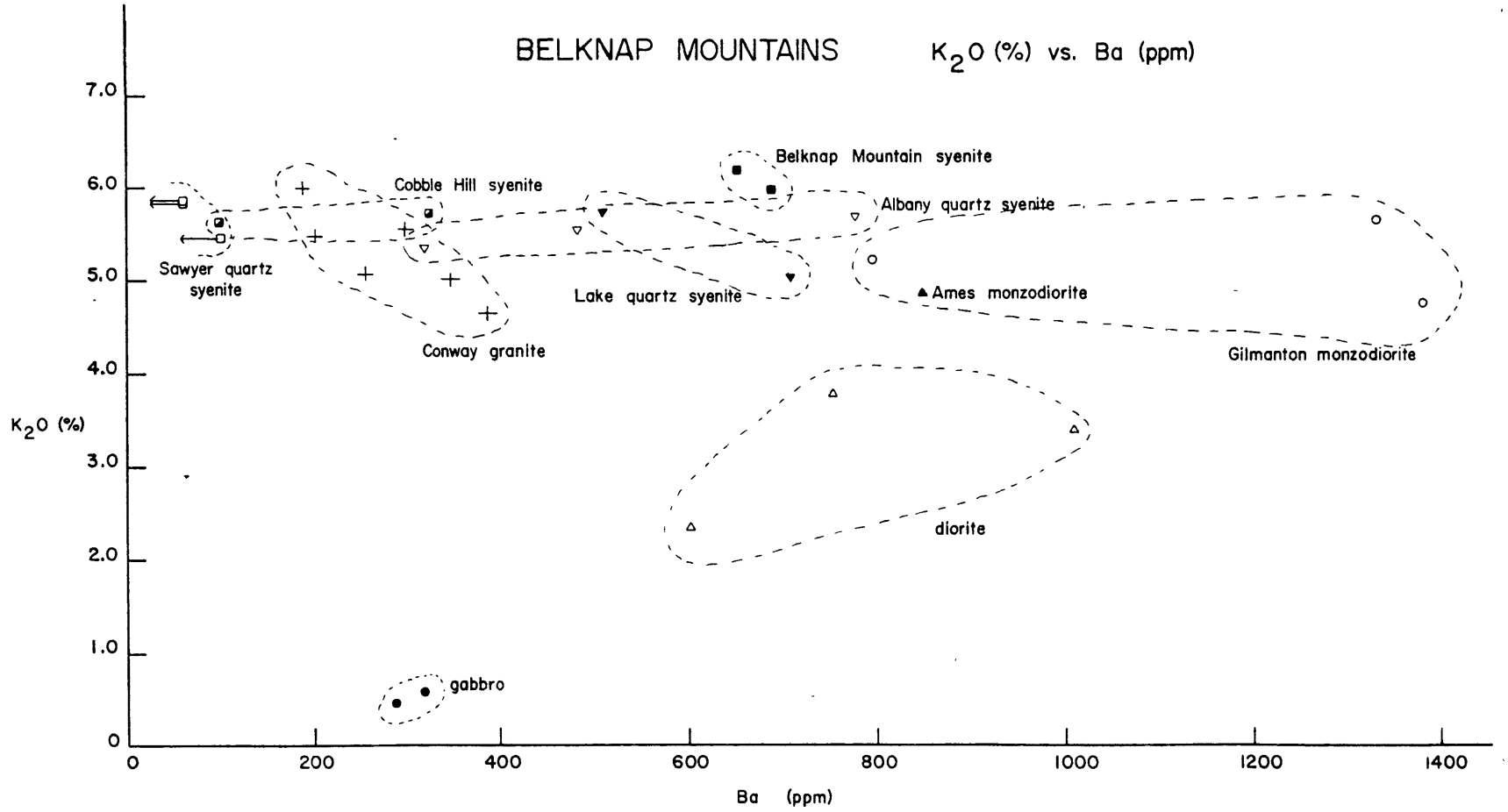
BELKNAP MOUNTAINS
K_2O (%) vs. Ba (ppm)
7.0
6.0
5.0
4.0
3.0
2.0
1.0
0
K_2O (%)
0
200
400
600
800
1000
1200
1400
Ba (ppm)
Belknap Mountain syenite
Albany quartz syenite
Cobble Hill syenite
Sawyer quartz syenite
Lake quartz syenite
Ames monzodiorite
Conway granite
Gilmanton monzodiorite
diorite
gabbro

Figure 30

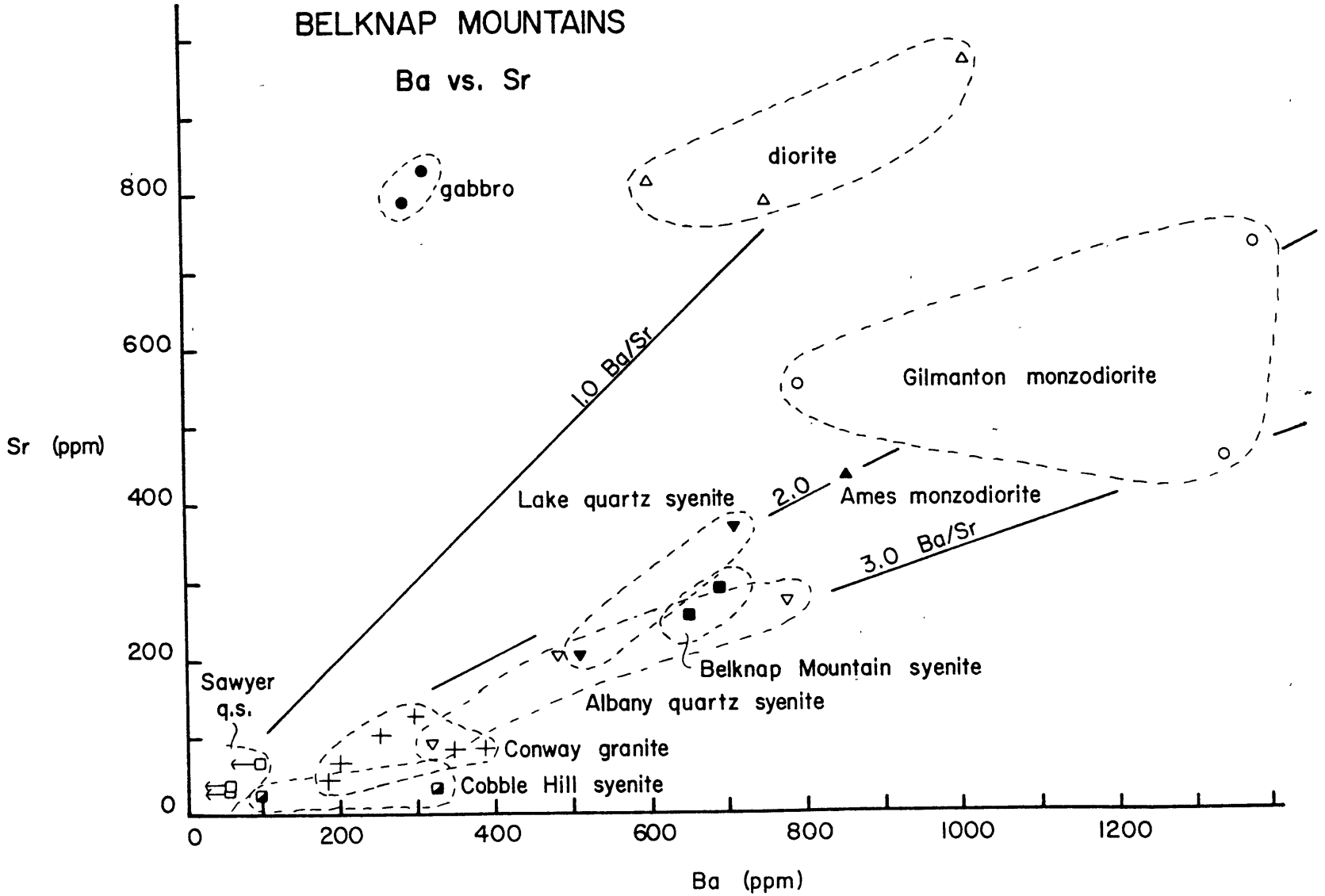
BELKNAP MOUNTAINS
Ba vs. Sr
gabbro
diorite
Gilmanton monzodiorite
1.0 Ba/Sr
2.0
3.0 Ba/Sr
Lake quartz syenite
Ames monzodiorite
Belknap Mountain syenite
Albany quartz syenite
Conway granite
Cobble Hill syenite
Sawyer q.s.
Sr (ppm)
Ba (ppm)
0
200
400
600
800
1000
1200

Figure 31

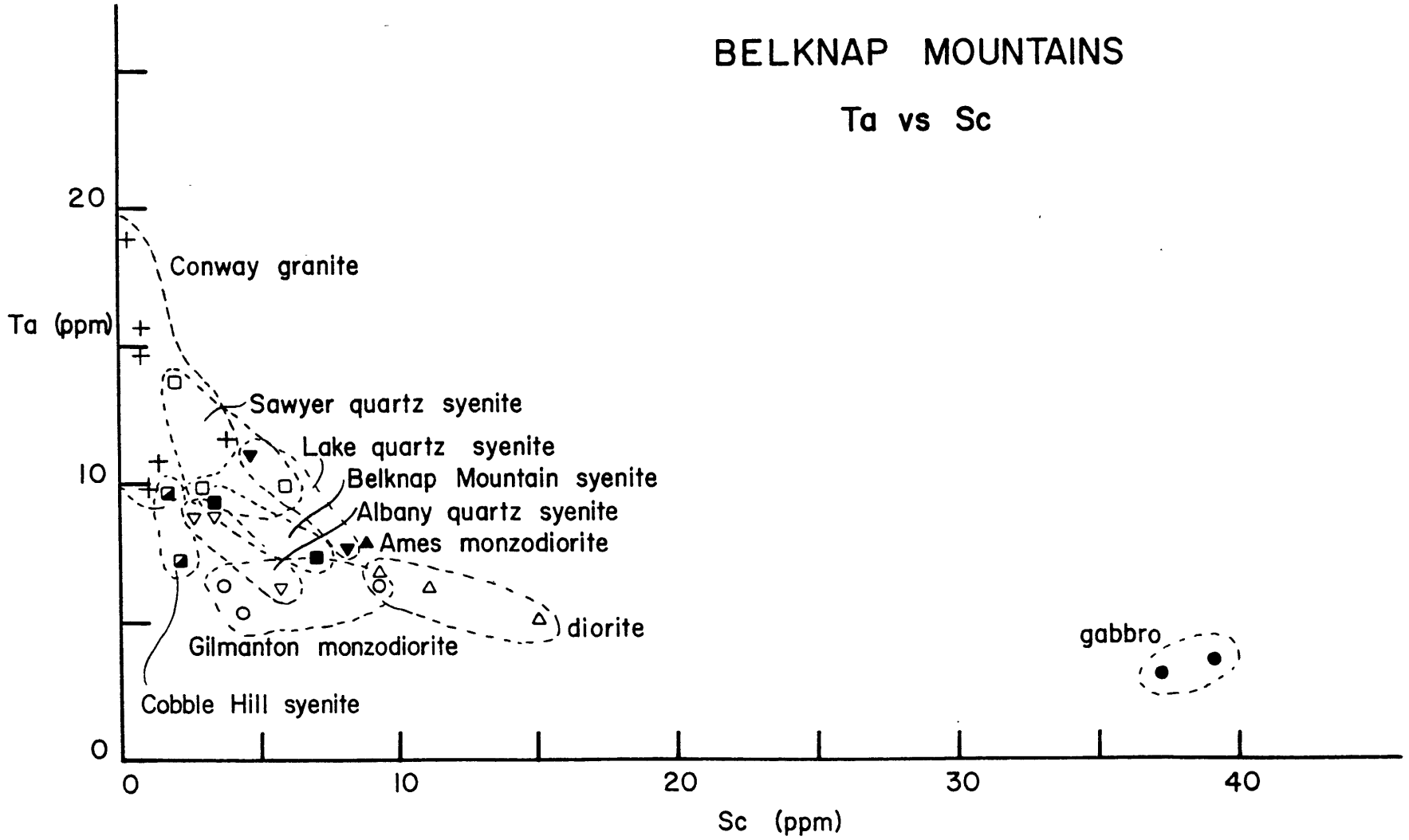
BELKNAP MOUNTAINS
Ta vs Sc
Ta (ppm)
20
10
0
0
10
20
30
40
Sc (ppm)
Conway granite
Sawyer quartz syenite
Lake quartz syenite
Belknap Mountain syenite
Albany quartz syenite
Ames monzodiorite
diorite
Gilmanton monzodiorite
Cobble Hill syenite
gabbro

Figure 32

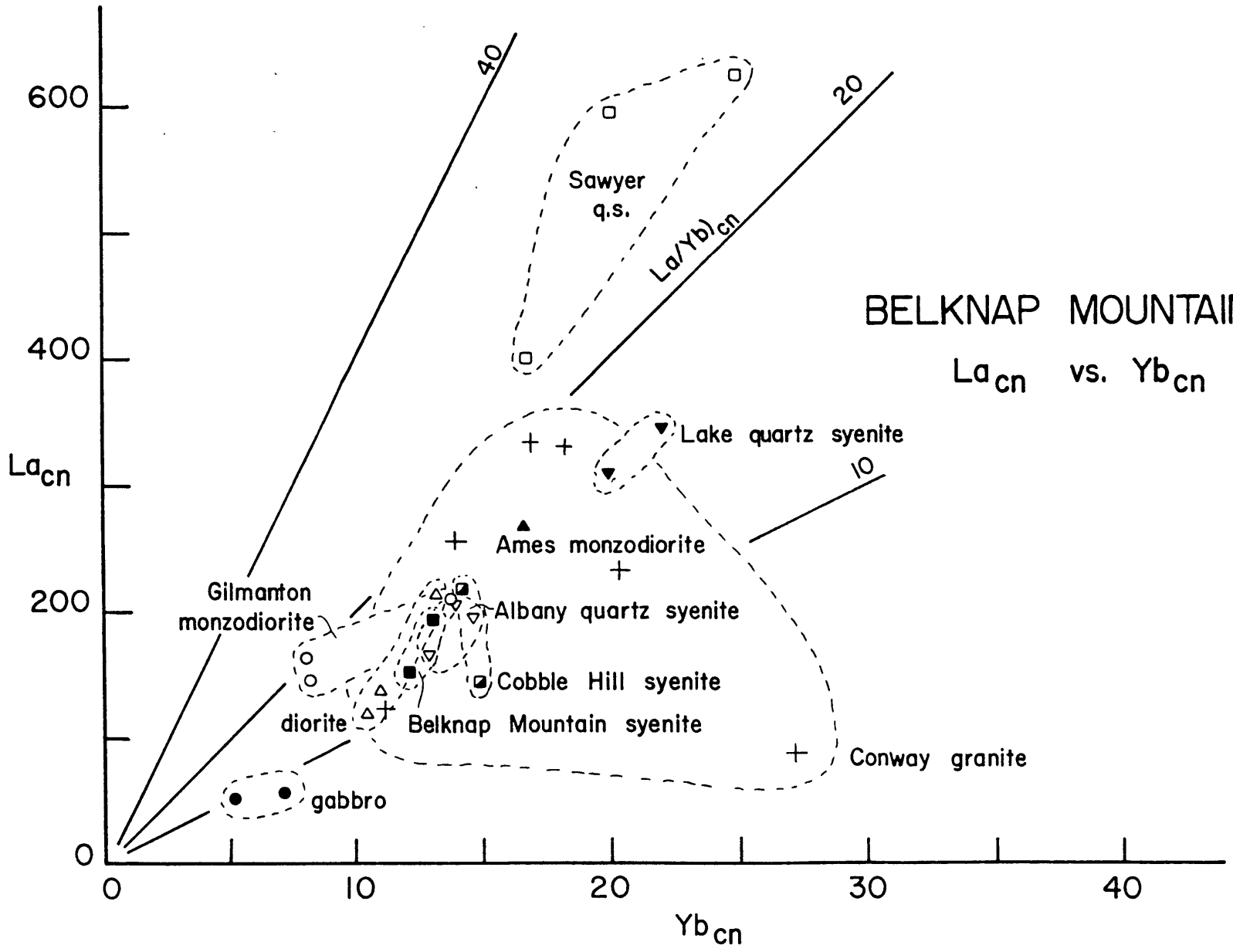
BELKNAP MOUNTAINS
La_{cn} vs. Yb_{cn}
La_{cn}
Yb_{cn}
600
400
200
0
0
10
20
30
40
40
20
10
$(La/Yb)_{cn}$
Sawyer q.s.
Lake quartz syenite
Ames monzodiorite
Albany quartz syenite
Cobble Hill syenite
Belknap Mountain syenite
Conway granite
Gilmanton monzodiorite
diorite
gabbro

Figure 33

CHAPTER 6. GEOCHEMICAL MODELING: RELATIONSHIPS AMONG THE BELKNAP MOUNTAINS COMPLEX UNITS

Introduction

This chapter presents the results of major and trace element modeling of the Belknap Mountains complex data. Isotopic data indicate that a comagmatic relation may exist between the gabbro, diorite, Belknap Mountain syenite, Cobble Hill syenite, Sawyer quartz syenite, and Conway granite (Chapter 3). The isotopic relations are necessary but not sufficient criteria to define a comagmatic relation. If geologically and geochemically reasonable models relating the rock units on the lower regression line can be constructed, they will provide strong evidence for a comagmatic relation. In this sense, much of this chapter deals with attempting to verify the relations suggested by the isotopic data.

There is also the question of the relation of the Gilmanton monzodiorite to the other Belknap magmas. No isochron relation for the Gilmanton was obtained, and there is the possibility of significant post-magmatic effects on the Rb/Sr isotope relations. In terms of major and trace element contents, the Gilmanton plotted in an ambiguous position. Part of this chapter examines the relation of the Gilmanton to the felsic units on the lower regression line.

Major Element Modeling: General Comments

Data on the composition of mafic silicate phases and the range of plagioclase composition in each of the units on the lower regression line were obtained as an input into a Wright-Doherty least squares mixing model program (Wright and Doherty, 1970). The mixing model approach attempts to relate liquid compositions by the addition and subtraction of reasonable mineral phases, although Wright (1974) has pointed out that this approach cannot see through complex fractionation processes (such as the superposition of more than one fractionation). Most applications have dealt with volcanic rocks where a liquid composition can be determined with some certainty (Wright and Doherty, 1970; Wright, 1974; Zielinski, 1975). Before applying this mixing model to the Belknap rocks, we must consider if such models are appropriate for plutonic rocks. Many plutonic rocks may consist of mixtures of crystalline material and residual liquid that do not have the bulk composition of the original liquid. In fact, White and Chappell (1977) proposed a model for the origin of granitoid rocks in orogenic belts that involves a spectrum of bulk compositions ranging from minimum melts which have entirely separated from their residual solid source material to rocks containing very high amounts of restite carried upward in the magma during emplacement. This range in solid-liquid mixtures may occur in the emplacement of any mixture of crystals and liquid, thereby creating residual liquids and mixes of liquids with varying amounts of

residual or cumulate crystals. Specifically, two samples (G17 and G18) of the Gilmanton monzodiorite have geochemical characteristics (high CaO, high Al_2O_3, high Sr, (+)Eu anomaly, low Sc) indicating the presence of cumulate plagioclase.

Mixing and separation of liquids and solids can be achieved by a variety of processes. For example, cauldron subsidence may provide a means of separating early crystalline material from residual liquid (Kingsley, 1931; Modell, 1936). As blocks of the rock fall into the magma chamber, magma is forced upward creating an effect similar to filter pressing. The material intruded as ring dikes may be dominantly residual liquid, or a mush with considerable early crystalline material, depending on the extent of subsidence. In another process, Bateman and Chappell (1978) suggest that accretion of early crystals on wall rocks has created the zoned Tuolumne Lake complex. Although gravitational settling is not considered to be as significant in intermediate and silicic magmas as in basic magmas, the syenites at Kungnât (Upton, 1960) show unmistakable signs of crystal settling; therefore this process may also produce separation of solids and silicic liquids.

Note that the lack of obvious cumulate textures such as observed in mafic layered intrusions (Wager and Brown, 1968) does not preclude cumulate material in the sense of early crystallized material in excess of closed system crystallization. One reason is the orthocumulate growth may completely mask earlier cumulate features. (An extreme case is the Conway granite where the orthocumulate mineralogy is

probably identical in proportions and composition to the cumulate material.)

Another complication in least squares mixing models is that when a large degree of fractionation is involved there are likely to be significant changes in the composition of crystallizing minerals or the appearance of a new phase which may be removed from the magma.

Figure 34 illustrates these problems schematically. Points A, B, C, and D represent the composition of four liquids on an oxide variation diagram of MgO (wt.%) vs. SiO_2 (wt.%). Points A', B', C', and D' represent compositions of the bulk crystalline material in equilibrium with these liquids. A least squares mixing model could be used to relate liquids A and B by addition of solid material A' to liquid B to derive liquid A. As long as the degree of fractionation is small (as from A to B) the variation of MgO with SiO_2 is nearly linear and a good match to the liquid composition A can be calculated. If the degree of fractionation is large, however, as in the case of liquids A and D, any attempt to derive liquid A by addition of solid material A' to D will yield a composition on the line A'-D and provide a poor match to A. Or, consider the case where the degree of fractionation appears small (as in the case B to D"), but where D" does not represent a liquid composition but a partial cumulate of crystalline material D'. Attempting to derive liquid B by addition of B' to D" will not yield a reasonable match.

As a consequence of these complexities an approach such as Wright-Doherty which relates different whole rocks interpreted as liquids by varying amount of liquidus phases may not be appropriate for the Belknap Mountains complex. It may be that a simple mixing relation between bulk rock compositions and liquidus mineral phases does not exist, and attempts to model the petrogenic relations between rocks by a mixing model may only yield solutions with high residuals that are not easily interpretable.

Major Element Modeling: Diorite-Gabbro

From the mafic silicate Fe/Fe+Mg ratios and the range of plagioclase compositions in the diorite, it is clear that the diorite is too fractionated to yield the gabbro as a cumulate (Figures 24, 25). A least squares mixing model yielded very high residuals ($\Sigma R^2 = 9.36$). The relationship between the gabbro and the diorite will be discussed further in the section on trace element modeling.

Major Element Modeling: Diorite-Gilmanton Monzodiorite or Belknap Mountain Syenite

Least squares mixing models were also used to evaluate the diorite as a parental magma for either the Gilmanton monzodiorite (sample 19) or the average Belknap Mountain syenite (Table 9). End member feldspars (An, Ab) were used in two cases, and the ratio of An:Ab in the solution was examined to see if it was geologically reasonable. In the

TABLE 9. WRIGHT-DOHERTY LEAST SQUARES MIXING MODEL SOLUTIONS

FOR DIORITE-GILMANTON MONZODIORITE AND DIORITE-BELKNAP MOUNTAIN SYENITE*

	Clinopyroxene**	Hornblende	Anorthite	Albite	Apatite	Ilmenite	% Crystallization	ΣR^2
Diorite - Gilmanton Monzodiorite (19)	--	47.1	22.2	19.1	2.7	8.9	51.8	2.28
Diorite - Belknap Mtn. Syenite	--	46.3	22.8	19.8	3.0	8.0	56.1	1.67

	Clinopyroxene**	Hornblende	An_{30} Plagioclase	Apatite	Ilmenite	% Crystallization	ΣR^2
Diorite - Gilmanton Monzodiorite (19)	--	40.0	48.7	3.7	7.6	61.9	3.13
Diorite - Belknap Mtn. Syenite	--	40.8	48.5	3.6	7.1	67.4	3.69

* Solutions normalized to 100%

** See Table 7 for mineral compositions

other solutions the feldspar composition was fixed as An_{30} (close to the upper limit of plagioclase observed in the diorite).

The two models which did not fix the An content of the plagioclase yield similar results, with approximately 50-55% crystallization required. Each has high ratios of An to Ab (higher than observed in the diorite) and a high ratio of hornblende to plagioclase. They also both have high values of ΣR^2. Models with fixed An content of the plagioclase also have high residuals, but a lower ratio of hornblende to feldspar, although this ratio ($\sim$0.83) is still higher than that observed in the diorite (average $\sim$0.29). All four models specify that no clinopyroxene fractionation is involved, which conflicts with the presence of moderately abundant clinopyroxene in diorite samples 5 and 17. Because of the high residuals, the lack of clinopyroxene involvement, the high hornblende/plagioclase ratio in the solutions, and the high An/Ab ratio in the first two models, these models are unreasonable.

Major Element Modeling: Gilmanton Monzodiorite and Belknap Mountain Syenite

The Gilmanton monzodiorite (sample 19) was considered as a potential parent liquid from which the Belknap Mountain syenite was derived, and samples G17 and G18 of the Gilmanton were considered as cumulates possibly derived from the average Belknap Mountain syenite. The derivation of the

Belknap Mountain syenite from the monzodiorite (Table 10) yielded moderate residuals ($\Sigma R^2 = 0.28$), and indicated only minor amounts of fractionation of hornblende and anorthite. This last feature (end member anorthite) is unreasonable considering the average An content of the Gilmanton monzodiorite plagioclase (Figure 25). Models with the Gilmanton monzodiorite (samples 17 and 18) as a partial cumulate derived from the Belknap Mountain syenite yielded higher residuals, but more significantly, only small amounts (<3%) of crystalline material was required which seems far too low considering the lower REE contents and marked (+)Eu anomaly in G17 and G18.

The significance of these solutions is particularly difficult to assess because cumulate material in G17 and G18 raises the possibility that major element variations between the samples of monzodiorite and syenite are not produced by a single, simple process. If the samples do not represent a liquid composition, models starting with this assumption will yield meaningless solutions. Because of these uncertainties, the results of the Wright-Doherty modeling do not eliminate the possibility of a relation between the monzodiorite and the Belknap Mountain syenite. The trace element data are used in examining the relationship between the units below.

TABLE 10. WRIGHT-DOHERTY LEAST SQUARES MIXING MODEL SOLUTIONS

FOR GILMANTON MONZODIORITE

	Clinopyroxene**	Hornblende	An	Ab	Or	Apatite	Ilmenite	% Crystallization	ΣR^2
Gilmanton Monzodiorite (19) - Belknap Mtn. Syenite*	--	65.1	34.9	--	--	--	--	11.1	0.28

	Hornblende**	An	Ab	Or	Apatite	Ilmenite	% Trapped Liquid	ΣR^2
Gilmanton Monzodiorite (G17, G18) from Belknap Mtn. Syenite	0.1	2.6	--	--	0.5	--	96.8	0.93

* Solution normalized to 100%

** See Table 7 for mineral compositions

Major Element Modeling: Syenite-Quartz Syenites-Granite

Table 11 lists results of modeling the Sawyer quartz syenite as a liquid derived from the Belknap Mountain syenite. The fit is extremely good ($\Sigma R^2 = 0.003$), and the proportions of the crystallizing phases are in good agreement with petrography (Table 19). The ratio of An:Ab:Or also agrees very well with the normative ratio of these components in the Belknap Mountain syenite (Table 6).

A model deriving the Cobble Hill syenite (here considered a liquid) from the Belknap Mountain syenite also yields a low residual (Table 11), but the Ab/Or ratio is considerably lower than the normative ratio in the Belknap Mountain. This reflects the position of Cobble Hill relative to the Belknap Mountain syenite in the normative Q-Or-Ab diagram. Since the liquidus phases of the Belknap Mountain syenite are not going to have a lower Ab/Or ratio than the whole rock, the model solution is unreasonable. In addition, the small amounts of apatite (0.50%) that must be subtracted from the Belknap Mountain are not sufficient to keep the REE abundances in the Cobble Hill similar to those in the Belknap Mountain after ∿63% crystallization.

The Cobble Hill syenite is not a possible parent magma for the Sawyer quartz syenite because the 60-70% crystallization required to derive the Sawyer would drive the Ba and Sr abundance to less than 10 ppm.

It was not possible to model the Conway granite as a cumulate derived from the Sawyer quartz syenite (as discussed

TABLE 11. WRIGHT-DOHERTY LEAST SQUARES MIXING MODEL SOLUTIONS FOR BELKNAP MOUNTAIN SYENITE, COBBLE HILL SYENITE, AND SAWYER QUARTZ SYENITE*

	Hornblende**	An	Ab	Or	Apatite	Opaque	% Crystallization	ΣR^2
n. Syenite - uartz Syenite	6.9	5.1	47.6	36.3	0.5	3.5	83.4	0.03
n. Syenite - ill Syenite	7.8	6.9	43.3	37.7	0.5	3.8	63.2	0.01

tions normalized to 100%

Table 7 for mineral compositions

in Chapter 5) because the potential cumulate phases (feldspar, quartz) are the normative components of the Conway, and all that was achieved in the modeling was the calculation of an average mode for the Conway granite with no Sawyer liquid involved.

Major Element Modeling: Conclusions

In summary, the Wright-Doherty least squares mixing models provide no support for a cogenetic relation between the diorite and the more evolved rocks. The model requirements of a high hornblende/plagioclase ratio, and a high An/Ab ratio for the subtracted crystalline material lead to the conclusion that this modeling approach is not realistic for evaluating the relationship of the diorite to the other Belknap Mountain complex rocks. However, because of the large gap in SiO_2 from diorite to monzodiorite and syenite, the high residuals may be due to a change in composition of minerals exhibiting solid solution (i.e., hornblende), or fractionation of phases (such as alkali feldspar) not considered in the parent, in addition to the uncertainties produced by samples consisting of partially cumulate material.

As mentioned earlier, the Wright-Doherty modeling of the monzodiorite is difficult to interpret, but does not preclude a relation between the monzodiorite and the Belknap Mountain syenite. A positive result is that a comagmatic relation between the Belknap Mountain syenite and Sawyer

quartz syenite is supported by the mixing models. The relation of the Cobble Hill syenite to both the Belknap Mountain syenite and Sawyer quartz syenite is better examined from the viewpoint of trace elements, and is considered in the next section.

Trace Element Modeling: General Comments

Quantitative modeling of trace element behavior has been reviewed most recently by Allegre and Minster (1978). Hanson (1978) discusses specific applications to granitic rocks. Trace element behavior during crystallization and melting are usually modeled by two end member cases: total equilibrium crystallization (or batch melting) and Rayleigh fractionation/surface equilibrium crystallization (or fractional melting). Shaw (1970) derived equations for partial melting in these two cases, and these equations are also applicable to crystallization.

In the case of total equilibrium between the solid and the liquid, the concentration in the residual liquid over the initial concentration is given by

$$\frac{C_l}{C_o} = \frac{1}{D_o + F(1-D_o)} \qquad (1)$$

where C_l = concentration in the residual liquid; C_o = initial concentration; D_o = bulk solid/liquid distribution coefficient; and F = fraction of liquid remaining or (1 - degree of crystallization).

The concentration in the crystalline material, C_s, is given by

$$\frac{C_s}{C_o} = \frac{D_o}{D_o + F(1-D_o)} \qquad (2)$$

These equations can be used for batch melting. In this case F is the degree of melting (i.e., 90% crystallization and 10% melting both have F = 0.1).

In the case of surface equilibrium, for crystallization

$$\frac{C_l}{C_0} = F^{(D_o-1)} \qquad (3)$$

and

$$\frac{\bar{C}_s}{C_o} = \frac{1-F^{D_o}}{(1-F)} \qquad (4)$$

where $\bar{C}_s$ is the concentration of the aggregate solid. Again, F is the fraction of liquid remaining.

In fractional melting,

$$\frac{\bar{C}_l}{C_o} = \frac{1 - (1-F)^{\frac{1}{D_o}}}{F} \qquad (5)$$

where $\bar{C}_l$ is the aggregate liquid, and

$$\frac{C_s}{C_o} = (1-F)^{(1/D_o - 1)} \qquad (6)$$

gives the concentration in the residual solid. F is the degree of melting.

In equations (1)-(6), D_o is the bulk solid/liquid distribution coefficient for a particular element given by

$$D_o = \sum_{i=1}^{n} D_n x_n \qquad (7)$$

where D_n = solid/liquid distribution coefficient for mineral n; x_n = fraction of phase n in the solid ($\sum_{i=1}^{n} x_n = 1$).

The equations describing trace element behavior during melting ((1), (2), (5), (6)) are for the case of modal melting, i.e. where the phases melt in proportion to their abundances in the rock. The analogous equations for non-modal melting are (Shaw, 1970)

$$\frac{C_l}{C_o} = \frac{1}{D_o + F(1-P)} \qquad (8)$$

$$\frac{C_s}{C_o} = \frac{D}{D_o + F(1-P)} \qquad (9)$$

for total equilibrium and

$$\frac{\overline{C}_l}{C_o} = \frac{1}{F}\left(1 - \left(1-\frac{PF}{D_o}\right)^{1/P}\right) \tag{10}$$

$$\frac{C_s}{C_o} = \frac{1}{1-F}\left(1-\frac{PF}{D_o}\right)^{1/P}) \tag{11}$$

for fractional melting, where if x_n is the initial fraction of phase n in the solid and p_n is the fraction that phase n contributes to the melt

$$D_o = \sum_{i=1}^{n} D_n x_n \tag{12}$$

$$P = \sum_{i=1}^{n} p_n D_n \tag{13}$$

and

$$D = \frac{D_o - PF}{1 - F} \tag{14}$$

In the case of total equilibrium, the assumption is that diffusion in the solid is rapid enough to maintain equilibrium between solid and liquid during crystallization of a liquid (or melting in an initially homogeneous solid). In the case of surface equilibrium crystallization, diffusion in the solid is assumed slow with respect to the crystal growth rate so that only the surface layer of the solid is in equilibrium with the liquid at any time. For fractional

melting, the assumption is that the liquid is removed from contact with the (homogeneous) solid as it is formed, and collected in a magma chamber. Therefore, fractional melting is not a Rayleigh process in the same sense as fractional crystallization because the solid is homogeneous throughout the process.

A decision as to which set of assumptions is valid depends on cooling rate, crystal growth rate, and values of diffusion coefficients in the solid (in the case of crystallization) or on the state of stress in the region of melting and geometry of partial melting (Allegre and Minster, 1978).

An alternative model in the case of crystallization is incremental fractional crystallization (McCarthy and Hasty, 1976). This model assumes some finite amount of crystallization before diffusion becomes inadequate to maintain equilibrium between the solid and the liquid. From McCarthy and Hasty (1976)

$$\frac{C_l}{C_o} = \prod_{i=1}^{n} \left[\frac{1}{f_i'(D_i-1)+1}\right] \qquad (15)$$

where f_i' is the increment of the existing liquid that crystallizes during the i^{th} interval, and C_l/C_o gives the liquid concentration after the n^{th} interval.

The concentration of the n^{th} solid increment is

$$\frac{C_{s,n}}{C_o} = D_n \prod_{i=1}^{n} \left[\frac{1}{f_i'(D_i-1)+1}\right] \qquad (16)$$

with f_i' and D_i as above and D_n the distribution coefficient for the n^{th} interval. The bulk solid concentration can be obtained by numerically summing over the n solid increments. Incremental melting (Suen, 1978) is similar in that it assumes a certain finite amount of melting prior to separation of the residual solid and liquid. The results for incremental processes lie between the two end members. At the last stages of surface equilibrium crystallization C_l/C_o for elements with $D << 1.0$ approaches infinity (as does the concentration of the instantaneous solid). Incremental fractional crystallization eliminates this singularity.

Results for total equilibrium and surface equilibrium crystallization were considered in the modeling of the Belknap magmas. The best fit in some cases is provided by an intermediate case.

One of the major assumptions in trace element modeling is the selection of a set of solid/liquid distribution coefficients for the mineral phases involved in the modeling. McIntire (1963) and Arth (1976) provide detailed reviews of the theory of solid/liquid distribution coefficients. In general, equilibrium partitioning of an element will depend on temperature, total pressure, other intensive parameters (most notably fo_2), and composition of the solid and the

silicate melt.

The effect of total pressure is probably negligible for the Belknap Mountains complex. Shimizu (1974) showed that for K, Rb, Cs, Sr, and Ba in clinopyroxene the effect of total pressure is minor between 0-10 kilobars. Since the pressure of crystallization of the Belknap Mountains and similar subvolcanic complexes is on the order of 1-2 kilobars (Chapter 4, also Czamanske et al., 1977), the effect of pressure is insignificant compared to other uncertainties.

Drake (1975) examined the effect of fo_2 on the partitioning of Eu into plagioclase. Eu is easily reduced to the +2 state (in contrast to the other REE) and the partitioning of Eu into feldspar is a sensitive function of fo_2. As a result the uncertainty associated with choosing an Eu distribution coefficient for feldspar is compounded. This problem is summarized in Figure 35, which is a plot of phenocryst/matrix distribution coefficients from a set of feldspars. (Data is from Schnetzler and Philpotts, 1970). With the exception of GSFC 271, the Sr data are very linear with respect to An content of the feldspar (which reflects effects of temperature, melt, and mineral composition). On the other hand, Eu (for which Sr is considered an analogue in the +2 state because of similar ionic radii) shows a wide scatter of points (note the different scales used for D_{Eu} and D_{Sr}). This is interpreted as a result of fo_2 effects on the Eu distribution coefficient.

The effects of temperature and mineral/melt composition

have only been separated in a few studies (Watson, 1977; Hart and Davis, 1978). They dealt with Mn and Ni in the system forsterite/liquid, and their results can only be a general guide for modeling the Belknap Mountains complex. In solid solution series such as the feldspars or hornblende, the effect of temperature and mineral/melt composition are difficult to separate. Drake and Weill (1975) studied partitioning of Ba, Sr, and REE into plagioclase and obtained absolute values of D_{Sr}, D_{Ba}, and D_{REE} in reasonable agreement with phenocryst/matrix data. However, they did not separate the temperature effects from the mineral/melt composition effects, and while they interpreted their results to indicate an increase in D_{Ba}, D_{Sr}, and D_{LREE} with decreasing temperature much of the increase in D may be due to compositional effects.

Unfortunately, there is little experimental trace element partitioning data in the relevant system (haplogranite plus hornblende). Therefore, the distribution coefficient data used in modeling are from phenocryst/matrix studies. There are major problems in using phenocryst/matrix distribution coefficients, for example, the unknown dependence on temperature and mineral/melt composition. The ideal situation is to use distribution coefficient data from your own suite of rocks (as suggested by Hanson, 1978), but this is not practical for plutonic rocks. The next best approach is to use distribution coefficient data from rocks with a similar bulk composition to the rock being studied. This is the approach suggested by Arth and Hanson (1975) and Arth

(1976). Since the composition of the liquid (and therefore the composition of the mineral phases in a solid solution series) is roughly a function of temperature (degree of crystallization), selecting distribution coefficients from rocks with similar bulk composition will tend to compensate for the temperature and mineral/melt composition dependence. This will work best for a relatively simple series like plagioclase as opposed to hornblende which shows much greater variation in composition.

Another problem is the assumption of equilibrium made in phenocryst/matrix studies. Albarede and Bottinga (1972) have discussed the effect of trace element zoning in the solid and liquid on the measured value of the distribution coefficient. Since the approach to equilibrium in slowly cooled plutonic rocks will not be the same as in volcanics, the applicability of phenocryst/matrix data from volcanics to plutonics is questionable.

A final problem with applying distribution coefficients obtained from such studies is the difficulty of obtaining mineral separates free from contaminant matrix material (high in "incompatible" elements) and free of inclusions. Hart and Brooks (1974) showed the considerable effect cloudy inclusions of clinopyroxene can have on the measured distribution coefficients of K, Rb, Cs, Sr, and Ba.

An observation which provides a positive point for the use of phenocryst/matrix data is that while there may be significant variation in the absolute value of a distribution

coefficient in a series like the REE, there is little relative change in values of D between the REE (Eu excepted). Therefore, the effect of a mineral on the relative REE pattern of a derived liquid will remain the same despite the uncertainty in the absolute value of D.

The uncertainty in absolute value of D is most critical for elements with D values appreciably greater than 1 (i.e., Sr in feldspar; Ba in alkali feldspar; Sc in hornblende). This is because depletion of a "compatible" element during crystallization is a more efficient process than enrichment of an "incompatible" element, particularly at high degrees of crystallization (Gast, 1968). (The opposite is true for small degrees of partial melting.)

With these considerations in mind, Table 12 lists the solid/liquid trace element distribution coefficients used in the geochemical modeling of the Belknap magmas. Following Arth and Hanson (1975) and Arth (1976) the table is divided into three general rock types: basic and intermediate; dacitic; and rhyolitic (corresponding to gabbroic and dioritic, syenitic, and granitic). The distribution coefficients for Rb, Sr, Ba, and the REE are very similar to those suggested by Arth (1976) since the same data base was used to compile the list. There is considerably less data available for the remaining elements used in the modeling (Sc, Ta, Th, U, Hf).

The distribution coefficients for Ta, Th, U, and Hf in major rock forming phases are considered to be small

TABLE 12. SOLID/LIQUID TRACE ELEMENT DISTRIBUTION COEFFICIENTS USED IN GEOCHEMICAL MODELING[a]

Basic and Intermediate Magma

	Diopside	Hornblende	Plagioclase	Apatite[c]
La[b]	0.05	0.14	0.15	11
Ce	0.08	0.20	0.12	17
Nd	0.12	0.33	0.08	26
Sm	0.18	0.52	0.066	31
Eu	0.18	0.59	0.4-2.0	15
Ho[b]	0.19	0.59	0.06	21
Yb	0.16	0.49	0.06	12
Lu	0.13	0.43	0.06	10
Rb	0.015	0.30	0.02	--[d]
Sr	0.12	0.45	1.2-3.0	3
Ba	0.01	0.42	0.20	--
Sc	3	2-4	--	--

Dacitic (Syenitic) Magma

	Hornblende	Plagioclase	Alkali Feldspar
La[b]	0.43	0.18	0.07
Ce	0.90	0.18	0.045
Nd	2.80	0.17	0.025
Sm	3.90	0.10	0.018
Eu	3.40	0.80-2.0	1.0-2.0(?)
Ho[b]	6.00	0.06	0.006

TABLE 12. continued

Dacitic (Syenitic) Magma

	Hornblende	Plagioclase	Alkali Feldspar
Yb	4.80	0.054	0.006
Lu	4.00	0.052	0.006
Rb	0.02	0.05	0.4
Sr	0.2	2.5-3.5	3.75
Ba	0.05	0.25	6.
Sc	3-10(?)	--	--

Rhyolitic (Granitic) Magma

	Hornblende	Plagioclase	Alkali Feldspar	Apatite	Zircon[e]
La[b]	0.8	0.33	0.07	22	
Ce	1.5	0.27	0.045	35	
Nd	4.3	0.21	0.025	58	
Sm	7.6	0.13	0.018	62	
Eu	5.1	1.5-2.5	1.0-2.0(?)	30	
Ho[b]	12.5	0.06	0.006	43	
Yb	8.3	0.05	0.006	24	
Lu	5.5	0.045	0.006	20	
Rb	0.02	0.10	0.4	--	
Sr	0.2	3.5-4.5(?)	3.75	4	
Ba	0.05	0.3	6.	--	
Sc	5-??	--	--	--	

TABLE 12. continued

a Where a range of distribution coefficients is given (Sr, Eu, Sc), the value used in a model is indicated in the appropriate table or figure, or in the discussion.

b Determined by extrapolation or interpolation of published data.

c Since no data for apatite in intermediate rocks were found, values assumed to be 1/2 those in dacites and rhyolites.

d Assumed to be <0.01.

e See section on modeling of Conway granite for discussion of zircon REE distribution coefficients.

References

Arth (1976)

Arth and Hanson (1975)

Ewart and Taylor (1969)

Higuchi and Nagasawa (1969)

Philpotts and Schnetzler (1970)

Schnetzler and Philpotts (1970)

Noble and Hedge (1970)

Nagasawa (1970)

Nagasawa (1971)

Nagasawa and Schnetzler (1971)

Sun and Hanson (1975)

Arth and Barker (1976)

(less than 0.01-0.05). However, they may occur in significant quantities in accessory phases such allanite (Th, U, REE), sphene (Th, U, Sc, Hf, Ta) (Noyes, 1978), and zircon (Th, U, Hf, and possibly Sc and Ta). The problem of accessory phases and their effect on the trace element abundance in the Belknap samples must be considered before models involving primarily the major rock forming phases can be discussed. Because of large values of D for certain trace elements in phases such as apatite, allantie, and zircon, trace element characteristics in a analyzed sample may be a function of the inhomogeneous distribution of these phases in the sample of rock unit (see Appendix II for a discussion of this problem with respect to splits).

However, it should be possible to determine the role of an accessory phase in determining unusual abundances by examination of several trace elements. For example, a large contribution to the REE abundance by apatite should be accompanied by a high value of P_2O_5, whereas allanite will raise Th and U, as well as the LREE.

Using this approach of correlated trace elements to identify the contribution of accessory phases to anomalous trace element abundances allows an estimation of the significance of geochemical models not involving these phases.

A final input into the trace element modeling is the mineral proportions in the crystallizing assemblage (or source for partial melting). These proportions are obtained either from the Wright-Doherty least squares mixing models

(in the case of the Belknap Mountain syenite to Sawyer quartz syenite) from the modal proportions of the phases in the parent rock or inferred cumulate material. These proportions are necessary for calculation of the bulk distribution coefficient, which is assumed constant for the entire episode of crystallization. This last assumption indicates that only the average bulk distribution coefficient is considered, and the fact that D_{Sr} in plagioxlase or D_{HREE} in hornblende may change over the course of 50-70% crystallization must be discussed when necessary.

Because of reasonably abundant phenocryst/matrix data for the REE, Rb, Sr, and Ba, and their sensitivity to major mineral phases involved in the evolution of magmas, emphasis has been placed on modeling these elements. Sc has also been used to evaluate the role of hornblende (and clinopyroxene), but less emphasis is placed on the behavior of Th, Hf, and Ta.

Trace Element Modeling: Diorite-Gabbro

We know from the mineral composition of the diorite that it is too fractionated to serve as a parent for the partly cumulate gabbroic material. However, fractional crystallization is not very efficient in enriching a liquid in incompatible elements in the early stages of crystallization. In addition, the relative abundance of elements with $D < 1$ will change by only small amounts. Therefore, modeling the gabbro as a cumulate derived from the diorite

should indicate whether a less fractionated diorite could serve as a parent.

Figure 36 shows the results of REE models for the gabbro. D_{Eu}^{Plag} was assumed to be 0.6, reflecting the high An content (average An_{50-60}) of the plagioclase in the gabbro. The relative proportions of the cumulate phases (clinopyroxene, plagioclase, opaques) were obtained from the modes of the gabbro. Models with 0.5% cumulate apatite were also considered. A reasonable fit to the observed rare earth pattern of the gabbro was obtained with ∿35-45% trapped liquid (average of diorite samples 5 and 17). If no cumulate apatite is assumed, the trapped liquid controls the REE abundance of the model gabbro. The 0.5% apatite will contain up to 20% of the REE if it is a cumulate phase. The model REE patterns are too steep, which might be expected if the diorite is fractionated from the original parent for the gabbro. However, the degree of LREE enrichment $(La/Yb)_{model}/La/Yb)_{gabbro} \simeq 1.30$) is too large for the bulk distribution coefficients of the crystalline material ($D_{La}^{Model\ C} = 0.068$; $D_{Yb}^{Model\ C} = 0.058$). The LREE in diorite sample 18 appear to have been enriched considerably by introduction of LREE-rich material from the Conway granite (Chapter 5). Diorite samples 5 and 17 may also have been affected, but to a much smaller degree, and this may be the cause of the higher La/Yb ratios in the models.

Predicted abundances for Rb, Sr, Ba, Ta, Hf, Th, U, and Sc based on REE models B and C (35-45% trapped liquid,

no cumulate apatite) are shown in Table 13. Mineral/liquid distribution coefficients were assumed equal to zero except for Sr and Ba in plagioclase and Sc in clinopyroxene and opaques. As the results indicate, Rb, Th, and U all yield high to slightly high abundances, suggesting some contribution of incompatible element-enriched material to the diorite from a source such as the Conway granite. This is especially true for Rb.

Calculated Sr abundances agree very well with the actual gabbro concentrations. D_{Sr}^{Plag} appears to be in the range 1.50-1.75, in agreement with the high An content of the plagioclase. Model Ba abundances are ∿20% high, but diorite samples 5 and 17 have very different Ba concentrations (600 ppm and 1000 ppm, respectively), and the average concentration may be too high. An initial value of 600 ppm Ba (sample 5) yields excellent agreement with the gabbro abundances.

Ta results show <u>low</u> predicted abundances, suggesting a Ta-bearing phase in the gabbro, possibly apatite(?). Sc also yields very low model abundances. This is probably because the diorite liquid has been fractionated (with removal of Sc in clinopyroxene, hornblende, and opaques) from the true gabbro parent. The same is true for Co (60 ppm in the gabbro; 16 ppm in the diorite).

In summary, trace elements such as Sr, and to a lesser degree Ba, are consistent with the comagmatic relationship implied by the isotopic data. However, strongly incompatible trace elements (LREE, Rb, Th, U) require that even diorite

TABLE 13. PREDICTED TRACE ELEMENT CONCENTRATIONS IN THE GABBRO BASED ON REE MODEL

Element	Parent Magma Concentration[a]	Predicted Concentration	Actual Concentration[b]	Comments
Rb	84	30-38 ppm	12-15 ppm	
Sr	875 ppm	840-930 ppm 760-850 ppm	790-830 ppm	$D_{Sr}^{Plag}=1.75$ $D_{Sr}^{Plag}=1.50$
Ba	800 ppm 600 ppm[c]	340-410 ppm 260-320 ppm	290-320 ppm	$D_{Ba}^{Plag}=0.20$
Ta	5.8 ppm	2.0-2.6 ppm	3.0-3.5 ppm	
Hf	7.5 ppm	2.6-3.4 ppm	2.9-3.2 ppm	
Th	4.8 ppm	1.7-2.2 ppm	1.0-1.5 ppm	
U	1.7 ppm	0.6-0.8 ppm	0.4 ppm	
Sc	12.5 ppm	16-17 ppm	34-38 ppm	$D_{Sc}^{Ilm}=1.8$ [d]

[a] Average of diorite samples 5 and 17 except for Rb (sample 17).

[b] Range of gabbro concentrations.

[c] Ba concentration in diorite sample 5.

[d] Paster et al., 1974.

samples 5 and 17 have been enriched in these elements by contamination (see Chapter 5) or later fractionation. Compatible trace elements such as Sc confirm the mineral composition data that these diorite samples are too fractionated to serve as the parent magma of the gabbro.

Trace Element Modeling: Diorite - Gilmanton Monzodiorite and Belknap Mountain Syenite

The modeling of liquids derived by fractional crystallization of the diorite is complicated by several unknowns. The large gap in SiO_2 from the diorite to the monzodiorite and syenite make it difficult to estimate the crystalline assemblage removed from the diorite. Furthermore, this range in SiO_2 implies a significant range in temperature and mineral/melt composition, introducing the possibility of significant changes in solid/liquid distribution coefficients during crystallization. Finally, it appears likely that the diorite samples were enriched in incompatible elements during intrusion of the Conway granite.

However, Sr and Ba abundances were probably not affected by intrusion of the Conway, and are useful in placing constraints on the bulk crystalline assemblage necessary to provide liquids like the Gilmanton (sample 19) or the Belknap Mountain.

The Wright-Doherty models indicate that $\sim$60% crystallization is required to produce liquids with SiO_2 contents similar to the monzodiorite and syenite. Given initial Sr

and Ba concentrations in the diorite of 875 ppm and 600 ppm, respectively, we can calculate the bulk solid/liquid distribution coefficient required to derive the Gilmanton and Belknap Mountain abundances. For total equilibrium and surface equilibrium cases we get:

	Gilmanton (19)		Ave. Belknap Mtn.	
	D_{Sr}	D_{Ba}	D_{Sr}	D_{Ba}
Total Equilibrium	2.32	0.08	4.82	0.85
Surface Equilibrium	1.71	0.12	2.30	0.90

The total equilibrium case yields bulk D_{Sr} values which are unreasonably high given the range of phenocryst/matrix values for D_{Sr} in plagioclase and alkali feldspar. Thus, surface equilibrium is the best model. A bulk D_{Ba} close to 1 for the Belknap Mountain syenite model implies that significant amounts of alkali feldspar are required. This was not indicated in the Wright-Doherty modeling because inclusion of alkali feldspar (end-member Or) as a possible fractionating phase yielded an average mode for the diorite as a solution, with no derived liquid included (similar to problems in modeling the Conway granite as a cumulate from the Sawyer quartz syenite). No alkali felspar is indicated in the bulk D_{Ba} calculated for the Gilmanton monzodiorite.

Using these values of bulk D_{Sr} we can calculate the ratio of hornblende to plagioclase required to obtain the Gilmanton monzodiorite from the diorite liquid. This ratio

is ∿0.8 using values of 3.0 for D_{Sr}^{Plag} and 0.45 for D_{Sr}^{Hbd}, and assuming plagioclase and hornblende make up 90% of the crystalline assemblage. (The contribution of apatite and opaques to the bulk D_{Sr} is negligible.) The ratio is very similar to the hornblende/plagioclase ratio of the Wright-Doherty model specifying An_{30} plagioclase (= 0.82) (Table 9). The bulk D_{Ba} for this assemblage is 0.27, which gives Ba concentrations of ∿1200 ppm at 60% crystallization, compared to an actual value of 1330 ppm. This low model value may be due to uncertainty in the Ba mineral/liquid distribution coefficients for plagioclase and hornblende.

Models for the REE using a crystalline assemblage of 40% hornblende, 50% plagioclase, 1.5-2.5% apatite, and 7.5% opaques were tried for a range of D_{REE}^{Hbd} ranging from basic to dacitic. Results indicate that the best fit was obtained with basic or .75 basic/.25 dacitic distribution coefficients and 2.5% apatite (Figure 37). D_{Eu}^{Plag} was taken as 1.0.

Using an initial concentration of 12.5 ppm Sc in the diorite with D_{Sc}^{Hbd} ∿ 3 and D_{Sc}^{Opaque} ∿ 1.8, the calculated Sc concentration in the derived liquid (with the same mineral proportions as the REE model (Figure 37)) would be 9.1 ppm, very close to the observed Sc in sample 19 (9.2 ppm). With average diorite values for initial concentrations Rb, Ta, and Hf yielded high predicted abundances, and Th and U good matches in Gilmanton monzodiorite sample 19.

The reasonable match to the observed REE, Sr, Ba, and

Sc abundances in Gilmanton monzodiorite sample 19 with a mineral assemblage and degree of crystallization in agreement with major element modeling would normally strongly suggest a comagmatic relation. In this case, the uncertainties associated with the REE modeling and the high percentage of hornblende in the model assemblage relative to that observed in the diorite makes the relationship questionable.

The calculated bulk D_{Sr} and D_{Ba} for the Belknap Mountain syenite indicate an average assemblage of ∿10-12% alkali feldspar, 57-58% plagioclase, and 20% hornblende (plus apatite and opaque oxides) is necessary to match the Sr and Ba concentrations at 60% crystallization. This assemblage has a very low hornblende/feldspar ratio (∿0.31), and has too high an average SiO_2 content to allow the diorite (initially Ne normative) to fractionate to SiO_2 saturated and oversaturated compositions (as indicated by the Wright-Doherty modeling which suggests a ratio closer to 0.8).

REE modeling using an average of diorite samples 5 and 17 as an initial concentration indicates LREE abundances too high in the predicted patterns for any reasonable set of D^{Hbd}_{Ree} and proportions of apatite. Again, the uncertainty in the diorite LREE abundances makes these results difficult to interpret.

The conclusions drawn from the geochemical modeling of the diorite are that major and trace element abundances suggest a possible relation to the Gilmanton monzodiorite (sample 19), but that the modal hornblende in the diorite appears

insufficient to generate the calculated liquids by hornblende subtraction. The amount of hornblende necessary to generate the Belknap Mountain syenite Sr and Ba concentrations is not reasonable from a major element standpoint, and there is also difficulty in obtaining a match to the observed REE abundances in the syenite. The major problem is a lack of intermediate compositions in the sample suite. Without intermediate rock compositions there are too many uncertainties to rigorously conclude whether the diorite is related to the more felsic units in the complex.

Trace Element Modeling: Gilmanton Monzodiorite and Belknap Mountain Syenite

Major element modeling of the relation between the Gilmanton monzodiorite and Belknap Mountain syenite did not yield any easily interpretable results. It was concluded that the Wright-Doherty modeling neither precluded nor strongly supported a relation between the units, possibly because of the presence of cumulate early-formed crystalline material in the samples. Sample 19 of the Gilmanton monzodiorite is the only sample from that unit which is likely to have a bulk composition close to a liquid. (The high Al_2O_3, high CaO, and (+)Eu anomaly in samples G17 and G18 suggest cumulate plagioclase.) However, the REE, Sr, and Ba abundances in sample 19 are not consistent with a parent-daughter relation for the Gilmanton (19) and the Belknap Mountain syenite.

Sample 19 has much higher Sr and Ba, and moderately higher overall REE than the Belknap Mountain syenites. Major elements suggest only limited (∿11%) fractionation is required to derive the syenite from sample 19 (Table 10), but this is not sufficient to lower the Sr and Ba by the 50-60% observed; or produce the marked (-)Eu anomaly in Belknap Mountain syenite samples 20 and G20. Also, without subtraction of several percent of a REE-bearing phase as apatite, the overall reduction of rare earths is impossible to justify. Therefore, it is concluded that this sample of the Gilmanton monzodiorite is not reasonable as a parent for a Belknap Mountain syenite liquid.

Samples G17 and G18 of the Gilmanton monzodiorite contain an appreciable amount of cumulate feldspar. Logical candidates for the parent liquid are sample 19 of the Gilmanton or the Belknap Mountain syenite. Sample 19 has a very high Ba (1335 ppm) and moderately high Sr (455 ppm), severely limiting the amount of cumulate feldspar allowed in G17 and G18. However, the rare earths indicate an upper limit of 60% liquid contribution to G17 and G18. Assuming the remaining 40% is dominantly feldspar (which the Sc concentration suggests), the calculated Sr concentrations in G17 and G18 are 15% (G18) to 50% (G17) too high ($D_{Sr}^{Feldspar} = 3.5$). The maximum of 60% trapped liquid also yields very low model Rb abundances (∿80 ppm). For these reasons sample 19 is not considered a reasonable parent liquid for either G17 or G18.

The average Belknap Mountain syenite has considerably

less Sr (266 ppm) and Ba (670 ppm) than Gilmanton monzodiorite sample 19, allowing larger amounts of cumulate feldspar in samples G17 and G18. The syenite also has lower REE than sample 19 allowing slightly more trapped liquid. Figure 38 shows the results of REE modeling assuming an average Belknap Mountain syenite as a parent. The models involve 0-10% hornblende, 20-30% plagioclase, 5-10% alkali feldspar, and 60-70% trapped liquid. These models provide a reasonably good fit to the observed patterns. The amount of cumulate hornblende is constrained by the low Sc in G17 and G18. If $D_{Sc}^{Hbd} = 3.0$, ∿3% cumulate hornblende provides a good match to the observed Sc (Table 14).

Table 14 also gives the predicted abundance of the remaining trace elements (Rb, Sr, Ba, Th, Ta, Hf) based on the REE models. Rb and Ba fit sample G17 very well; Sr is low by ∿10%; the Belknap Mountain syenite contains too little Sr and Ba to yield sample G18. Ta and Hf also fit the observed abundance, but Th is far too low. Furthermore, 60% trapped liquid is only 2/3 the amount indicated by Wright-Doherty modeling (Table 10). Thus, a model can be produced to predict the REE, Rb, Sr, Ba, and Sc in sample G17 of the Gilmanton monzodiorite, but the major element model is not consistent.

Because samples G17 and G18 have trace element characteristics indicating cumulate plagioclase; because samples 20 and G20 show a reversal of "incompatible" elements and major oxide indicators of fractionation; and because rather mafic

TABLE 14. PREDICTED TRACE ELEMENT CONCENTRATIONS IN GILMANTON MONZODIORITE SAMPLES G17 AND G18 BASED ON REE MODEL WITH 65% TRAPPED LIQUID (FIGURE 38)

Element	Parent Magma Concentration[a]	Predicted Concentration	Actual Concentration G17	Actual Concentration G18	comments
Rb	161 ppm	106 ppm	112 ppm	126 ppm	$D_{Rb}^{AF} = 0.4$
Sr	266 ppm	497 ppm	549 ppm	727 ppm	$D_{Sr}^{Plag} = 3.5$ $D_{Sr}^{AF} = 3.75$
Ba	670 ppm	791 ppm	795 ppm	1380 ppm	
Th*	13 ppm	8.1 ppm	14.4 ppm	13.0 ppm	
Ta*	8.4 ppm	5.5 ppm	6.4 ppm	5.5 ppm	
Hf*	17 ppm	11.0 ppm	9.7 ppm	12.1 ppm	
Sc**	5.2 ppm	3.9 ppm	3.6 ppm	4.5 ppm	$D_{Sc}^{Hbd} = 3$

[a] Average Belknap Mountain syenite

* Solid/liquid distribution coefficient assumed equal to zero

** ∿3% cumulate hornblende

sample 19 shows higher abundances of some incompatible elements than syenite samples 20 and G20, it is possible that the physical processes that produced ambiguities in the major element modeling may also have produced trace element characteristics in individual samples that are not indicative of the general fractionation series. The problem may also lie in unrepresentative sampling of the units, or in the variation between splits (Appendix II). Therefore, the exact relationship of the monzodiorite to the more felsic units is not clear. Further careful isotope studies and better screening to obtain samples clearly representative of liquid compositions might allow resolution of the relations.

Trace Element Modeling: Belknap Mountain Syenite and Sawyer Quartz Syenite

Trace element modeling of the Sawyer quartz syenite as a liquid derived from the average Belknap Mountain syenite provides additional evidence to support the comagmatic relation suggested by the isotope and major element data. Using an assemblage of hornblende, plagioclase, alkali feldspar, apatite, and opaque oxide in the proportions indicated by the Wright-Doherty mixing model (Table 11), it was possible to obtain a very good fit to the observed REE, Sr, and Ba abundances in the Sawyer at ∿80% crystallization.

Table 15 gives the predicted concentration of Rb, Sr, Ba, and Sc. Ba and Sr yield excellent matches to the observed

TABLE 15. PREDICTED TRACE ELEMENT CONCENTRATION IN THE SAWYER QUARTZ SYENITE BASED ON REE MODELS*

Element	Parent Magma Concentration[a]	Predicted Concentration	Actual Concentration	Comments
Rb	161 ppm	>400 ppm	187-224 ppm	
Sr	266 ppm	33-50 ppm	33-62 ppm	
Ba	670 ppm	65-103 ppm	<60-100 ppm	
Sc	5.2 ppm	3.4-3.6 ppm	3-6 ppm	$D_{Sc}^{Hbd} = 17$ $D_{Sc}^{Opaque} = 2$

* At 80% crystallization.

Assumes either 30% total equilibrium/70% surface equilibrium or 50% total equilibrium/50% surface equilibrium.

[a] Average Belknap Mountain syenite.

abundances. An interesting consequence of the modeling of these two elements is that neither surface equilibrium nor total equilibrium will produce a match to the observed Sr and Ba concentrations in the Sawyer. A mix between the two (essentially an incremental fractional crystallization process) with between 50-70% surface equilibrium crystallization does yield a good match.

Figure 39 shows the calculated REE patterns. The upper diagram used dacitic hornblende mineral/liquid distribution coefficients; the lower diagram used rhyolitic distribution coefficients. Calculated REE patterns for 50% to 90% total equilibrium and surface equilibrium crystallization are shown. Rhyolitic values of D_{REE}^{Hbd} produced insufficient enrichment in the middle rare earths (Nd, Sm, Ho) at ∿80% crystallization. Dacitic values of D_{REE}^{Hbd} produced a close fit to the observed range of Sawyer quartz syenite abundances, with calculated heavy rare earth concentrations ∿10% too high. This suggests <u>average</u> D_{REE}^{Hbd} close to, but slightly greater than, dacitic values. Assuming between 50-70% surface equilibrium/30-50% total equilibrium crystallization the values of D_{Eu} used for plagioclase and alkali feldspar (2.0 in each case) appear slightly low.

Because of the low amounts of hornblende and opaque oxides removed from the Belknap Mountain syenite, a high D_{Sc}^{Hbd} must be used (∿17). Ewart and Taylor (1969) report extremely high D_{Sc}^{Hbd} in andesitic and rhyolitic volcanics.

The extremely high Rb abundances in the model present

a problem. There is a fairly large amount of data on the partitioning of Rb into alkali feldspar, all indicating a $D_{Rb}^{\text{alkali feldspar}} \sim 0.40$. However, these are for volcanic rocks and it may be that, as with Ba in plagioclase (Drake and Weill, 1975), there is a fairly strong temperature/composition dependence on the Rb distribution coefficient. A bulk D_{Rb} of $\sim$0.8-0.9 is indicated by the small change in Rb from the syenite to the quartz syenite. This suggests a $D_{Rb}^{\text{alkali feldspar}}$ of $\sim$1.2-1.4.

Overall, the geochemical modeling of the relations between the Sawyer quartz syenite and the Belknap Mountain syenite strongly supports the comagmatic relation indicated by the isotope data.

Trace Element Modeling: Cobble Hill Syenite

As discussed in Chapters 4 and 5, a number of features in the Cobble Hill syenite (isotopes; essentially zero normative An; high normative Ab/Or; low REE, Sc, Co, Hf, Zr; high total alkalis) are consistent with an origin for the syenite as a cumulate of dominantly alkali feldspar. The chief objections to this hypothesis are the extremely low Sr and relatively low Ba in the two samples, and the unique hornblende composition. If we assume an average Sawyer quartz syenite is the parent for the cumulate, the rare earth abundances allow a maximum of 50-60% trapped liquid, or a minimum of 40-50% cumulate alkali feldspar. The Sr concentration in a liquid in equilibrium with the cumulate

feldspar would have to have Sr concentrations of between 12-17 ppm, much lower than the Sawyer quartz syenite (33-62 ppm). For the Ba concentration in Cobble Hill syenite sample G8 (∿100 ppm), the liquid would have to contain ∿35 ppm Ba. The precise Ba in the Sawyer is not known, but it is unlikely to be this low. These low Sr and Ba concentrations required in the parent liquid for a Cobble Hill syenite cumulate and the unique hornblende composition appear to eliminate this model. An alternative must be found that will explain the extremely low Sr concentration at only moderate SiO_2 enrichment, in contrast to the Belknap Mtn. syenite which has ∿10 times the Sr of the Cobble Hill syenite.

Morse (1969), in a discussion of syenites, pointed out that one of the problems faced in explaining syenitic rocks was maintaining critical silica saturation (but not oversaturation) during their evolution. The Sr concentration in Cobble Hill syenite samples G7 and G8 provide another statement of the problem of maintaining low normative quartz during the protracted crystallization of feldspar necessary to reduce the Sr abundances. A possibility is that the Cobble Hill syenite magma evolved from a common parent but under more anhydrous conditions than the Belknap Mtn. syenite, suppressing the crystallization of hornblende (low in SiO_2 , and therefore efficient in increasing SiO_2 in the residual liquid). The presence of well preserved clinopyroxene crystals in sample G7 and lack of biotite in the Cobble Hill (except as interstitial material) might indicate low f_{H_2O}. An assemblage clinopyroxene plus feldspars plus opaque oxides would be much less silica undersaturated than a

similar assemblage with hornblende substituting for clinopyroxene. This would tend to suppress SiO_2 enrichment in the residual liquid until f_{H_2O} was high enough for hornblende to form. Suppression of hornblende crystallization would also maintain a higher Na_2O content in the liquid, since hornblende in the Belknaps contains up to 2-2.5% Na_2O (diorite hornblende). This might explain the position of the Cobble Hill syenite relative to the Belknap Mountain syenite on the normative Q-Or-Ab diagram (Figure 23).

The lower REE content of Cobble Hill syenite sample G8 relative to sample G7 in spite of higher SiO_2, lower FeO, MgO, and CaO; the lower Sc, and higher Rb is interpreted as reflecting a partly cumulate origin for G8, supported by the cumulate texture of the sample. About 35% crystallization of dominantly alkali feldspar from sample G7 would reduce the Sr and Ba concentrations to levels reasonable for a parent for such a cumulate. The REE content of such a parent liquid (fractionated Cobble Hill syenite sample G7) would imply ∿50-55% trapped liquid and 45-50% cumulate alkali feldspar and hornblende in sample G8.

This hypothesis for the origin of the Cobble Hill syenite (fractionation under more anhydrous conditions than the Belknap Mountain syenite) is proposed to explain the very low Sr, Ba, and normative An contents (features of highly fractionated liquids) in rocks of only moderate SiO_2 enrichment. The similar initial $^{87}Sr/^{86}Sr$ of the Cobble Hill syenite and the other felsic Belknap rocks suggests evolution

of a magma generated from similar source materials under different P_{H_2O} conditions.

Trace Element Modeling: Conway Granite

The Conway granite is the most fractionated rock type in terms of major elements, but as pointed out in Chapter 5, it has significantly lower amounts of most "incompatible" elements while containing higher concentrations of feldspar compatible trace elements (Sr, Ba, Eu). The model proposed in Chapter 5 suggested an origin for the Conway granite through accumulation of early formed alkali feldspar, quartz, and plagioclase and final crystallization with varying amounts of residual liquid enriched in the REE, Rb, Ta, Th, etc. Such an origin would also explain the large variation in REE abundances in the Conway, which covers most of the range of the other rock units in the Belknaps (Figures 26-28). The series of sub-parallel REE patterns in Figure 28 (Chapter 5) is a feature to be expected from mixing a REE-depleted crystalline material with an enriched residual liquid.

Crystallization at, or near, a eutectic (or minimum) composition can produce extreme changes in trace element abundances in a residual liquid with little or no change in major element bulk composition. (Hanson, 1978, makes this point with respect to the K_2O content of a partial melt in the system Q-Or-Ab.) The major element bulk composition of the crystalline assemblage and residual liquid are virtually identical, but they will have extremely different

concentrations of trace elements. Mixing the liquid and crystalline material in various proportions can yield the wide range of trace element concentrations observed in the Conway granite, from sample G34 (small percentage of trapped liquid) to sample G29 (high percentage of trapped liquid). If the Conway granite is related to the Sawyer quartz syenite (as isotopes indicate), no Conway granite sample crystallized as a closed system without loss of residual liquid. Barker and Arth (1976) propose a similar process of dilution of REE abundances by quartz and feldspar in the Kroenke batholith.

Figure 40 shows the REE patterns produced by mixing early formed feldspar plus quartz with varying amounts of residual liquid similar to the more enriched Sawyer quartz syenite. Variation in the ratio of plagioclase:alkali feldspar:quartz has little effect on the calculated REE pattern compared to the effect of trapped liquid, and an average assemblage of 15% plagioclase, 55% alkali feldspar, and 30% quartz was used as the crystalline assemblage. The LREE abundances seem to indicate between 12 and 50% trapped liquid is necessary to generate the REE patterns in the Conway granite. However, the HREE abundances in the model are far too low compared to the actual HREE concentrations in the Conway. This indicates that either the liquid from which the Conway granite crystallized had a considerably lower $La/Yb)_{cn}$ ratio than the Sawyer liquid ($\sim$12-18 as opposed to $\sim$25 in the Sawyer), or a phase other than feldspar, quartz, or trapped residual liquid is controlling the HREE abundance.

An accessory phase which has a large effect on the HREE in comparison to its effect on the LREE is zircon (Nagasawa, 1970). The D^{Zircon}_{HREE} are several orders of magnitude higher than the LREE distribution coefficients, so a small fraction of cumulate zircon in the Conway granite could raise the HREE abundances well above the level expected from only trapped residual liquid. The middle portion of Figure 40 shows the effects of 0.03% cumulate zircon on the calculated HREE patterns, using the REE distribution coefficients for zircon given in Arth (1976). The predicted HREE are still too low by 3-4 times. The amount of zircon in the Conway is limited by the Zr concentration in the Conway (an average of $\sim$200 ppm based on the analysis of sample 7 and roughly similar Hf concentrations, and excluding sample G28, which is much closer to the Sawyer quartz syenite in most geochemical characteristics, Chapter 5). About 200 ppm Zr implies a maximum of 0.035% zircon. Therefore, if zircon is the controlling factor on the HREE abundances, the distribution coefficients from Arth (1976) must be too low. The lower portion of Figure 5 shows predicted abundances of the REE assuming HREE distribution coefficients for zircon 4 times the average values in Arth (1976). (About 3.5 times the high values listed.) The match to the REE patterns in the Conway is quite good, as expected since the values of D^{Zircon}_{HREE} were calculated to produce a good fit. The values used are given in Figure 40, and are similar to a zircon from a granite studied by Nagasawa (1970) that had REE_{Zircon}/

$REE_{Whole\ Rock}$ values of 890 and 1230 for Yb and Lu. The D^{Zircon}_{LREE} were not multiplied by 4 based on Nagasawa's (1970) comment that he felt the relatively flat light rare earth distribution for the zircons he studied were too high due to either contaminants in the zircon separates or analytical problems. Also, the percentage of trapped liquid indicated by the LREE abundances in Figure 40 work well for the Sr and Ba abundances in the Conway, suggesting that zircon does not contribute significantly to the LREE abundances. The increase in the zircon distribution coefficient, if real, would be due to the lower crystallization temperatue of the Sawyer-Conway versus the dacites studied by Nagasawa (1970), and the slightly different melt composition. The combined effect of temperature and melt composition might be sufficient to raise the D^{Zircon}_{HREE} by the needed 3.5-4 times.

Table 16 gives predicted Rb, Sr, Ba abundances in the Conway. The predicted Sr abundances agree very well with the range observed in the granite. The model predicts higher Sr (and Ba, Eu; and lower Eu/Eu*) in the samples with the least amount of trapped liquid, a feature generally observed in the granite samples, e.g., as the LREE increase, Sr, Ba, and Eu decrease. The coherence of Sr (and Ba and Eu) with trapped liquid would not be exact because the amount of cumulate quartz and plagioclase/alkali feldspar ratio will affect these concentrations.

Model Rb concentrations are too low. In modeling of the Sawyer quartz syenite, it was suggested that values of

TABLE 16. PREDICTED CONCENTRATIONS OF Rb, Sr, AND Ba IN THE CONWAY GRANITE*

Element	Parent Magma Concentration[a]	Predicted Concentration	Actual** Concentration	Comments
Rb	190-225 ppm (210 ppm average)	100-135 ppm	181-225 ppm	
Sr	33-62 ppm (43 ppm average)	90-115 ppm	84-116 ppm	
Ba	<60-100 ppm	140-200 ppm	201-348 ppm	$D_{Ba}^{Alkali\ Feldspar}=6$

* Assuming 15-50% trapped liquid; crystalline assemblage as in REE model.

** Excluding sample G28.

[a] Sawyer quartz syenite range and average

$D_{Rb}^{alkali\ feldspar}$ in the range 1.2-1.4 would produce a better fit to Rb in the quartz syenite. The same range of Rb distribution coefficients would produce model Rb concentrations in good agreement with the Conway values. The Ba values are also slightly low. $D_{Ba}^{alkali\ feldspar}$ of 7-8 would yield a good match to observed abundances.

In summary, the general trace element features of the Conway granite support a model involving cumulus phases mixed with evolved Sawyer quartz syenite liquid. This model also accounts for similar $^{87}Sr/^{86}Sr)_o$ in the Sawyer quartz syenite and Conway granite, and for several distinctive features of the Conway granite; in particular, the evolved major element composition with relatively low contents of incompatible trace elements, the wide range of REE abundances, and the high concentration of feldspar compatible trace elements. REE abundances can be modeled providing assumptions are made concerning the rare earth distribution coefficients in zircon, i.e., increasing published values 3.5-4 times. This assumption may be checked by separating zircon from the Conway granite and determining the fraction of heavy rare earths in zircon. Since the model predicts 70-80% of the HREE should be in zircon, anything less than 50-60% (given the difficulty in obtaining 100% of the zircon from a sample) would indicate that the model was incorrect.

An alternative to the model discussed above is that the Conway granite crystallized from a magma with much lower La/Yb ratio than the Sawyer quartz syenite. In this case,

the variation in the REE cannot be ascribed simply to fractional crystallization at a eutectic because the 2-3 times enrichment of the rare earths between samples would require at least 60% crystallization. With a value of $D_{Sr}^{feldspar}$ = 2.4-5 and a crystalline assemblage with 65% feldspar, this would reduce the Sr concentration in the granite by 70% from ∿120 ppm to ∿37 ppm. This large range in Sr is not observed. Similarly for Ba, by assuming 45% alkali feldspar fractionation, Ba would drop from ∿350 ppm to ∿70 ppm.

If we eliminate fractional crystallization of the Conway at a eutectic as a source for the wide range in REE abundances, we could apply a model similar to the one discussed in detail above, but with a liquid that would not require an appeal to zircon as an accessory phase controlling HREE concentrations. The range of La/Yb in the Conway (Figure 33) (excluding sample 6) would indicate some effect of some accessory mineral on the HREE abundances, but not the 70-80% required if the Sawyer is the parent. (In this case, sample G28 would be grouped with the Sawyer quartz syenite as discussed in Chapter 5.)

As mentioned in Chapter 5, sample 6 of the Conway granite has anomalous trace element abundances relative to the other Conway granite samples. These include high concentrations of heavy rare earths, an extremely low $(La/Yb)_{cn}$ ratio (∿3.3), a very high concentration of U, and higher Th and Ta abundances. Sample 6 is similar to the other

Conway granite samples in having higher Sr and Ba than the Sawyer quartz syenite. Petrographically (Appendix I), the sample is a fine-grained, mafic-poor felsite with common disseminated fluorites and accessory zircon and allanite.

The high U and Th concentrations may be related to the relatively abundant disseminated fluorite as Heinrich (1965) indicates that uranite commonly occurs with disseminated fluorite. Hon and Noyes (1977) suggested that the LREE depletion in fine-grained aplites associated with granites in the Sierra Nevada, California, and Mount Katahdin, Maine, was due to subtraction of allanite (which has very high D_{LREE}) from the liquid, but this should also deplete the liquid in uranium and thorium (Deer et al., 1962). Sample 6 of the Conway granite has been affected by some process which has apparently not affected the remaining samples (at least to the same degree). The exact process resulting in LREE depletion in sample 6 (and aplites) is not understood at this time.

Figure Captions

Figure 34. Oxide variation of MgO (wt.%) vs. SiO_2 (wt.%) illustrating some problems in applying the Wright-Doherty least squares mixing models in specific instances. A, B, C, and D represent hypothetical liquids; A', B', C', and D' represent the crystalline assemblage in equilibrium with A, B, C, and D; D" represents a mix of liquid D and crystalline D'. See text for discussion.

Figure 35. Plot of $D_{Eu}^{Plagioclase}$ and $D_{Sr}^{Plagioclase}$ vs. An content. Data from Schnetzler and Philpotts (1970).

Figure 36. Results of geochemical modeling of the gabbro as a partial cumulate derived from diorite samples 5 and 17. See text for discussion.

Figure 37. Results of geochemical modeling of the Gilmanton monzodiorite (sample 19) as a liquid derived by fractional crystallization of diorite (samples 5 and 17). See text for discussion.

Figure 38. Results of geochemical modeling of the Gilmanton monzodiorite (samples G17 and G18) as a partial cumulate derived from the Belknap Mountain syenite

(samples 20 and G20). See text for discussion.

Figure 39. Results of geochemical modeling of the Sawyer quartz syenite as a liquid derived from the Belknap Mountain syenite by fractional crystallization. See text for discussion.

Figure 40. Results of geochemical modeling of the Conway granite as a partial cumulate derived from a liquid similar in REE abundances to the Sawyer quartz syenite. See text for discussion.

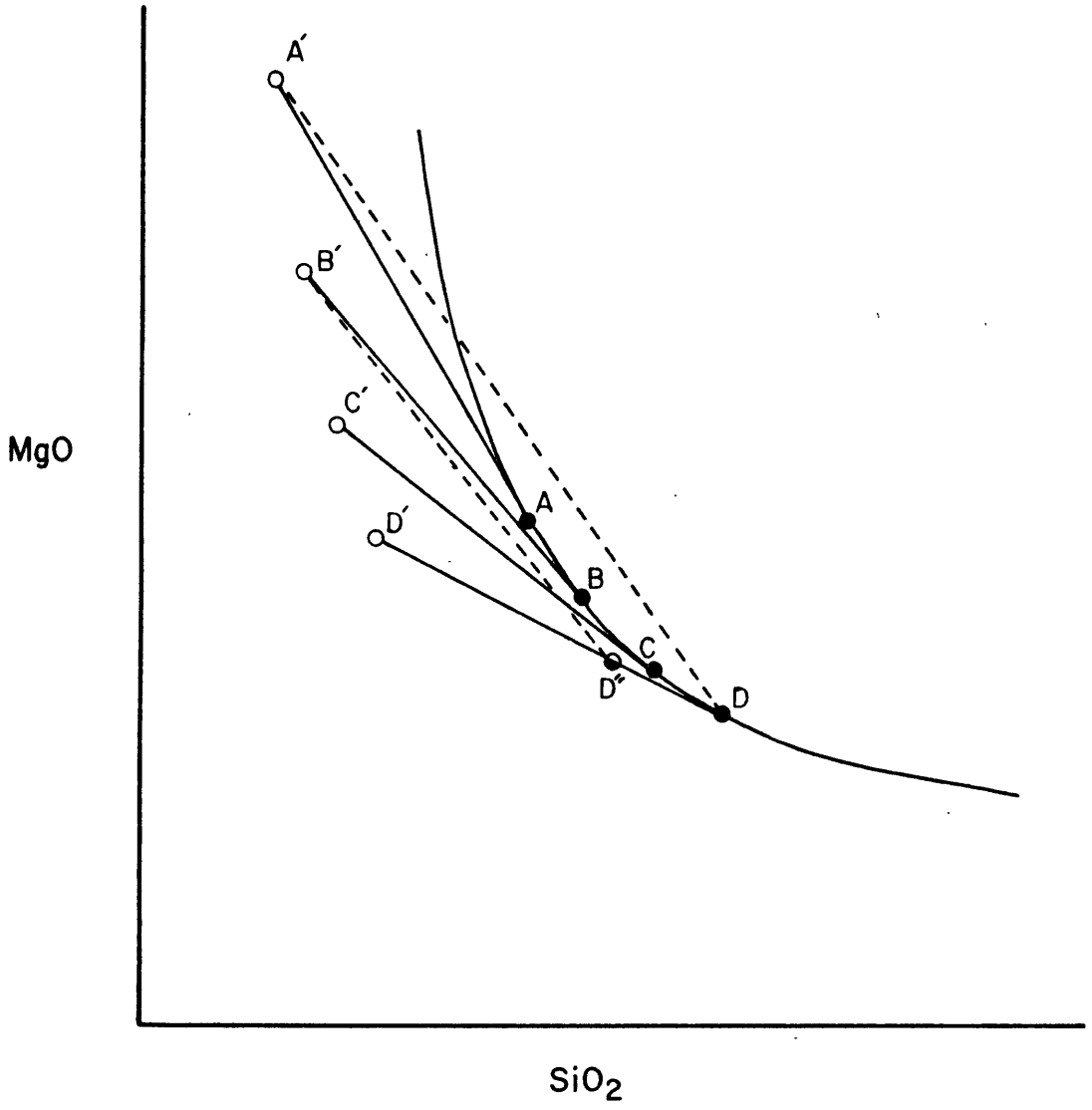
A´
B´
C´
D´
A
B
C
D
D´
MgO
SiO2

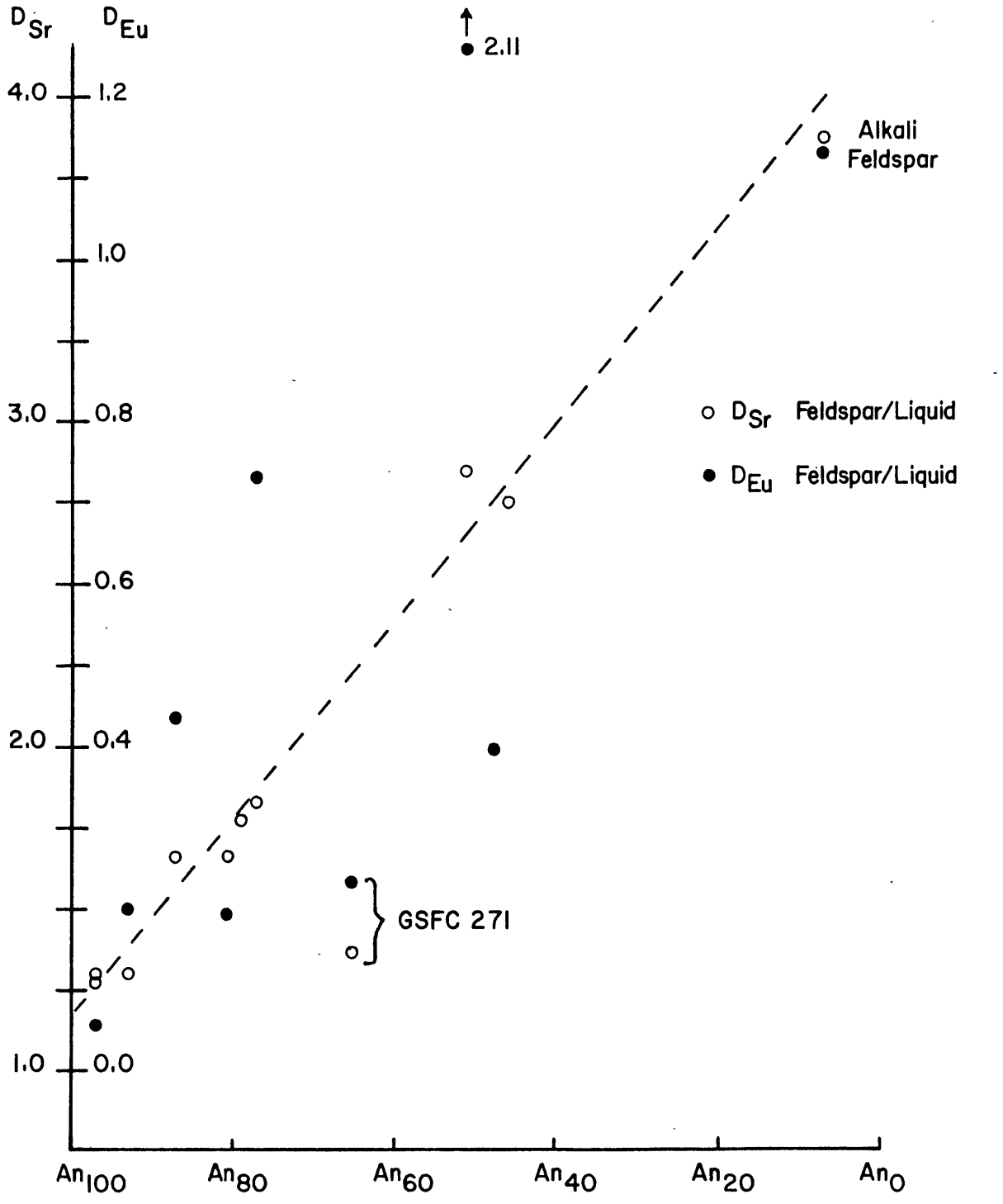
D_{Sr}
D_{Eu}
4.0
1.2
1.0
3.0
0.8
0.6
2.0
0.4
1.0
0.0
2.11
Alkali Feldspar
D_{Sr} Feldspar/Liquid
D_{Eu} Feldspar/Liquid
GSFC 271
An_{100}
An_{80}
An_{60}
An_{40}
An_{20}
An_0

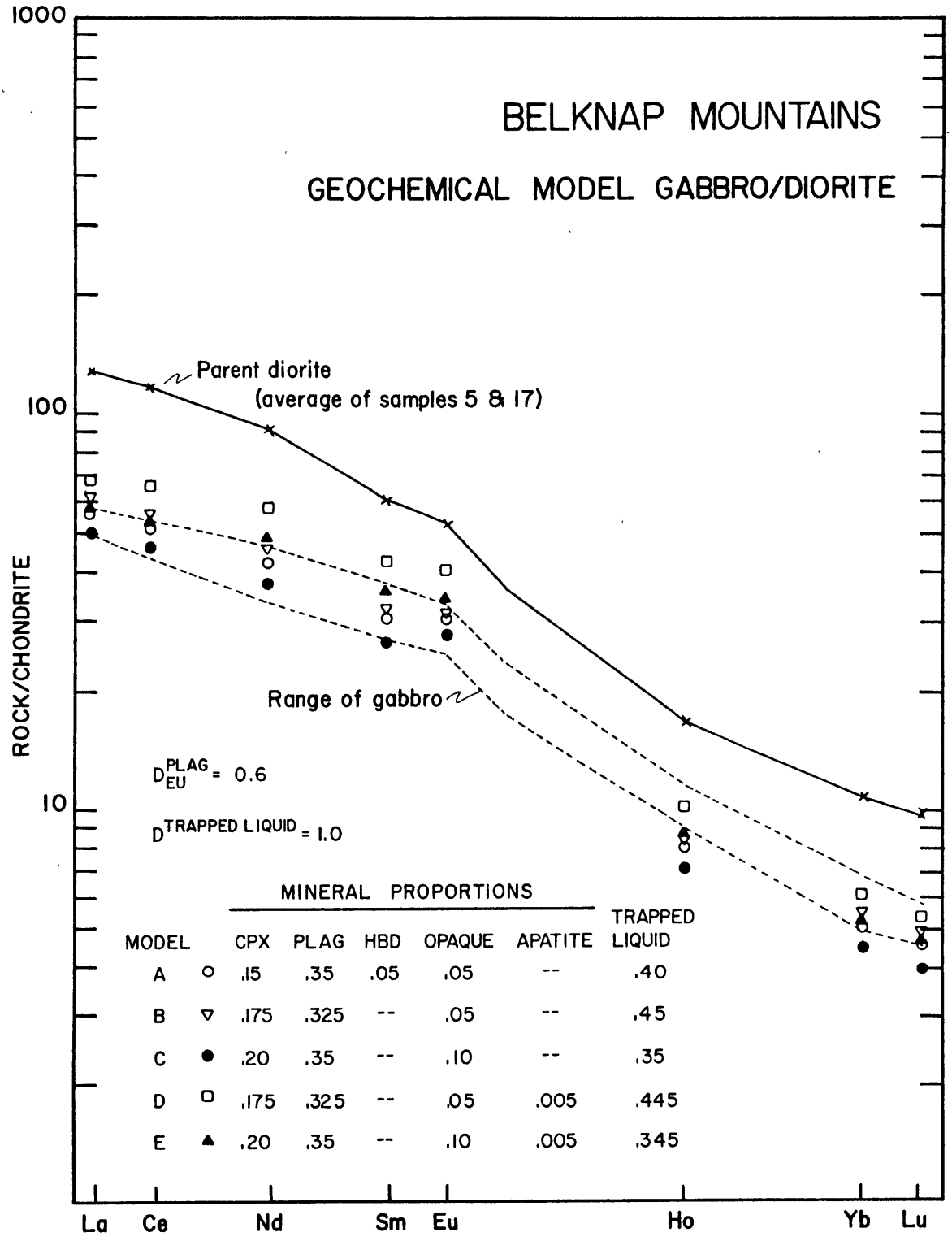
BELKNAP MOUNTAINS
GEOCHEMICAL MODEL GABBRO/DIORITE
Parent diorite
(average of samples 5 & 17)
Range of gabbro
D_{EU}^{PLAG} = 0.6
$D^{TRAPPED\ LIQUID}$ = 1.0
ROCK/CHONDRITE
1000
100
10
La
Ce
Nd
Sm
Eu
Ho
Yb
Lu
MINERAL PROPORTIONS
MODEL CPX PLAG HBD OPAQUE APATITE TRAPPED LIQUID
A .15 .35 .05 .05 -- .40
B .175 .325 -- .05 -- .45
C .20 .35 -- .10 -- .35
D .175 .325 -- .05 .005 .445
E .20 .35 -- .10 .005 .345

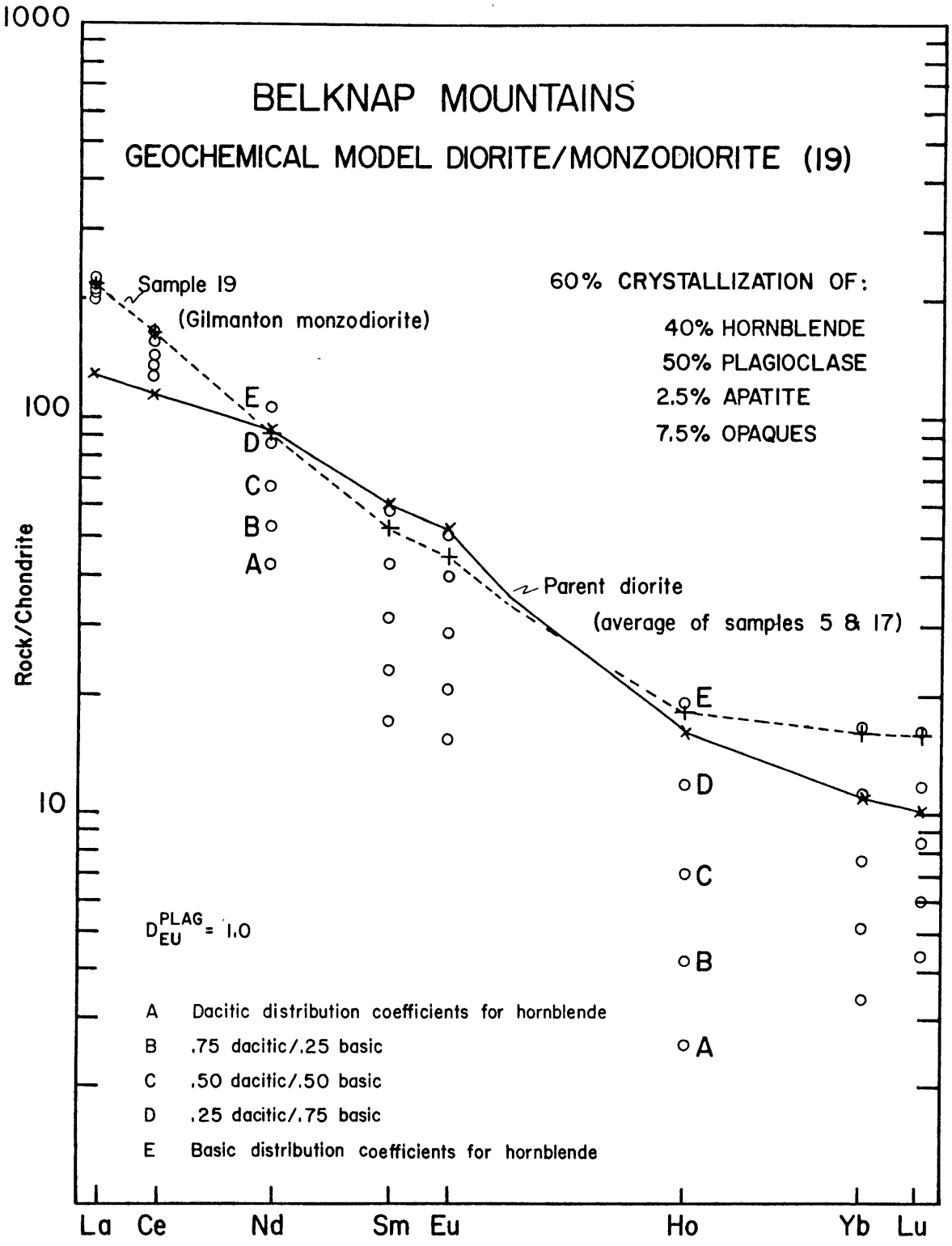
BELKNAP MOUNTAINS
GEOCHEMICAL MODEL DIORITE/MONZODIORITE (19)
Sample 19
(Gilmanton monzodiorite)
60% CRYSTALLIZATION OF:
40% HORNBLENDE
50% PLAGIOCLASE
2.5% APATITE
7.5% OPAQUES
Parent diorite
(average of samples 5 & 17)
Rock/Chondrite
1000
100
10
La
Ce
Nd
Sm
Eu
Ho
Yb
Lu
A
B
C
D
E
D_{EU}^{PLAG} = 1.0
A Dacitic distribution coefficients for hornblende
B .75 dacitic/.25 basic
C .50 dacitic/.50 basic
D .25 dacitic/.75 basic
E Basic distribution coefficients for hornblende

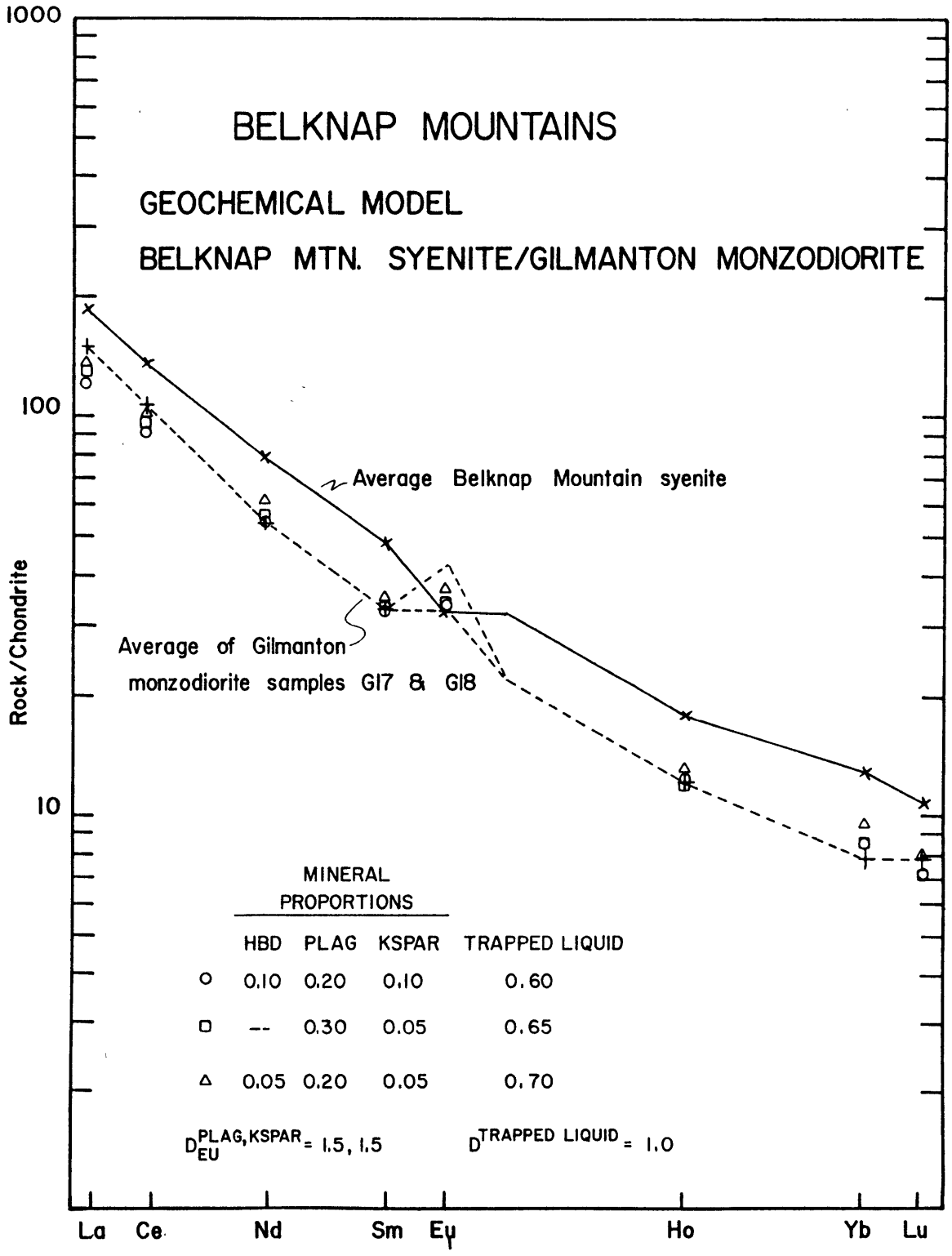
BELKNAP MOUNTAINS
GEOCHEMICAL MODEL
BELKNAP MTN. SYENITE/GILMANTON MONZODIORITE
1000
100
10
Rock/Chondrite
Average Belknap Mountain syenite
Average of Gilmanton monzodiorite samples GI7 & GI8
MINERAL PROPORTIONS
HBD PLAG KSPAR TRAPPED LIQUID
○ 0.10 0.20 0.10 0.60
□ -- 0.30 0.05 0.65
△ 0.05 0.20 0.05 0.70
$D_{EU}^{PLAG,KSPAR}$ = 1.5, 1.5
$D^{TRAPPED\ LIQUID}$ = 1.0
La Ce Nd Sm Eu Ho Yb Lu

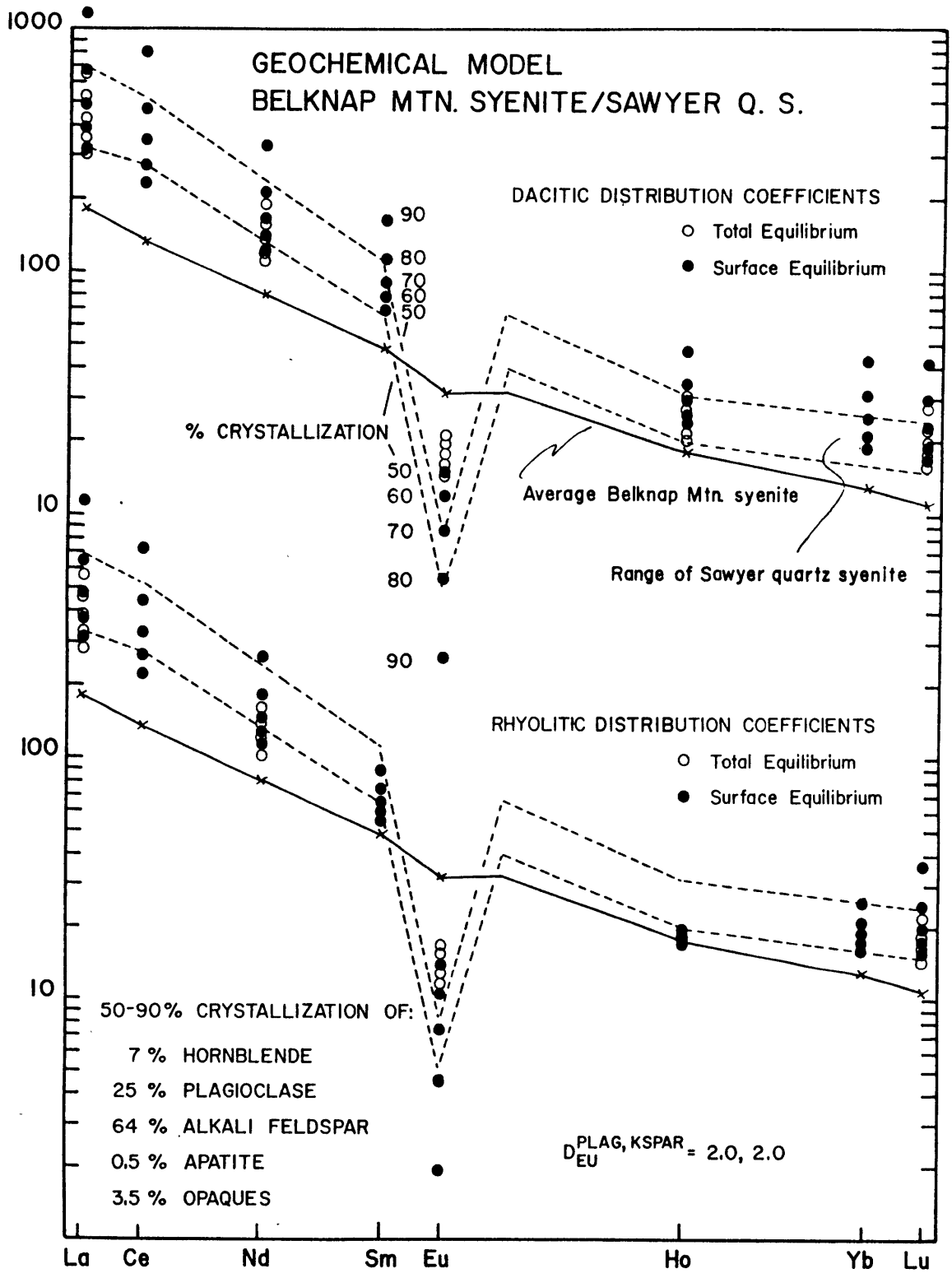
GEOCHEMICAL MODEL
BELKNAP MTN. SYENITE/SAWYER Q. S.
DACITIC DISTRIBUTION COEFFICIENTS
Total Equilibrium
Surface Equilibrium
% CRYSTALLIZATION
90
80
70
60
50
Average Belknap Mtn. syenite
Range of Sawyer quartz syenite
RHYOLITIC DISTRIBUTION COEFFICIENTS
Total Equilibrium
Surface Equilibrium
50-90% CRYSTALLIZATION OF:
7 % HORNBLENDE
25 % PLAGIOCLASE
64 % ALKALI FELDSPAR
0.5 % APATITE
3.5 % OPAQUES
$D_{EU}^{PLAG, KSPAR}$ = 2.0, 2.0
1000
100
10
100
10
La
Ce
Nd
Sm
Eu
Ho
Yb
Lu

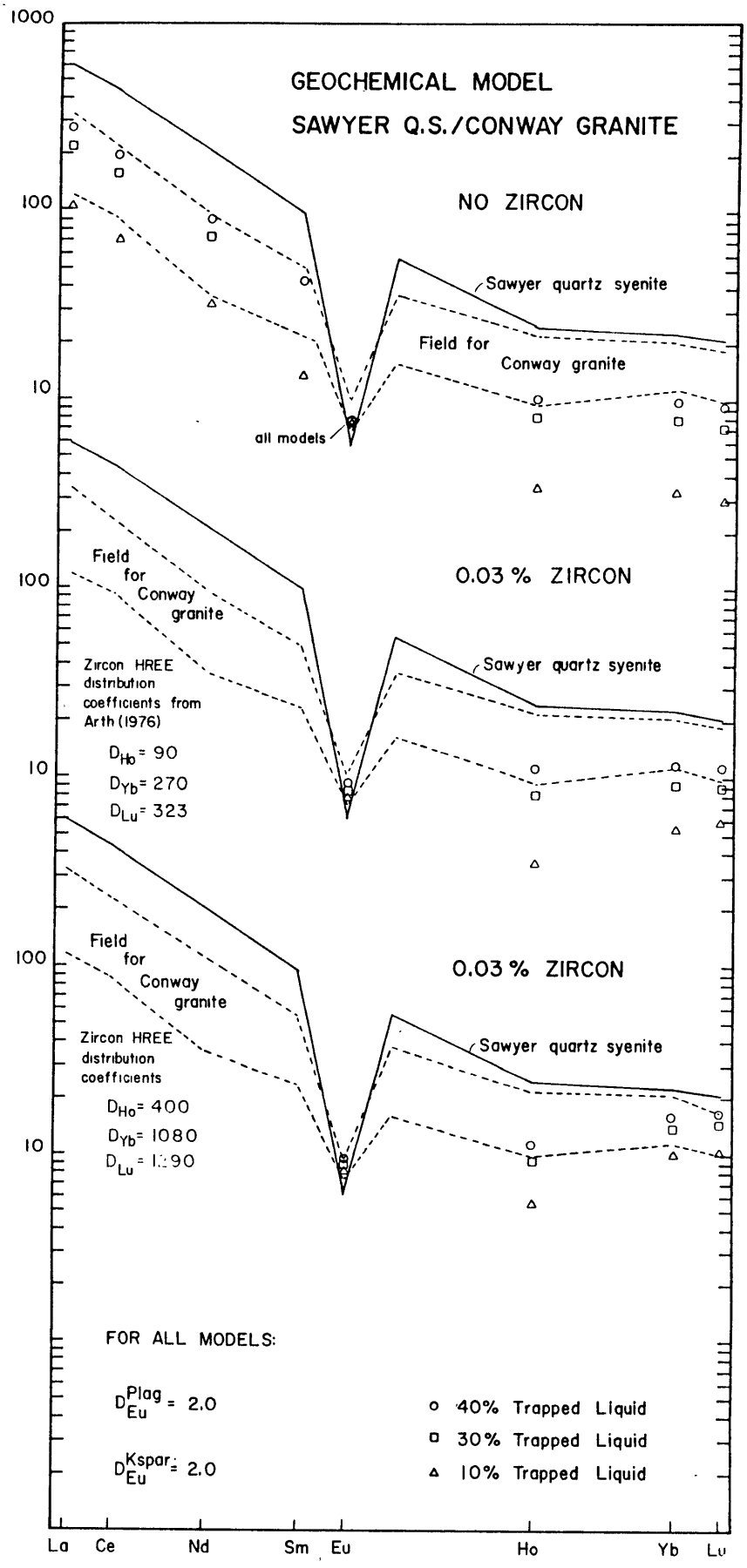
GEOCHEMICAL MODEL
SAWYER Q.S./CONWAY GRANITE
NO ZIRCON
Sawyer quartz syenite
Field for
Conway granite
all models
0.03 % ZIRCON
Field
for
Conway
granite
Zircon HREE
distribution
coefficients from
Arth (1976)
D_{Ho} = 90
D_{Yb} = 270
D_{Lu} = 323
Sawyer quartz syenite
0.03 % ZIRCON
Field
for
Conway
granite
Zircon HREE
distribution
coefficients
D_{Ho} = 400
D_{Yb} = 1080
D_{Lu} = 1290
Sawyer quartz syenite
FOR ALL MODELS:
D^{Plag}_{Eu} = 2.0
D^{Kspar}_{Eu} = 2.0
40% Trapped Liquid
30% Trapped Liquid
10% Trapped Liquid
1000
100
10
100
10
100
10
La
Ce
Nd
Sm
Eu
Ho
Yb
Lu

CHAPTER 7. POSSIBLE SOURCES OF BELKNAP MOUNTAINS COMPLEX MAGMAS

Introduction

Chapter 6 examined the relationships between the various units of the Belknap Mountains complex, concentrating almost entirely on the units with initial $^{87}Sr/^{86}Sr \simeq 0.7035$. This chapter deals with the constraints that the major and trace element and isotopic data place on the source material for the Belknap Mountains complex magmas.

Following the conclusions based on the isotope data (Chapter 3), we must be concerned with:

- A source for a parental gabbro/diorite magma with $^{87}Sr/^{86}Sr)_o \simeq 0.7035$.
- If the felsic units with similar initial Sr isotope ratios (Belknap Mountain syenite, Sawyer quartz syenite, Conway granite) are not related to the gabbro and diorite by fractional crystallization, we must consider a source for a parental syenitic magma similar to, or slightly more basic than, the Belknap Mountain syenite from which the Sawyer quartz syenite and Conway granite were derived.
- A source, or mechanism of formation, for the Albany quartz syenite magma with $^{87}Sr/^{86}Sr)_o \simeq 0.7040$.
- Sources, or mechanisms of formation, for the Ames monzodiorite, possibly the Gilmanton monzodiorite,

and Lake quartz syenite, all of which show indications of possessing initial Sr isotope ratios greater than ∿0.7040.

Because of the uncertain relation of the Gilmanton monzodiorite to the units with $^{87}Sr/^{86}Sr)_o \simeq 0.7035$, and the limited amount of data on the Ames monzodiorite and Lake quartz syenite, this chapter concentrates on the first three problems.

Basic Rocks: Gabbro and Diorite

The gabbro appears to be a partial cumulate derived from a magma similar to the diorite. Therefore, the major question is the source of the Endicott diorite magma. As mentioned in Chapter 5, the diorite has REE abundances similar to typical alkali basalt. Kay and Gast (1973) reviewed in detail the REE, Rb, Sr, and Ba content and origin of alkali-rich basalt, and concluded such liquids are formed by several percent partial melting of a garnet peridotite mantle with initial rare earth concentrations 2-5 times chondrites. Also, Sun and Hanson (1976), in a study of basanitoids from Ross Island, Antarctica, suggested a LREE-enriched mantle source and 7-15% partial melting for the generation of alkali basalt. Compared to direct melts of mantle peridotite the diorite studied is clearly a fractionated rock which may also have undergone a slight enrichment of LREE during intrusion of the Conway granite. Nevertheless, the general similarity in normative nepheline and REE content to alkali basalt implies that the primary diorite could have formed by ∿5% melting of

garnet lherzolite with relative REE abundances as in chondrites (Kay and Gast, 1973) or by higher degrees of melting (∿10%) of a garnet lherzolite with relative LREE enrichment compared to chondrite (Sun and Hanson, 1976).

Felsic Rocks with $^{87}Sr/^{86}Sr)_o \simeq 0.7035$

Modeling of major and trace element data in Chapter 6 was unsuccessful in showing a direct relationship between the Belknap Mountain syenite (and its derivatives) and the more mafic Belknap Mountains complex rocks. However, the isochron relationship of the samples on the "high" regression line in Chapter 3 must be considered strong evidence favoring a comagmatic relationship. Considering the large gap in SiO_2 between the diorite and the Belknap Mountain syenite and the uncertainties this introduces into the geochemical modeling, it is not clear which evidence is more compelling - the positive result indicated by the isotopic data or the negative results of the geochemical modeling. A number of studies of volcanic associations on oceanic islands (e.g., St. Helena, Baker (1969); Ascension, Daly (1925); Gough, Zielinski and Frey (1970)) and continental volcanic series (e.g., New South Wales, Abbott (1969); New Zealand, Coombs and Wilkinson (1969)) have demonstrated the origin of trachytic magma through fractional crystallization of basalt. However, in all these examples (plus others described in Carmichael et al., 1974), the original normative character of the parental basalt, either saturated or

undersaturated with respect to silica, persisted in their felsic derivatives. Modeling of the major element data (Chapter 6) indicated that if sufficient hornblende was subtracted from the Ne-normative diorite the oversaturated Belknap Mountain syenite could be derived, but the large hornblende/plagioclase ratio was not consistent with either the trace element models or the diorite petrography. Because of this conflicting evidence, the possibility that the Belknap Mountain syenite (or some more basic syenitic magma) was derived from an independent source will be examined.

The low initial Sr isotope ratios and non-peraluminous composition of the Belknap Mountain syenite rule out the involvement of the dominantly pelitic Devonian Littleton Formation in the genesis of the syenite. Involvement of older, less pelitic sediments (greywacke composition) exposed in central Maine (and presumably underlying the Devonian rocks of the Belknap Mountains region) is probably also precluded by the Sr isotope data. Even assuming an initial $^{87}Sr/^{86}Sr$ ratio of $\sim$0.7035 at the time of deposition (unlikely to be this low based on Rb/Sr work on northern New England metasediments by Brookins, 1976), clastic rocks with a Rb/Sr weight ratio between 0.1 and 0.2 (similar to most greywackes; Condie, 1967; Arth and Hanson, 1975) will show an increase in $^{87}Sr/^{86}Sr$ of 0.0064-0.0128 in $\sim$150 m.y. This would produce ratios in the sediments too high for the Belknap Mountain syenite. Furthermore, experimental studies summarized by Winkler (1974) indicate that partial melting of greywacke

composition does not yield melts of syenitic compositions.

The calc-alkaline New Hampshire Plutonic Series appears to have $^{87}Sr/^{86}Sr$ ratios too high (0.7040 and above) at ∿170 m.y. (Foland and Friedman, 1977) to yield the Belknap Mountain syenite. Also, gravity studies (Nielson et al., 1976) indicate that the intrusions are shallow, sheet-like bodies, and therefore they are not likely to be major source rocks in the generation of the Belknap Mountains complex magmas.

Another type of source rock to be considered is basic material. Based on 1 atmosphere experiments in the system Na_2O-Al_2O_3-Fe_2O_3-SiO_2, Baily and Schairer (1966) suggested that syenitic magma may be generated by partial melting of alkali basalt. Also, Chayes (1963) suggested that the bimodal distribution of alkali basalt and trachyte on oceanic islands can be explained by partial melting of alkali basalt to yield trachytic liquid. More recently, Helz (1973, 1976) studied melting of basalts at 5 kilobars with $P_{H_2O} = P_{Total}$. Her results indicate that silica oversaturated melts were formed from nepheline and hypersthene normative basalts at all temperatures due to the stability of hornblende in the residue. These results contrast with the expected early liquids formed from anhydrous melting of nepheline normative basalts which, based on fractionation trends observed in alkali basalt sequences, would be silica undersaturated.

The composition of melts produced by partial melting of

a hydrous alkali basalt are quartz and corundum normative, high in normative anorthite, and have Na_2O/K_2O greater than 1, increasing with increasing degree of partial melting (Helz, 1976). In this respect, the melts are not strict analogues for syenitic rocks (with low normative quartz and anorthite, and no normative corundum). However, the initial composition of the basalt, gabbro and, more importantly, the relation of P_{H_2O} to P_{Total} can significantly alter the composition of the melt. For example, a major point made by Helz (1976) is that as long as P_{H_2O} is sufficient to stabilize hornblende in the residue, the melts will tend towards silica saturation or oversaturation. Also, the high CaO and Al_2O_3 in the experimental liquids is probably due to high P_{H_2O}, since Yoder (1965) has shown that solubility of plagioclase in a silicate melt is greatly increased at high values of P_{H_2O}. The following is a reasonable conjecture based on the effects of reduced P_{H_2O} on the composition of melts produced by partial melting of alkaline gabbro.

Reduced P_{H_2O}, i.e. $<P_{Total}$, will decrease the plagioclase solubility, and the melt will be lower in Al_2O_3, CaO, and possibly Na_2O. This eliminates normative corundum and decreases the Na_2O/K_2O in the liquid. A lower P_{H_2O} will also tend to destabilize hornblende with respect to clinopyroxene, olivine, and Fe-Ti oxides. Therefore, the silica enrichment at a given degree of melting will not be as great as for conditions of $P_{H_2O} = P_{Total}$. Thus, the degree of melting required to obtain a given SiO_2 content is lower and the

alkali enrichment (and incompatible trace element enrichment) is proportionately greater. Of course, this is only conjecture, and detailed studies such as Helz (1976) at $P_{H_2O} < P_{Total}$ are required to accurately determine partial melt composition under such conditions.

A model deriving the Belknap Mountain syenite by partial melting of alkaline gabbro, possibly an earlier member of the Belknap Mountains complex, satisfies the constraint of similar initial ratios for the basic and felsic material, provides a broadly suitably source material in terms of alkalis and trace elements, and explains the apparent lack of intermediate (50-60% SiO_2) rocks (although this may be a sampling effect). The trace element characteristics of the source must differ from the diorite, however, because it is not possible to derive the trace element abundances of the Belknap Mountain syenite from the concentrations of Rb, Sr, Ba, and REE in diorite samples 5 and 17 (Table 8). The concentrations of these elements are too high in the diorite which leads to unrealistically high concentrations in the partial melt. At 15-20% partial melting the calculated liquid in equilibrium with 60% plagioclase, 20-30% clinopyroxene, and 10-20% hornblende contained ∿320 ppm Rb, ∿800 ppm Sr, ∿1900 ppm Ba, and La ∿350 times chondrites, compared to ∿150-170 ppm Rb, 250-275 ppm Sr, 650-770 ppm Ba, and La ∿160-190 times chondrites in the Belknap Mtn. syenite. (The 15-20% melting is an estimate based on the SiO_2 contents of melts at $P_{H_2O} = P_{Total}$ (Helz, 1976), and assuming $P_{H_2O} \simeq 0.5\ P_{Total}$.) Leaving 5-10% biotite in the residue (a

feature not noted by Helz (1976) in any of her runs at $P_{H_2O} = P_{Total}$) will reduce Rb and Ba in the melt, but not by a sufficient amount, and this does not effect the Sr and REE concentrations which are also too high. Gabbro samples 9 and 15, with ∿800 ppm Sr and ∿300 ppm Ba also yield concentrations of Sr and Ba in a 15-20% partial melt that are higher than those in the syenite.

For a model with ∿15-20% partial melt in equilibrium with a residue of 50-60% plagioclase, 20-30% clinopyroxene and/or olivine, and 10-20% hornblende, a source with ∿35-40 ppm Rb, ∿250-300 ppm Sr, 200-225 ppm Ba, and La ∿40 times chondrites is consistent with the trace element content of the Belknap Mountain syenite. Of these only the Rb abundance is similar to an average alkali basalt, with the Sr, Ba, and La abundances lower than in typical alkali basalts (Kay and Gast, 1973; Sun and Hanson, 1976; Price and Chappell, 1975; Price and Taylor, 1973). It appears, then, that the trace element characteristics of the Belknap Mountain syenite cannot be matched by simple partial melting of a typical alkali basalt at reasonable (?) degrees of partial melting (15-20%). A possibility is that the Belknap Mountain syenite was produced by partial melting of a partial cumulate similar in origin to gabbro samples 9 and 15, but derived from a liquid with lower abundances of Sr, Ba, and REE than diorite samples 5 and 17. Large positive gravity and aeromagnetic anomalies associated with the Belknap Mountains (Sharp and Simmons, 1978) indicate considerable material at depth which may have

provided source material for the syenite.

Larger degrees of melting (∿40%) of a typical alkali basalt could account for the trace element abundances in the Belknap Mountain syenite, but the major element composition would be more basic than Belknap Mountain syenite samples 20 and G20. Possibly, the product of such melts was a more basic syenite which fractionated to the Belknap Mountain syenite, but at this point there are no longer any constraints on the source and intermediate magma, and the model becomes ad hoc.

Units with $^{87}Sr/^{86}Sr)_o \simeq 0.7040$ and Higher

From earlier modeling of the various Belknap rock units it was not clear whether the Gilmanton monzodiorite was related to the units on the lower regression line. Also, major element modeling of the Gilmanton and the Belknap Mountain syenite were complicated by bulk compositions not equivalent to liquids. Therefore, the possibility exists that the Gilmanton, along with the Ames monzodiorite, Albany quartz syenite, and Lake quartz syenite were formed by reaction or assimilation of crustal material into a mantle-derived alkali basalt (Barker et al., 1975).

The process of reaction melting as described by Barker et al. (1975) is complex. It involves a combination of assimilation, crystallization, and reaction of mineral phases with the liquid as equilibrium is approached. Luth (1974) has described the possible effects of resorption of silicate

minerals into a liquid, and his discussion illustrates the complexity of reactions involving biotite and hornblende. Barker et al. (1975) indicate in their description of reaction melting that iron enrichment of the liquid is an early feature of the process. But, as Figure 15 shows, the Albany and Lake quartz syenites are not significantly enriched in FeO* relative to the Belknap Mountain syenite and Sawyer quartz syenite. However, they have significantly higher concentrations of MgO, CaO, and TiO_2 and lower total alkalis (Table 6). These trends are opposite to those predicted by Barker et al. (1975) for a reaction melting process. Possibly the higher $^{87}Sr/^{86}Sr)_o$, higher values of MgO and CaO, and lower total alkalis in the Albany quartz syenite and Lake quartz syenite are due to assimilation of some percentage of metamorphosed basic material at the base of the Merrimack synclinorium by a mantle-derived alkali basalt. Aleinikoff (1977) has concluded that sections of the Ordovician Ammonoosuc volcanics on the flank of the synclinorium are comparable to modern day abyssal tholeiites and island arc tholeiites. While it cannot be demonstrated that similar material underlies the synclinorium to the southeast, there is no evidence for an older crystalline basement. Because of the low Rb/Sr of tholeiitic volcanic material, the $^{87}Sr/^{86}Sr$ at $\sim$168 m.y. would not be as high as for sedimentary material. Assimilation of such material could produce the slight increase in $^{87}Sr/^{86}Sr)_o$ observed in the Albany quartz syenite, the higher MgO and CaO, lower total alkalis, and also possibly the lower

REE at a given SiO_2. The Ammonoosuc volcanics are high in TiO_2 (Aleinikoff, 1977), so assimilation may also explain the high TiO_2 concentration. The effect of assimilation on trace elements, however, is hard to evaluate because of alteration and metamorphic effects on the assimilated material and also because the Albany quartz syenite has undergone considerable fractional crystallization.

Whitney (1972) used the results of his phase assemblage studies on synthetic granitic systems to conclude that the Albany quartz syenite in the North Conway Quadrangle and the Ossipee Mountains was formed at a pressure of at least 10 kilobars (∿30-35 kilometers), and intruded rapidly to the present level of erosion. Embayed quartz phenocrysts similar to ones described by Whitney (1972) in the Albany quartz syenite occur in sample 1 of Albany quartz syenite from the Belknap Mountains complex (Appendix I). The major element composition of sample 1 is similar to the quartz syenite samples discussed by Whitney (1972), suggesting that the Albany quartz syenite in the Belknap Mountains was also rapidly intruded from a depth of 30-35 kilometers. Because Taylor (1978) has determined a crustal thickness of ∿40 km in the Merrimack synclinorium this is not inconsistent with assimilation of metamorphosed basic material at the base of the Merrimack synclinorium prior to emplacement of the Albany quartz syenite.

The REE concentrations in the Lake quartz syenite are unique (Figure 28). These high abundances are not consistent

with simple assimilation of tholeiitic basalt, and they may reflect differences in initial REE content of the alkali basalt (due to different percents of partial melting (?)), or may be the result of more complex processes occurring in the crust. The data are inadequate for constraining the origin of the Lake quartz syenite.

With only one sample very little can be said about the origin of the Ames monzodiorite. The ubiquitous mafic clots or inclusions mentioned by Modell (1936) and the high Co and Sc contents may reflect assimilation of, or reaction with, mafic crustal material. If the liquid equilibrated with a residue containing plagioclase, the (-)Eu anomaly would be explained.

The data for the Gilmanton monzodiorite are equivocal insofar as a relation to either the diorite or Belknap Mountain syenite. Most trace element data can be modeled satisfactorily for the diorite-monzodiorite relation, but the major element abundances are not consistent with models based on trace elements. Possible relationships to the Belknap Mountain syenite are obscured by cumulate effects. Further analytical work on carefully selected samples is necessary.

CHAPTER 8. SUMMARY AND DISCUSSION

This chapter summarizes the conclusions drawn from the isotope, major and trace element data, and petrography, and a model for the evolution of the complex consistent with this data is presented. This model and the general characteristics of the Belknap Mountains complex are then compared with other complexes (most notably the Pikes Peak batholith and the Younger Granites of Nigeria).

Summary

Conclusions drawn from the isotope data, as outlined in Chapter 3, were that a comagmatic relation is possible between the gabbro, diorite, Belknap Mountain syenite, Cobble Hill syenite, Sawyer quartz syenite, and Conway granite. The Albany quartz syenite has a significantly higher initial ratio (obtained from an isochron relation), indicating a different source for the magma, or a mixture of material from several sources. The remaining units, the two monzodiorites and the Lake quartz syenite, fell above the lower isochron without defining an isochron. The Ames monzodiorite yielded a whole rock-mineral isochron with a low age and $^{87}Sr/^{86}Sr)_o \sim 0.7043$, and the isotope data for the Gilmanton monzodiorite are difficult to interpret. The scatter of data may reflect weathering or post-magmatic exchange with meteoric water (Chapter 3).

In agreement with the grouping based on isotopic data,

the major element data of the Albany and Lake quartz syenites are significantly higher in MgO, CaO, and TiO_2 and lower in total alkalis and Fe/Fe+Mg than the felsic units on the lower regression line. The Gilmanton monzodiorite has equivocal major element data, with only some oxides falling on a trend defined by the possibly comagmatic units. The major and trace element characteristics of the Gilmanton monzodiorite are affected by cumulate processes, and further work on carefully screened samples is necessary to clarify its relation to the units on the lower regression line.

Major and trace element data strongly support a comagmatic relation between the Belknap Mountain syenite, Sawyer quartz syenite, and Conway granite. However, the Cobble Hill syenite seems to have fractionated under different conditions of P_{H_2O} (and fo_2?) than the Belknap Mountain syenite, leading to radically different Sr and Ba abundances and mafic silicate composition. A common source for the Cobble Hill syenite and Belknap Mountain syenite is not ruled out.

Modeling of the gabbro/diorite (particularly Ba and Sr) provided some support for the comagmatic relation permitted by the isotopes, but the diorite may have had its LREE, Th, and Rb concentrations raised by contamination during intrusion of the Conway granite. Possible relations between the diorite and felsic units are obscured by the large SiO_2 range between samples ($\sim$10%) and the lack of intermediate samples. It is concluded that with the present data a cogenetic origin

is not ruled out. The chief obstacle is the mechanism of SiO_2 enrichment within the diorites. Between diorite samples 5, 17, and 18 there is a trend of silica enrichment which is not understood as it requires much more hornblende than observed in the rocks.

Because there is no clear relation between the diorite and the more felsic units, an origin for the Belknap Mountain syenite by partial melting of an alkaline gabbro was investigated. A source which satisfies the isotope, major, and trace element data would be a gabbro similar to samples 9 and 15 but with lower Sr, Ba, and REE. Such a rock was not sampled, but the large positive gravity and aeromagnetic anomalies beneath the Belknaps (Sharp and Simmons, 1978) suggests such a source at depth. These gravity and aeromagnetic anomalies also support an origin for the felsic units by fractional crystallization.

The ambiguity in the relation of the diorite to the felsic units inhibits the development of a unique model consistent with all the data. Two possibilities are considered (Figure 41).

Model A makes the assumption that the isotope data is the overriding factor in indicating a cogenetic relation for all units on the lower regression line. The sequence gabbro ← diorite → Belknap Mountain syenite → Sawyer quartz syenite → Conway granite is related by crystal fractionation, with the Cobble Hill syenite derived from the same magma

under conditions of low P_{H_2O}. This produces the large positive gravity anomaly and aeromagnetic high (Sharp and Simmons, 1978). In this case, surface exposures are not representative of the actual proportions of rock types in the complex.

Model B assumes the difficulty in establishing a comagmatic relation between the diorite and felsic units with low initial $^{87}Sr/^{86}Sr$ by geochemical modeling indicates an origin for the Belknap Mountain syenite → Sawyer quartz syenite → Conway granite sequence by partial melting of alkaline gabbro derived from a less fractionated source than than diorite. In this model the Cobble Hill syenite is produced by fractional crystallization of alkali basalt since a magma with ∿30 ppm Sr cannot be produced from a basic source by partial melting.

In both models A and B it is assumed that the scatter of Gilmanton monzodiorite isotope data is due to weathering of a unit with initially high $^{87}Sr/^{86}Sr)_o$ (Chapter 3). The ambiguity in the major and trace element modeling (Chapter 6) of the Gilmanton monzodiorite, however, makes a comagmatic relation with other Belknap Mountains complex units possible. Both models show the Albany and Lake quartz syenites as produced by fractionation of alkali basalt which has assimilated or reacted with metamorphosed tholeiitic basalt at the base of the Merrimack synclinorium. A similar origin is indicated for the monzodiorites.

Discussion

As discussed in Chapter 3, detailed isotopic studies on similar complexes (sub-alkaline and alkaline) have indicated several different modes of formation from wholly comagmatic (Marangudzi, Foland and Henderson, 1976) to the type complex for the reaction melting hypothesis (Pikes Peak, Barker et al., 1975). When the number of variables involved in the genesis of such complexes is considered (quantity and composition of mantle-derived liquid, nature of the crustal section, thermal state of the lower and intermediate crust, etc.) it would be surprising if there was little or no diversity in the origin of anorogenic continental intrusives.

One of the most thoroughly studied intrusives of this type is the Precambrian Pikes Peak batholith (Barker et al., 1975, 1976). The batholith is composed dominantly of biotite and biotite-hornblende granite with lesser amounts of fayalite granite, riebeckite granite, and quartz syenite. There is also a marginal, coeval stock of gabbro and syenite. Initial Sr isotope ratios range from 0.7044 for the gabbro; 0.7044-0.7063 for the syenite and quartz syenites, through 0.7063-0.7114 for the granites (Hedge and Barker, 1975). This increase in $^{87}Sr/^{86}Sr)_o$ is matched by an increase in δO^{18} values for the whole rocks from +6.4 ‰ (gabbro) to +8.1 ‰ (syenite) and +8.8 ‰ (biotite granite) (Barker and O'Neil, 1975). The rare earth patterns of the felsic rocks are broadly similar to the patterns for the Belknap Mountains complex rocks in that they have enriched LREE, moderate to

large (-)Eu anomalies, and flat HREE (Barker et al., 1976). There are two trends of granitic rocks present, a well defined sodic trend consisting of the quartz syenites and fayalite and riebeckite granites, and a less well defined potassic trend consisting of the biotite and biotite-hornblende granites (Barker et al., 1975). Barker et al. (1975) presented a model for the origin of the batholith which is summarized in Figure 2 (Chapter 1). The sodic trend results from differentiation of syenitic magma formed in the lower crust; the potassic biotite granites by reaction melting in the intermediate crust. Fractional crystallization has played a role in the genesis of the quartz syenites and fayalite and reibeckite granites, as evidenced by their low Sr concentrations (Hedge and Barker, 1975) and large (-)Eu anomalies (Barker et al., 1976).

Similar high level, anorogenic granitic complexes make up the Niger-Nigeria province (Bowden and Turner, 1974). Acidic rocks occupy over 95% of the total area of the province, and both peralkaline and non-peralkaline types are represented. Sr isotope studies (van Breeman et al., 1973) strongly suggest a crustal origin for most of the granites. No isotope data is available for the minor basic material, but syenite from one complex has a model $^{87}Sr/^{86}Sr)_o \simeq 0.7048$, substantially lower than the associated granites (van Breeman et al., 1975). Bowden and Turner (1974) propose a model where basic material generated in the upper mantle produced partial melting of granodioritic lower crust to yield

alumimous granites and granitic upper crust to yield peralkaline magmas

The origin of the Sawyer quartz syenite and Conway granite through extensive fractional crystallization of a syenitic liquid contrasts strongly with the origins of the biotite granites in the Pikes Peak batholith and Niger-Nigeria complexes. The low $^{87}Sr/^{86}Sr)_o$ of the Conway precluded the involvement of any older crustal material in its genesis. The identical initial Sr isotope ratio of the Belknap Mountains complex basic rocks and the syenite-quartz syenite-granite sequence is similar to the isotope relations in the Marangudzi complex (Foland and Henderson, 1976), where a wide range of rock types was developed by fractional crystallization (C.M.B. Henderson, pers. comm., 1976). However, as noted above, fractional crystallization has played a role in the generation of the Pikes Peak rocks, and the REE patterns and Sr abundances of the fayalite quartz syenite are strikingly similar to the Sawyer quartz syenite (compare Figure 6 of Barker et al., 1976, with the Sawyer REE pattern, Figure 28). Fractional crystallization is also evident at Kûngnât, Gardar province (Upton, 1960).

A significant feature of the Belknap magmas which contrasts with complexes that have undergone extensive reaction melting is a lack of Fe enrichment on a molecular AFM diagram (Figure 42). In this respect the Belknap Mountains complex is very similar to the Marangudzi complex. It appears that a characteristic feature of reaction melting, Fe enrichment, is

not produced to a similar degree in complexes where felsic rocks are produced by fractional crystallization (at least under conditions that existed during the evolution of the Belknap and Marangudzi magmas).

The position of the sodic differentiation trend of Barker et al. (1975) relative to their potassic trend on a normative Q-Or-Ab diagram is similar to the position of the Cobble Hill syenite relative to the sequence Belknap Mountain syenite - Sawyer quartz syenite - Conway granite on Q-Or-Ab (Figure 23). Barker et al. (1975) concluded the rocks of the sodic trend evolved under conditions of lower P_{H_2O} than the associated biotite granites. The same conclusion was drawn concerning the Cobble Hill syenite relative to the Belknap Mountain syenite (Chapter 6).

In terms of the two end member models discussed in Chapter 1 (Figure 2), the Belknap Mountains complex must have evolved via both models, but reaction or assimilation played only a minor role in the evolution of most Belknap Mountains complex magmas. Fractional crystallization has played a major role (more so in Model A) in the genesis of the magmas, and has had a greater control on the rock compositions.

No claim is made that the model applies to other White Mountain complexes. For example, the isotope data for Red Hill (Foland and Friedman, 1977), unlike the Belknap Mountains complex isotope data, indicate a considerable contribution of crustal material to the granite magma. Obviously, isotope

data are extremely critical in interpreting the relations between rock units. Interpretation of geochemical data without accompanying isotope data can be frustrating and lead to ambiguous solutions (viz. the Gilmanton monzodiorite).

Figure Captions

Figure 41. Models relating the various rock units of the Belknap Mountains complex based on major and trace element and isotope data. See text for assumptions made in developing models A and B.

Figure 42. Molecular A-F-M diagram comparing the Belknap Mountains complex to the Pikes Peak batholith (data from Barker et al., 1975); the Nigerian Younger Granite complexes (data from Jacobson et al., 1958; MacLeod et al., 1971); and the Marangudzi complex, Rhodesia (Foland and Henderson, 1976).

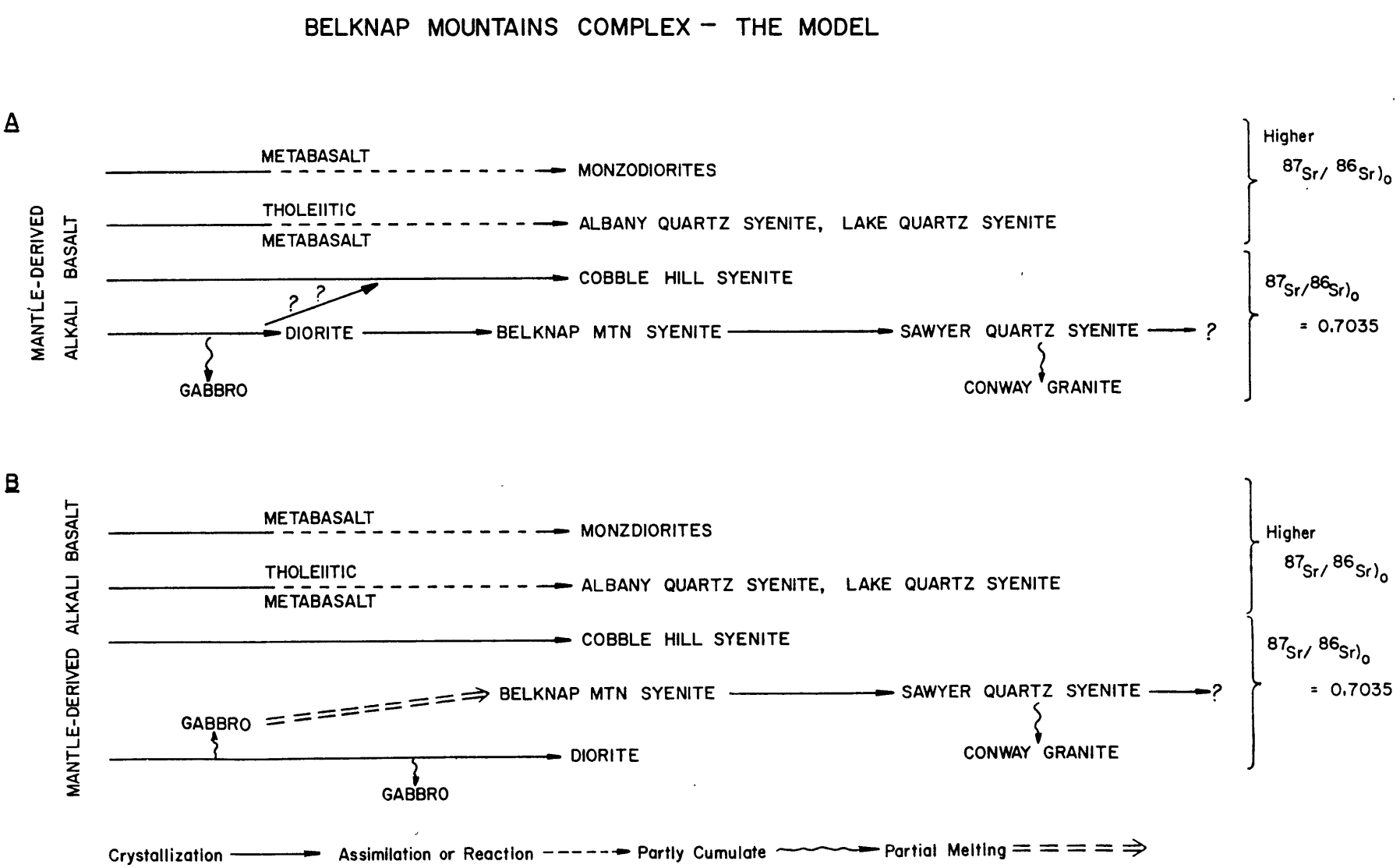
BELKNAP MOUNTAINS COMPLEX – THE MODEL
A
MANTLE-DERIVED ALKALI BASALT
METABASALT
MONZODIORITES
THOLEIITIC METABASALT
ALBANY QUARTZ SYENITE, LAKE QUARTZ SYENITE
COBBLE HILL SYENITE
? ?
DIORITE
BELKNAP MTN SYENITE
SAWYER QUARTZ SYENITE
?
GABBRO
CONWAY GRANITE
Higher $^{87}Sr/^{86}Sr)_o$
$^{87}Sr/^{86}Sr)_o$ = 0.7035
B
MANTLE-DERIVED ALKALI BASALT
METABASALT
MONZDIORITES
THOLEIITIC METABASALT
ALBANY QUARTZ SYENITE, LAKE QUARTZ SYENITE
COBBLE HILL SYENITE
GABBRO
BELKNAP MTN SYENITE
SAWYER QUARTZ SYENITE
?
CONWAY GRANITE
DIORITE
GABBRO
Higher $^{87}Sr/^{86}Sr)_o$
$^{87}Sr/^{86}Sr)_o$ = 0.7035
Crystallization
Assimilation or Reaction
Partly Cumulate
Partial Melting

Figure 41

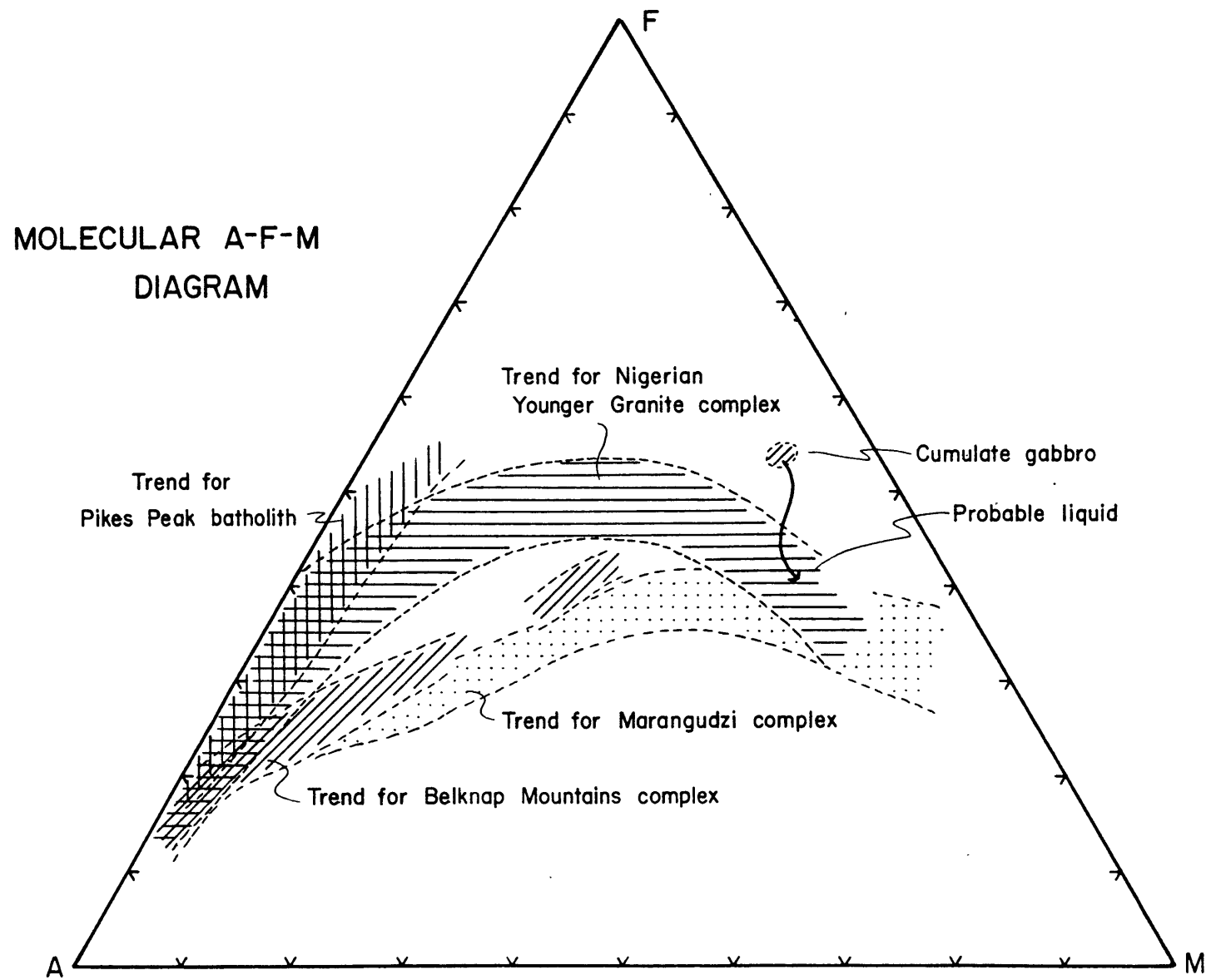
MOLECULAR A-F-M
DIAGRAM
F
A
M
Trend for Nigerian
Younger Granite complex
Cumulate gabbro
Trend for
Pikes Peak batholith
Probable liquid
Trend for Marangudzi complex
Trend for Belknap Mountains complex

Figure 42

CHAPTER 9. RESULTS OF ANALYSIS OF PLINY RANGE SAMPLES

Introduction

As discussed in Chapter 2, the White Mountain series rocks of the Pliny Range were intruded into the Bronson Hill anticlinorium, which had a more complex pre-Mesozoic crustal history than the Merrimack synclinorium. Since in any model involving reaction of magma with crustal material the nature of the crust will have a significant effect on the composition of the resulting magma, a comparison of samples from the Pliny Range with material from the Belknap Mountains complex might show the effects of the different crustal sections. Czamanske et al. (1977) studied the mineralogy and petrology of the Pliny Range, and concluded that a model similar to the reaction melting model of Barker et al. (1975) was necessary to explain the relations between the rocks. Trace element analysis of samples analyzed by Czamanske et al. (1977) was initially undertaken to supplement their study, and the work was later expanded with the collection of additional samples.

No isotope data for the Pliny Range samples are available at this time, so there is no information as to which units are likely to be related by fractional crystallization. Therefore, no detailed modeling of possible relationships between Pliny Range units was done. However, there were significant features in the compositions of some Pliny Range units (notably the older syenites and the hastingsite quartz syenite) which indicate processes different from those which acted in the

Belknap Mountains complex occurred.

The analytical procedures for major and trace element analyses of Pliny Range samples are the same as those used for the Belknap Mountains samples (Appendix II). An exception is that all Rb and Sr data for the Pliny Range samples were obtained by X-ray fluorescence analysis, not by isotope dilution analysis. Table 17 gives the results of major element analyses of new samples, together with data on samples reported in Czamanske et al. (1977), and CIPW norms of all samples. Table 18 gives the results of trace element analyses of all samples.

Discussion of Major and Trace Element Data

Figures 43 to 49 are oxide variation diagrams for the Pliny Range samples; Figure 50 is a plot of whole rock Fe/Fe+Mg vs. SiO_2, and Figure 51 is a molecular A-F-M diagram for the Pliny Range rocks. Figures 52 -54 are chondrite normalized rare earth diagrams for the Pliny Range samples.

One of the most striking features is the significant iron enrichment in the hastingsite quartz syenite relative to the other Pliny Range units and the trend for Belknap Mountains complex samples (Figure 51). In this respect the hastingsite quartz syenite is similar to rocks from the Pikes Peak batholith (Barker et al., 1975) and the Nigerian Younger granites (Jacobsen et al., 1958) (see Figure 42). Barker et al. (1975) indicate this feature of iron enrichment is characteristic of the early stages of reaction melting, and may

TABLE 17. MAJOR ELEMENT ANALYSES AND CIPW NORMS

FOR PLINY RANGE SAMPLES[a]

	Diorite		Quartz Monzodiorite		Porphyritic Quartz Monzonite		Hastingsite Quartz Syenite		Pink Biotite Granite	
	E-W	14	E-70	4	E-78	10	E-SK	12	E-115	5
SiO_2	50.1	49.7	54.1	58.3	69.3	69.5	69.3	65.6	74.5	72.9
TiO_2	2.9	2.59	2.5	1.45	0.30	0.31	0.31	0.45	0.16	0.16
Al_2O_3	15.6	16.0	16.5	15.8	15.6	15.6	14.7	15.0	13.0	13.7
Fe_2O_3[b]	3.37	--	1.80	--	1.75	--	3.39	--	1.34	--
FeO	8.25	10.9	7.72	7.71	0.91	1.93	1.40	6.12	0.44	1.95
MgO	4.6	4.63	3.1	1.75	0.47	0.45	0.05	0.04	0.11	0.06
CaO[c]	7.1	7.06	5.8	4.27	0.30	1.26	0.29	1.94	0.50	0.40
Na_2O[c]	3.67	3.31	3.68	3.69	4.50	3.78	5.47	4.79	3.30	3.59
K_2O	2.35	2.02	3.53	3.83	5.51	5.97	4.37	5.58	5.60	5.82
P_2O_5	0.56	0.71	0.82	0.75	0.07	0.07	0.02	0.05	n.d.	n.d.
H_2O^+	1.1	--	1.3	--	0.76	--	0.54	--	0.72	--
CO_2	--	--	--	--	--	--	--	--	--	--
TOTAL[d]	99.88	96.92	101.17	97.55	100.61	98.87	99.89	99.57	99.69	98.58

TABLE 17. continued

	Diorite		Quartz Monzodiorite		Porphyritic Quartz Monzonite		Hastingsite Quartz Syenite		Pink Biotite Granite	
	E-W	14	E-70	4	E-78	10	E-SK	12	E-115	5
Q	--	0.87	1.69	9.37	18.52	21.70	20.15	13.68	32.75	29.18
C	--	--	--	--	--	0.83	0.49	--	0.60	0.76
Or	13.90	12.27	20.68	23.17	32.37	35.62	25.87	32.99	33.20	34.84
Ab	31.09	28.79	30.88	31.97	37.85	32.30	46.36	40.56	28.02	30.77
An	19.18	23.38	17.93	15.46	6.06	5.85	1.31	2.81	2.50	2.01
Wo	5.10	3.28	2.21	0.51	0.15	--	--	2.71	--	--
En	7.92	11.85	7.66	4.46	1.16	1.13	0.13	0.10	0.28	0.16
Fs	5.49	7.95	8.49	8.26	--	--	--	--	--	--
Fo	2.49	--	--	--	--	--	--	--	--	--
Fa	1.90	--	--	--	--	--	--	--	--	--
Mt	4.89	4.87	2.59	2.21	2.15	1.47	3.62	4.88	0.96	1.23
Hm	--	--	--	--	0.26	0.34	0.90	1.29	0.69	0.75
Il	5.51	5.06	4.70	2.82	0.57	0.60	0.59	0.86	0.31	0.31
Ap	1.33	1.73	1.93	1.82	0.17	0.17	0.05	0.12	--	--
Fe/Fe+Mg	0.58	0.57	0.63	0.72	0.75	0.71	0.98	0.99	0.89	0.94
Na+K/Al	0.55	0.48	0.60	0.65	0.86	0.81	0.93	0.93	0.88	0.89

TABLE 17. continued

	Granite Porphyry		Hastingsite Biotite Granite			Conway Granite			Coarse Syenite			Medium Syenite	
	E-34	1	E-169	11	13	E-171	3	6	E-177	2	7	E-119	8
SiO_2	72.1	70.1	73.0	74.2	75.0	72.7	74.9	75.4	64.4	70.8	60.7	65.5	67.7
TiO_2	0.29	0.40	0.31	0.19	0.22	0.22	0.17	0.20	0.43	0.29	0.42	0.28	0.27
Al_2O_3	13.9	14.1	13.5	13.1	12.7	14.4	12.7	12.8	18.1	14.3	18.6	17.5	16.5
Fe_2O_3[b]	0.94	--	0.29	--	--	0.91	--	--	1.60	--	--	1.56	--
FeO	1.29	2.60	1.34	1.79	1.92	1.18	1.61	1.67	1.00	1.86	3.14	0.93	1.95
MgO	0.20	0.41	0.34	0.11	0.17	0.15	0.06	0.17	0.55	0.51	1.04	0.40	0.28
CaO[c]	0.82	1.17	0.89	0.50	0.65	0.61	0.32	0.54	2.0	1.72	2.05	1.2	0.60
Na_2O[c]	4.35	4.24	3.82	3.78	3.68	4.02	3.69	3.59	4.91	3.41	4.38	5.37	4.67
K_2O	5.14	5.19	5.12	5.27	4.98	5.41	5.26	5.06	6.43	5.61	7.42	6.58	6.85
P_2O_5	0.04	0.10	0.05	n.d.	n.d.	n.d.	n.d.	n.d.	0.13	0.15	0.32	0.06	0.02
H_2O^+	0.81	--	0.63	--	--	0.13	--	--	0.92	--	--	--	--
CO_2	--	--	--	--	--	--	--	--	--	--	--	--	--
TOTAL[D]	100.01	98.31	99.40	98.94	99.32	99.78	98.71	99.43	100.56	98.65	98.07	100.22	98.84

TABLE 17. continued

	Granite Porphyry		Hastingsite Biotite Granite			Conway Granite			Coarse Syenite			Medium Syenite	
	E-34	1	E-169	11	13	E-171	3	6	E-177	2	7	E-119	8
Q	24.84	22.72	28.34	30.14	32.04	26.68	32.49	33.53	6.12	25.89	1.77	6.37	12.81
C	--	--	0.18	0.23	0.05	0.83	0.40	0.43	--	--	0.40	--	0.37
Or	30.41	31.17	30.47	31.48	29.64	32.06	31.47	30.05	37.82	33.60	44.65	38.83	40.90
Ab	36.85	36.46	32.55	32.33	31.36	34.11	31.61	30.53	41.35	29.24	37.74	45.38	39.93
An	3.23	4.21	4.11	2.51	3.25	3.04	1.61	2.69	8.32	7.10	8.23	4.21	2.88
Wo	0.24	0.43	--	--	--	--	--	--	0.30	0.23	--	0.56	--
En	0.50	1.04	0.85	0.28	0.43	0.38	0.15	0.43	1.36	1.29	2.64	0.99	0.71
Fs	1.12	1.30	1.72	2.20	2.32	1.06	0.87	0.87	--	--	--	--	--
Fo	--	--	--	--	--	--	--	--	--	--	--	--	--
Fa	--	--	--	--	--	--	--	--	--	--	--	--	--
Mt	1.37	1.68	0.42	0.46	0.51	1.32	1.07	1.11	1.97	1.63	2.99	2.18	1.75
Hm	--	--	--	--	--	--	--	--	0.24	0.10	0.02	0.05	0.11
Il	0.55	0.77	0.59	0.37	0.42	0.42	0.33	0.38	0.81	0.56	0.81	0.53	0.52
Ap	0.10	0.24	0.12	--	--	--	--	--	0.31	0.36	0.77	0.14	0.05
Fe/Fe+Mg	0.86	0.78	0.72	0.90	0.86	0.88	0.94	0.85	0.71	0.67	0.63	0.76	0.80
Na+K/Al	0.92	0.89	0.88	0.91	0.90	0.87	0.92	0.89	0.83	0.82	0.82	0.91	0.92

TABLE 17. continued

Notes

a Includes data from Czamanske et al. (1977). Norms for samples from Czamanske et al. (1977) recalculated at the same time other samples were calculated to insure consistency of results.

b Where Fe_2O_3 not given, total iron reported as FeO.

c See Appendix II for details of CaO and Na_2O analyses.

d Total for samples from Czamanske et al. (1977) includes components not given here.

n.d. not detected

-- not determined

TABLE 18. TRACE ELEMENT DATA FOR PLINY RANGE SAMPLES[a]

	Diorite		Quartz Monzodiorite		Porphyritic Quartz Monzonite		Hastingsite Quartz Syenite		Pink Biotite Granite	
	E-W	E-14	E-70	4	E-78	10	E-SK	12	E-115	5
Rb[b]	81.	52.	112.	120.	174.	121.	270.	163.	222.	198.
Sr[b]	790.	844.	752.	607.	476.	501.	38.	23.	72.	112.
Ba	c	511.	c	1180.	525.	506.	c	359.	174.	249.
Sc	23.	20.	21.	15.	2.9	3.2	3.3	9.2	1.9	2.8
Co	36.	--	15.	--	2.3	--	0.65	--	0.39	--
La	c	44.6	c	108.	65.2	86.1	c	134.	58.0	142.
Ce	82.9	107.	169.	287.	139.	183.	214.	313.	128.	319.
Nd	35.0	53.2	66.0	97.6	75.2	58.2	58.8	115.	36.7	106.
Sm	8.1	7.9	13.4	14.6	8.0	8.7	10.9	17.6	6.6	12.9
Eu	2.4	2.4	2.9	3.0	1.5	1.7	0.40	2.8	0.60	0.64
Ho	1.1	1.1	1.5	1.5	1.2	1.1	3.5	2.3	0.8	2.6
Yb	1.9	2.1	3.5	3.5	2.2	1.7	7.2	5.3	2.0	3.9
Lu	0.29	0.27	0.52	0.33	0.31	0.23	1.09	0.79	0.38	0.58
Zr[b]	217.	229.	346.	449.	297.	327.	675.[d]	521.	148.	372.
Hf	6.0	5.4	8.2	12.6	10.4	11.3	24.0	14.8	6.2	15.4
Th	6.4	6.8	13.4	33.0	23.3	25.5	31.8	24.6	58.8	73.8
U	2.1	c	2.6	4.2	c	7.4	5.9	5.4	6.0	12.8

TABLE 18. continued

	Granite Porphyry		Hastingsite Biotite Granite			Conway Granite			Coarse Syenite			Medium Syenite	
	E-34	1	E-169	11	13	E-171	3	6	E-177	2	7	E-119	8
Rb[b]	178.	175.	259.	186.	219.	211.	170.	210.	120.	115.	134.	137.	155.
Sr[b]	80.	48.	103.	47.	62.	49.	39.	60.	675.	751.	753.	143.	135.
Ba	c	439.	c	167.	223.	148.	148.	221.	695.	1190.	1049.	92.	197.
Sc	3.3	4.1	3.2	3.0	3.1	3.4	3.2	2.8	3.8	3.2	5.8	6.2	4.5
Co	1.05	--	2.28	--	--	0.85	--	--	3.1			1.2	
La	65.4	94.1	c	98.1	72.1	49.1	83.1	66.3	92.5	79.3	107.	152.	85.6
Ce	154.	216.	184.	207.	171.	119.	160.	145.	230.	165.	233.	327.	243.
Nd	51.0	74.8	33.2	67.9	51.7	36.7	47.4	48.5	70.3	44.0	69.8	93.1	24.3
Sm	10.8	11.6	7.3	10.6	9.4	6.8	8.7	8.8	10.2	6.0	11.2	12.4	10.7
Eu	0.74	1.1	0.74	0.46	0.59	0.45	0.36	0.53	2.1	1.5	3.1	2.0	1.5
Ho	1.5	1.6	1.1	1.4	1.3	1.0	1.5	1.4	0. 9	0.6	0.7	0.8	0.9
Yb	4.4	3.7	3.1	3.1	3.5	2.4	2.6	2.9	2.1	1.1	1.5	1.5	1.8
Lu	0.63	0.47	0.40	0.41	0.43	0.42	0.41	0.38	0.35	0.18	0.23	0.23	0.25
Zr[b]	294.	324.	205.	235.	215.	255.	227.	181.	363.	254.	681.[d]	560.[d]	155.
Hf	11.4	10.8	9.2	8.0	8.5	10.9	9.5	8.0	17.2	7.8	20.0	18.6	15.6
Th	32.9	40.4	26.2	50.4	60.2	37.6	51.9	44.0	42.3	29.0	13.1	32.8	34.1
U	11.4	c	3.0	6.7	10.5	4.3	8.6	10.8	4.2	7.5	3.2	3.7	4.2

TABLE 18. continued

Notes

a See Appendix II for details of analytical procedure.

b Rb, Sr, and Sr by XRF.

c Data not available due to instrument malfunctions.

d Out of range of Zr standards. See Appendix II.

reflect the interaction of an alkali basalt with an anhydrous lower crust beneath the Bronson Hill anticlinorium to produce the Hastingsite quartz syenite.

The two samples of hastingsite quartz syenite also have the lowest Sr abundances of all the Pliny Range samples, and sample E-SK has the largest (-)Eu anomaly, indicating considerable fractionation of feldspar. This may also be reflected in the high HREE abundances of the hastingsite quartz syenite. The low Sr at moderate values of SiO_2 (65-69%) is the same feature observed in the Cobble Hill syenite (Belknap Mountains complex). The suggestion by Czamanske et al. (1977) that the hastingsite quartz syenite (23-38 ppm Sr) was produced from the porphyritic quartz monzonite (∿500 ppm Sr) by alkali feldspar accumulation is untenable for the same reason the Cobble Hill syenite cannot be a cumulate from any Belknap Mountain samples analyzed (Chapter 6). This relationship is also precluded on the basis of REE, Zr, Hf, and Th abundances.

As noted by Czamanske et al. (1977), the hastingsite biotite granite and Conway granite are very similar in terms of their major element compositions (Figures 43-49) and Fe/Fe+Mg (Figure 50). In addition, they are also very similar in their trace element compositions (Table 18). With the exception of sample E-169 (which has higher Sr and Rb) the samples of granite all have similar Sr, Rb, and Ba. On a chondrite normalized REE diagram (Figure 54), fields composed of samples of hastingsite biotite granite and Conway granite would be virtually indistinguishable. Thus, the two late

granites which form circular stocks are identical in major and trace element compositions. Relative to the Conway granite from the Belknap Mountains complex, the hastingsite biotite granite and Conway granite from the Pliny Range show a much smaller range of REE abundances, and have slightly lower concentrations of Sr and Ba (on the average). The concentrations of Sr and Ba are the lowest of any of the Pliny Range units (except the hastingsite quartz syenite which has major element and petrologic characteristics indicating it is a separate magma, Czamanske et al., 1977), and this combined with the limited range of REE abundances indicates they are probably liquids resulting from some unknown amount of fractionation. Isotope data is necessary in order to evaluate their relation to the earlier granitic rocks in the Pliny Range which form ring dikes.

Sample 5 of the pink biotite granite has high abundances of "incompatible" elements (REE, Th, U, Zr, Hf) despite major element similarities to pink biotite granite sample E115, and this may be due to larger amounts of accessory phases such as allanite and zircon, both present in the unit.

The Pliny Range diorite REE patterns are similar to the patterns for the diorite from the Belknap Mountains complex, but the Pliny Range diorites have much more Sc and Co, and marginally lower abundances of incompatible elements Zr, Hf, and REE. Comparisons of incompatible element abundances, however, are complicated by possible contamination of the diorite from the Belknap Mountains complex during intrusion of

the Conway granite. The most significant difference between the two diorites is the much lower P_2O_5 (less than 0.75% vs. greater than 1.0%).

The older syenites provide the most interesting results in terms of comparison with other Pliny Range rocks and with the Belknap Mountains syenites and quartz syenites. With respect to major elements the older syenites are similar to the syenites of the Belknap Mountain complex. The more siliceous samples, however, are quite distinct from the hastingsite quartz syenite and to a lesser degree the porphyritic quartz monzonite (Figures 43-49), particularly in terms of the relatively low Fe/Fe+Mg of the coarse syenite, and high total alkalis. However, the most striking features are the REE abundance patterns and the Ba and Sr concentrations.

On a chondrite normalized rare earth diagram the older syenites of the Pliny Range show extremely fractionated patterns $(La/Yb)_{cn}$ = 31-47) with very low HREE abundances, and either no Eu anomaly or a slight (-)Eu anomaly. This is in contrast to the syenites and quartz syenites of the Belknap Mountains complex and the later hastingsite quartz syenite of the Pliny Range which are characterized by moderate to large (-)Eu anomalies, generally flat HREE abundances, and $La/Yb)_{cn} < 30$. The two samples of the medium syenite have slightly higher LREE abundances and larger (-)Eu anomalies, supporting the observation of Czamanske et al. (1977) that it is more fractionated than the coarse syenite. This is also reflected in the lower Ba and Sr in the medium syenite

relative to the coarse syenite.

The Sr concentrations in the coarse syenite (675-750 ppm) are 2 to 3 times the Sr abundances in the Belknap Mountain syenite, and are similar to the values in the Gilmanton monzodiorite (Belknap Mountains) and quartz monzonite (Pliny Range). Ba concentrations in the coarse syenite (700-1200 ppm) are also higher (on average) than the other White Mountain series syenitic rocks studied. The medium syenite (actually a quartz syenite - see Figure 5) has Ba and Sr more like the syenitic rocks from the Belknap Mountains complex. Thus, the older syenites are not only unusual in their age relative to the other Pliny Range magmas and the presence of a weak foliation (Czamanske et al., 1977; also Chapter 2), but also possess geochemical features unlike other White Mountain series syenitic and quartz syenitic rocks studied.

The rare earth abundance patterns, Ba, and Sr concentrations and Rb/Sr ratio of the older coarse syenites are similar to the Precambrian Icarus syenodiorite studied by Arth and Hanson (1975), and the monzonites described and analyzed by Miller (1977a,b). Arth and Hanson (1975) and Miller (1977a,b) both suggest that their magmas formed by limited partial melting of eclogite or quartz eclogite. The lack of a significant Eu anomaly and low HREE abundances in the older syenites would indicate a source lacking plagioclase in the residue and containing a phase such as garnet or amphibole (with relatively large D_{HREE}). Such a source may also apply to the older syenites of the Pliny Range.

Czamanske et al. (1977) concluded that data on intensive parameters during crystallization of the magma precluded a simple genetic model involving a single magma. As pointed out by Czamanske et al. (1977), however, some differences in the intensive parameters during crystallization of the magmas may be due to late processes occurring during intrusion and emplacement, and thus would not necessarily preclude genetic relations between some units such as the ring dike granites and the later hastingsite biotite granite and Conway granite. Preliminary inspection of the major and trace element data supports some of their conclusions, but evaluation and detailed modeling of possible cogenetic relations must await isotope data (specifically values of $^{87}Sr/^{86}Sr)_o$ for the various units).

Figure Captions

Figure 43. Plot of TiO_2 (wt.%) vs. SiO_2 (wt.%) for Pliny Range samples.

- ■ coarse syenite
- ◪ medium syenite
- ● diorite
- ○ quartz monzodiorite
- △ porphyritic quartz monzonite
- ▲ hastingsite biotite granite
- ▽ pink biotite granite
- ▼ granite porphyry
- □ hastingsite biotite granite
- + Conway granite

Figure 44. Plot of Al_2O_3 (wt.%) vs. SiO_2 (wt.%) for Pliny Range samples.

Figure 45. Plot of FeO* (wt.%) vs. SiO_2 (wt.%) for Pliny Range samples.

Figure 46. Plot of MgO (wt.%) vs. SiO_2 (wt.%) for Pliny Range samples.

Figure 47. Plot of CaO (wt.%) vs. SiO_2 (wt.%) for Pliny Range samples.

Figure 48. Plot of Na_2O+K_2O (wt.%) vs. SiO_2 (wt.%) for Pliny Range samples.

Figure 49. Plot of P_2O_5 (wt.%) vs. SiO_2 (wt.%) for Pliny Range samples.

Figure 50. Plot of Fe/Fe+Mg vs. SiO_2 (wt.%) for Pliny Range samples. Fe/Fe+Mg calculated from total iron content of samples.

Figure 51. Molecular A (Na_2O+K_2O) - F (total iron as FeO) - M (MgO) diagram for Pliny Range samples. Because of overlap of points, fields for various rock units are shown instead of individual data points.

Figure 52. Chondrite normalized rare earth diagram for the older syenites, diorite, and quartz monzodiorite. Data normalized to chondrite values of Haskin et al. (1968).

Figure 53. Chondrite normalized rare earth diagram for the hastingsite quartz syenite and porphyritic quartz monzonite. Data normalized to chondrite values of Haskin et al. (1968).

Figure 54. Chondrite normalized rare earth diagram for the pink biotite granite, granite porphyry, hastingsite biotite granite, and Conway granite. Data normalized to chondrite values of Haskin et al. (1968).

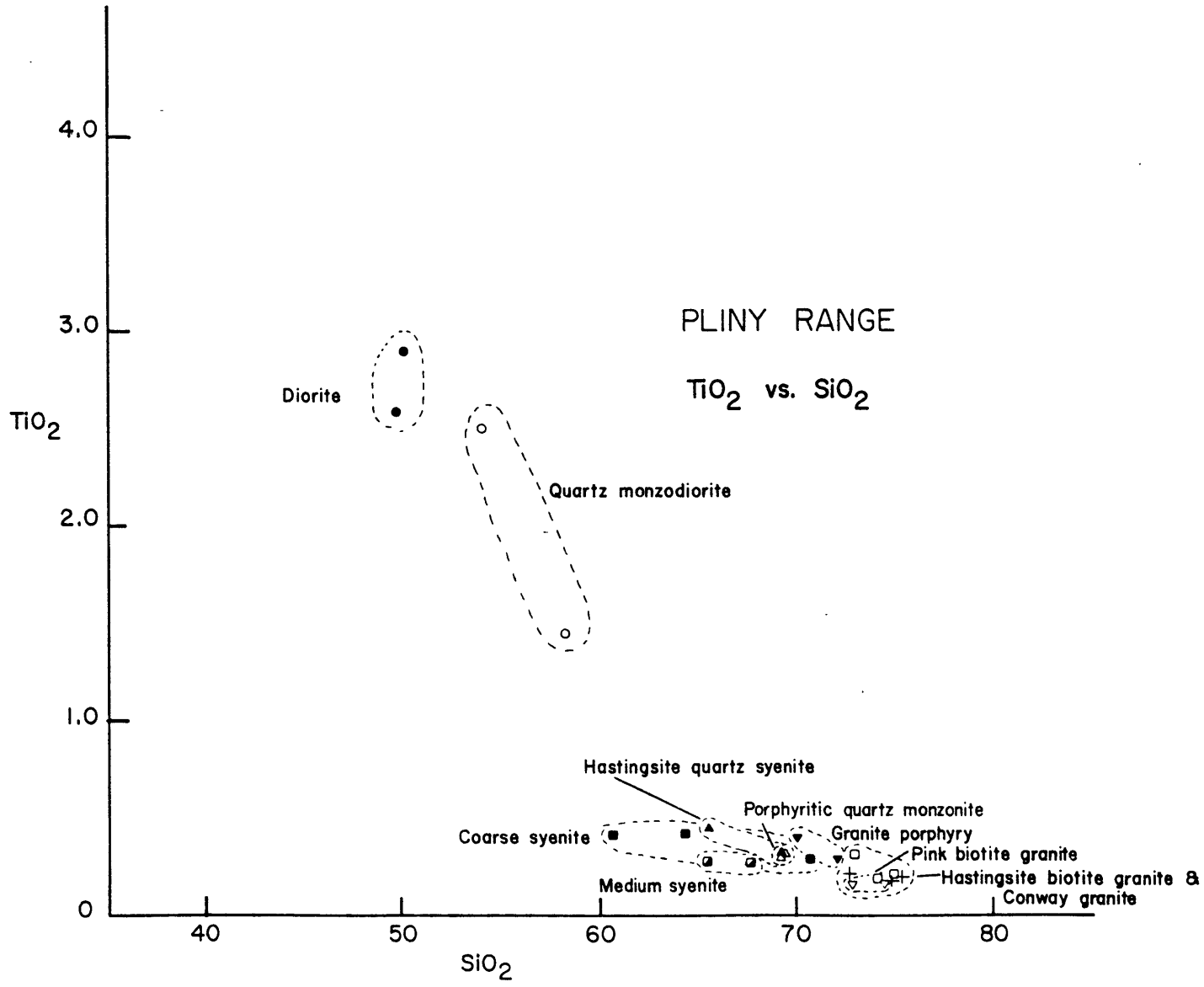
PLINY RANGE
TiO2 vs. SiO2
TiO2
SiO2
4.0
3.0
2.0
1.0
0
40
50
60
70
80
Diorite
Quartz monzodiorite
Hastingsite quartz syenite
Porphyritic quartz monzonite
Coarse syenite
Granite porphyry
Pink biotite granite
Hastingsite biotite granite &
Conway granite
Medium syenite

Figure 43

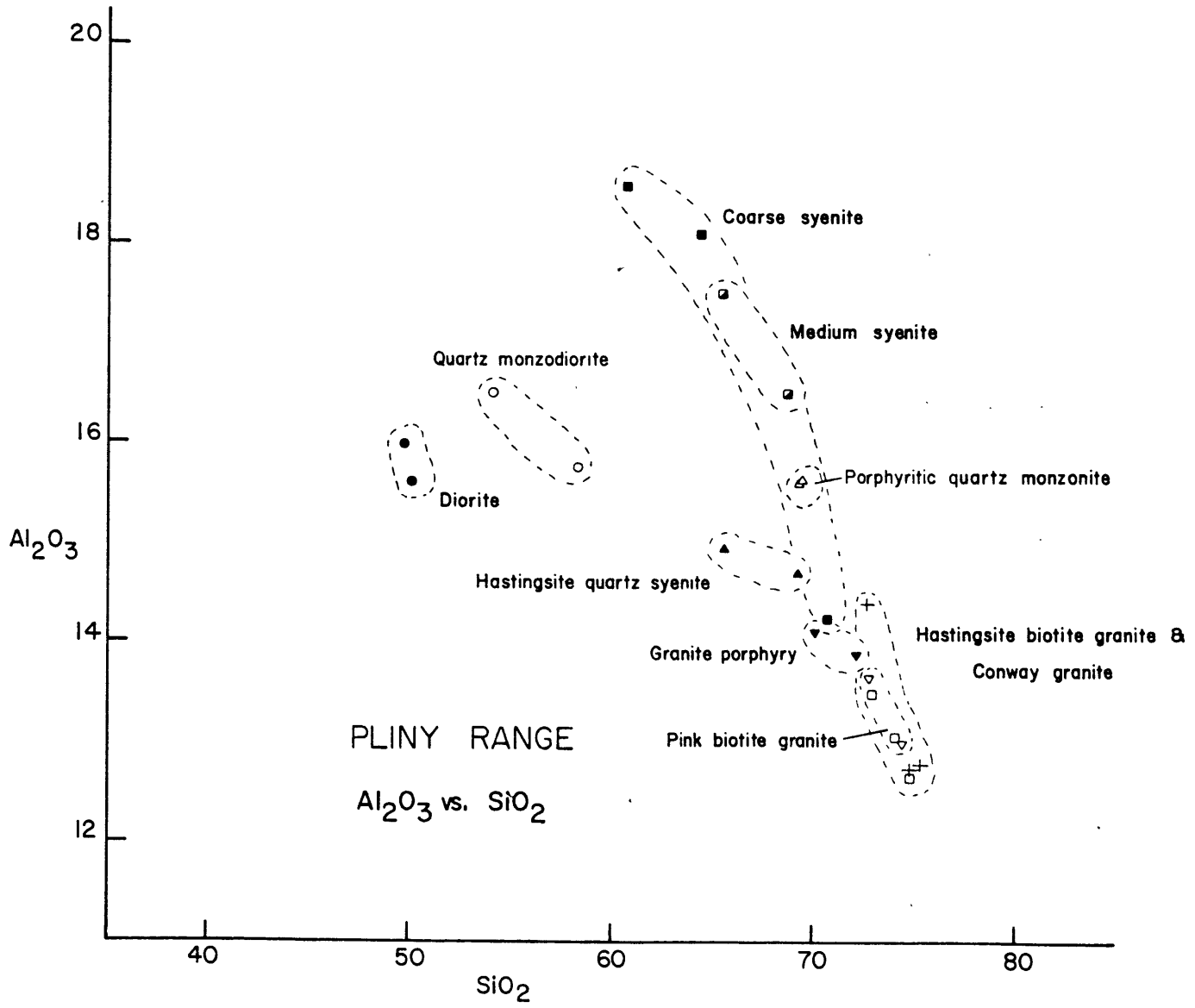
20
18
16
14
12
Al_2O_3
40
50
60
70
80
SiO_2
Coarse syenite
Medium syenite
Quartz monzodiorite
Porphyritic quartz monzonite
Diorite
Hastingsite quartz syenite
Hastingsite biotite granite &
Conway granite
Granite porphyry
Pink biotite granite
PLINY RANGE
Al_2O_3 vs. SiO_2

Figure 44

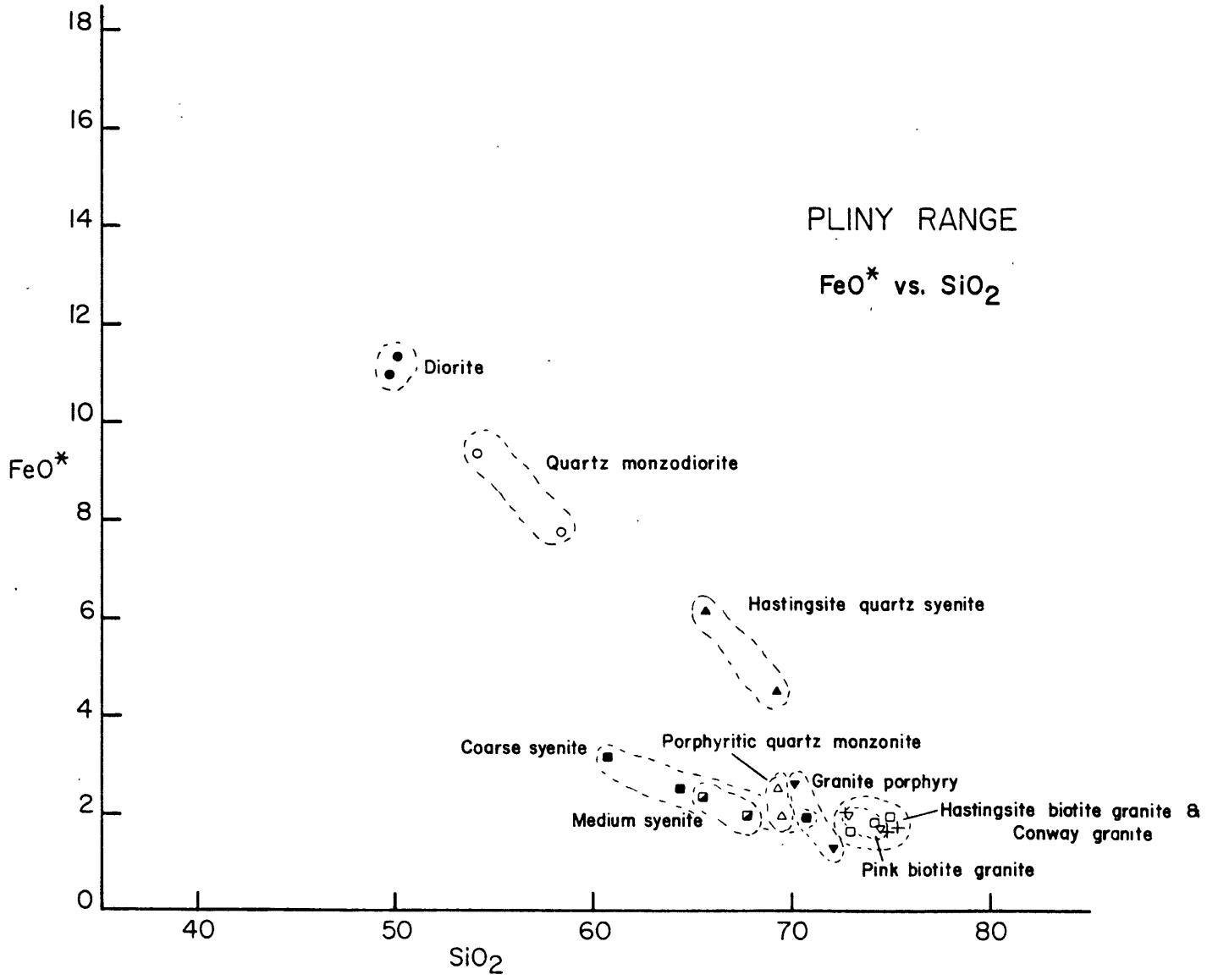
PLINY RANGE
FeO* vs. SiO2
FeO*
SiO2
18
16
14
12
10
8
6
4
2
0
40
50
60
70
80
Diorite
Quartz monzodiorite
Hastingsite quartz syenite
Coarse syenite
Porphyritic quartz monzonite
Granite porphyry
Medium syenite
Hastingsite biotite granite &
Conway granite
Pink biotite granite

Figure 45

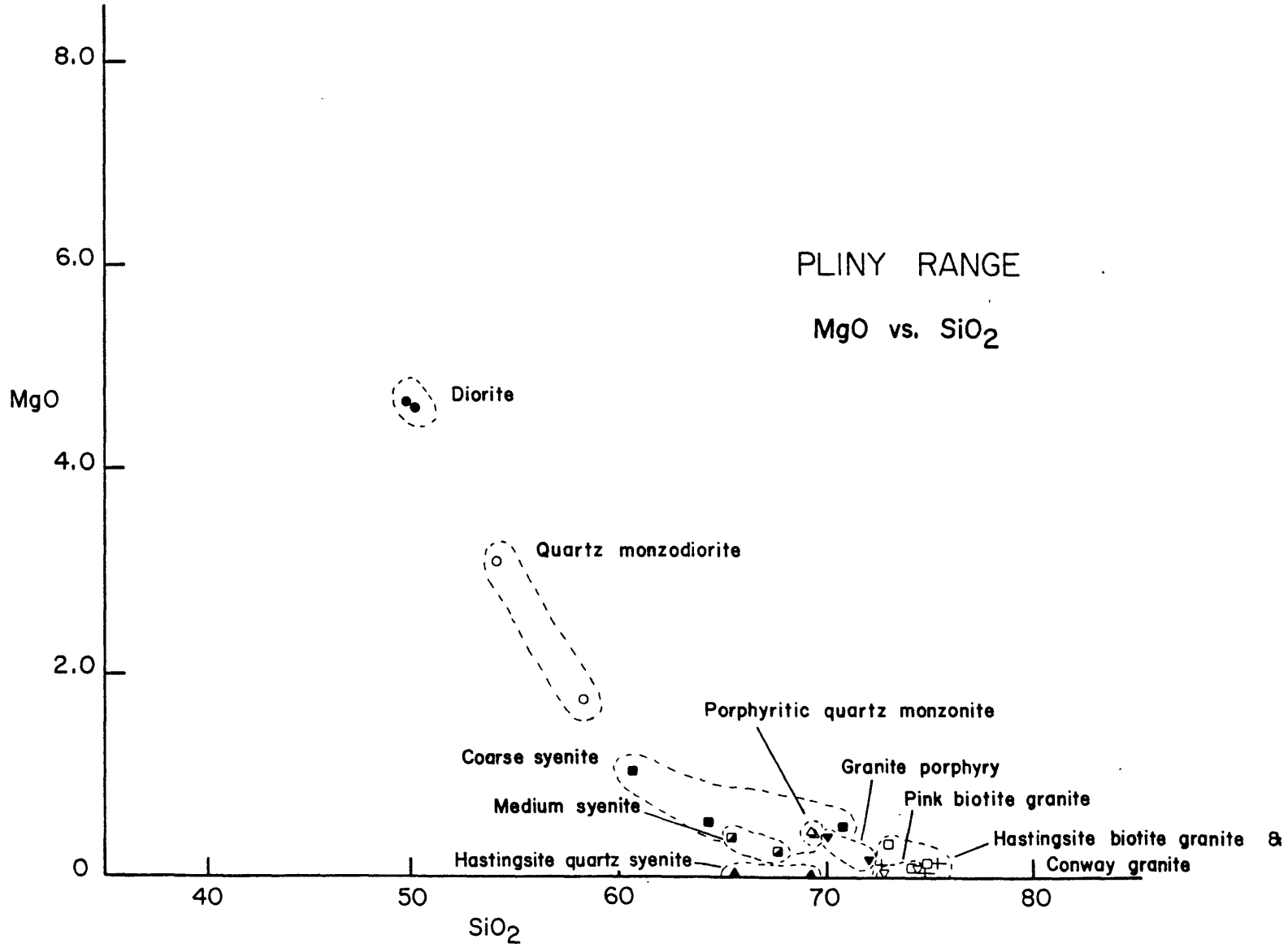
PLINY RANGE
MgO vs. SiO2
MgO
8.0
6.0
4.0
2.0
0
40
50
60
70
80
SiO2
Diorite
Quartz monzodiorite
Porphyritic quartz monzonite
Coarse syenite
Granite porphyry
Medium syenite
Pink biotite granite
Hastingsite biotite granite &
Hastingsite quartz syenite
Conway granite

Figure 46

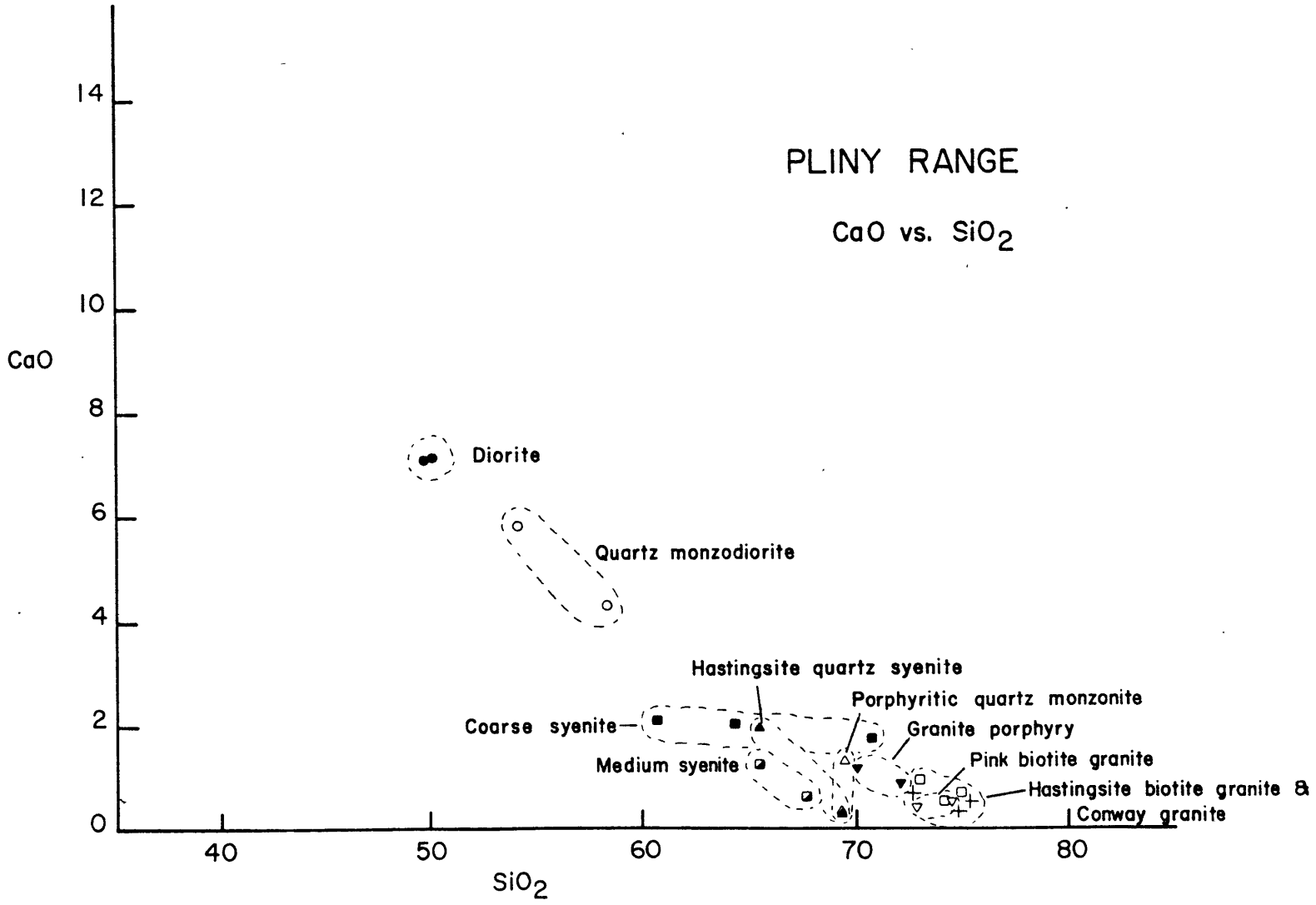
PLINY RANGE
CaO vs. SiO2
CaO
SiO2
14
12
10
8
6
4
2
0
40
50
60
70
80
Diorite
Quartz monzodiorite
Hastingsite quartz syenite
Porphyritic quartz monzonite
Coarse syenite
Granite porphyry
Medium syenite
Pink biotite granite
Hastingsite biotite granite &
Conway granite

Figure 47

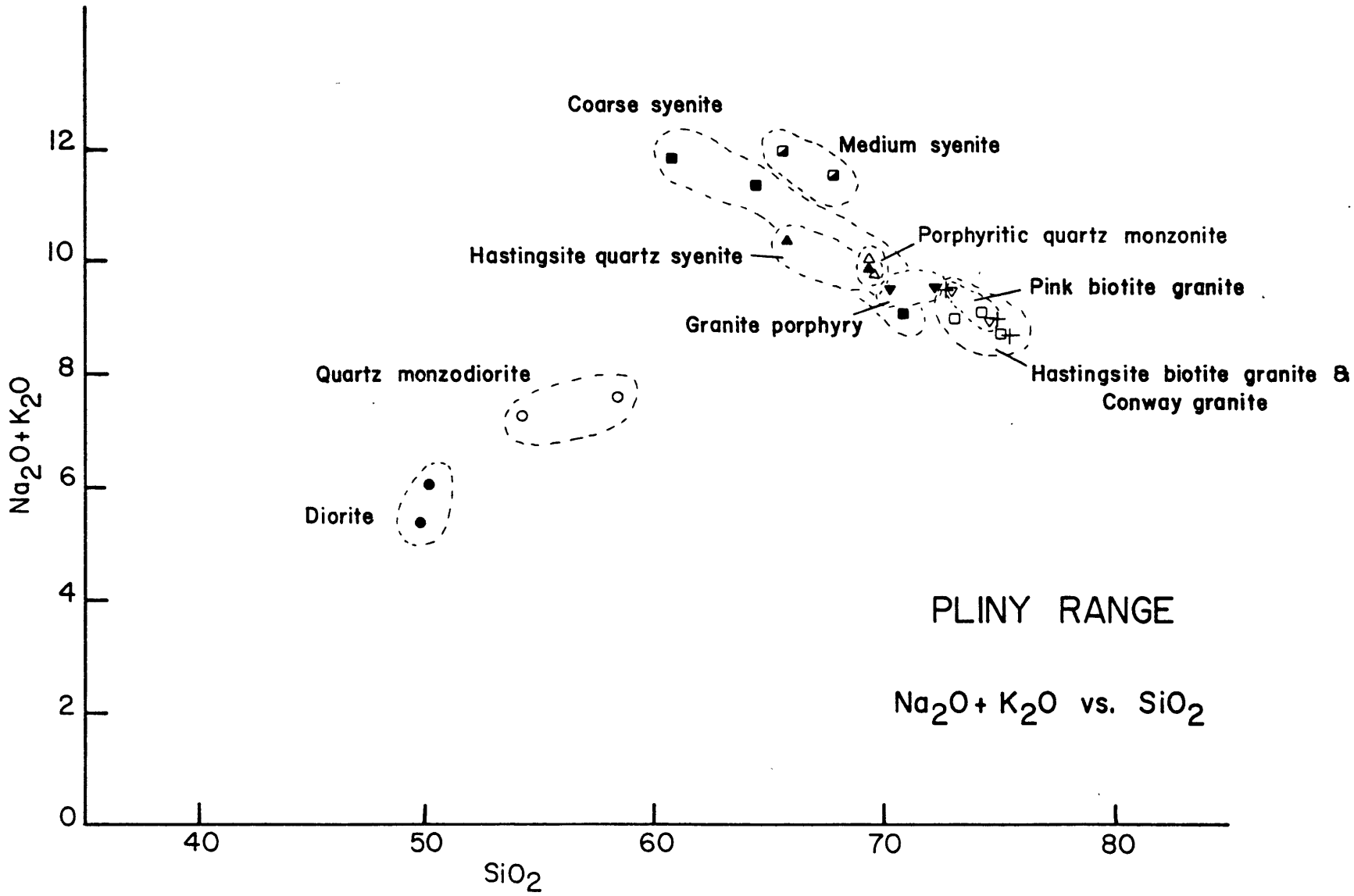
Coarse syenite
Medium syenite
Hastingsite quartz syenite
Porphyritic quartz monzonite
Pink biotite granite
Granite porphyry
Hastingsite biotite granite &
Conway granite
Quartz monzodiorite
Diorite
PLINY RANGE
Na2O + K2O vs. SiO2
Na2O + K2O
SiO2
0
2
4
6
8
10
12
40
50
60
70
80

Figure 48

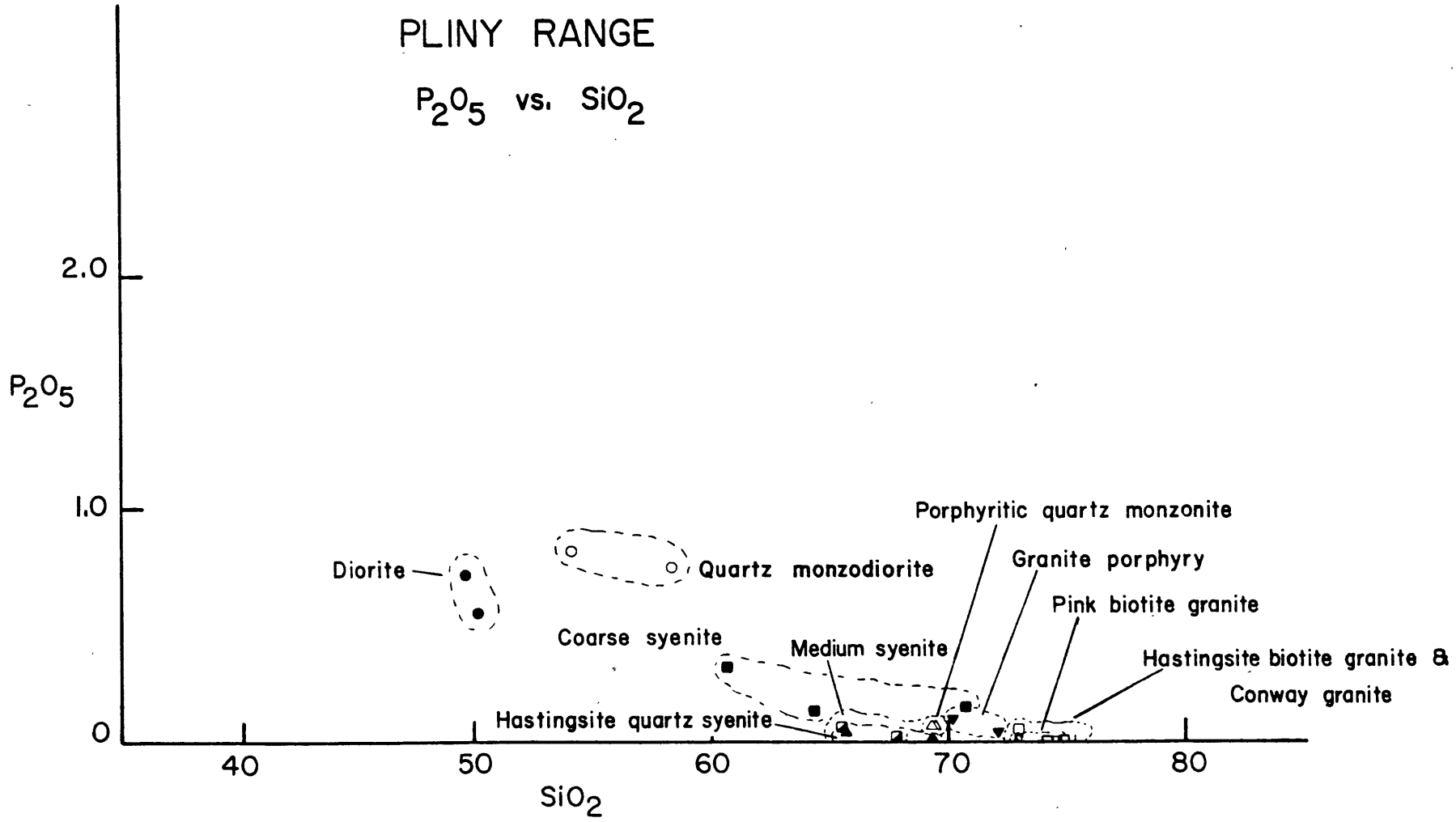
PLINY RANGE
P_2O_5 vs. SiO_2
2.0
1.0
0
P_2O_5
40
50
60
70
80
SiO_2
Diorite
Quartz monzodiorite
Coarse syenite
Medium syenite
Hastingsite quartz syenite
Porphyritic quartz monzonite
Granite porphyry
Pink biotite granite
Hastingsite biotite granite &
Conway granite

Figure 49

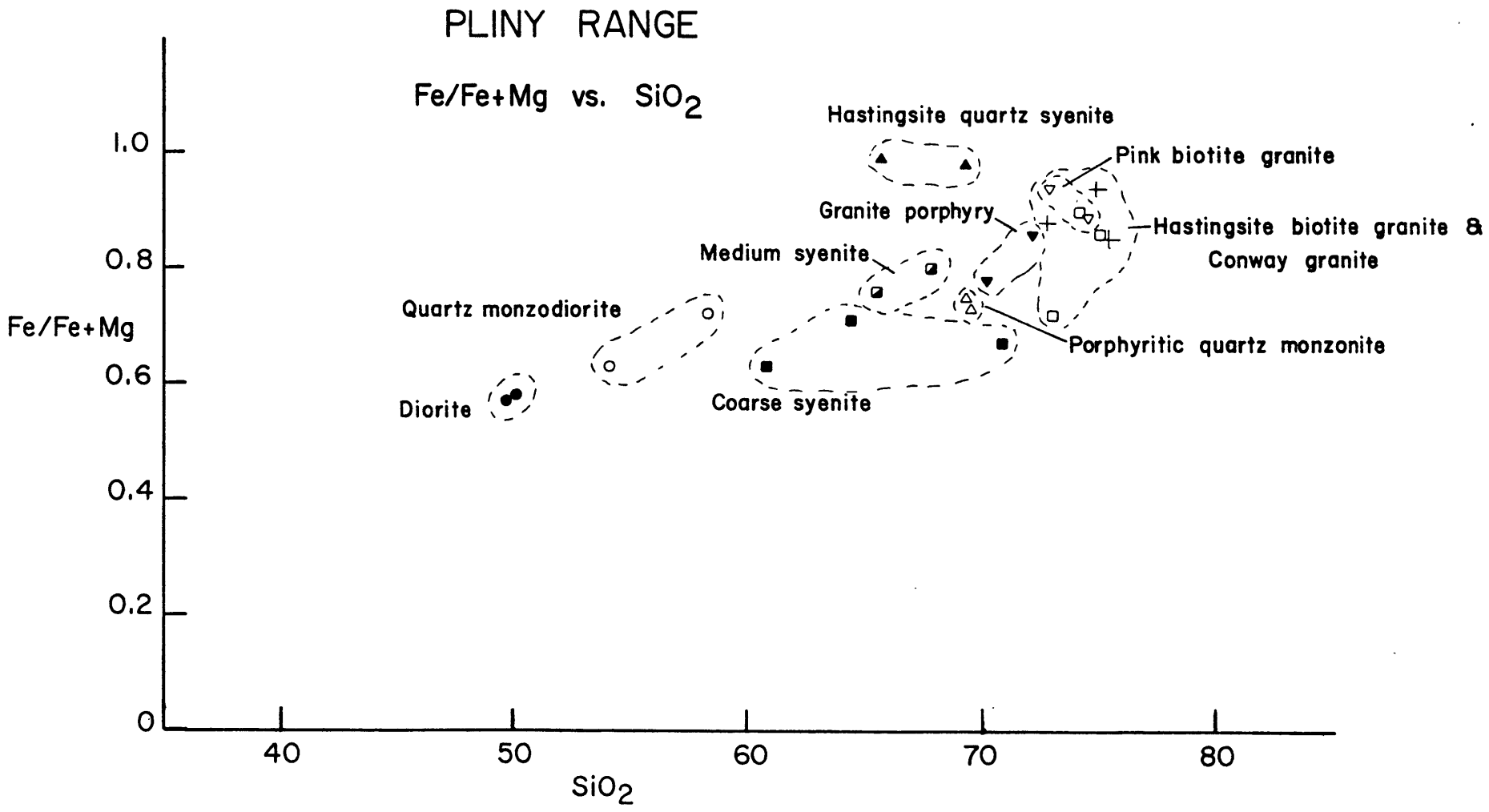
PLINY RANGE
Fe/Fe+Mg vs. SiO2
Hastingsite quartz syenite
Pink biotite granite
Granite porphyry
Hastingsite biotite granite &
Conway granite
Medium syenite
Quartz monzodiorite
Porphyritic quartz monzonite
Diorite
Coarse syenite
Fe/Fe+Mg
1.0
0.8
0.6
0.4
0.2
0
40
50
60
70
80
SiO2

Figure 50

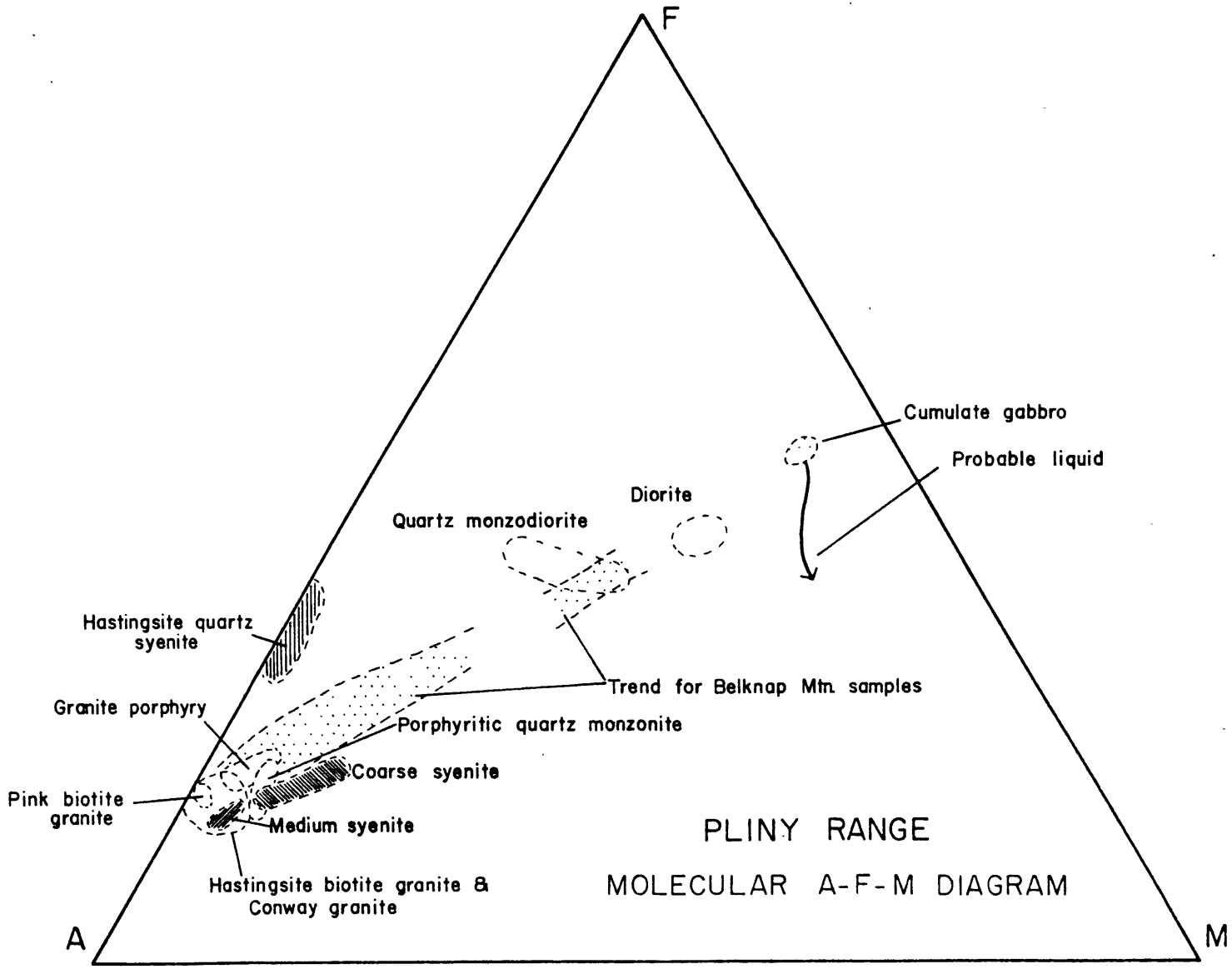
F
A
M
Cumulate gabbro
Probable liquid
Diorite
Quartz monzodiorite
Hastingsite quartz syenite
Trend for Belknap Mtn. samples
Granite porphyry
Porphyritic quartz monzonite
Coarse syenite
Pink biotite granite
Medium syenite
Hastingsite biotite granite & Conway granite
PLINY RANGE
MOLECULAR A-F-M DIAGRAM

Figure 51

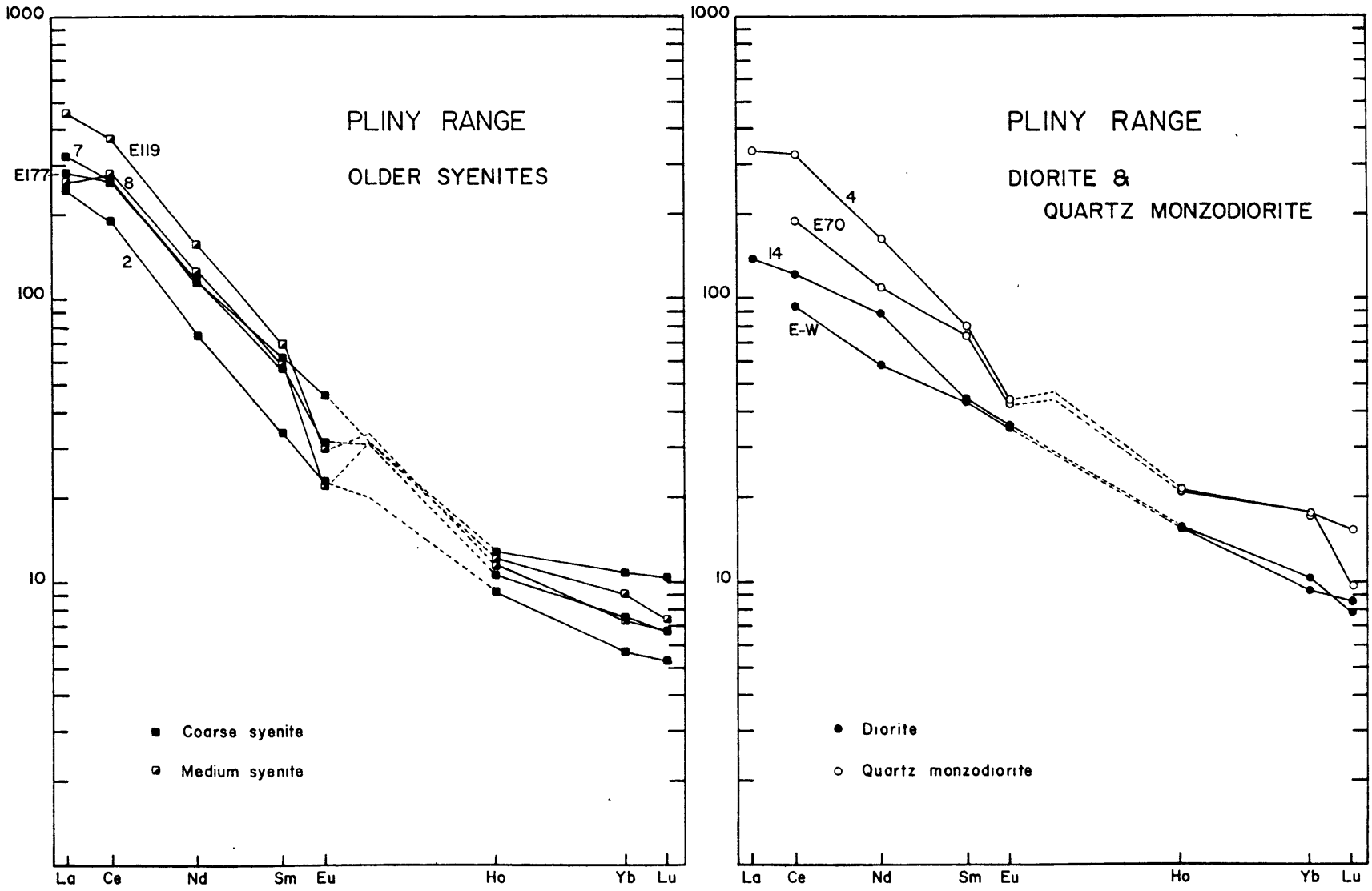
1000
100
10
PLINY RANGE
OLDER SYENITES
E177
E119
7
8
2
Coarse syenite
Medium syenite
La
Ce
Nd
Sm
Eu
Ho
Yb
Lu
1000
100
10
PLINY RANGE
DIORITE &
QUARTZ MONZODIORITE
4
E70
14
E-W
Diorite
Quartz monzodiorite
La
Ce
Nd
Sm
Eu
Ho
Yb
Lu

Figure 52

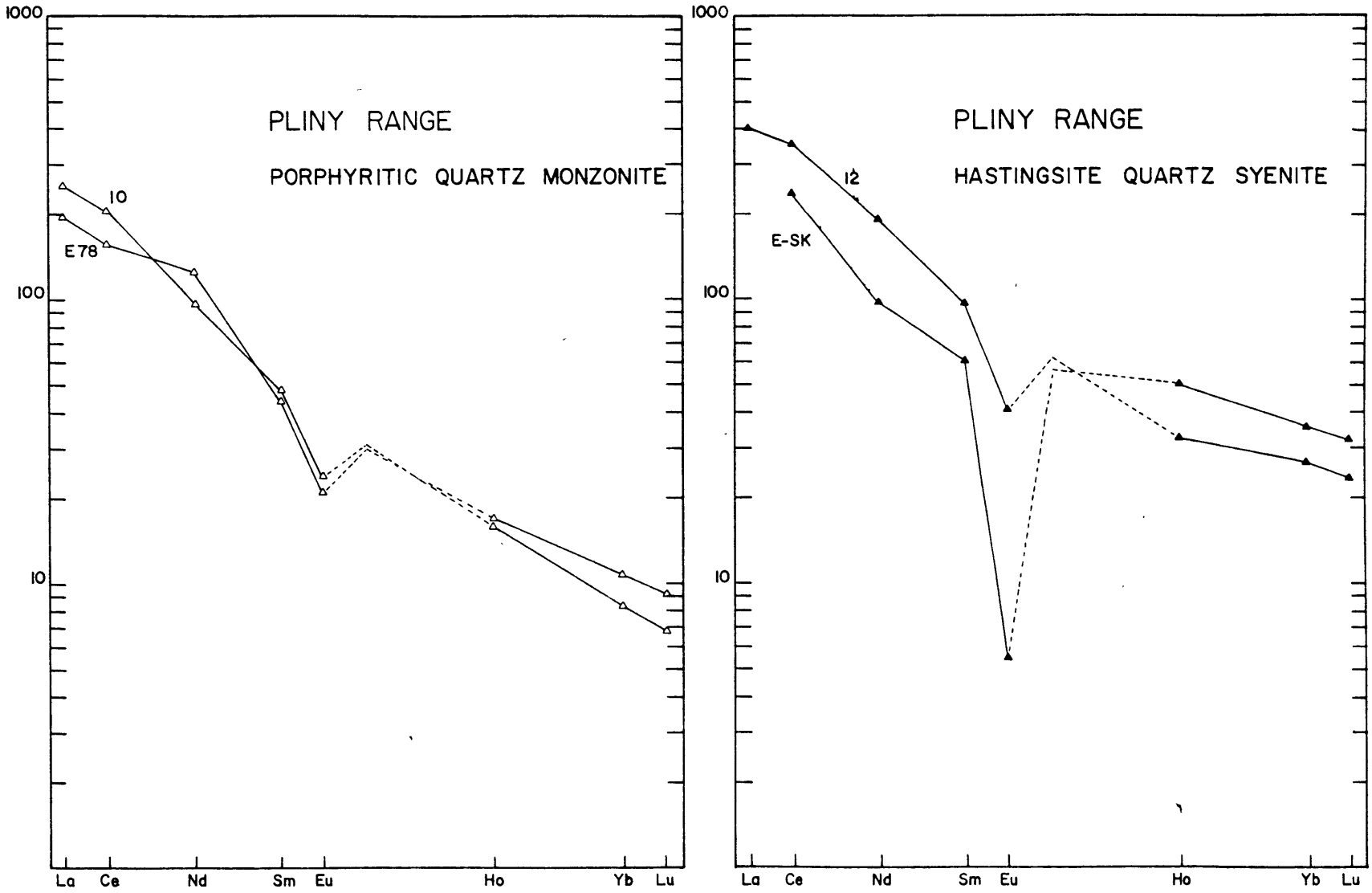
PLINY RANGE
PORPHYRITIC QUARTZ MONZONITE
10
E78
1000
100
10
La
Ce
Nd
Sm
Eu
Ho
Yb
Lu
PLINY RANGE
HASTINGSITE QUARTZ SYENITE
12
E-SK
1000
100
10
La
Ce
Nd
Sm
Eu
Ho
Yb
Lu

Figure 53

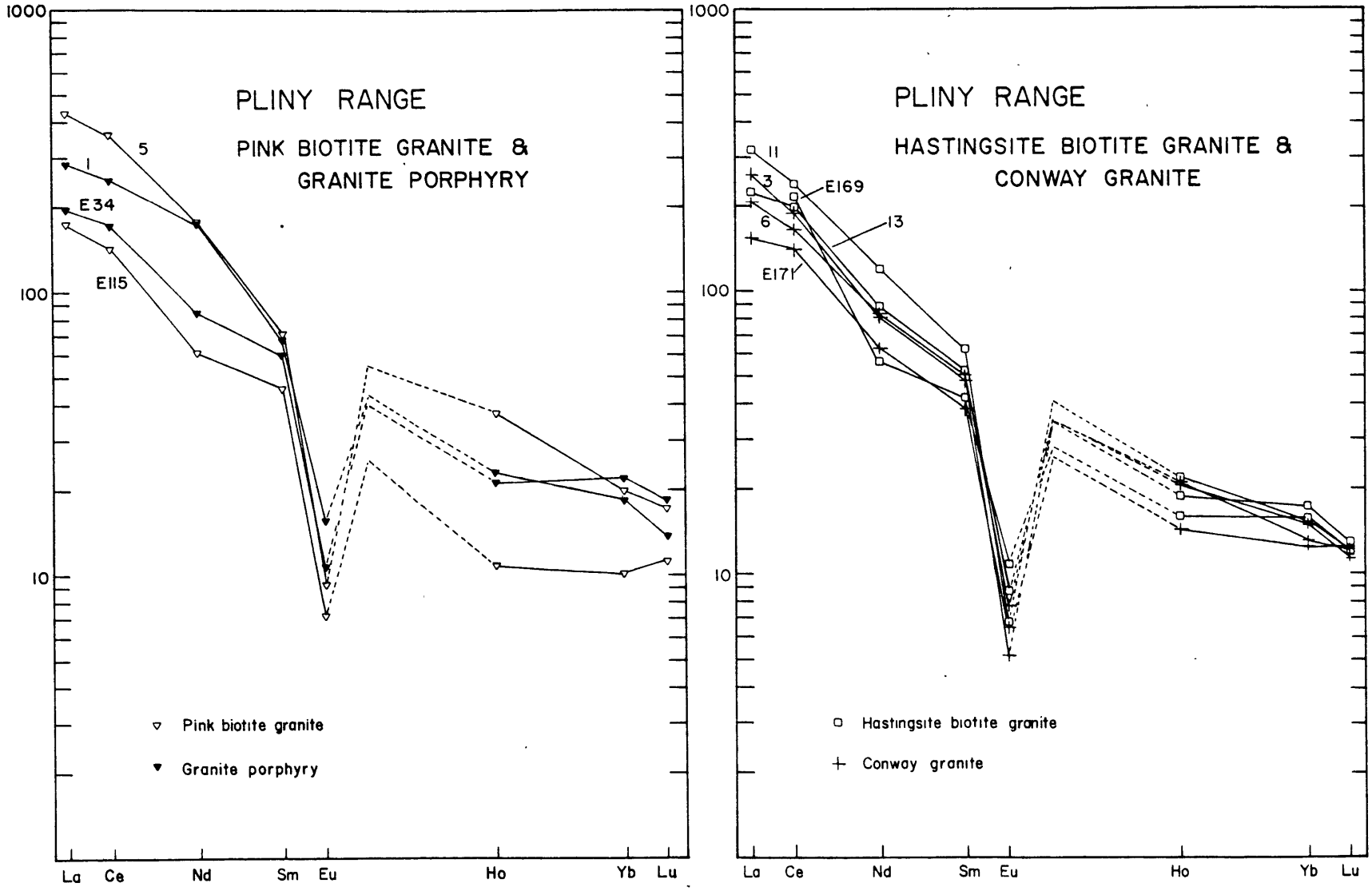
PLINY RANGE
PINK BIOTITE GRANITE &
GRANITE PORPHYRY
5
1
E34
E115
Pink biotite granite
Granite porphyry
PLINY RANGE
HASTINGSITE BIOTITE GRANITE &
CONWAY GRANITE
11
3
E169
6
13
E171
Hastingsite biotite granite
Conway granite
1000
100
10
La
Ce
Nd
Sm
Eu
Ho
Yb
Lu

Figure 54

APPENDIX I. PETROGRAPHY

A. BELKNAP MOUNTAINS

Gabbro (Samples 9 and 15)

Samples 9 and 15 of the gabbro are both coarse grained, holocrystalline rocks with a subophitic to diabasic texture. They are composed of laths of plagioclase (up to 6 mm) and clinopyroxene (up to 4 mm), with subhedral to anhedral grains of ilmenite (up to 2.5mm) and coarse (up to 2 cm) grains of poikilitic interstitial brown hornblends enclosing and surrounding all the other major phases. Biotite, chlorite, apatite, pyrite, epidote, and sphene constitute minor and accessory phases. The sequence of crystallization is: apatite and opaques followed closely by plagioclase and clinopyroxene, with hornblende much later. Some interstitial biotite may be primary. The plagioclase has been partly altered to epidote and sericite; clinopyroxene has been partly altered and replaced by a green hornblende which has partly altered to biotite and chlorite. Except for the replacement sequence clinopyroxene→hornblende→biotite and chlorite grain boundaries are very sharp. The brown hornblende is pleochroic in shades of light and dark reddish brown; the green hornblende is buff to medium green. Biotite is pleochroic from straw to dark brown. Sample 15 is more altered than sample 9, containing more epidote and chlorite.

Diorite (Samples 5,17,and 18)

The diorite samples are equigranular, fine grained, and holocrystalline, with a dominantly diabasic texture. Samples 5 and 18 have a grain size less than 1-1.5 mm; sample 17 has plagioclase laths up to 3 mm. Plagioclase, clinopyroxene, hornblende, and biotite are the essential phases present with minor or accessory alkali feldspar, apatite, sphene, chlorite, sericite, and epidote. The sequence of crystallization is apatite and clinopyroxene, plagioclase and opaques, hornblende, biotite, and alkali feldspar (interstitial). Alkali feldspar is present only as traces in sample 5, but is much more abundant in samples 17 and 18. In sample 18 the alkali feldspar is concentrated in several 4-6 mm irregular bands suggesting injection of K_2O-rich material into the diorite. Apatite is extremely abundant in all three samples. The plagioclase has partly altered to epidote and sericite, and shows irregular, serrated grain boundaries suggesting recrystallization. Plagioclase is weakly zoned from approximately An_{27} to An_{20-22}. Hornblende is pleochroic from olive green to brown; biotite is pleochroic from light brownish yellow to dark brown. Sample 17 is slightly more altered than 5 and 18, containing more chlorite and sericite. Samples 17 also has a ratio of hornblende to biotite greater than 1.0, where samples 5 and 18 have more biotite than hornblende.

Gilmanton Monzodiorite (Samples g17, g18, and 19)

The Gilmanton monzodiorite is medium grained, holocrystalline, hypidiomorphic, with a seriate to equigranular texture. The crystallization sequence appears to be early opaques, clinopyroxene, and plagioclse, followed by hornblende, and finishing with interstitial biotite, alkali feldspar, and quartz. Apatite, sphene, zircon, chlorite, minor epidote, and feldspar clay alteration are accesories. The plagioclase in samples G17 and G18 are euhedral to subhedral grains up to 1 cm in length, with occasional oriented strings of inclusions of opaques. Twin lamellae are frequently strained and bent, and show irregular and undulose extinction. Clinopyroxene is minor, usually as cores of hornblende grains. Hornblende (2-6 mm) is subhedral but obviously crystallized later than plagioclase. It is pleochroic from light brown to light green, and is partly replaced by chlorite. Biotite (2-5 mm, pleochroism light buff to red brown) is interstitial and partly replaced by chlorite. Alkali feldspar (3-7 mm) is microperthite, with cores and inclusions of plagioclase. It also occurs as interstitial grains. Quartz is always interstitial, and always shows undulose extinction. There are patches of myrmekite at alkali feldspar grain boundaries. Strings of fine grained, granulated material occur at many grain boundaries, and together with the deformed plagiclase twin lamellae and strained quartz indicate minor cataclasis. Sample 19 has a much higher color index that samples G17 and G18, with abundant hornblende.

Ames Monzodiorite (Sample 11)

The Ames monzodiorite is holocrystalline, medium grained, and has a hypidiomorphic granular texture. Plagioclase, alkali feldspar, hornblende, and biotite are the essential phases, with minor clinopyroxene and quartz, and accessory opaques, apatite, sphene,pyrite, chlorite, and feldspar clay alteration. Clinopyroxene occurs as infrequent cores in hornblende grains. Plagioclase occurs both as euhedral to subhedral laths and interlocking anhedra. Alkali feldspar (microperthite) is mostly anhedral, but a few large (7-8 mm) subhedral grains occur, one with a plagioclase core. Hornblende is subhedral to anhedral, with pleochroism from buff to light and dark greens. Biotite (pleochroism brownish yellow to red brown) and quartz are interstitial. Opaques occur in two habits: a few large (3-5 mm), partly resorbed grains and small (less than 1 mm) scattered anhedra. Mafic phases appear to be undergoing several complex reactions, including clinopyroxene→hornblende→ biotite and chlorite and biotite→chlorite plus opaques plus sphene. One mafic inclusion in a thin section is almost certainly Endicott diorite, but a second is much richer in hornblende.

Belknap Mountain Syenite (Samples G20 and 20)

The samples of Belknap Mountain syenite are medium grained, hypidiomorphic to allotriomorphic in texture. The samples are dominantly perthitic alkali feldspar (up to 1 cm) with lesser amounts of plagioclase (chiefly as cores to perthite,

but some discreet grains do occur). Hornblende (2-4 mm, pleochroism buff to green) is the chief mafic mineral, with rare cores of clinopyroxene. Biotite (pleochroism brownish yellow to brown) crystallizes as a late, interstitial mineral, as does quartz. Minor opaques, apatite, zircon, sphene, chlorite, and feldspar alteration are also present. The crystallization sequence was clinopyroxene, plagioclase, and hornblende, followed closely by alkali feldspar, with biotite and quartz later. Irregular extinction in quartz and deformed plagioclase twin lamellae suggest cataclasis as in the Gilmanton monzodiorite.

Cobble Hill Syenite (Samples G7 and G8)

Sample G7 is holocrystalline, allotriomorphic granular. It is composed of anhedral grains of perthitic alkali feldspar (up to 1.5 cm), with rare cores of plagioclase. Average grain size is 7-8 mm. Clinopyroxene (1-2 mm) occurs as well preserved inclusions in the alkali feldspar. Hornblende (pleochroism buff to very dark green) is interstitial. Quartz is a minor (less than 1%) interstitial phase. Accessories include opaques, apatite, zircon, and sphene (plus feldspar alteration). In contrast, sample G8 is hypidiomorphic granular with euhedral to subhedral grains of perthitic alkali feldspar (up to 1 cm, average 5 mm), laths and irregular (partly resorbed) grains of hornblende (pleochroism dark tan to very dark green) with rare cores of clinopyroxene, and interstitial biotite (pleochroism buff to dark brown) and quartz (approximately 7%).

Plagioclase is extremely minor and occurs as a few discreet anhedral grains (2-3 mm). Accessories are the same as in G7. Grain boundaries in sample G8 are very straight and clean. There is significantly less apatite in sample G8 relative to sample G7. G8 has a texture very much like a cumulate of alkali feldspar with an interstitial quartz matrix.

Lake Quartz Syenite (Samples 21 and 22)

The Lake quartz syenite samples are holocrystalline, hypidiomorphic, and slightly porphyritic. There are two generations of hornblende (both with pleochroism light brown to light green): larger (up to 6 mm) grains with irregular, resorbed grain boundaries, and smaller (1-2 mm) euhedral crystals. Both samples have subhedral phenocrysts of plagioclase (up to 8mm, and much more abundant in sample 22) rimmed by alkali feldspar, and slightly smaller subhedral alkali feldspar crystals. In addition there is anhedral and interstitial alkali feldspar, biotite (minor), and quartz. Accessories include opaques (with resorbed grain boundaries), apatite, zircon, and sphene (plus chlorite and feldspar alteration). The crystallization sequence involved early opaques and hornblende; plagioclase followed closely by alkali feldspar; and a second generation of hornblende together with alkali feldspar, quartz, and biotite. Sample 22 is slightly more altered that sample 21, and both samples have considerable chlorite and feldspar alteration products.

Albany Quartz Syenite (Samples G14,G27, and 1)

All three samples of Albany quartz syenite are holocrystalline, hypidiomorphic, and subporphyritic. Sample 1 is most porphyritic, with euhedral to anhedral (rounded) alkali feldspar (up tp 9 mm) and quartz (up to 5 mm) phenocrysts in a matrix of quartz and feldspar. The quartz phenocrysts are all embayed, but were obviously once euhedral. Mafic phases consist of corroded hornblende (up to 4 mm, pleochroism buff to light green) and interstitial, anhedral biotite. Myrmekite is common around alkali feldspsr phenocrysts. Plagioclase occurs in the groundmass and as occasional cores to alkali feldspar phenocrysts. Apatite, opaques, sphene, and zircon(?) are accessories. Samples G14 and G27 are less obviously porphyritic, contain much more plagioclase, hornblende, and biotite, and less quartz. The sequence of crystallization is similar to sample 1, i.e., minor opaques, hornblende, and plagioclase, followed by alkali feldspar, quartz, and biotite. Sphene always occurs with corroded hornblende and opaques, not as individual grains, indicating it is not primary but a reaction product. Samples 21 and 22 are more altered that sample 1.

Sawyer Quartz Syenite (Samples G11, 12, and 13)

All three samples of Sawyer quartz syenite are holocrystalline, allotriomorphic to hypidiomorphic granular. The samples have very even grain size (approximately 3-5 mm). The crystallization sequence is early, euhedral to subhedral

hornblende (1-3 mm, pleochroism light brown to green), alkali feldspar (a coarse, patchy perthite), and later plagioclase, quartz, and biotite (pleochroism buff to dark brown). Accessories include apatite, zircon, allanite, sphene (some primary sphene as well as sphene associated with opaques and hornblende), and minor opaques. The amount of plagioclase varies considerably in the samples studied. Samples G11 and 13 have slightly irregular grain boundaries, while sample 12 has much more regular, "clean" grain boundaries.

Conway Granite (Samples G28, G29, G34, G38, 6, and 7)

The Conway granite samples are medium to fine grained (less than 5 mm), holocrystalline, allotriomorphic granular. They are composed of anhedral alkali feldspar, quartz, plagioclase, and minor hornblende and biotite. Opaques, apatite, zircon, allanite, and fluorite (as large, anhedral grains in samples G28 and G29 and as fine grained, disseminated inclusions in feldspars in sample 6) are accessories. The sequence of crystallization appears to be hornblende (pleochroism light brown to greenish brown), alkali feldspar, and plagioclase/quartz/biotite (pleochroism straw to dark brown). Sample 6 is finer grained that the other samples (average grain size approximately 2 mm), and is extremely poor in mafics. Grain boundaries in all the samples are sharp.

TABLE 19. MODES OF BELKNAP MOUNTAINS SAMPLES[a]

Rock Type	Sample No.	Quartz	Alkali Feldspar	Plagioclase[b]	Clinopyroxene	Hornblende	Biotite	Opaque	Rest
Gabbro	9	--	--	48	27[c]	11	--	12	2[d]
	15	--	--	43	24[c]	21	--	9	3[d]
Diorite	5	--	<1	57	4	21	12	3	2[e]
	17	--	4	61	2	11	18	1	3[e]
	18	--	5	65	2	20	7	1	2[e]
Gilmanton Monzodiorite	G17	--	34	52	--	6	4	<1	3[f]
	G18	--	30	54	--	9	4	<1	2[f]
	19	--	33	45	--	13	6	<1	2[f]
Ames Monzodiorite	11	--	33	50	--	8	7	--	2[g]
Belknap Mountain Syenite	G20	--	71	16	--	7	3	--	3[h]
	20	--	75	12	--	9	3	--	3[h]
Cobble Hill Syenite	G7	<1	87	3	--	7	<1	--	1[i]
	G8	7	85	2	--	4	2	--	1[i]

TABLE 19. continued

Rock Type	Sample No.	Quartz	Alkali Feldspar	Plagioclase[b]	Clinopyroxene	Hornblende	Biotite	Opaque	Rest
Lake Quartz Syenite	21	7	62	20	--	8	1	--	2[j]
	22	12	69	11	--	4	2	--	2[j]
Sawyer Quartz Syenite	G11	15	73	8	--	2	1	--	1[k]
	12	17	72	10	--	1	3	--	1[k]
	13	9	83	4	--	3	1	--	1[k]
Albany Quartz Syenite	G14	1	58	23	--	6	3	--	1[l]
	G27	7	65	17	--	7	3	--	1[l]
	1	14	75	7	--	2	1	--	1[l]
Conway Granite	G28	14	62	20	--	3	1	--	<1[m]
	G29	24	57	16	--	1	2	--	<1[m]
	G34	33	45	20	--	--	2	--	<1[m]
	G38	29	52	14	--	--	4	--	1[m]
	6	36	59	15	--	--	<1	--	<1[m]
	7	26	48	14	--	1	1	--	<1[m]

TABLE 19. continued

Notes

a Modes based on 1000-1200 counts per thin section, one thin section per sample, except for gabbro samples 9 and 15, where two sections were counted. Modes rounded to nearest 1%.

b Primary plagioclase only. Exsolution plagioclase included with alkali feldspar.

c Includes green hornblende after clinopyroxene.

d Biotite, chlorite, apatite, pyrite, sphene, epidote, sericite.

e Apatite, zircon (?), sphene, chlorite, sericite, epidote.

f Clinopyroxene, apatite, quartz, sphene, zircon, chlorite, feldspar alteration, epidote.

g Clinopyroxene, opaques, quartz, apatite, pyrite, sphene, chlorite, feldspar alteration.

h Clinopyroxene, quartz, opaques, apatite, zircon, sphene, chlorite, feldspar alteration.

i Clinopyroxene, apatite, opaques, sphene, zircon, feldspar alteration.

j Opaques, apatite, sphene, zircon, chlorite, feldspar alteration.

k Apatite, zircon, sphene, allanite, opaques, chlorite, feldspar alteration.

l Opaques, apatite, sphene, zircon, chlorite, feldspar alteration.

m Hornblende, opaques, apatite, sphene, zircon, allanite, fluorite, chlorite, feldspar alteration.

B. PLINY RANGE

Older Syenites (Samples 2, 7, and 8)

Samples of the coarse syenite (2 and 7) contain irregular perthitic alkali feldspar phenocrysts up to 1.5 cm in length and smaller zoned plagioclase phenocrysts in a matrix of anhedral alkali feldspar and interstitial quartz. Myrmekite is present in some matrix feldspar. Mats of fine grained (0.2-0.5 mm) biotite (pleochroism buff to brown) are present in both samples; amphibole is conspicuous in sample 7 (pleochroism yellow to green). Sphene, opaques, apatite, chlorite, and feldspar alteration are accessories. Irregular and embayed phenocrysts, matted biotite, and intergrown matrix material suggest recrystallization as noted by Czamanske et al. (1977).

Medium syenite sample 8 is much more equigranular, with an average grain size of 3-4 mm. Interlocking perthitic alkali feldspar, anhedral plagioclase, and interstitial quartz all have irregular grain boundaries. The major mafic is biotite (pleochroism straw to brown), with only traces of amphibole. Minor opaques, sphene, apatite, zircon, chlorite, and feldspar alteration are accessories.

Diorite (Sample 14)

Sample 14 has a diabasic texture, and is dominated by plagioclase, with hornblende, biotite and clinopyroxene, and chlorite making up the bulk of the rest of the rock. Accessories include opaques, interstitial alkali feldspar and

quartz, apatite, sphene, and feldspar alteration. Grain size is <2 mm (∿1 mm average). Hornblende pleochroism is tan to greenish brown; biotite, yellow brown to reddish brown. The degree of feldspar and mafic alteration is quite high, as indicated by the 5% modal chlorite.

Quartz Monzodiorite (Sample 4)

The sample has hypidiomorphic granular texture, with an average grain size of ∿2 mm. Plagioclase (subhedral to euhedral) dominates with subhedral hornblende (pleochroism buff to dark olive green) and biotite (pleochroism straw to brown), and anhedral alkali feldspar (perthite) and interstitial quartz. A second bluish amphibole irregularly replaces the olive green amphibole (as noted by Czamanske et al., 1977). Opaques, apatite, clinopyroxene, sphene, chlorite, and feldspar alteration are accessories.

Porphyritic Quartz Monzonite (Sample 10)

Sample 10 is a medium grained, holocrystalline rock composed of anhedral quartz, alkali feldspar (perthite), and plagioclase. Average grain size is 6-7 mm. Minor hornblende (pleochroism light yellow to pale green) and biotite (pleochroism buff to brown), opaques, chlorite, epidote, and sericite also are present. The grain boundaries are irregular, and minor myrmekite is present at alkali feldspar grain boundaries. Patches of finer grained quartz and feldspar (0.1-0.5 mm) plus mafics are present

between some grains, giving the rock its porphyritic texture.

Hastingsite Quartz Syenite (Sample 12)

The sample of the Hastingsite quartz syenite is sub-porphyritic, with laths of perthitic alkali feldspar (up to 6 mm) surrounded by smaller laths of alkali feldspar (1-2 mm) and anhedral quartz grains (1-2 mm). Mafics consist of pale green clinopryoxene (subhedral to anhedral, 1-3 mm), interstitial amphibole (pleochroism brownish yellow to dark green) and minor biotite (light brown to dark brown). Accessories include minor opaques, apatite, zircon, allanite (?), chlorite, and feldspar alteration.

Pink Biotite Granite (Sample 5)

Sample 5 is holocrystalline, allotriomorphic granular. The average grain size is 0.5 to 1.5 mm. Anhedral perthitic alkali feldspar, plagioclase, and quartz make up 95% of the rock. Mafics consist of subequal amounts of subhedral to anhedral amphibole (pleochroism pale straw to yellow green) and anhedral biotite (pleochroism yellow to brown). Opaques, sphene, zircon (?), allanite (?), chlorite, and feldspar alteration are accessories.

Granite Porphyry (Sample 1)

Sample 1 is holocrystalline, sub-porphyritic, hypidiomorphic to allotriomorphic. Subhedral to anhedral perthitic alkali feldspar (up to 3 mm), resorbed rounded quartz grains

(up to 2 mm), and slightly smaller plagioclase (up to 1.5 mm) are set in a finer (up to 0.8 mm) matrix of quartz plus feldspars. Amphibole (pleochroism buff to olive green) and biotite (pleochroism straw to brown) (both up to 0.8 mm) are irregular and often contain inclusions of feldspar. Minor opaques, apatite, zircon, chlorite, and feldspar alteration are accessories.

Hastingsite Biotite Granite (Samples 11 and 13)

The two samples are very similar. Both are holocrystalline, hypidiomorphic granular. Average grain size is 2-4 mm. Subhedral perthitic alkali feldspar (with rare cores of plagioclase) and plagioclase and anhedral, interstitial quartz, show irregular grain boundaries. Biotite (pleochroism straw to dark brown) is the major mafic mineral, and is partially altered to chlorite. Amphibole (pleochroism pale yellow green to olive green) is a minor phase in both samples. Both mafics crystallized late in the history of the samples. Accessories include minor opaques, sphene, zircon, allanite, chlorite, and feldspar alteration.

Conway Granite (Samples 3 and 6)

Both samples are medium grained (3-5 mm average grain size), hypidiomorphic granular. Perthitic alkali feldspar (with rare plagioclase cores in sample 3), plagioclase, and quartz make up >95% of the samples. Biotite (pleochroism light yellow to dark brown) is interstitial, as is minor

amphibole (pleochroism light brown to brownish green). Accessories include minor opaques, sphene, apatite, zircon, allanite (?), chlorite, and feldspar alteration.

TABLE 20. MODES OF PLINY RANGE SAMPLES[a]

Rock Type	Sample No.	Quartz	Alkali Feldspar	Plagioclase[b]	Clinopyroxene	Hornblende	Biotite	Opaques	Rest
Coarse Syenite	2	17	63	18	--	Tr	3	-	2[c]
	7	3	75	15	--	2	3	-	2[c]
Medium Syenite	8	10	71	17	--	Tr	1	-	2[d]
Diorite	14	--	2	59	5	13	10	3	8[e]
Quartz Monzodiorite	4	9	14	45	--	12	16	2	2[f]
Porphyritic Quartz Monzonite	10	20	38	37	--	2	2	-	1[g]
Hastingsite Quartz Syenite	12	13	62	14	4	5	1	-	1[h]
Pink Biotite Granite	5	26	51	19	--	1	1	1	1[i]
Granite Porphyry	1	30	51	11	--	5	2	-	<1[j]

TABLE 20. continued

Rock Type	Sample No.	Quartz	Alkali Feldspar	Plagioclase[b]	Clinopyroxene	Hornblende	Biotite	Opaques	Rest
Hastingsite Biotite Granite	11	35	45	15	--	Tr	3	-	<1[k]
	13	34	47	14	--	1	3	-	<1[k]
Conway Granite	3	33	49	15	--	Tr	2	-	<1[l]
	6	34	45	17	--	1	2	-	<1[l]

a Modes based on 1000-1200 counts per thin section, one thin section per sample. Modes rounded to nearest 1%.

b Primary plagioclase only. Exsolution plagioclase included with alkali feldspar.

c Sphene, opaques, apatite, chlorite, feldspar alteration.

d Sphene, opaques, apatite, zircon, chlorite, feldspar alteration.

e 5% chlorite, quartz, apatite, sphene, epidote, sericite.

f Apatite, clinopyroxene, sphene, chlorite, feldspar alteration.

g Opaques, chlorite, feldspar alteration.

h Opaques, apatite, zircon, allanite (?), chlorite, feldspar alteration.

i Sphene, zircon (?), allanite (?), chlorite, feldspar alteration.

j Opaques, apatite, zircon, chlorite, feldspar alteration.

k Opaques, sphene, zircon, allanite, chlorite, feldspar alteration.

l Opaques, sphene, apatite, zircon, allanite (?), chlorite, feldspar alteration.

APPENDIX II. ANALYTICAL PROCEDURES

A. Sample Preparation

Pliny Range samples with an "E-" prefix were obtained from D.R. Wones as powders. The remaining samples were prepared for analysis by first breaking large pieces of rock in a large jaw crusher. Fragments of ∿50-200 grams with no weathered surfaces were selected from this crushed material and blown clean, then crushed in a small jaw crusher to material ranging in size from ∿1 cm to a fine powder. ∿500 gm total of this material was prepared for each sample. This material was split into equal parts, and ∿150 gm was crushed in a tool steel percussion mortar to pass 80 mesh, then in a tungsten carbide ball mill to a fine powder. Several samples were sieved and >95% (by weight) passed 200 mesh. Splits for several rocks were prepared in different ways, and the general question of the representative nature of the splits prepared is discussed in Section E.

B. Procedure for Isotope Dilution Analysis of Rb and Sr and Sr Isotopic Analysis

The procedure followed during analysis of the Belknap Mountain whole rocks and mineral separates is essentially identical to that described in Appendix II of Hart and Brooks (1977).

H_2O, HCl and Hf used in sample dissolution and cation

exchange were produced by sub-boiling distillation in teflon; Also used were minor quantities of Baker Ultrex brand $HClO_4$, HNO_3, and H_2SO_4. Teflon beakers (TFE) were cleaned by soaking in a warm 50:50 HNO_3:H_2O bath for at least several days followed by leaching with hot HF prior to being rinsed with H_2O prepared by sub-boiling distillation.

For whole rocks between 100-200 mg of rock powder was weighed (±0.02 mg) into a clean teflon beaker, and a mixed spike of ^{87}Rb and ^{84}Sr weighed in. Two spikes were used: one for samples with Rb/Sr weight ratio <1 and one for samples with Rb/Sr > 1. This arrangement provided for adequate values of the ratio of normal to spike Sr and Rb except for the case of the normal to spiked Sr in several biotite separates with very low ppm Sr. These ratios were far from optimum, but are not believed to have introduced sufficient uncertainty in either the measured Sr concentration or calculated $^{87}Sr/^{86}Sr$ ratio to change the conclusions drawn in Chapter 3.

After addition of the spike, ∿5 ml of a 4:1 mix of HF (distilled) and $HClO_4$ (Ultrex) were added to the beaker, and the sample covered with a teflon watch glass and allowed to digest overnight at ∿90°C. This was followed by evaporation of the HF and $HClO_4$ to near dryness, followed by 3 dilutions and evaporations with ∿2 ml of 2.5 N HCl (distilled). After the third drying the samples were diluted in ∿0.5-1 ml of 2.5 N HCl and placed in a centrifuge tube, centrifuged, and 1/2 of this liquid loaded into a cation column. The column consisted of 3 ml of Dowex 50w-x8, 200-400 mesh resin with

a bed length of 19 cm and diameter of 0.5 cm which had been conditioned in 2.5 N HCl. The resin was pre-cleaned prior to making up the columns by eluting ∿25 gm with at least 1000 ml of reagent grade of 6.2 N HCl. The columns were constructed from pyrex glass fitted with a polyethylene filter disk, and cleaned for several days in 50:50 HNO_3:H_2O. Columns were calibrated with a ^{85}Sr tracer, and the position of the alkali aliquot calculated from information supplied by S.R. Hart on the behavior of Rb and Sr in similar columns.

After loading the sample on the column, Rb and Sr were eluted with 2.5 N HCl (distilled). Rb was collected between 7.5 and 12.5 ml, and Sr between 15 and 19 ml. The columns were then cleaned with 10 ml of 6.2 N HCl (distilled) followed by 20 ml of 6.2 N HCl distilled in vycor glass. Prior to the next use the columns were conditioned by back-washing with 2.5 N HCl (distilled). The procedure for the mineral separates was identical except that the separates were cleaned in acetone prior to weighing, and since ∿50 mg was used in all cases, smaller quantities of HF+$HClO_4$ and HCl were used during the dissolution.

After elution several drops of 20% Ultrex H_2SO_4 were added to the Rb fraction to convert the chlorides to sulfates. After drying Rb was run as a sulfate. Several drops of Ultrex $HClO_4$ were added to the Sr fraction to dissolve any resin beads which may have passed through the filter disk. After drying, several drops of Ultrex HNO_3 were added to the beaker, followed by drying to convert the Sr to nitrate.

This step was repeated three times.

Rb was run as a sulfate on a previously degassed Ta filament. Sr was run as a nitrate on a degassed Ta filament onto which a slurry of fine Ta_2O_5 had been dried to produce a coating of the oxide. After loading and drying, a drop of the Sr taken up in very dilute ($\sim$0.2 N) HNO_3, the filament was brought up to a dull red glow in air. The filament was then placed in the mass spectrometer and run.

Analyses were made on a 9 inch-60° mass spectrometer with complete automation. The magnetic field was switched by a PDP computer and controlled by a Varian FR-41 gaussmeter/controller. One second counts on each mass peak were integrated on an HP integrating digital voltmeter and processed by the computer.

Sr concentration and Sr isotopic composition were determined on the same sample aliquot. All values of $^{87}Sr/^{86}Sr$ measured were normalized to a $^{87}Sr/^{86}Sr$ ratio of 0.11940. The normal/spike Sr ratio of the sample and the normalized $^{87}Sr/^{86}Sr$ ratio of the sample were then calculated from a knowledge of the isotopic composition of the spike.

An average of two procedure blanks run during the course of the analyses gave blank values of 0.18 ±0.06 ng Rb and 2.21 ±0.51 ng Sr.

Duplicate analyses on several rock types for both Rb and Sr concentration and $^{87}Sr/^{86}Sr$ ratio yielded precision estimates of 1% for $^{87}Rb/^{86}Sr$ and 0.02% for $^{87}Sr/^{86}Sr$.

$^{87}Sr/^{86}Sr$ values reported have been normalized to a

value of $^{87}Sr/^{86}Sr$ = 0.70800 for the Eimer and Armand $SrCO_3$. The average value for the $SrCO_3$ obtained during the time period of the analyses was 0.70765 ±.00011 (2σ standard deviation of six analyses).

C. Neutron Activation Analysis

Selected REE (La, Ce, Nd, Sm, Eu, Ho, Yb, Lu), Th, U, Ba, Hf, Ta, Sc, Cs (and on certain splits of some samples, Co), were determined via Instrumental Neutron Activation analysis.

Approximately 0.5 gm of rock powder were placed in a 2/5 dram polyethylene vial, and an accurately weighed iron wire taped to the outside to act as a flux monitor. 5 or 6 samples plus a standard were then irradiated for 8 hours in the M.I.T. research reactor. Irradiation of all Belknap samples was performed in a lazy susan facility to minimize flux corrections. For these irradiations, the flux corrections (as determined from the specific activity of the iron wires) were in all cases less than 2-1/2 %. The Pliny samples were irradiated in a pneumatic facility, and had somewhat higher flux corrections (up to 6%). Pliny samples with "E" prefixes were irradiated at the Georgia Institute of Technology with similar (<6%) flux corrections.

The standard used was a solution with known trace element concentrations accurately pipetted (0.4 ±0.001 ml) onto specpure SiO_2 in a 2/5 dram vial and dried. The specpure SiO_2 was to insure a similar geometry for sample and standard

during irradiation and counting.

Samples and standards were counted four times over the next 30 days on two high resolution Ge(Li) detectors: at 5 and 15 days after irradiation on an ORTEC LEPS detector (low energy photon spectrometer) with a resolution of ∿0.65 keV. Pliny samples with an "E-" prefic were counted on the detector with ∿4.0 keV resolution; the remaining Pliny samples and all Belknap samples were counted on the higher resolution detector.

The gamma ray spectrum was collected on a 4096 multichannel analyzer, printed out, and peak areas calculated from this raw data using a linear fit to the background.

Table 21 lists the gamma ray peaks used for particular elements, the count on which they were obtained, the average percent uncertainty of the concentration based on counting statistics (1σ), and the percent standard deviation (1σ) of six samples of Los Pinos granite irradiated during analysis of the Belknap samples, and the percent difference of the extremes of these six analyses from the mean. The average analysis for the Los Pinos granite is also given in Table 21.

The larger of the two values, $\bar{\sigma}_c$ or Δ, should be considered the maximum uncertainty of any concentration for a given analysis; σ_A represents the optimum uncertainty for a sample analyzed a number of times.

USGS standard rock G2 was also analyzed several times during the course of analysis. Table 22 gives the results of these analyses plus values collected from literature.

TABLE 21. GAMMA RAY PEAKS USED IN NEUTRON ACTIVATION ANALYSIS

Element	Peak Energy (keV)	Count/Detector	$\bar{\sigma}_c$ [a]	σ_A [b]	Δ [c]	Average Los Pinos Granite (± 1σ)
La	816.	8D/high energy	1.6	3.5	6.1	74.8 ±2.6
	1596.		1.5	3.6	5.3	75.2 ±2.7
Ce	145.	15D/LEPS	0.9	4.0	5.6	173. ±7
Nd	91.	15D/LEPS	1.8	4.5	7.9	75.0 ±3.4
Sm	103.	5D/LEPS	0.6	2.4	3.6	16.9 ±0.4
Eu	1408.	30D/high energy	1.4	3.0	5.0	2.71 ±0.08
Ho	80.6	5D/LEPS	24.8	9.8	12.5	4.1 ±0.4
Yb	283.	8D/high energy	5.6	5.8	11.1	--
	177.	15D/LEPS	12.3	10.0	15.1	--
Lu [d]	208.	8D/high energy	3.6	2.8	5.3	1.76 ±0.05
		15D/LEPS	6.0	4.5	6.0	1.77 ±0.08
Th	94.	15D/LEPS	4.5	2.2	3.4	18.1 ±0.4
	311.	30D/high energy	1.0	4.7	9.0	19.2 ±0.9
U	106.	5D/LEPS	28.0	15.8	20.7	3.8 ±0.6
Ba	496.	8D/high energy	11.8	4.1	6.3	980. ±40.
Hf	482.	30D/high energy	0.6	3.3	6.1	--
Ta	1222.	30D/high energy	0.8	3.7	6.1	3.9 ±0.2
Sc	889.	30D/high energy	0.5	5.1	9.0	
Cs	605.	30D/high energy	2.6	2.0	2.7	2.01 ±0.04
	795.		2.9	3.2	6.2	1.89 ±0.06
Co [f]	1332.	30D/high energy	--[e]	--[e]	--[e]	--

TABLE 21. continued

Notes

a Average percent uncertainty of concentration based on counting statistics (1σ).

b Percent standard deviation from the mean of six analyses of Los Pinos granite radiated during analysis of Belknap samples.

c Percent difference of the extreme of the six samples of Los Pinos granite from the mean calculated using

$$\Delta = 100 \times \frac{|\text{extreme value} - \text{mean value}|}{\text{mean value}}$$

d In samples ground in tungsten carbide, the 15 day Lu value must be used due to contribution by tungsten to the 208 keV peak used in Lu analysis. For samples ground in agate or tool steel, the 8 day value may be used.

e No detailed data on Los Pinos granite. Believed as good as or better than Hf.

f Co can not be analyzed for in samples ground in tungsten carbide.

TABLE 22. ANALYSES OF USGS STANDARD ROCK G2 (ppm)

	This Study[a]	Arth & Hanson[d] (1975)	Smet et al. (in press) (e)	(f)
La	82.6 ±3.3	--	86.0 ±4.3	87.4 ±1.7
Ce	159 ±9.5	165.	160 ±8	161 ±3
Nd	45.1 ±1.9	51.1	52.6 ±2.6	54.6 ±1.1
Sm	7.2 ±0.2	6.93	6.88 ±0.34	6.98 ±0.14
Eu	1.37 ±0.06	1.35	1.33 ±0.07	1.63 ±0.03
Ho[b]	0.40	--	0.37 ±0.07	0.39 ±0.09
Yb	0.69 ±0.07	0.543	0.72 ±0.04	0.79 ±0.02
Lu	0.117±0.04	0.0775	0.114±0.006	0.108±0.007
Th	22.4 ±1.9	--	24.2 ±1.2	24.5 ±0.5
U[b]	1.4	--	--	--
Ba[b]	2047.	1872.	1860. ±93	1939. ±70
Hf	8.4 ±0.2	--	7.55 ±0.38	8.13 ±0.16
Ta[b]	1.7	--	0.86 ±0.04	0.96 ±0.04
Sc	3.67 ±0.06	--	--	--
Cs[b]	1.4	--	1.42 ±0.04	1.30 ±0.14
Co[c]	--	--		

a Average of 3 analyses ±1 standard deviation from the mean.

b One analysis only.

c No data.

d Isotope dilution

e RNAA

f INAA

Values from my analyses are quite similar to those from the literature with the exception of Nd, which is ∿10-15% lower than reported values, and Ta, which is ∿100% higher. However, USGS G2 is low in Ta (relative to Belknap Mountain samples), and only one analysis was available, so the accuracy is probably better than indicated. In general, accuracy should be considered comparable to precision.

D. X-Ray Fluorescence Analysis

Major elements for Belknap and Pliny samples (other than those reported in Czamanske et al., 1977) were analyzed using a fused glass disk. The method of sample preparation is essentially identical to that of Norrish and Hutton (1969) as modified by Harvey et al. (1973).

A commercial fluxing compound (spectroflux 105; Harvey et al., 1973) was used. Prior to use it was ignited at 500°C and stored in a dissicator. Where H_2O^+ and CO_2 analyses were available for samples, concentrations were corrected to account for volatile loss during fluxing. Where not available (as for the Pliny samples and several Belknap samples) average H_2O^+ and CO_2 values from analyzed samples of the rock unit were used in the correction.

Powders were dried at 110° overnight and stored in a dessicator prior to making up the glass disks. A flux-to-rock ratio of 5:1 (identical to Woods Hole procedure) was used. Sample and flux were weighed and placed directly into a PT/5%Au crucible, and heated at ∿1050°C over a meeker burner

for 12-15 minutes. The molten glass was then poured into an aluminum planchet kept at ∿450°C and quenched by pressing with a polished aliminun plunger. After quenching, the planchet with the glass disk was transferred to a transite cooling block kept at ∿400°C and covered. After a block was full (6 samples) it was removed from the hot plate and the samples allowed to cool slowly. The crucibles were cleaned between uses by fluxing with $NaCO_3$ and soaking in dilute (∿2 N) HCl then rinsing with distilled H_2O.

Two major problems were encountered in the analyses: lack of adequate standards at high values of Na_2O, and a consistent 0.2 weight percent offset in CaO values of rock analyzed at ANU by B.W. Chappell.

The latter problem was solved by adding 0.2 weight percent to all CaO values obtained from Woods Hole.

The first problem was solved by using Na_2O values from samples analyzed at ANU and corrected intensities of sodium peaks from the output to construct an empirical standard line. Linear regression of the line yielded a correlation coefficient of 0.986. This procedure was only necessary for samples with >4.0% Na_2O. Samples with <4.0% Na_2O were within the range of Woods Hole standards.

This procedure of using analyses performed at ANU on different splits of samples is justified by the excellent agreement for other major oxides on samples analyzed in both laboratories (see Section E).

Trace element analyses for Rb, Sr, and Zr were made on

pressed powders made with 10 weight percent H_3BO_3 as a binder. USGS standard rocks W-1. BCR-1, AGU-1, GSP-1, G-1, and G-2 pressed in a similar fashion were used as Rb and Zr standards; these rocks plus high and low Sr samples from the Belknaps analysed by isotope dilution were used as Sr standards, since the range of Sr concentration in the USGS rocks was not sufficient to cover the range of observed Sr concentrations. Several high Zr samples were outside the standard range, and these values must be considered to have a larger uncertainty than the remaining samples within the standard range. These samples are indicated in the appropriate tables. No blank was observed for a pellet of pure H_3BO_3 analyzed with the samples. Estimated precision of the analyses are: Zr ±5%; Rb ±4%; Sr ±7% at <200 ppm, ±4% at >200 ppm.

E. Comparison of Analyses of Independently Prepared Splits

While not undertaken as an exhaustive study of the effects of split preparation on the variation of major and trace element abundances in granitic rocks, several opportunities arose during the study which allowed for comparison of independently prepared splits.

Approximately twenty samples of Belknap Mountain rocks were initially analyzed for major elements by B.W. Chappell at ANU. Second splits of these samples were later prepared and analyzed at WHOI. Since different analytical laboratories were used for the analyses, detailed comparison is not

justified, but with the exception of sample 9 (a very coarse gabbro), the results of the two analyses agreed quite well (Na_2O and CaO excepted, see Section D).

Trace element analyses do show significant differences. Table 23 gives results of analyses of 4 splits of sample G7. Split A is a large volume of powder prepared in a spex iron shatter box; split B is a large tungsten carbide prepared split (∿2/3 the size of split A), and was prepared the same as all the powders analyzed for this study; splits C and D are smaller tungsten carbide splits (∿1/3 the size of B).

Split A should be considered "most representative" of the bulk rock abundances. Split B differs significantly from split A, most notably La and Ce. The remaining elements are within the uncertainties of the analytical method. Split D, however, is significantly higher in almost all trace elements. This is probably due to preferential sampling of incompatible enriched minor phases in G7 (apatite, zircon, sphene). Assessing the problem with other samples prepared similarly to split B is difficult without an analysis of independent split. It must be kept in mind, however, that variations in excess of analytical error may be present.

TABLE 23. COMPARISON OF TRACE ELEMENT ANALYSES ON INDEPENDENTLY PREPARED SPLITS (CONCENTRATIONS IN PPM)

	A	B	C	D
La	62.5	73.1	62.6	87.2
Ce	143.	162.	137.	189.
Nd	57.6	60.4	42.1	67.7
Sm	10.0	10.0	9.0	10.5
Eu	1.18	1.18	1.07	1.27
Ho	1.0	1.2	1.1	1.4
Yb	2.6	2.8	2.4	2.9
Lu	0.42	0.46	0.41	0.53
Th	14.1	15.6	12.0	15.5
U	3.2	4.7	--	--
Hf	8.4	8.2	6.6	8.2
Sc	2.5	2.2	2.2	2.5

A SPEX shatter box

B Large tungsten carbide split

C,D Independent small tungsten carbide splits

REFERENCES

Abbott, M.J., 1969. Petrology of the Nandewar volcano, N.S.W. Australia, Contrib. Mineral. Petrol., 20:115-134.

Albarede, F. and Y. Bottinga, 1972. Kinetic disequilibrium in trace element partitioning between phenocrysts and host lava, Geochim. Cosmochim. Acta, 36:141-156.

Aleinikoff, J.N., 1977. Petrochemistry and tectonic origin of the Ammonoosuc Volcanics, New Hampshire-Vermont, Bull. Geol. Soc. Am., 88:1546-1552.

Allegre, C.J. and J.F. Minster, 1978. Quantitative models of trace element behavior in magmatic processes, Earth Planet. Sci. Lett., 38:1-25.

Allegre, C.J., M. Treuil, J.F. Minster, B. Minster, and F. Albarede, 1977. Systematic use of trace elements in igneous process. Part I. Fractional crystallization processes in volcanic suites, Contrib. Mineral. Petrol., 60:57-75.

Almond, D.C., 1977. The Sabaloka igneous complex, Sudan, Phil. Trans. Roy. Soc. London, Ser. A., 287:595-633.

Armstrong, R.L. and E. Stump, 1971. Additional K-Ar dates, White Mountain magma series, New England, Am. Jour. Sci., 270:331-333.

Arth, J.G., 1976. Behavior of trace elements during magmatic processes - a summary of theoretical models and their applications, Jour. Resch. U.S. Geol. Surv., 4:41-47.

Arth, J.G. and F. Barker, 1976. Rare earth partitioning between hornblende and dacitic liquid and implications for the genesis of trondhjemitic-tonalitic magmas, Geology, 4: 534-552.

Arth, J.G. and G.N. Hanson, 1975. Geochemistry and origin of the early Precambrian crust of northeastern Minnesota, Geochim. Cosmochim. Acta, 39:325-362.

Bailey, D.K. and J.F. Schairer, 1966. The system Na_2O-Al_2O_3-Fe_2O_3-SiO_2 at 1 atmosphere, and the petrogenesis of alkaline rocks, Jour. Petrol., 7:114-170.

Baker, I., 1969. Petrology of the volcanic rocks of Saint Helena Island, South Atlantic, Bull. Geol. Soc. Am., 80: 1283-1310.

Ballard, R.D. and E. Uchupi, 1972. Carboniferous and Triassic rifting: a preliminary outline of the tectonic history of the Gulf of Maine, Bull. Geol. Soc. Am., 83:2285-2302.

Barker, F. and J.G. Arth, 1976. Generation of trondhjemitic-tonalitic liquids and Archean bimodal trondhjemite-basalt suites, Geology, 4:596-600.

Barker, F., C.E. Hedge, H.T. Millard, Jr., and J.R. O'Neil, 1976. Pikes Peak batholith: geochemistry of some minor elements and isotopes, and implications for magma genesis, in R.C. Epis and R.J. Weimer (eds.) Studies in Colorado Field Geology, Prof. Contrib. Colorado School of Mines, 8:552.

Barker, F. and J.R. O'Neil, 1975. Oxygen and hydrogen isotope variations in the Pikes Peak batholith (abstract), Abstracts with Programs, Geol. Soc. Am., 7:989.

Barker, F., D.R. Wones, W.N. Sharp, and G.A. Desborough, 1975. The Pikes Peak batholith, Colorado Front Range, and a model for the origin of the gabbro-anorthosite-syenite-potassic granite suite, Precambrian Research, 2:97-160.

Bateman, P.C. and B.W. Chappell, 1978. Crystallization, fractionation, and solidification of the Tuolumne Intrusive Series, Yosemite National Park, submitted.

Billings, M.P., 1956. The Geology of New Hampshire, Part II. Bedrock Geology, New Hampshire State Planning and Development Comm., Concord.

Blaxland, A.B., 1974. Geochemistry and geochronology of chemical weathering, Butler Hill granite, Missouri, Geochim. Cosmochim. Acta, 38:843-852.

Bothner, W.A. and H.E. Gaudette, 1971. Geologic review of the Belknap Mountain complex, N.E.I.G.C. Guidebook for Field Trips in Central New Hampshire and Contiguous Areas, 88-99.

Bottino, M.L. and P.D. Fullager, 1968. Effects of weathering on whole rock Rb-Sr ages of granitic rocks, Am. Jour. Sci., 266:661-670.

Boudette, E.L. and G.M. Boone, 1976. Pre-Silurian stratigraphic succession in central western Maine, in L.R. Page (ed.) Contributions to the Stratigraphy of New England, Geol. Soc. Am. Memoir 148, 79-96.

Bowden, P. and D.C. Turner, 1974. Peralkaline and associated ring complexes in the Nigeria-Niger Province, West Africa, in H. Sørenson (ed.) The Alkaline Rocks, J. Wiley and Sons, New York, 330-354.

Brookins, D.G., 1976. Geochronologic contributions to stratigraphic interpretation and correlation in the Penobscot Bay area, eastern Maine, in L.R. Page (ed.) Contributions to the Stratigraphy of New England, Geol. Soc. Am. Memoir 148, 129-146.

Brooks, C., S.R. Hart, and I. Wendt, 1972. Realistic use of two-error regression treatments as applied to Rb-Sr data, Rev. Geophys. Space Phys., 10:551-577.

Carmichael, I.S.E., F.J. Turner, and J. Verhoogen, 1974. Igneous Petrology, McGraw-Hill, New York, 739 pp.

Chapman, C.A., 1968. A comparison of the Maine coastal plutons and the magmatic central complexes of New Hampshire, in E.-A. Zen, W.S. White, J.B. Hadley, and J.B. Thompson, Jr. (eds.) Studies of Appalachian Geology: Northern and Maritime, John Wiley and Sons, New York, 385-396.

Chapman, C.A., 1976. Structural evolution of the White Mountain magma series, in P.C. Lyons and A.H. Brownlow (eds.) Studies in New England Geology, Geol. Soc. Am. Memoir 146, 281-300.

Chapman, C.A., M.P. Billings, and R.W. Chapman, 1944. Petrology and structure of the Oliverian magma series in the Mount Washington Quadrangle, New Hampshire, Bull. Geol. Soc. Am., 55:497-516.

Chapman, R.W., 1942. Ring structures of the Pliny Range, New Hampshire, Bull. Geol. Soc. Am., 53:1533-1568.

Chapman, R.W., 1948. Petrology and structure of the Percy Quadrangle, New Hampshire, Bull. Geol. Soc. Am., 59: 1059-1100.

Chapman, R.W., and C.R. Williams, 1935. Evolution of the White Mountain magma series, Part I. Data, Am. Mineral., 20: 502-530.

Chayes, F., 1963. Relative abundance of intermediate members of the oceanic basalt-trachyte association, J. Geophys. Res., 68:1519-1534.

Condie, K.C., 1967. Geochemistry of Early Precambrian graywackes from Wyoming, Geochim. Cosmochim. Acta, 31:2135-2149.

Coombs, D.S. and F.J.G. Wilkinson, 1969. Lineages and fractionation trends in undersaturated volcanic rocks from the East Otago Volcanic Province (New Zealand) and related rocks, J. Petrol., 10:440-501.

Creasy, J.W., 1974. Mineralogy and petrology of the White Mountain batholiths, Franconia and Crawford Notch quadrangles, New Hampshire, Ph.D. Thesis, Harvard Univ.

Czamanske, G.K. and D.R. Wones, 1973. Oxidation during magmatic differentiation, Finnmarker complex, Oslo area, Norway, Part 2. The mafic silicates, Jour. Petrol., 14:349-380.

Czamanske, G.K., D.R. Wones, and J.C. Eichelberger, 1977. Mineralogy and petrology of the intrusive complex of the

Pliny Range, New Hampshire, Am. Jour. Sci., 277:1073-1123.

Drake, M.J., 1975. The oxidation state of europium as an indicator of oxygen fugacity, Geochim. Cosmochim. Acta, 39:55-64.

Drake, M.J. and D.J. Weill, 1975. Partition of Sr, Ba, Ca, Y, Eu^{2+}, Eu^{3+}, and other REE between plagioclase feldspar and magmatic liquid: an experimental study, Geochim. Cosmochim. Acta, 39:689-712.

Eichelberger, J.C., 1971. Granites and syenites of the Pliny Range, New Hampshire, M.S. Thesis, Massachusetts Institute of Technology, Cambridge.

Ewart, A. and S.R. Taylor, 1969. Trace element geochemistry of the rhyolitic volcanic rocks, central North Island, New Zealand, phenocryst data, Contr. Mineral. Petrol., 22:127-146.

Foland, K.A. and H. Faul, 1977. Ages of the White Mountain intrusives - New Hampshire, Vermont, and Maine, U.S.A., Am. Jour. Sci., 277:888-904.

Foland, K.A. and I. Friedman, 1977. Application of Sr and O isotope relations to the petrogenesis of the alkaline rocks of the Red Hill complex, New Hampshire, U.S.A., Contr. Mineral. Petrol., 65:213-225.

Foland, K.A. and C.M.B. Henderson, 1976. Application of age and Sr isotope data to the petrogenesis of the Marangudzi ring complex, Rhodesia, Earth Planet. Sci. Lett., 29:291-301.

Foland, K.A., A.W. Quinn, and B.J. Giletti, 1971. K-Ar and Rb-Sr Jurassic and Cretaceous ages for intrusives of the White Mountain magma series, northern New England, Am. Jour. Sci., 270:321-330.

Forester, R.W. and H.P. Taylor, Jr., 1976. ^{18}O-depleted igneous rocks from the Tertiary complex of the Isle of Mull, Scotland, Earth Planet. Sci. Lett., 32:11-17.

Forester, R.W. and H.P. Taylor, Jr., 1977. $^{18}O/^{16}O$, D/H and $^{13}C/^{12}C$ studies of the Tertiary igneous complex of Skye, Scotland, Am. Jour. Sci., 277:136-177.

Fullagar, P.D. and P.C. Ragland, 1975. Chemical weathering and Rb-Sr whole rock ages, Geochim. Cosmochim. Acta, 39: 1245-1252.

Gast, P.W., 1968. Trace element fractionation and the origin of tholeiitic and alkaline magma types, Geochim. Cosmochim. Acta, 32:1057-1086.

Gaudette, H.E. and W.A. Bothner, 1969. Geochemistry of the Belknap Mountain complex, New Hampshire (abstract), Abstracts with Program, Geol. Soc. Am., 1:22.

Goldich, S.S. and P.W. Gast, 1966. Effects of weathering on the Rb-Sr and K-Ar ages of biotite from the Morton gneiss, Minnesota, Earth Planet. Sci. Lett., 1:372-375.

Gordon, G.E., K. Rangle, G.G. Coles, J.B. Corliss, M.H. Beeson, and S.S. Oxley, 1968. Instrumental activation analysis of standard rocks with high-resolution γ-ray detectors, Geochim. Cosmochim. Acta, 32:369-396.

Green, J.C., 1964. Stratigraphy and structure of the Boundary Mountain anticlinorium in the Errol quadrangle, New Hampshire-Maine, Geol. Soc. Am. Special Paper 77.

Green, J.C. and C.V. Guidotti, 1968. The Boundary Mountains anticlinorium in northern New Hampshire and northwestern Maine, in E.-A. Zen, W.S. White, J.B. Hadley, and J.B. Thompson, Jr. Studies of Appalachian Geology: Northern and Maritime, John Wiley and Sons, New York, 255-266.

Hanson, G.N., 1978. The application of trace elements to the petrogenesis of igneous rocks of granitic composition, Earth Planet. Sci. Lett., 38:26-43.

Hart, S.R., 1969. K, Rb, Cs contents and K/Rb, K/Cs ratios of fresh and altered submarine basalts, Earth Planet. Sci. Lett., 6:295-303.

Hart, S.R. and C. Brooks, 1974. Clinopyroxene-matrix partitioning of K, Rb, Cs, Sr, and Ba, Geochim. Cosmochim. Acta, 38:1799-1806.

Hart, S.R. and C. Brooks, 1977. The geochemistry and evolution of early Precambrian mantle, Contrib. Mineral. Petrol., 61:109-128.

Hart S.R., and K.E. Davis, 1978. Nickel partitioning between olivine and silicate melt, Earth Planet. Sci. Lett., 40:203-219.

Harvey, P.K., D.M. Taylor, R.D. Hendry, and F. Bancroft, 1973. An accurate fusion method for the analysis of rocks and chemically related materials by X-ray fluorescence

spectrometry, X-Ray Spectrometry, 2:33-44.

Haskin, L.A., M.A. Haskin, F.A. Frey, and T.R. Wildeman, 1968. Relative and absolute terrestrial abundances of the rare earth, in L.H. Ahrens (ed.) Origin and Distribution of the Elements, Pergamon Press, New York, 889 pp.

Hedge, C.E. and F. Barker, 1975. Strontium isotope and abundance systematics of the Pikes Peak batholith, Colorado (abstract), EOS, Trans. Am. Geophys. Un., 56: 1071.

Heinrich, E.W., 1965. Microscopic Identification of Minerals, McGraw-Hill, New York, 414 pp.

Helz, R.T., 1973. Phase relations of basalts in their melting range at P_{H_2O} = 5 kb as a function of oxygen fugacity. Part I. Mafic phases, J. Petrol., 14:249-302.

Helz, R.T., 1976. Phase relations of basalts in their melting ranges at P_{H_2O} = 5 kb. Part II. Melt compositions, J. Petrol., 17:139-193.

Henderson, D.M., M.P. Billings, J. Creasy, and S.A. Wood, 1977. Geology of the Crawford Notch Quadrangle, New Hampshire, Dept. of Resources and Economic Development, Concord, 29 pp.

Higuchi, H. and H. Nagasawa, 1969. Partition of trace elements between rock-forming minerals and the host volcanic rocks, Earth Planet. Sci. Lett., 7:281-287.

Hofmann, A.W. and S.R. Hart, 1978. An assessment of local and regional isotopic equilibrium in the mantle, Earth Planet. Sci. Lett., 38:44-62.

Hon, R., 1976. Petrology and geochemistry of the Mt. Katahdin batholith, Maine. Unpublished Ph.D. Thesis, Mass. Inst. of Technology

Hon, R. and H.J. Noyes, 1977. REE and other trace elements during fractionation of granitic aplites of Sierra Nevada batholith, California, and Katahdin pluton, Maine (abstract), Abstracts with Programs, Geol. Soc. Am., 9:1023.

I.U.G.S., 1973. Plutonic rocks: classification and nomenclature recommended by IUGS, Subcommission on the Systematics of Igneous Rocks, Geotimes, October:26-30.

Jacobsen, R.E., W.N. MacLeod, and R. Black, 1958. Ring Complexes in the Younger Granite Province of Northern Nigeria, Geol. Soc. London, Memoir No. 1., London.

James, R.S. and D.L. Hamilton, 1969. Phase relations in the system $NaAlSi_3O_8$-$KAlSi_3O_8$-$CaAl_2Si_2O_8$-SiO_2 at 1 kilobar water vapour pressure, Contrib. Mineral. Petrol., 21: 111-141.

Kay, R.W. and P.W. Gast, 1973. The rare earth content and origin of alkali-rich basalts, Jour. Geol., 81:653-682.

Kingsley, L., 1931. Cauldron subsidence of the Ossipee Mountains, Am. Jour. Sci., 5th Series, 12:134-167.

Ludman, A., 1976. Fossil-based stratigraphy in the Merrimack synclinorium, central Main, in L.R. Page (ed.) Contributions to the Stratigraphy of New England, Geol. Soc.

Am. Memoir 148, 65-78.

Luth, W.C., 1969. The systems $NaAlSi_3O_8$-SiO_2 and $KAlSi_3O_8$-SiO_2 at 20 kb and the relationship between H_2O content, P_{H_2O}, and P_{Total} in granitic magmas, Am. Jour. Sci., 267A:325-341.

Luth, W.C., R.H. Jahns, and O.F. Tuttle, 1964. The granite system at pressures of 4 to 10 kilobars, J. Geophys. Res., 69:759-773.

Lyons, J.B. and D.E. Livingston, 1977. Rb-Sr age of the New Hampshire magma series, Bull. Geol. Soc. Am., 88:1808-1812.

MacLeod, W.N., D.C. Turner, and E.P. Wright, 1971. The Geology of the Jos Plateau, Vol. 1. General Geology, Geol. Surv. Nigeria, Bulletin 32.

McCarthy, T.S. and R.A. Hasty, 1976. Trace element distribution patterns and their relationship to the crystallization of granitic melts, Geochim. Cosmochim. Acta, 40:1351-1359.

McHone, J.G., W.W. Black, W.J. Pegram, 1976. Origin of northwestern New England lamprophyres: Sr isotopes and geochemical evidence (abstract), Abstracts with Programs, Geol. Soc. Am., 8:227.

McIntire, W.L., 1963. Trace element partition coefficients - a review of theory and applications to geology, Geochim. Cosmochim. Acta, 27:1209-1264.

Miller, C.F., 1977a. Alkali-rich monzonites, California: origin of near silica-saturated alkaline rocks and their significance in a calc-alkaline batholithic belt, Ph.D.

Thesis, University of California, Los Angeles, 283 pp.

Miller, C.F., 1977b. Early alkalic plutonism in the calc-alkaline batholithic belt of California, Geology, 5: 685-688.

Modell, D., 1936. Ring-dike complex of the Belknap Mountains, New Hampshire, Bull. Geol. Soc. Am., 47, 1885-1932.

Moorbath, S. and J.D. Bell, 1965. Strontium isotope abundance studies and Rb-Sr age determinations on Tertiary igneous rocks from the Isle of Skye, northwest Scotland, J. Petrol., 6:37-66.

Moorbath, S. and H. Welke, 1969. Lead isotope studies on igneous rocks from the Isle of Skye, northwest Scotland, Earth Planet. Sci. Lett., 5:217-230.

Morgan, W.J., 1971. Convection plumes in the lower mantle, Nature, 230:42-43.

Morse, S.A., 1969. Syenites, Carnegie Inst. Washington Yb., 67:112-120.

Nagasawa, H., 1970. Rare earth concentrations in zircons and apatites and their host dacites and granites, Earth Planet. Sci. Lett., 9:359-364.

Nagasawa, H., 1971. Partitioning of Eu and Sr between co-existing plagioclase and K-feldspar, Earth Planet. Sci. Lett., 13:139-144.

Nagasawa, H. and C.C. Schnetzler, 1971. Partitioning of rare earth, alkali and alkaline earth elements between phenocrysts and acidic igneous magma, Geochim. Cosmochim. Acta, 35:953-968.

Naylor, R.S., 1968. Origin and regional relationships of the core-rocks of the Oliverian domes, in E.-A. Zen, W.S. White, J.B. Hadley, and J.B. Thompson, Jr. (eds.) Studies of Appalachian Geology: Northern and Maritime, John Wiley and Sons, New York, 231-240.

Naylor, R.S., 1969. Age and origin of Oliverian domes, central western New Hampshire, Bull. Geol. Soc. Am., 80:405-428.

Naylor, R.S., 1975. Age provinces in the northern Appalachians, Ann. Rev. Earth Sci., 3:387-400.

Naylor, R.S., G.M. Boone, E.L. Boudette, D.D. Ashenden, and P. Robinson, 1973. Pre-Ordivician rocks in the Bronson Hill and Boundary Mountain anticlinorium (abstract), EOS, Trans. Am. Geophys. Un., 50:495.

Neilson, D.L., R.G. Clark, J.B. Lyons, E.J. Englund, and D.J. Borns, 1976. Gravity models and mode of emplacement of the New Hampshire plutonic series, in P.C. Lyons and A.H. Brownlow (eds.) Studies in New England Geology, Geol. Soc. Am. Memoir 146, 301-318.

Noble, D.C. and C.E. Hedge, 1970. Distribution of rubidium between sodic sanidine and natural silicic liquid, Contrib. Mineral. Petrol., 29:234-241.

Norrish, K. and J.T. Hutton, 1969. An accurate X-ray spectrographic method for the analysis of a wide range of geological samples, Geochim. Cosmochim. Acta, 33:431-453.

Noyes, H.J., 1978. Petrogenesis of Sierran plutons: a petrologic and geochemical investigation into the origin and differentiation of granodioritic plutons of the central

Sierra Nevada batholith, Ph.D. Thesis, Massachusetts Institute of Technology, 324 pp.

Osberg, P.H., R.H. Muench, and J. Warner, 1968. Stratigraphy of the Merrimack synclinorium in west central Maine, in E.-A. Zen, W.S. White, J.B. Hadley, and J.B. Thompson, Jr. (eds.) Studies in Appalachian Geology: Northern and Maritime, John Wiley and Sons, New York, 241-253.

Page, L.R., 1968. Devonian plutonic rocks in New England, in E.-A. Zen, W.S. White, J.B. Hadley, J.B. Thompson, Jr. (eds.) Studies in Appalachian Geology: Northern and Maritime, John Wiley and Sons, New York, 371-383.

Pankhurst, R.J., R.D. Beckinsale, and C.K. Brooks, 1976. Strontium and oxygen isotope evidence relating to the petrogenesis of the Kanderdlugssuag alkaline intrusion, East Greenland, Contrib. Mineral. Petrol., 54:17-42.

Pankiwskyj, K.A., A. Ludman, J.R. Griffen, and W.B.N. Berry, 1976. Stratigraphic relationships on the southeast limb of the Merrimack synclinorium in central and west central Maine, in P.C. Lyons and A.H. Brownlow (eds.) Studies in New England Geology, Geol. Soc. Am. Memoir 146, 263-280.

Paster, T.P., D.S. Schauwecker, and L.A. Haskin, 1974. The behavior of some trace elements during solidification of the Skaergaard layered series, Geochim. Cosmochim. Acta, 38:1549-1577.

Philpotts, J.A. and C.C. Schnetzler, 1970. Phenocryst-matrix partition coefficients for K, Rb., Sr, and Ba, with applications to anorthosite and basalt genesis, Geochim.

Cosmochim. Acta, 34:307-322.

Pirsson, L.V. and H.S. Washington, 1905. Contributions to the geology of New Hampshire, I. Geology of the Belknap Mountains, Am. Jour. Sci., 4th Series, 20:344-352.

Pirsson, L.V. and H.S. Washington, 1906. Contributions to the geology of New Hampshire, II. Petrology of the Belknap Mountains, Am. Jour. Sci., 4th Series, 72:439-457, 493-514.

Price, R.C. and B.W. Chappell, 1975. Fractional crystallization and the petrology of Dunedin volcano, Contrib. Mineral. Petrol., 53:157-182.

Price, R.C. and S.R. Taylor, 1973. The geochemistry of the Dunedin volcano, East Otago, New Zealand: rare earth elements, Contrib. Mineral. Petrol., 40:195-205.

Quinn, A., 1937. Petrology of the alkaline rocks at Red Hill, New Hampshire, Bull. Geol. Soc. Am., 48:373-402.

Rodgers, J., 1970. Tectonics of the Appalachians, John Wiley and Sons, New York.

Roy, C.J. and J. Freedman, 1944. Petrology of the Pawtuckaway Mountains, New Hampshire, Bull. Geol. Soc. Am., 55: 905-920.

Schnetzler, C.C. and J.A. Philpotts, 1970. Partition coefficients of rare earth elements between igneous matrix material and rock forming mineral phenocrysts, II., Geochim. Cosmochim. Acta, 34:331-340.

Sharp, J.A. and G. Simmons, 1978. Geologic/geophysical models of intrusives of the White Mountain magma series (WMMS)

(abstract), Abstracts with Programs, Geol. Soc. Am., 10:85.

Shaw, D.M., 1970. Trace element fractionation during anatexis, Geochim. Cosmochim. Acta, 34:237-243.

Shimizu, N., 1974. An experimental study of the partitioning of K, Rb, Sc, Sr, and Ba between clinopyroxene and liquid at high pressure, Geochim. Cosmochim. Acta, 38:1789-1798.

Size, W.B., 1972. Petrology of the Red Hill syenitic complex, New Hampshire, Bull. Geol. Soc. Am., 83:3747-3760.

Smet, T., J. Hertogen, R. Gijbels, and J. Hoste, 1978. A group separation scheme for radiochemical neutron activation analyses of 24 trace elements in rock and minerals separates, in press.

Steiner, J.C., R.H. Jahns, and W.C. Luth, 1975. Crystallization of alkali feldspar and quartz in the haplogranite system $NaAlSi_3O_8$-$KAlSi_3O_8$-SiO_2-H_2O at 4 kb, Bull. Geol. Soc. Am., 86:83-98.

Suen, J., 1978. Geochemistry of perididites and associated mafic layers, Ronda ultramafic complex, Spain. Unpublished Ph.D. thesis, Mass. Inst. of Technology

Sun, S.S. and G.N. Hanson, 1975. Origin of Ross Island basanitiods and limitations upon the heterogeneity of mantle sources for alkali basalts and nephelinites, Contrib. Mineral. Petrol., 52, 77-106.

Sun, S.S. and G.N. Hanson, 1976. Rare earth element evidence for differentiation of McMurdo volcanics, Ross Island, Antarctica, Contrib. Mineral. Petrol., 54:139-155.

Taylor, H.P., Jr., 1974. The application of oxygen and hydrogen isotope studies to problems of hydrothermal alteration and ore deposition, Economic Geology, 69: 843-883.

Taylor, H.P., Jr., 1978. Oxygen and hydrogen isotope studies of plutonic granitic rocks, Earth Planet. Sci. Lett., 38: 177-210.

Thompson, J.B., Jr., P. Robinson, T.H. Clifford, and N.H. Trask, Jr., 1968. Nappes and gneiss domes in west central New England, in E.-A. Zen, W.S. White, J.B. Hadley, J.B. Thompson, Jr. (eds.) Studies in Appalachian Geology: Northern and Maritime, John Wiley and Sons, New York, 203-218.

Toulmin, P. III, 1960. Composition of feldspars and crystallization history of the granite-syenite complex near Salem, Essex County, Massachusetts, U.S.A. Rept. Intl. Geol. Cong. 21st, Copenhagen, Pt. 13, 275-286.

Tuttle, O.F. and N.L. Bowen, 1958. Origin of Granite in the Light of Experimental Studies in the System $NaAlSi_3O_8$-$KAlSi_3O_8$-SiO_2-H_2O, Geol. Soc. Am. Memoir 74.

Upton, E.G.J., 1960. The Alkaline Igneous Complex of Kûngnât Fjeld, South Greenland, Grønlands Geologiske Undersøgelese, Bulletin 27.

van Breeman, O., J. Hutchison, and P. Bowden, 1975. Age and origin of the Nigerian Mesozoic granites: a Rb-Sr isotopic study, Contrib. Mineral. Petrol., 50:157-172.

Wager, L.R. and G.M. Brown, 1968. Layered Igneous Rocks, Oliver and Boyd, London, 588 pp.

Watson, E.B., 1977. Partitioning of manganese between forsterite and silicate liquid, Geochim. Cosmochim. Acta, 41:1363-1375.

Wellman, T.R., 1971. Feldspathoidal rocks of the Red Hill igneous complex, New Hampshire, Jour. Geol., 79:621-627.

White, A.J.R. and B.W. Chappell, 1977. Ultrametamorphism and granitoid genesis, Tectonophysics, 43:7-22.

Whitney, J.A., 1972. History of granodioritic and related magma systems: an experimental study, unpublished Ph.D. thesis, Stanford University

Winkler, H.G.F., 1974. Petrogenesis of Metamorphic Rocks, Springer-Verlag, New York, 320 pp.

Wright, T.L., 1974. Presentation and interpretation of chemical data for igneous rocks, Contrib. Mineral. Petrol., 48:233-248.

Wright, T.L. and P.C. Doherty, 1970. A linear programming and least squares computer method for solving petrologic mixing problems, Bull. Geol. Soc. Am., 81:1995-2008.

Yoder, H.S., 1965. Diopside-anorthite-water at five and ten kilobars and its bearing on explosive volcanism, Carnegie

Inst. Washington Yb., 64:82-89.

York, D., 1969. Least-squares fitting of a straight line with correlated errors, Earth Planet. Sci. Lett., 5:320-324.

Zielinski, R.A., 1975. Trace element evaluation of a suite of rocks from Reunion Island, Indian Ocean, Geochim. Cosmochim. Acta, 39:713-734.

Zielinski, R.A. and F.A. Frey, 1970. Gough Island: evaluation of a fractional crystallization model, Contrib. Mineral. Petrol., 29:242-254.